The Influence of Cross-winds on the Performance of Natural Draft Dry-Cooling Towers.

by

Abraham Francois du Preez

Dissertation presented for the Degree of Doctor of Philosophy
(Mechanical Engineering) at the University of Stellenbosch.

Promoter: Prof. D.G. Kröger

Department of Mechanical Engineering
University of Stellenbosch
Stellenbosch, 7600
R.S.A.

Declaration

I, the undersigned, declare that the work contained in this thesis is my own original work and has not previously in its entirety or in part been submitted at any University for a degree.

Signature of candidate

Date: Nov 1992

Abstract

The effect of cross-winds on the performance of natural draft dry-cooling towers is studied by means of isothermal model tests, a numerical simulation and full scale measurements. The action of the wind on such towers is found to be complex and is influenced by a number of different parameters including the wind speed, the shape of the approaching wind profile, the inlet diameter to the inlet height ratio of the tower, the tower height, the shape of the tower shell, the pressure loss coefficient of the heat exchangers and the amount of heat rejected by the tower. For a horizontal arrangement of the heat exchangers the wind effect on the tower is shown to be strongly dependent on both the shape and pressure loss coefficient of the tower supports.

In practical cooling towers the heat exchangers are either arranged horizontally in the inlet cross-section of the tower or vertically around the circumference of the tower and the wind effect is found to be dependent on the particular layout. The wind effect on a tower is furthermore found to increase if the heat exchangers are arranged in the form of A-frames. Additional reductions in the heat rejection rate of the tower are caused by a non-uniform air temperature distribution inside the tower and flow distortions through the heat exchanger.

Significant reductions in the wind effect on a cooling tower can be achieved by installing windbreak walls below the heat exchangers if the latter are arranged horizontally in the tower inlet.

Opsomming

Die invloed van dwarswinde op die verkoelingsvermoë van natuurlike trek droë-koeltorings word bestudeer met behulp van isotermiese model toetse, 'n numeriese model en volskaal metings. Die windeffek op sulke koeltorings is kompleks en word bepaal deur 'n aantal faktore soos die windsnelheid, die windprofiel, die inlaatdiameter tot inlaathoogte verhouding van die toring, die toring hoogte, die vorm van die koeltoringwand, die drukverlieskoëffisiënt van die warmteruilers en die hoeveelheid warmte wat deur die koeltoring uitgeruil word. Vir 'n horisontale rangskikking van die warmteruilers word die invloed van die wind op die koeltoring ook bepaal deur die vorm en drukverlieskoëffisiënt van die koeltoringstutte.

In praktiese koeltorings word die warmteruilers gewoonlik óf horisontaal in die basisarea óf vertikaal langs die inlaatomtrek van die koeltoring geplaas en daar is gevind dat die windinvloed afhanklik is van die tipe rangskikking. Verder is 'n verhoging in die windeffek op die koeltoring gevind indien die warmteruilers in die vorm van A-rame geïnstalleer word. As gevolg van die wind word 'n nie-uniforme lugsnelheidsverdeling en gevolglik ook 'n versteurde temperatuurprofiel in die koeltoring verkry. Laasgenoemde faktore veroorsaak verdere verminderings in die verkoelingsvermoë van die koeltoring.

Die windeffek op die koeltoring met 'n horisontale warmteruiler uitleg kan aansienlik verminder word deur windwande onder die warmteruilers op te rig.

Acknowledgements

Upon completion of this study, I would like to acknowledge, with gratitude, the following persons and institutions without whom this research would not have been possible.

Prof. D.G. Kröger, my thesis supervisor, for his continuous inspiration and guidance, in some respects more than what was required for the completion of this dissertation. I would also like to thank Mrs Kröger for her encouragement when it was needed.

Dr. C.G. du Toit for his valuable contributions towards the numerical analysis.

Kobus Zietsman for his more-than-technical assistance with both the model tests and the full scale measurements. His friendliness and interest were much appreciated.

All my fellow-students, especially J.E. Hoffmann and A.E. Conradie, for their assistance with the full scale measurements.

Mr Attie Visser for reading the draft and correcting the English.

ESKOM for allowing us to perform measurements on the full scale cooling tower and for providing the weather data during the tests.

The FRD and Water Research Commission for their financial support.

Furthermore am I deeply grateful to my parents and my friends Elmarie, Jan (Mossie) and all the others who supported me morally and by their prayers throughout the course of this project.

Above all I give the honour to my Lord and Saviour who said in His Word "Apart from me you can do nothing" (John 15:5).

Contents

Nomenclature

A	Area, m^2
a	Coefficient
b	Exponent
C	Coefficient
C_D	Drag coefficient
c_p	Specific heat at constant pressure, J/kgK
c_v	Specific heat at constant volume, J/kgK
d	Diameter, m
d_e	Equivalent diameter, m
F	Correction factor or force, N
f	Friction factor
g	Gravitational acceleration, m/s^2
H	Height, m
h	Heat transfer coefficient, W/m^2K
K	Loss coefficient
k	Thermal conductivity, W/mK or roughness height, m
L	Length, m
m	Mass flow rate, kg/s
Ny	Characteristic heat transfer parameter, m^{-1}
n	Number or nozzle
Pr	Prandtl number
p	Pressure, N/m^2
Δp	Pressure differential, N/m^2
Q	Heat transfer rate, W or volume flow rate, m^3/s
R	Universal gas constant, J/kgK
Re	Reynolds number
Ry	Characteristic flow parameter, m^{-1}
r	Radius, m
T	Temperature, °C or K
t	Time, s
U	Overall heat transfer coefficient, W/m^2K
u	Velocity component, m/s

v	Velocity, m/s or velocity component
w	Vertical velocity component, m/s
Y	Velocity factor as defined by equation (C.1.7)
z	Elevation, m
α	Kinetic energy coefficient or thermal expansion coefficient or correction factor
α_Q	Heat transfer correction factor as defined by equation (2.3.2)
Δ	Differential
ϵ	Surface roughness or effectiveness
θ	Angle or circumferential position, °
μ	Dynamic viscosity, kg/ms
υ	Kinematic viscosity, m^2/s
ρ	Density,kg/m^3
σ	Area ratio
τ	Factor depending on the shape of wind tunnel outlet
ϕ	Expansion factor as defined by equation (C.1.6) or outlet angle
λ	Shape factor

Subscripts

a	Air or air-side
c	Cold or cone or contraction
con	Contraction
ct	Cooling tower
ctc	Cooling tower contraction
cte	Cooling tower expansion
e	Effective
fr	Frontal
g	Gas
h	Hot
he	Heat exchanger
i	Inlet
l	Local
lm	Logarithmic mean
m	Mean
n	Nozzle

o	Outlet
p	Pressure
Q	Heat transfer
ref	Reference
s	Static
T	Temperature
t	Throat
tr	Tube row
ts	Tower supports or tube or tunnel cross-section
u	Upstream or tangential direction
v	Normal
w	Wind or water
x	Co-ordinate
y	Co-ordinate
z	Elevation or Co-ordinate
θ	Circumferential position
∞	Free stream

Abbreviations

arr	Arrangement
AGL	Above ground level
e	East
ex	Exchanger
max	Maximum
min	Minimum
n	North
s	South
v	Velocity
w	West

CHAPTER 1

Introduction and background

1.0: Introduction

The second law of thermodynamics requires that a thermal power cycle has to exchange heat with more than one fixed temperature reservoir. In most existing power plants water is used as the working fluid with heat supplied to the cycle at a relative high temperature by means of coal or oil fired boilers or nuclear reactors. In a practical thermal power plant more than 50% of the heat delivered by the boiler to the working fluid has to be rejected (through a cooling system), to the low temperature reservoir. The latter normally includes a condenser in which the exit steam from the low pressure turbine is condensed by rejecting heat to a low temperature coolant, i.e. the low temperature reservoir. The lower the coolant temperature in the condenser, the higher the thermal efficiency of the thermal power cycle and the more economical the power generation process.

Originally most power generation plants relied on the hydrosphere as the low temperature reservoir. This is a very simple cooling method by which river, lake or sea water is passed "once though" the power plant condenser and afterwards returned to the source. However, due to the ever increasing electric demand, environmental concerns and the siting of power plants, this cooling method was limited in favour of wet or evaporative cooling towers. Wet cooling tower require relatively smaller quantities of cooling water and reject waste heat directly to the atmosphere, chiefly by means of evaporation.

The erection of power plants in arid areas and the exploitation of coal fields where the coal deposits could not be matched with an adequate supply of water at reasonable cost, necessitate a reconsideration of the type of cooling system to be used. As a result dry-cooling became a more attractive alternative. Basically two types of dry-cooling systems are employed in power plants, namely the direct condensing system and the indirect system. In the direct system the turbine exhaust steam is condensed in either forced or induced draft, air cooled, condensers. With the indirect system the turbine steam is condensed in a conventional, watercooled surface or direct contact spray condenser. The required cooling water flow is recooled in a closed circuit by means of a natural draft dry-cooling tower. Since the purpose of the present study is to investigate the influence of

cross-winds on the performance of natural draft dry-cooling towers, all subsequent references to a dry-cooling system imply an indirect system including a natural draft cooling tower.

The water in the cooling circuit of an indirect dry-cooling system is cooled in finned tube heat exchangers and is therefore not in contact with the air. The waste heat is rejected to the air entirely by convection whereby considerable quantities of make-up water are saved compared to the power plants where wet cooling systems are employed. However, due both to the additional thermal resistance caused by the finned tubes and to the fact that the transfer of heat is limited to convection, very large heat exchange areas and air mass flow rates are required in a dry-system for adequate cooling. Consequently the capital cost of a dry-cooled system designed to reject a given amount of heat would be higher than that of a wet system of comparable output.

As mentioned before, the efficiency of the power cycle is amongst others a function of the coolant temperature in the condenser. If an indirect dry-cooling system is employed in a power plant, the coolant temperature is determined by the temperature of the water returning from the cooling tower. Thus the performance of such a power plant depends on the performance of the cooling system. It is therefore important to identify the different atmospheric conditions which may have a negative effect on the performance of a dry-cooling system and to minimize the resulting losses by specific design.

It is well known that cross-winds have an adverse affect on the performance of natural draft dry-cooling towers. However, very little useful information is available in the literature quantifying the effect of winds on the heat rejection rate of such towers. For that reason the present study is undertaken with the aim to determine the factors affecting the performance of dry-cooling towers in windy conditions.

In chapter 2 results of comprehensive scale model tests are given and are used to predict the rise in the outlet water temperature of a specific dry-cooling tower. Measurements performed on a full scale dry-cooling towers subjected to cross-winds are discussed in chapter 3. In an attempt to duplicate results obtained by means of full scale measurements, a numerical procedure is employed as described in chapter 4 with conclusive remarks given in chapter 5.

1.1: Literature survey: Full scale measurements.

Measurements performed on full scale towers indicate a rise in the temperature of the water leaving the tower as the wind speed increases for a given heat rejection rate of the tower [67PR1, 69CH1, 76VA1, 77MA1, 87TR1, 88CA1]. A summary of these measurements is shown in figure 1.1.1.

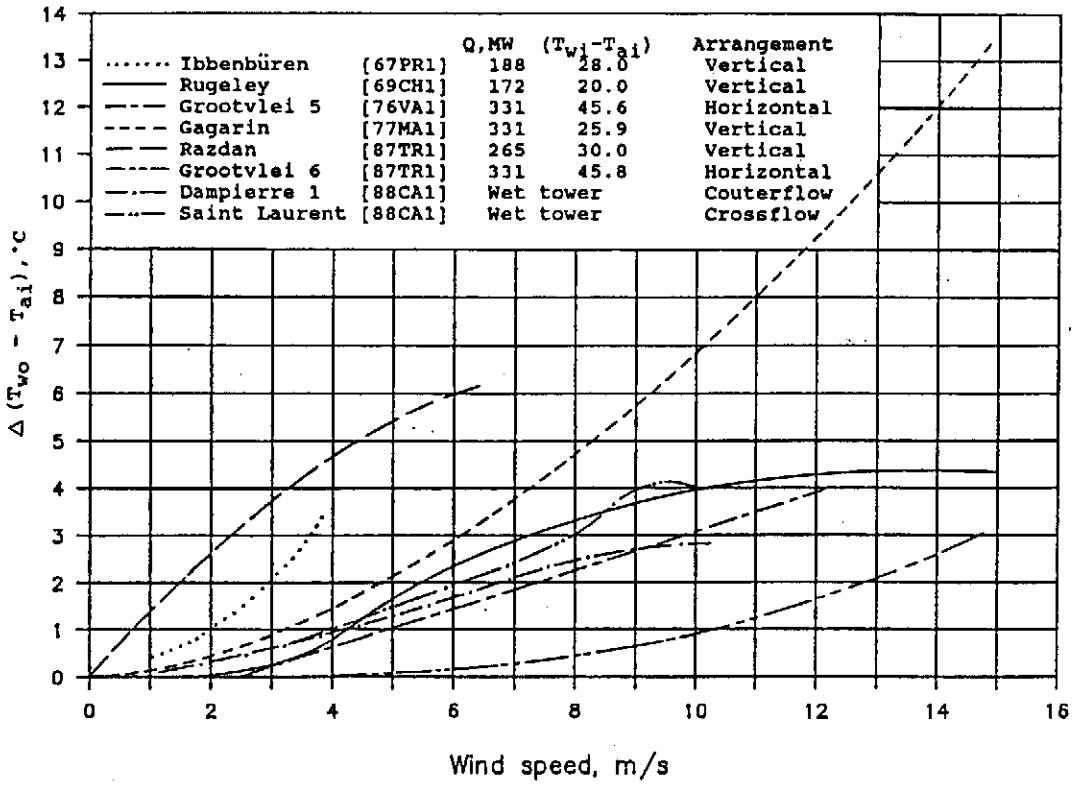

Figure 1.1.1: Rise in the cooling water temperature of cooling towers as a function of the wind speed.

As shown in the figure, the wind effect on a dry-cooling tower is usually expressed in terms of the change in the difference between the outlet water temperature, T_{wo}, and that of the ambient air entering the tower, T_{ai}, at a constant heat rejection rate as a function of the wind speed. The above-mentioned temperature difference is also defined as the approach temperature and may be expressed as follows.

$$\Delta(T_{wo} - T_{ai}) = (T_{wo} - T_{ai})_w - (T_{wo} - T_{ai}) \qquad (1.1.0)$$

where the first term on the right hand side of the equation represents the temperature difference during windy conditions while the second term is the difference in temperature in the absence of wind.

Although all the curves in figure 1.1.1 indicate a rise in the water temperature as the wind speed increases, some cooling towers seem to be much more sensitive to cross-winds than others. The exact reason for this trend is difficult to determine from the above mentioned literature, primarily due to a lack of adequate test details, but the following factors may contribute to the wide distribution in the data.

In existing dry-cooling towers, the rectangular heat exchanger bundles are arranged either vertically around the circumference of the tower as shown in figure 1.1.2(a), in a horizontal rectangular pattern, figure 1.1.2(b) or in a horizontal radial pattern, figure 1.1.2(c). Moore [76MO1] mentioned that according to the results of the tests performed on full scale towers, an internal horizontal arrangement of the heat exchangers is less wind-susceptible than an external vertical arrangement. In agreement Russell [78RU1] states that cross-wind effects are smallest when the intake arrangements create the minimum disturbances to the approaching wind profile. The latter seems to be confirmed by the results shown in figure 1.1.1 where the wind influence on the towers with a horizontal heat exchanger arrangement, namely Grootvlei 5 and Grootvlei 6, is less than on any of the towers with a vertical arrangement. Markòczy [77MA1] furthermore argues that the greater initial temperature difference of the Grootvlei towers may ensure a more stable air flow through the bundles and therefore the towers appear to be less affected by the wind.

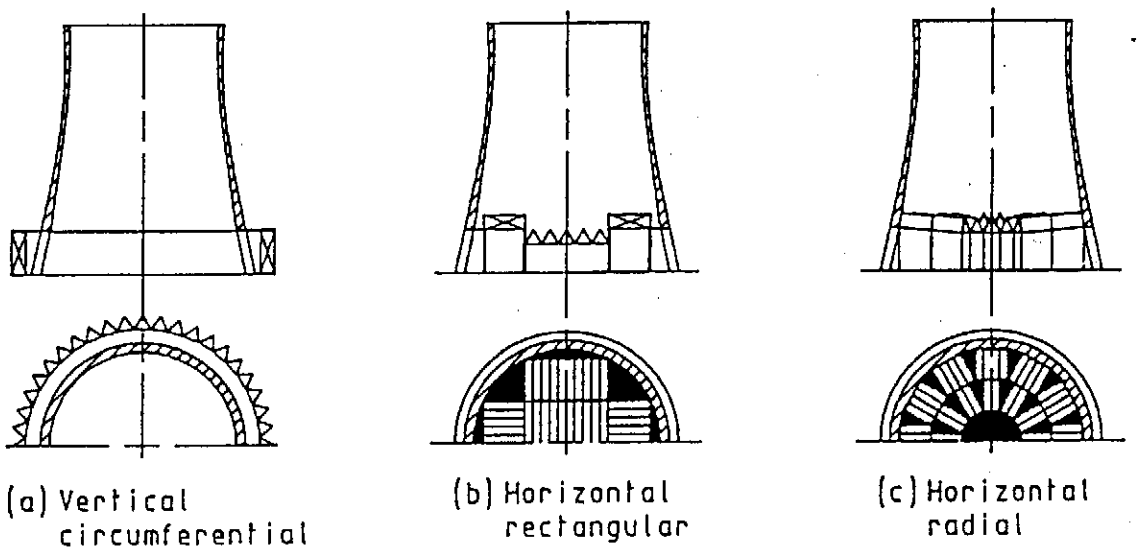

Figure 1.1.2: Different bundle arrangements in dry-cooling towers.

Based on results obtained during full scale measurements, Markòczy [77MA1] furthermore

found that the extent of disturbances caused by the wind is not only a function of the wind velocity, but also of the average air velocity through the heat exchangers. Since the latter is directly related to the tower performance, a reduction in the wind influence can be expected with increasing tower performance. This is found to be true if the heat exchangers are arranged in the form of A-frames.

Witte [83WI1] mentioned that the influence of winds on a cooling tower can only be tested reliably in the absence of vertical temperature inversions, which will also tend to increase the water outlet temperature of the tower. Markòczy [77MA1] mentioned that part of the apparent strong wind effect on the Ibbenbüren tower [67PR1] may be caused by inversions since some of the measurements were made during the night. Furthermore cold inflow at the tower top is not excluded, especially at low wind velocities. The wind influence on the Grootvlei 5 tower as published by Van der Walt [76VA1] was derived from tests where it was possible to distinguish between the individual effects of the wind and inversions.

According to Moore [78MO1] scatter in the data can be expected due to the unstable character of the wind, both in speed and direction. Markòczy [77MA1] based their test results on the average wind velocity over ten-minute periods and also mentioned that wind gusts will hardly affect the operating behaviour of the tower due to the thermal inertia of the cooling system. Van der Walt [76VA1] also found that the graphs based on five-minute observation periods were too spiky and the curves were smoothed by converting to a fifteen minute average basis. Bourillot [80BO1] states that less scatter in the data is found if the wind velocity is measured at a height corresponding to the outlet edge of the tower.

The wind profile is usually not uniform, and significant variations in the wind velocity may be found in the atmosphere near ground level. In the surface boundary layer, the wind velocity tends to increase with an increase in height above ground level and the wind profile can, for engineering applications, be described with a power law [83PA1] i.e.

$$\frac{v_w}{v_{wref}} = \left[\frac{z}{z_{ref}}\right]^b \qquad (1.1.1)$$

where v_{wref} is the wind speed at the reference height z_{ref}. The exponent, b, depends on the roughness of the ground surface with the vertical temperature distribution also having an important effect. During the night, when a stable surface layer is found, the value of the

exponent b is usually much higher than that which is found in daytime when the wind profile is more uniform. VDI 2049 [78VD1] recommended a value of b = 0.2 to be used for cooling tower measurements while the free stream wind velocity should be measured at the outlet height of the tower in an undisturbed flow. Should this be impossible, the wind velocity is to be measured 10 m above ground level.

Due to the variations in wind velocity it is important to know the wind velocity distribution, as well as the position and the height above ground level where the wind velocity was measured during any test. The closer to the ground level the wind velocity is measured, the more sensitive the cooling tower will appear to be to a cross-wind. Van der Walt [76VA1] measured the wind velocity with a cup-type anemometer at the inlet height of the tower, while for the Grootvlei 6 tower it was measured 7.5 m AGL. Markòczy [77MA1] only states that the atmospheric conditions were obtained from a meteorologic station 500 m from the tower, but does not mention at which height the wind velocity was measured. He furthermore mentioned that the position of the cooling tower on which the measurements were performed was such that for the prevailing wind direction the approaching wind was not disturbed by structures or obstacles. Caytan [88CA1], who published results of measurements performed on wet towers, used the wind velocity as measured on 11 metres as reference. Grange [82GR1], who performed measurements on the Saint-Laurent wet tower, based his observations on the wind velocity 140 meter AGL as obtained from a weather mast erected 200 m from the tower. Bourillot [80BO1] used the wind velocity as measured at the tower outlet level as reference while no relevant information is given by the rest of the authors whose results are shown in figure 1.1.1. It can therefore be expected that at least part of the apparent difference in the wind influence on the different towers is due to the fact that the wind velocities were measured at different elevations during the tests. Furthermore no details are given concerning the wind profiles which will be different for the various power station sites.

1.2: Literature survey: Model tests.

Due both to all the problems which arise during full scale tests, and to practical and economical considerations, some investigators [78BO1, 78RU1, 80BO1, 80LE1, 82BU1, 82CH1, 82GR1, 82RU1, 82SA1, 83BU1, 85VO1, 86BL1, 86VA1] preferred model tests for studying the wind effect on cooling towers. Völler [85VO1] did a dimensional analysis for a dry-cooling tower in a cross-flow and found at least seven dimensional groups as listed in table 1.2.1

Table 1.2.1: Dimensional groups for a dry-cooling tower in a cross-flow.

1.	$\frac{\rho v d}{\mu}$	Reynolds number based on the flow inside the tower.
2.	$\frac{d_i}{H_i}$	Ratio of the inlet diameter to inlet height.
3.	$\frac{\rho v^2}{\Delta\rho g d}$	Densimetric Froude number.
4.	$\frac{\Delta p}{\rho v^2}$	Euler number.
5.	$\frac{v_w}{v}$	Ratio of the wind velocity to the velocity of the air flow inside the tower.
6.	$\frac{\rho d v_w}{\mu}$	Reynolds number based on the wind velocity.
7.	$\frac{d}{vt}$	Strouhal number.

If the size of available wind tunnels is considered, cooling tower models of a scale larger than approximately 0.01 cannot be employed without the results being seriously affected by solid blockage effects. In a small scale model it is impossible to satisfy both the densimetric Froude number and the Reynolds number, as listed in table 1.2.1, with a single model test. Therefore model tests in the past were either based on Froude's similarity or on isothermal tests approximating Reynolds similarity. Each of the techniques offers some advantages, but because all the dimensional groups are not satisfied in either of the approximations, each technique also

has its limitations. Bourillot [80BO1], Buchlin [82BU1], Grange [82GR1], Ruscheweyh [82RU1] and Sabaton [82SA1] performed tests based on Froude's similarity. This is done by using non-isothermal tests with the tower draft simulated by buoyancy effects. Buchlin [82BU1] mentioned that these models allow a realistic simulation of the possible interaction between the inlet and outlet thermal and aerodynamic phenomena. The fluid velocities obtained in these models are very low and special measuring techniques usually have to be used. Consequently the Reynolds numbers are approximately three orders of magnitude less than those for a full scale tower, which may cause erroneous results. Bourillot [80BO1] furthermore observed large velocity fluctuations and tests were repeated several times to eliminate random errors. Although heating models can be of value for comparative surveys of different tower shapes [82RU1], it is still difficult to forecast the wind influence for a specific tower, due to uncertainties in the measurements.

If the densimetric Froude number is neglected, isothermal tests may be performed [78BO1, 78RU1, 80BO1, 80LE1, 82CH1, 83BU1, 85VO1, 86BL1, 86VA1]. The natural draft phenomenon is not represented in these tests and therefore the tower draft is achieved by sucking or blowing a fluid through the model. Although the Reynolds numbers obtained in these tests are much higher than those which are found in heating models, they are still much lower than those found in full scale towers. In Appendix A the inlet loss coefficient for a natural draft dry-cooling tower is shown to become independent of the Reynolds number inside the tower for Reynolds numbers higher than 0.03×10^6. Therefore, as far as the flow inside the tower is concerned no serious flow distortions due to Reynolds number effects are expected, provided that the Reynolds number inside the model is kept above this limit. The inlet pressure coefficient is found to be affected by the wind Reynolds number on the outside of the model as shown in Appendix E. It is however possible to perform model tests in the supercritical range of Reynolds numbers by roughening the outer surface of the model. Furthermore the Reynolds number effect can also be eliminated by using a constant wind speed as also mentioned by Leene [80LE1]. The main disadvantage of isothermal models is that wind effects on the inlet and outlet of the tower are decoupled and the effects have to be studied separately. The advantage of this method is that the mean fluid velocity inside the tower can easily be determined because the fluid is forced through the model. Furthermore the measurements performed on these models are accurate and stable and both Bourillot [80BO1] and Buchlin [82BU1] mentioned that good reproducibility is obtained.

As mentioned before, another problem which arises when testing models in a wind tunnel, is

that of solid blockage. If the working section of the wind tunnel has straight, rigid boundaries, continuity of mass flow in the tunnel requires that the axial velocity in the vicinity of the model shall exceed the free stream value. On the other hand it is found that with an open test section, the effective velocity past the model is less than the free stream value which should be taken into account when evaluating results of model tests. Lock [29LO1] determined correction factors for three-dimensional bodies in open and closed working sections. Völler [85VO1] used the latter to correct his experimental results while Leene [80LE1] and Chaboseau [82CH1] found that the wall effect could be neglected due to a large enough test section.

Other investigators tried to solve the problem numerically. Radosavljevic [88RA1] did a comprehensive numerical analysis of the influence of a cross-wind on a natural draft wet cooling tower by using the general purpose PHOENICS computer code for fluid flow simulation. Dibelius [79DI1] did a theoretical analysis on the influence of a cross-flow on the plume of a cooling tower. The analysis was done analogous to a jet issuing into a free stream and the effect of the tower shell was ignored.

CHAPTER 2

Experimental investigation of the influence of a cross-flow on the performance of a dry-cooling tower.

2.1: Introduction.

Although the effect of a cross-flow on the performance of a natural draft cooling tower was studied by a number of investigators during the last 25 years as discussed in chapter one, it is clear when reading the available literature that little agreement exists between the authors about various aspects of the problem. Reports on full scale tests are found to be poorly documented and due to a lack of test details the results are not suitable for comparative purposes. Many of the investigators who used model tests, considered only a specific aspect of the problem or used a model of a specific cooling tower to perform the tests. Furthermore very few of the authors [83WI1, 85VO1, 86BU1] used their results to predict the effect of a cross-wind on the performance of a full scale tower.

Witte [83WI1] suggested that the wind effect on a cooling tower can be predicted by using the pressure distribution round the outside of the tower shell. The results obtained with this method agree well with full scale measurements as published by Markòczy [77MA1]. Witte, however, totally ignores the wind effect at the outlet of the tower, while others [72EC1, 79DI1, 80BO1, 82BU1, 82CH1, 82RU1, 83BU1, 85VO1] found that the wind has a significant influence at the top of the tower and tends partly to counterbalance the negative action at the inlet for high wind speeds. Furthermore the proposal made by Witte fails to give the correct velocity distribution through the heat exchanger for a horizontal arrangement [85VO1].

Buxmann [83BU1] and Völler [85VO1] performed isothermal model tests to determine the effect of different outlet shapes of the cooling tower and the arrangement of the heat exchangers on the performance of the cooling tower in the presence of wind. To quantify the influence of wind on the air mass flow rate through the tower, Buxmann [83BU1] defined pressure coefficients for the inlet, C_{pi}, and outlet, C_{po}, in terms of the static pressure difference between the throat of the tower and the ambient.

$$C_{pi},C_{po} = \frac{\Delta p_w - \Delta p}{0.5\rho v_w^2} \qquad (2.1.1)$$

where Δp_w is the static pressure difference between the throat of the tower and the ambient

with wind and Δp is the static pressure difference without wind, for the same mean air mass flow rate through the tower. Their tests were all done for the same d_i/H_i ratio of the tower model and except for the vertical arrangement of the heat exchangers, the pressure loss coefficient of the heat exchangers was kept at a constant value for all the tests. The velocity distribution through the heat exchangers in the presence of a cross-wind was measured separately and an air-side heat transfer correction factor was defined to calculate the reduction in the heat transfer due to the flow distortions through the heat exchanger.

By using the experimental results, Völler calculated the influence of the wind effect on two dry-cooling towers and compared the results with the measurements made on the full scale towers. Good agreement is found between the predicted values and the results as published by Van der Walt [76VA1] for the Grootvlei 5 tower. For the Rugeley tower, with the heat exchangers arranged vertically around the circumference of the tower, the rise in water outlet temperature as calculated by Völler is considerably lower than that which was measured by Christopher [69CH1]. Völler determined the inlet pressure coefficient in a uniform cross-flow, but because a wind profile is usually found in the atmosphere, equation (1.1.1), he assumed that the effective wind velocity which acts upon the inlet of a tower is equal to the average wind velocity across the inlet height of the tower. This wind velocity was therefore used in equation (2.1.1) to obtain the static pressure difference in the tower as a result of the wind. This assumption however was never confirmed by model tests.

Due to all the uncertainties, comprehensive scale model tests were performed in the present investigation. Specific reference is made to circular natural draft dry-cooling towers with the finned tube heat exchangers arranged uniformly and horizontally (not A-frames) over the entire inlet cross-section of the tower. The following effects are addressed:

1. Two different open wind tunnels were used to simulate the cross-flow. Because of the flexibility and availability of the smaller tunnel (330 mm x 660 mm) it was used for most of the tests. By using a second tunnel with a much larger outlet section (1710 mm diameter), shown schematically in figure C.2.2, the influence of the blockage effect on the experimental results was determined. The blockage effect in an open jet will cause the effective velocity across the model to be less than that of the free stream. For both wind tunnels the effective wind velocity across the model was determined by using a solid blockage correction factor as determined by Lock [29LO1].

2. According to full scale measurements it seems as if a horizontal arrangement of the

heat exchangers is less sensitive to cross-winds than a vertical arrangement. In agreement Russell [78RU1] found that a horizontal layout gives a significantly better performance than the vertical layout. Völler [85VO1] however found with his experimental tests that both the inlet pressure coefficient and the velocity distribution through the heat exchangers for a vertical arrangement are less sensitive to cross-winds than those of a horizontal arrangement. Although not much emphasis was placed on the vertical arrangement in the present investigation, the inlet pressure coefficient for both arrangements was determined in an attempt to clarify the problem.

3. In the past most investigators modelled the heat exchangers with perforated plates or gauze screens [78BO1, 78RU1, 82BU1, 83BU1, 85VO1, 86BL1] while Vauzanges [86VA1] used porous foam to simulate the heat exchangers. Geldenhuys and Kröger [86GE1] argued that an incorrect modelling of these resistances may cause erroneous results. For a horizontal layout of the heat exchangers, with the finned tubes arranged in a radial pattern, the flow through the bundles is directed in an axial direction while for a vertical arrangement the flow is directed in a radial direction. The effect of the different heat exchanger simulations on the value of C_{pi} was investigated by using screen layers with and without honeycomb in different tests.

4. The heat exchanger pressure loss coefficient is defined as:

$$K_{he} = \frac{\Delta p_{he}}{0.5\rho v_{he}^2} \qquad (2.1.2)$$

where Δp_{he} is the difference in total pressure across the core while v_{he} is the mean normal free-stream velocity based on the frontal area of the core. The value of K_{he} is twice as large as the Euler number listed in table 1.2.1 as one of the dimensionless groups which should be the same in the model as that in the full scale tower. In figure 2.1.1 typical pressure loss coefficients of a dry and wet cooling tower are shown as a function of the characteristic flow parameter, Ry, defined as:

$$Ry = \rho v_{he}/\mu = m_a/\mu A_{fr} \qquad (2.1.3)$$

If the heat exchangers cover the entire inlet cross-section of the tower, such as in the present model, v_{he} is equal to the mean air velocity, v, based on the inlet cross-section

of the tower.

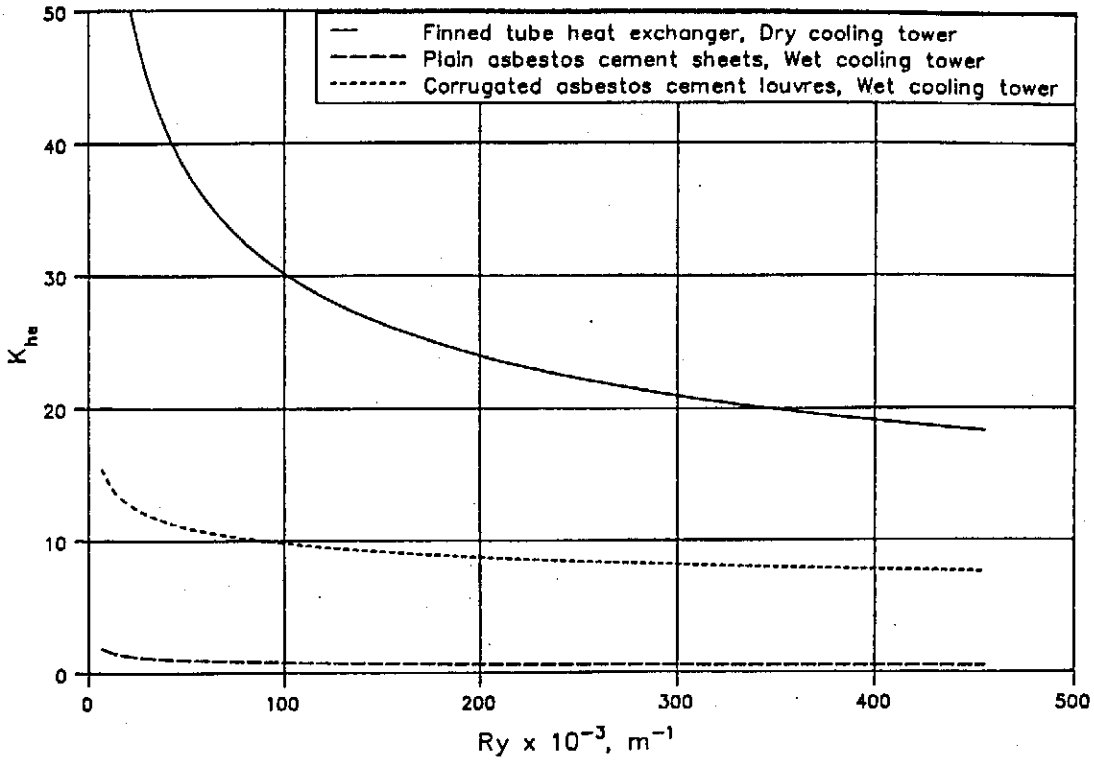

Figure 2.1.1: Typical heat exchanger loss coefficients in dry and wet cooling towers.

The influence of the K_{he} value of the heat exchangers on the wind effect on a cooling tower was only investigated by Völler [85VO1] and Leene [80LE1]. Both performed their tests for a vertical arrangement of the heat exchangers while no similar data could be found in the literature for a horizontal arrangement. By using different numbers of screen layers in series with the honeycomb, the effect of the K_{he} value of the heat exchangers on the inlet pressure coefficient as well as the velocity distribution through the heat exchangers was investigated.

5. Although most dry-cooling towers have a diameter to inlet height ratio, d_i/H_i, of roughly six, the effect of the latter on the inlet pressure coefficient has never been investigated.

6. Völler [85VO1] and Vauzanges [86VA1] performed model tests to determine the effect of the tower supports on the value of C_{pi} for a horizontal arrangement of the heat exchangers. In the present investigation a complete model of the support arrangement of an representative dry-cooling tower was incorporated in the tower model.

7. The wind profile was simulated by a number of investigators [78BO1, 78RU1, 80LE1, 82GR1, 82RU1, 86BL1] in their model tests. The effect of a variation in the approaching wind profile on the tower performance, however has never been quantified.

8. The velocity distribution through the horizontal heat exchangers was determined for different values of the d_i/H_i ratio, K_{he} values, form of the wind profile and also with various windbreak walls below the heat exchanger.

9. With isothermal tests the wind effect on the inlet and outlet of a cooling tower has to be studied separately, and is it assumed that the wind effect on the inlet and outlet is independent of each other. The effect of a distorted flow pattern inside the tower on the outlet pressure coefficient was determined.

10. In an attempt to reduce the negative action of the wind effect on the inlet of a tower, several tests were performed with different wind break walls positioned below the horizontal heat exchangers. Results or suggestions of similar tests were published by Leene [80LE1], Grange [82GR1], Sabaton [82SA1], Völler [85VO1] and Blanquet [86BL1].

2.2: The inlet pressure coefficient of a dry-cooling tower in a cross-wind.

By using the cooling tower model as described in appendix C, the inlet pressure coefficient, C_{pi} was determined for different values of the relative wind velocity v_{wo}/v with v_{wo} the wind velocity at the cooling tower outlet height while v is the mean air velocity based on the inlet cross-sectional area of the tower model. For a horizontal arrangement of the heat exchangers the air velocity, v, is also equal to the air velocity based on the frontal area of the heat exchangers, v_{he}. Different values of the relative wind velocity, v_{wo}/v, was obtained by varying the air velocity through the model for a constant wind speed to eliminate the wind Reynolds number effect as discussed in appendix E. Furthermore the tests were usually performed at the maximum wind velocity of the wind tunnel, except where stated differently.

In figure 2.2.1. the inlet pressure coefficient as determined in the two different wind tunnels, as described in appendix C, is shown for three different values of the d_i/H_i ratio. The results suggest that the value of C_{pi} as determined in the smaller wind tunnel is approximately 4% more than the value as obtained in the larger tunnel. The discrepancy cannot be a result of the different Reynolds numbers used in the tests, since the value of C_{pi} for a roughened model tends to decrease for an increase in the Reynolds number according to figure E.3. If it is assumed that the inlet pressure coefficient as determined on the larger wind tunnel is correct, and the difference in the value of C_{pi} is caused by the blockage effect on the smaller tunnel, the blockage correction factor for the smaller tunnel, as calculated in Appendix C, is incorrect. The correct blockage factor required for a reduction of 4 % in the C_{pi} value on the smaller tunnel is found to be equal to 0.987 which is almost identical to the correction factor on the larger tunnel. This however is not possible since the area of the test section of the larger tunnel is 10.5 times that of the smaller tunnel. It is therefore concluded that the difference in the value of C_{pi} is due to experimental inaccuracies. Except for the difference in the absolute values of C_{pi} good agreement is found in the variation in the value of the inlet pressure coefficient for a change in the value of the d_i/H_i ratio.

Völler [85VO1] plotted his experimental observations as a function of the velocity ratio v_w/v_2 where v_2 is the average air velocity in the vertical inlet cross-sectional area of the tower as shown in figure B.1.1. In figure 2.2.2 the results in figure 2.2.1 are shown as a function of the relative wind velocity v_w/v_2. According to the latter, it appears as if cooling towers with larger d_i/H_i ratios are less affected by cross-winds than towers with smaller d_i/H_i ratios. The variation of the static pressure inside the tower model, for the data shown in figure 2.2.2, is given in figure 2.2.3 for different values of the mean axial velocity inside the tower.

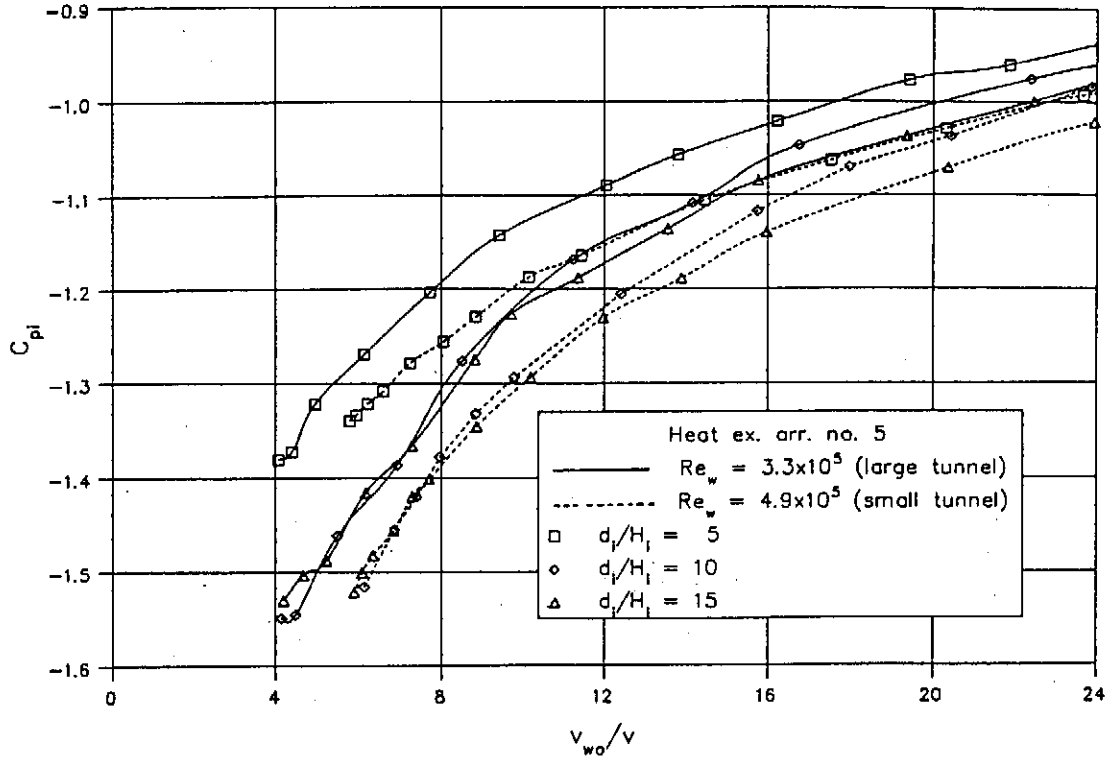

Figure 2.2.1: C_{pi} values as obtained in the two wind tunnels.

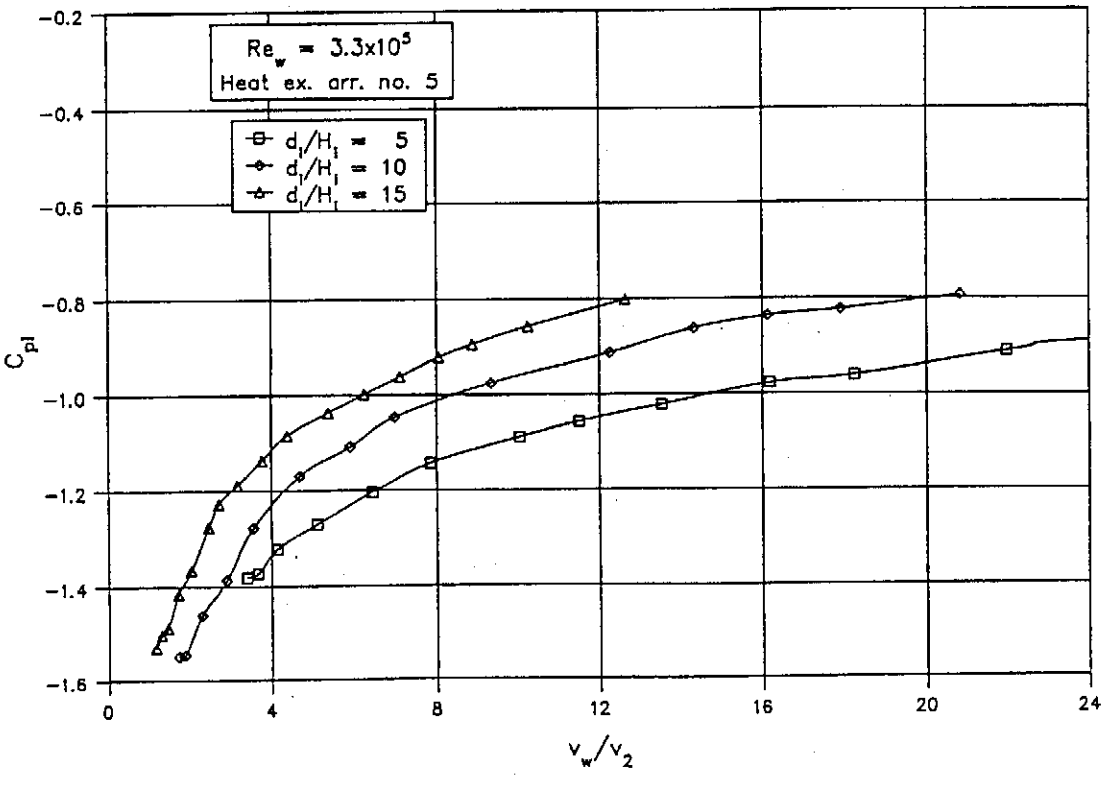

Figure 2.2.2: Inlet pressure coefficient as a function of the velocity ratio v_w/v_2.

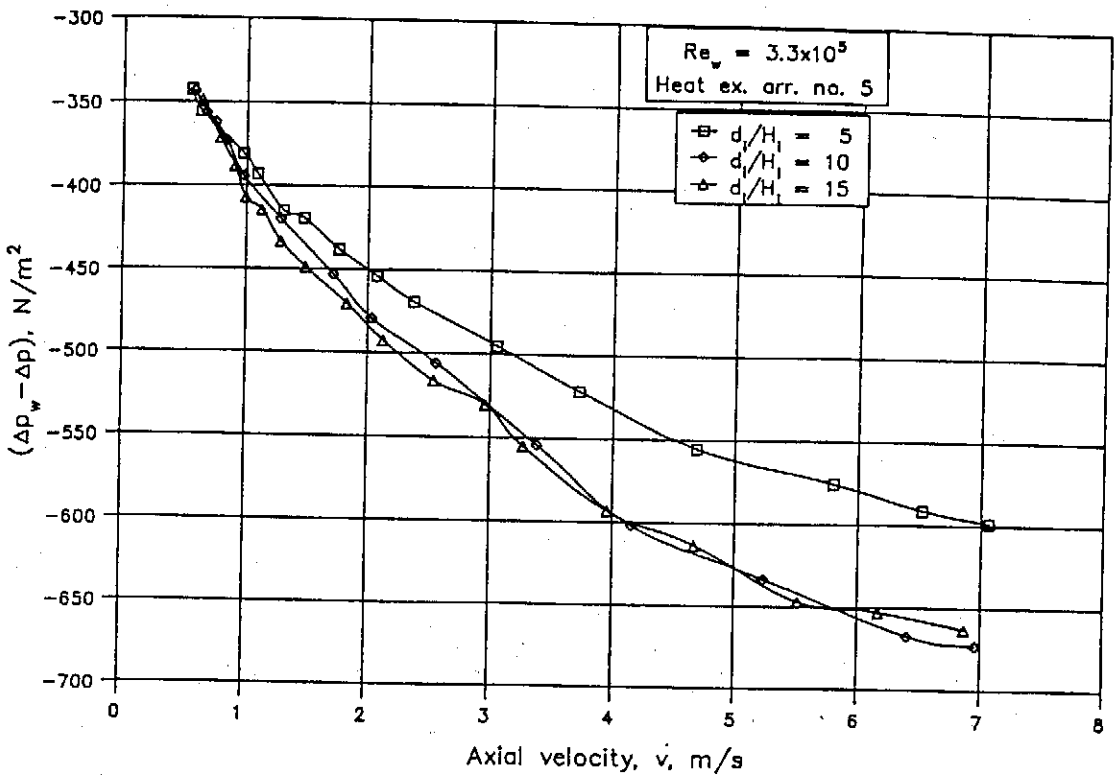

Figure 2.2.3: Increase in the static pressure as a result of the wind.

The results indicate that the actual change in static pressure is less for a tower with a small d_i/H_i ratio, and therefore the presentation of the results as shown in figure 2.2.1 is less confusing.

According to figure A.1.3 the inlet loss coefficient is affected by Reynolds number effects for Reynolds numbers less than 0.03×10^{-6}. The corresponding mean air velocity in the tower is:

$$v = Re\ \mu/d\ \rho = 0.03 \times 10^{6} \times 1.82 \times 10^{-5}/0.192 \times 1.2 = 2.4 \text{ m/s}$$

To prevent flow distortions due to Reynolds number effects, the air velocity should therefore not be reduced to values less than 2.4 m/s. It is however found that the value of C_{pi} will hardly be affected if the above mentioned limit is exceeded. In table 2.2.1 the experimental data for the results shown in figure 2.2.1 is listed as obtained for a d_i/H_i ratio of 5. The inlet pressure coefficient is calculated by substituting the pressure differences given in columns four and five in equation (2.1.1).

The air velocity in the model for the second test is 0.63 m/s and therefore the value of the

pressure difference given in the fourth column will be affected by the Reynolds number effect. Say an error of 100% was made in the static pressure difference above the heat exchangers and the ambient, the correct pressure difference for this particular test should be -9.496/2 = -4.748 N/m^2. The corresponding value of the inlet pressure coefficient is then obtained as -0.833 which differs only by 1.33% from the value given in table 2.2.1. It follows therefore that the value of C_{pi} is almost independent of the Reynolds number effect.

Table 2.2.1: Static pressure difference between inside of tower and surroundings with and without wind.

Test no.	v_{wo} m/s	v m/s	(p_s-p_∞) N/m^2	$(p_s-p_\infty)_w$ N/m^2	C_{pi}
1	28.62	0.55	-7.63	-350.75	-0.80
2	28.73	0.63	-9.50	-365.89	-0.82
3	28.64	0.97	-20.15	-401.81	-0.89
4	28.70	1.09	-24.55	-418.41	-0.91
5	28.51	1.30	-33.78	-443.35	-0.96
6	28.62	1.47	-42.13	-462.33	-0.98
7	28.60	1.76	-58.23	-497.31	-1.02
8	28.62	2.07	-78.40	-533.31	-1.06
9	28.63	2.38	-100.87	-569.97	-1.09
10	28.75	3.05	-160.85	-657.06	-1.14
11	28.75	3.72	-234.25	-756.93	-1.20
12	28.73	4.69	-363.30	-913.77	-1.27
13	28.72	5.80	-547.00	-1119.66	-1.32
14	28.67	6.52	-686.86	-1279.07	-1.37
15	28.76	7.06	-801.23	-1400.87	-1.38

Without tower supports, any changes in the inlet shape (taper) of the tower or inlet edge of the tower shell has significant influences on the value of C_{pi}. In figure 2.2.4 the results of tests are shown with a rounded inlet installed at the tower inlet. In comparison with figure 2.2.1 a reduction of roughly 20% in the value of the inlet pressure coefficient is obtained.

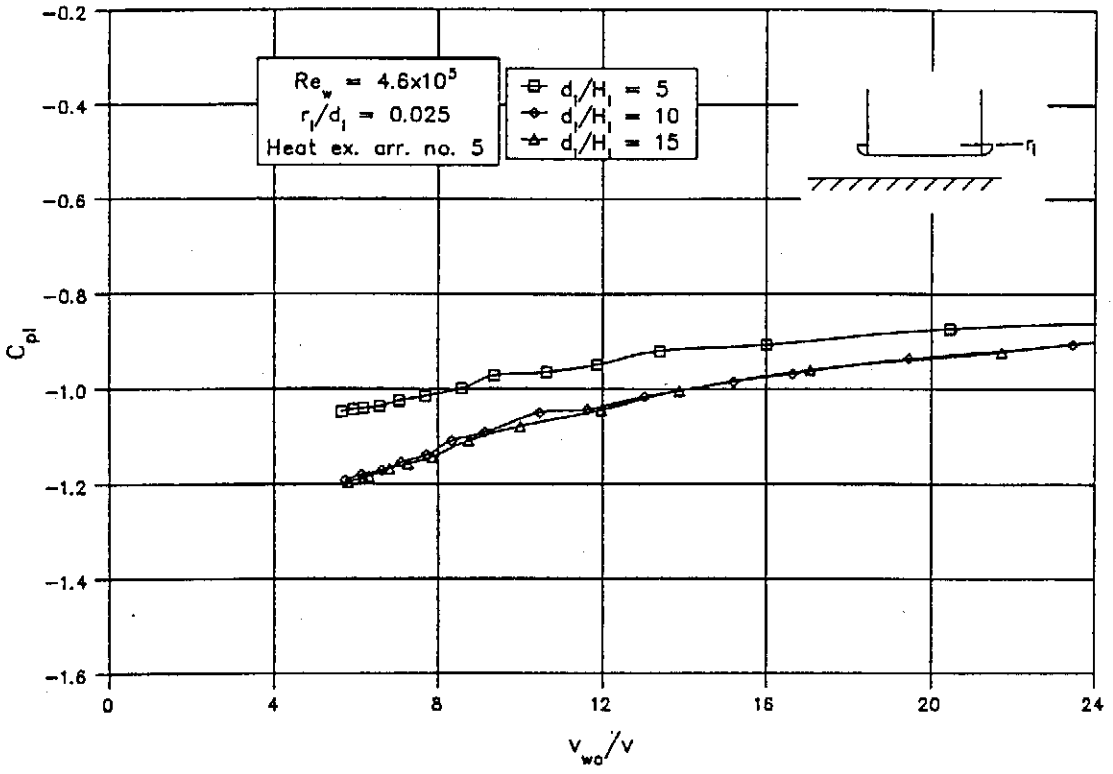

Figure 2.2.4: C_{pi} for a cooling tower with a rounded inlet.

In figure 2.2.5 the inlet pressure coefficient is shown for different d_i/H_i ratios and heat exchanger pressure loss coefficients. The results suggest that C_{pi} becomes increasingly more dependent on the value of K_{he} as the d_i/H_i ratio of the tower increases especially for smaller values of the velocity ratio v_{wo}/v.

A possible explanation for the latter can be found from data presented by Geldenhuys and Krõger [86GE1] who determined K_{ct} for different K_{he} and d_i/H_i values of the tower. The results suggest that for an increase in the value of K_{he} from zero to 30, K_{ct} remains almost constant for a d_i/H_i ratio of 5 while a significant reduction in K_{ct} is found for a d_i/H_i value of 15. It was furthermore argued that the increase in the cooling tower loss coefficient as the heat exchanger resistance decreases is due to a tendency for the axial velocity distribution above the heat exchangers to become more non-uniform. Measurements made by Völler

[85VO1] show that cross-winds will also cause a non-uniform axial velocity distribution in the tower. According to the definition of C_{pi} in equation (2.1.1), the latter gives an indication of the increase in the value of the inlet loss coefficient of a cooling tower in a cross-wind. It would therefore be expected that a cooling tower with a poor velocity distribution in windless conditions will be less affected by cross-winds than a tower with a more uniform distribution in windless conditions. Therefore the wind influence on a cooling tower with a d_i/H_i ratio of 15 and a small K_{he} value is much less than that for a tower with a small d_i/H_i value where a much more uniform velocity distribution in the tower is found in windless conditions.

In figure 2.2.6 C_{pi} is shown for different wind Reynolds numbers for a tower with a d_i/H_i ratio of 15. The wind Reynolds number effect as shown in figure E.3 seems to have very little effect on the value of the inlet pressure coefficient. For small wind velocities the measurements seem to become a bit more unstable.

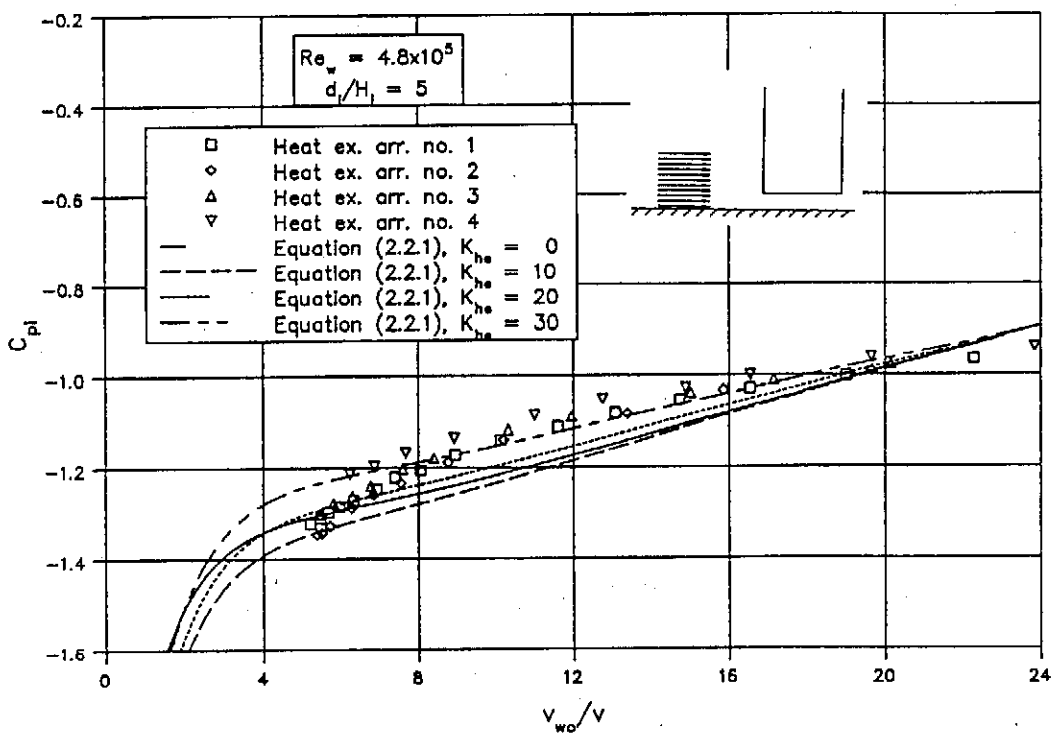

(a)

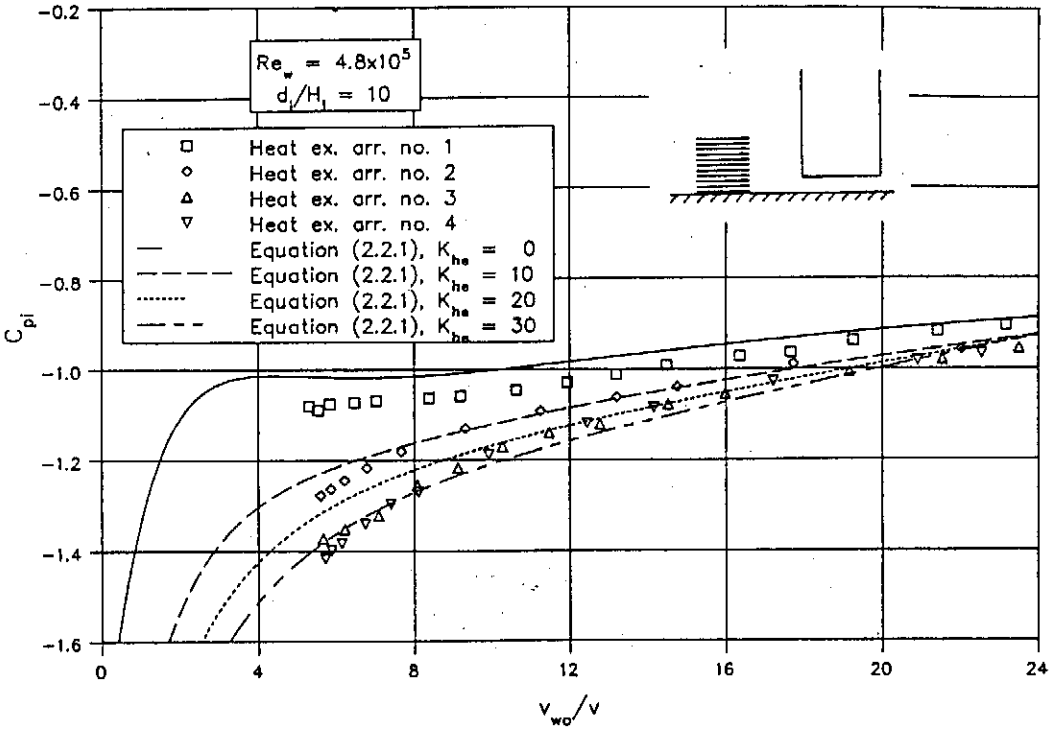

(b)

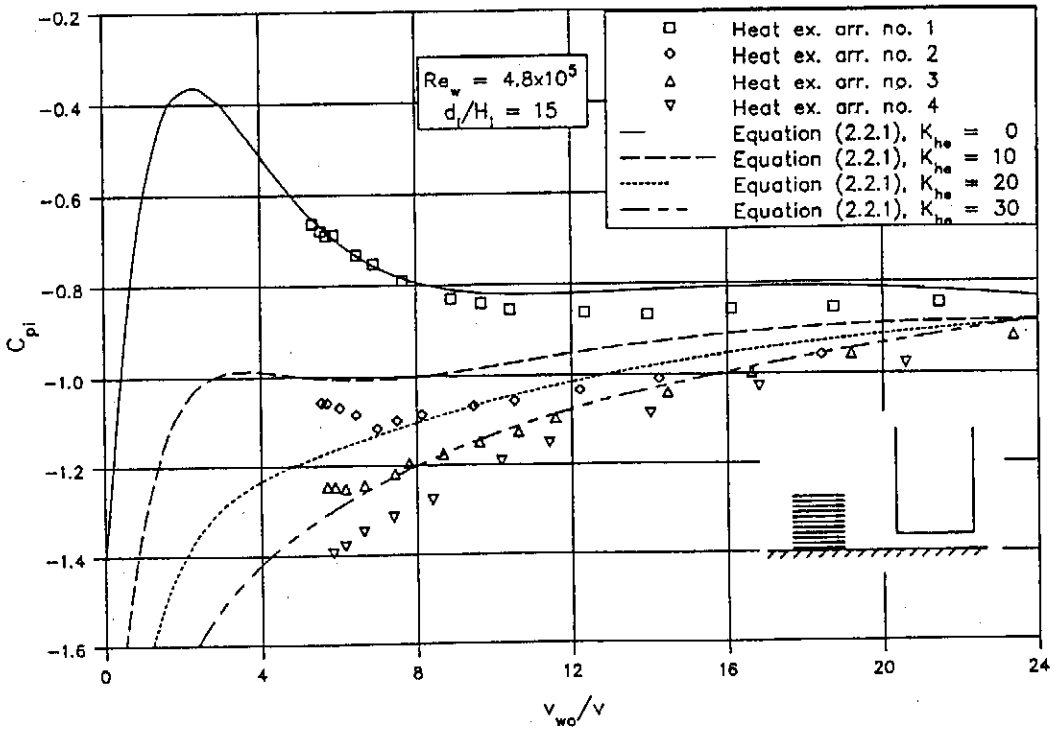

(c)

Figure 2.2.5: Inlet pressure coefficient for different d_i/H_i and K_{he} values.

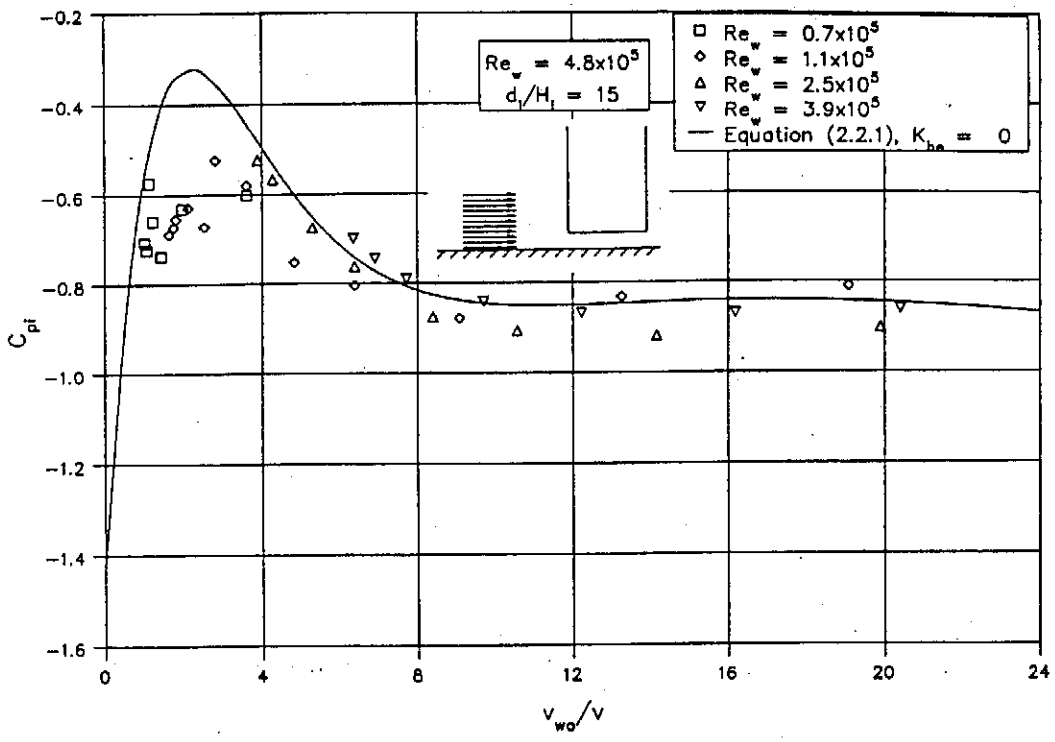

Figure 2.2.6: C_{pi} for different wind Reynolds numbers.

In the previous tests the horizontal heat exchangers were modelled with mesh layers in series with honeycomb as shown in figure A.1.4 with the honeycomb being used to direct the flow. In figure 2.2.7 the results are shown with the heat exchangers being modelled only with a couple of mesh layers. The flow through the heat exchangers in this case is not necessarily directed in an axial direction. The difference in the value of C_{pi} obtained with and without the honeycomb is found to be insignificant and it is therefore sufficient to model the horizontal arranged finned tube heat exchangers, found in dry-cooling towers (relatively high loss coefficient), only with mesh layers to determine the inlet pressure coefficient in the presence of a cross-wind.

As described in chapter 1, a wind profile is usually found in the atmosphere. The effect of the wind profile on value of C_{pi} was determined experimentally by creating a boundary layer artificially. This was done by arranging dowels, 6 mm in diameter, at such a distance upstream of the model that the flow through the dowels was not influenced by the presence of the model. The profile obtained at the location of the model is shown in figure 2.2.8 and is compared with the distribution given by the power law.

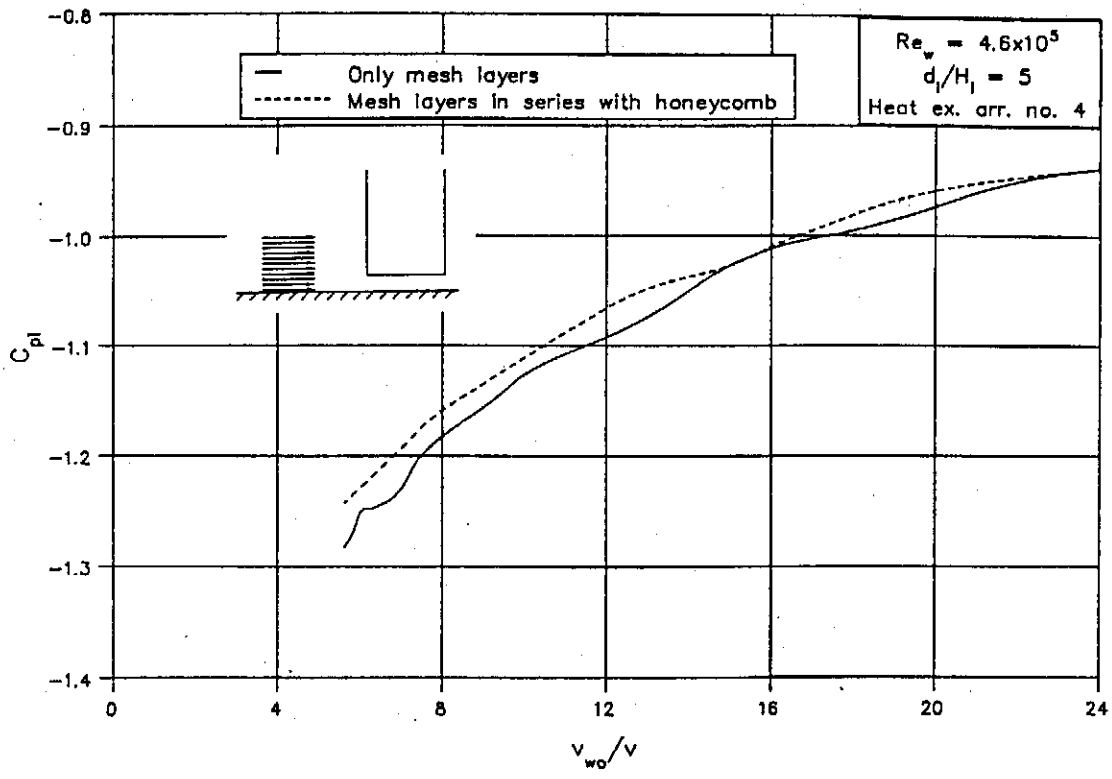

Figure 2.2.7: Inlet pressure coefficient for different simulations of the horizontal heat exchangers.

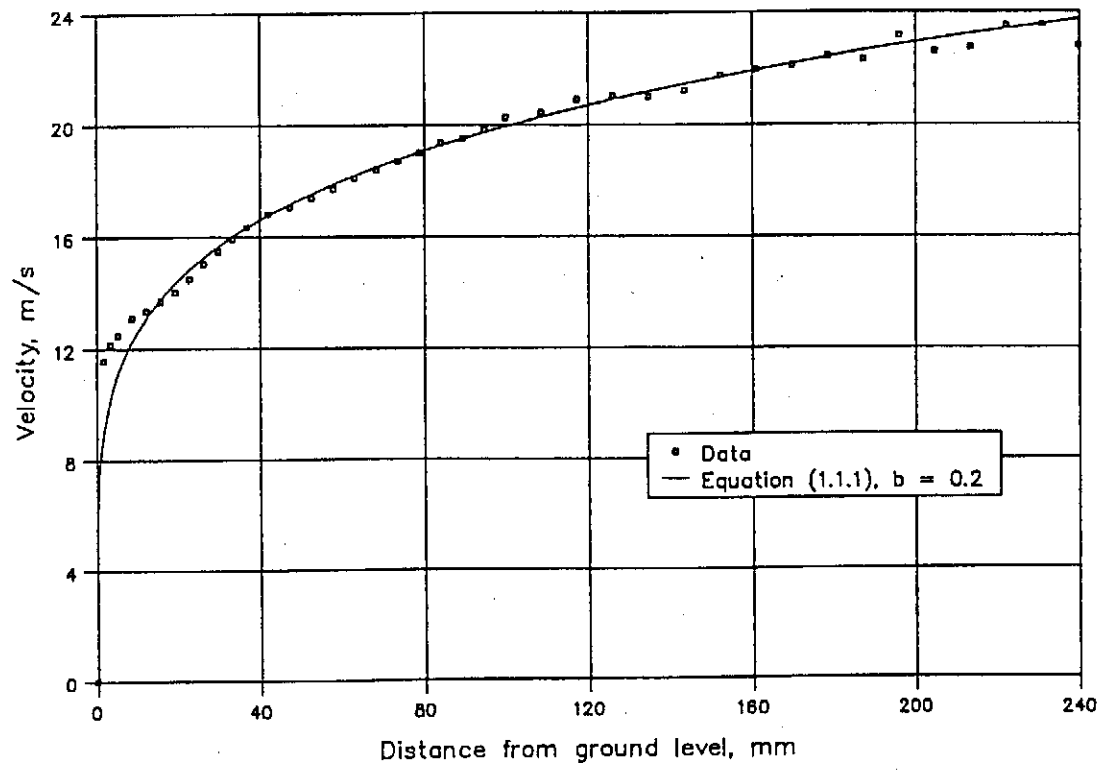

Figure 2.2.8: Wind profile.

The inlet pressure coefficient as determined with the wind profile is shown in figure 2.2.9. Because the wind velocity over the cooling tower height is no longer uniform, the reference height at which the wind velocity is being measured has to be specified. The inlet pressure coefficients shown in figure 2.2.9 are based on the relatively high wind velocity at the outlet height of the tower. If compared with figure 2.2.5, the wind profile causes a reduction of roughly 25% in the value of the inlet pressure coefficient. The variation in the value of C_{pi} for changes in the value of the heat exchanger pressure loss coefficient is in agreement with that observed in figure 2.2.5. If the inlet pressure coefficient is based on the mean wind velocity over the inlet height of the tower as suggested by Völler [85VO1], the value of C_{pi} would be approximately three times as much as that shown in figure 2.2.9. Therefore the assumption made by Völler is found to be without foundation.

Most natural draft cooling towers found in practice have a hyperbolic shell shape. In the present investigation the conical inlet shape of such towers is simulated by a conical section as shown in figure 2.2.13a. In figure 2.2.10 the results obtained without a wind profile are shown. The trend in the data follows that shown in figure 2.2.5 closely with the absolute value of C_{pi} approximately 12% less. If the same tests are repeated with a wind profile, a further reduction of 30% in the value of C_{pi} is observed as shown in figure 2.2.11.

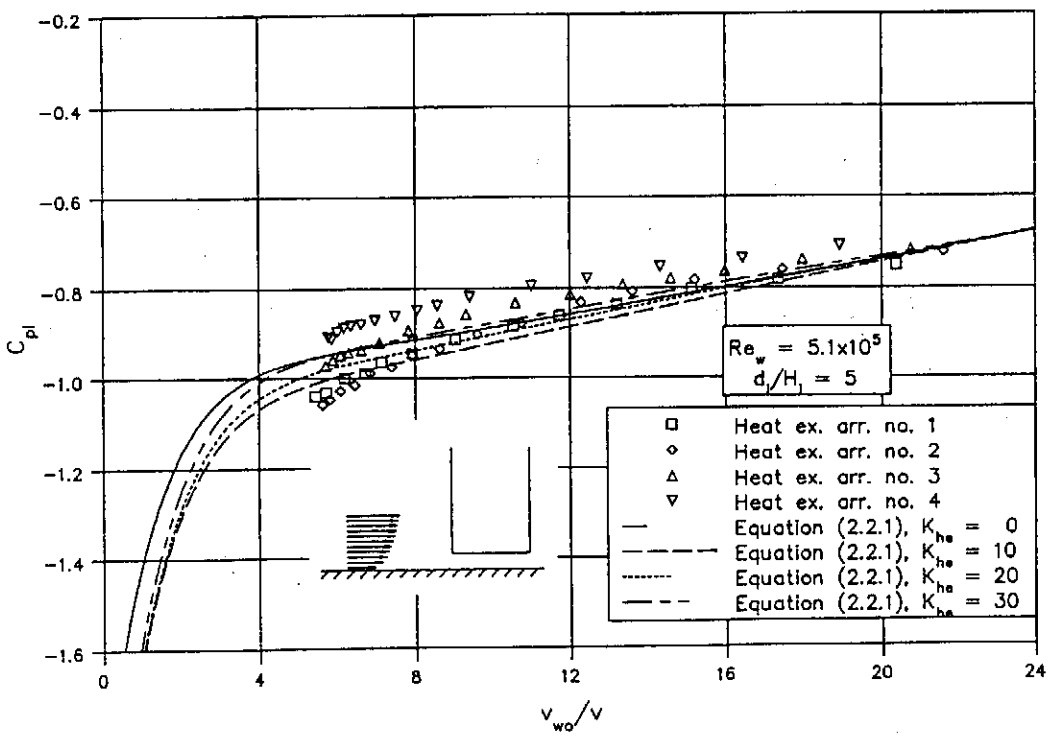

(a)

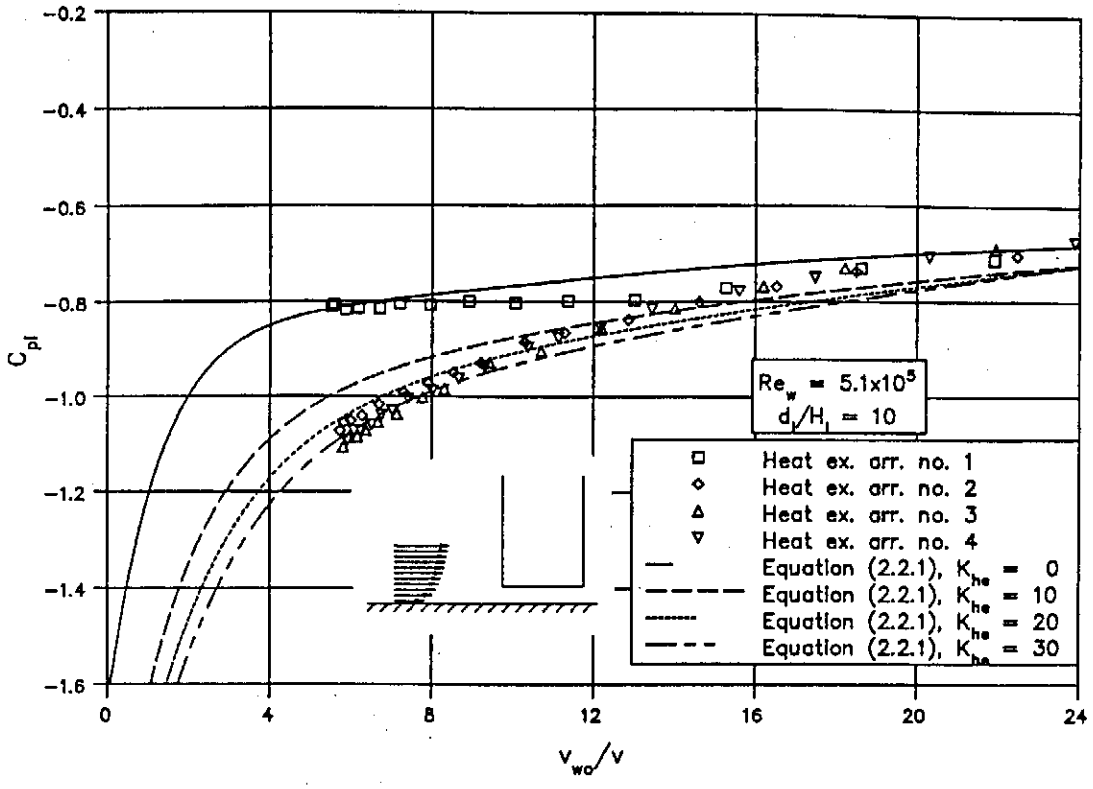

(b)

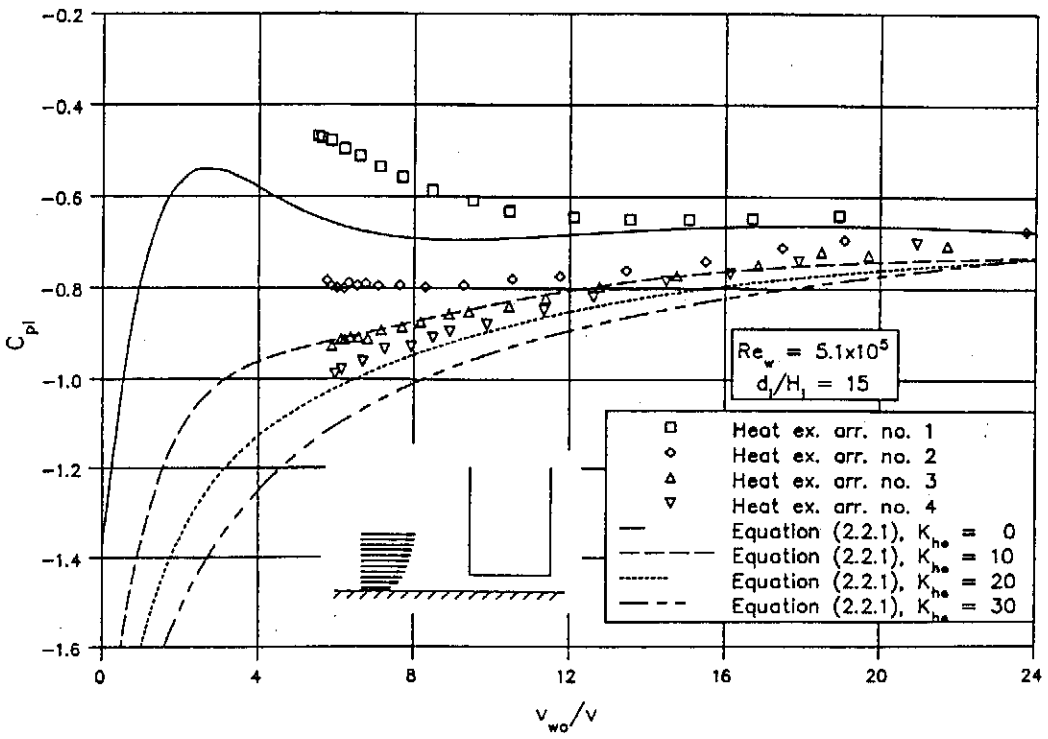

(c)

Figure 2.2.9: Inlet pressure coefficient for cooling tower with wind profile.

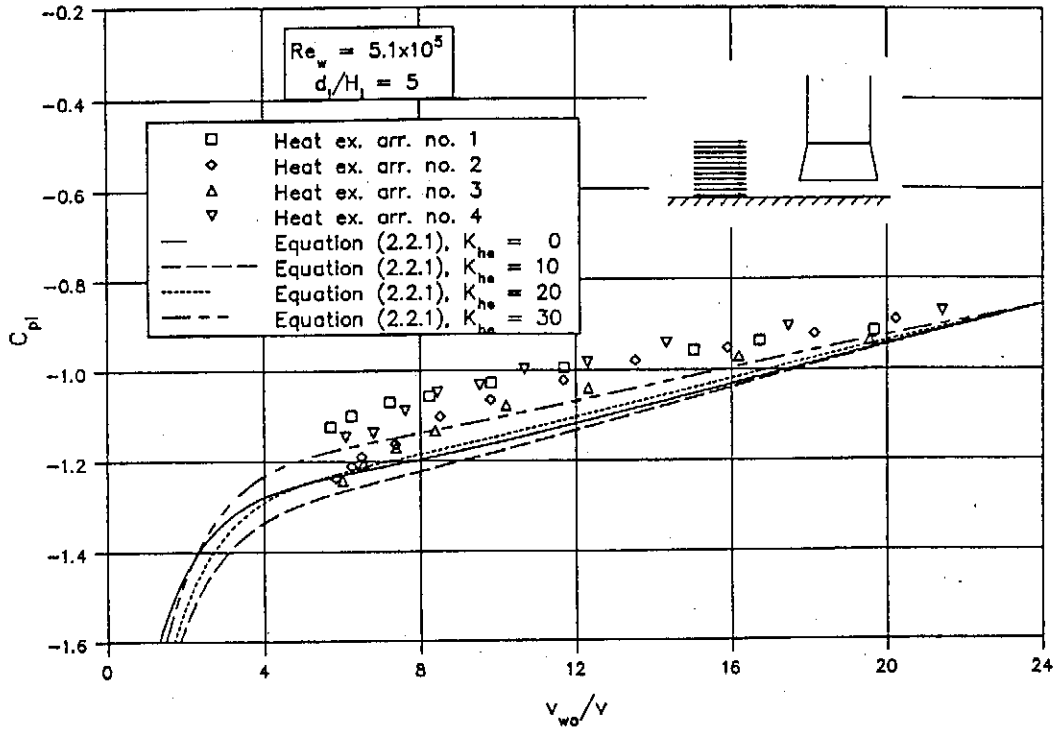
Re_w = 5.1x10^5
d_t/H_t = 5
Heat ex. arr. no. 1
Heat ex. arr. no. 2
Heat ex. arr. no. 3
Heat ex. arr. no. 4
Equation (2.2.1), K_he = 0
Equation (2.2.1), K_he = 10
Equation (2.2.1), K_he = 20
Equation (2.2.1), K_he = 30
C_pl
V_wo/V
-0.2
-0.4
-0.6
-0.8
-1.0
-1.2
-1.4
-1.6
0
4
8
12
16
20
24

(a)

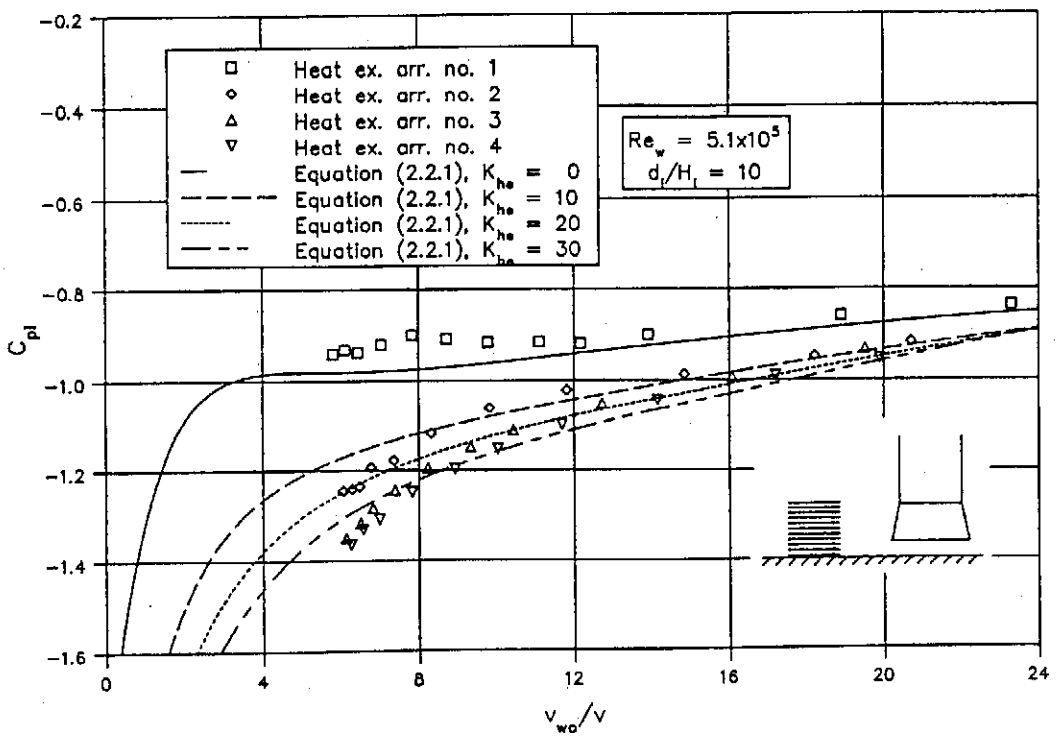
Heat ex. arr. no. 1
Heat ex. arr. no. 2
Heat ex. arr. no. 3
Heat ex. arr. no. 4
Equation (2.2.1), K_he = 0
Equation (2.2.1), K_he = 10
Equation (2.2.1), K_he = 20
Equation (2.2.1), K_he = 30
Re_w = 5.1x10^5
d_t/H_t = 10
C_pl
V_wo/V
-0.2
-0.4
-0.6
-0.8
-1.0
-1.2
-1.4
-1.6
0
4
8
12
16
20
24

(b)

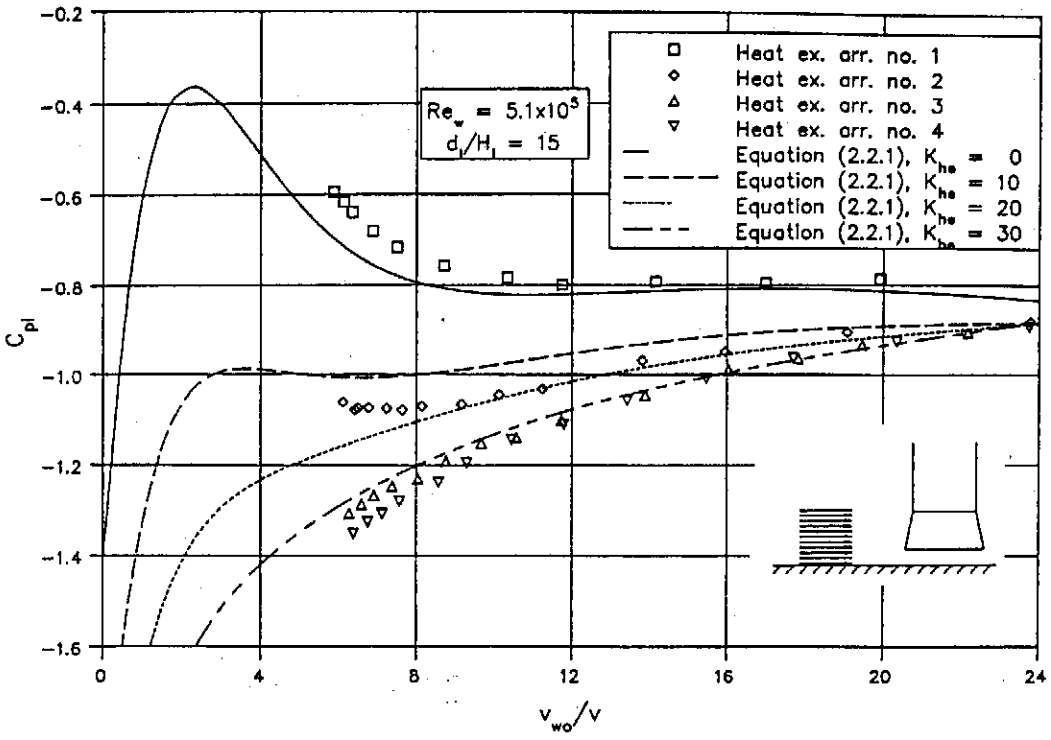

(c)

Figure 2.2.10: C_{pi} for a cooling tower with a conical inlet.

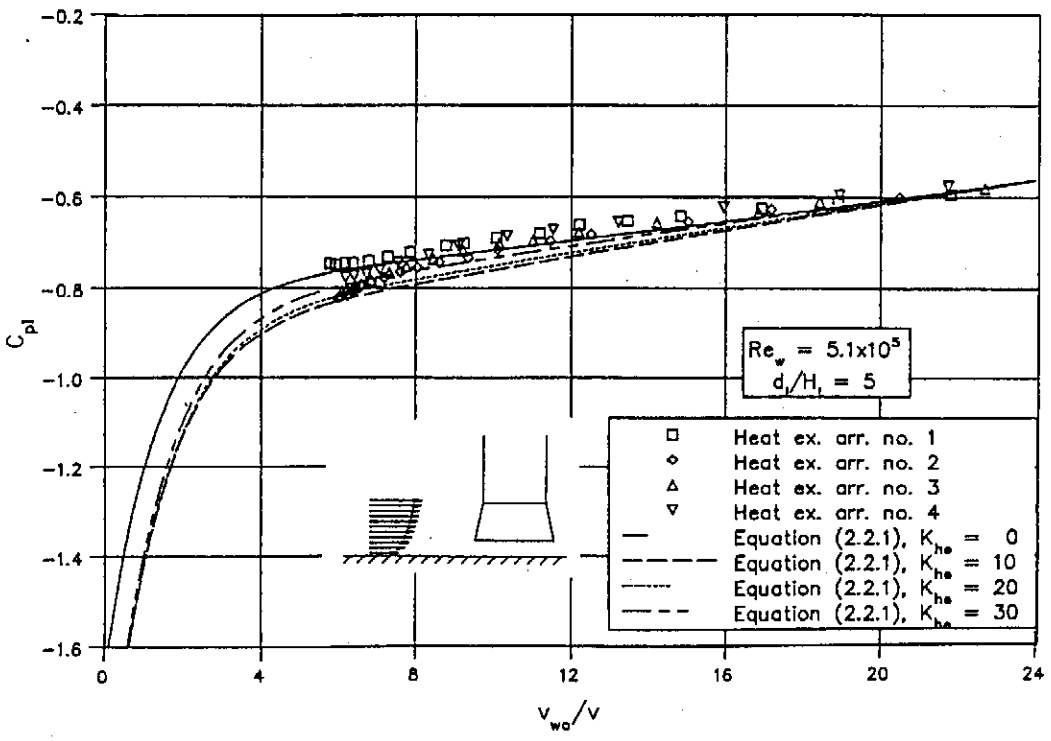

(a)

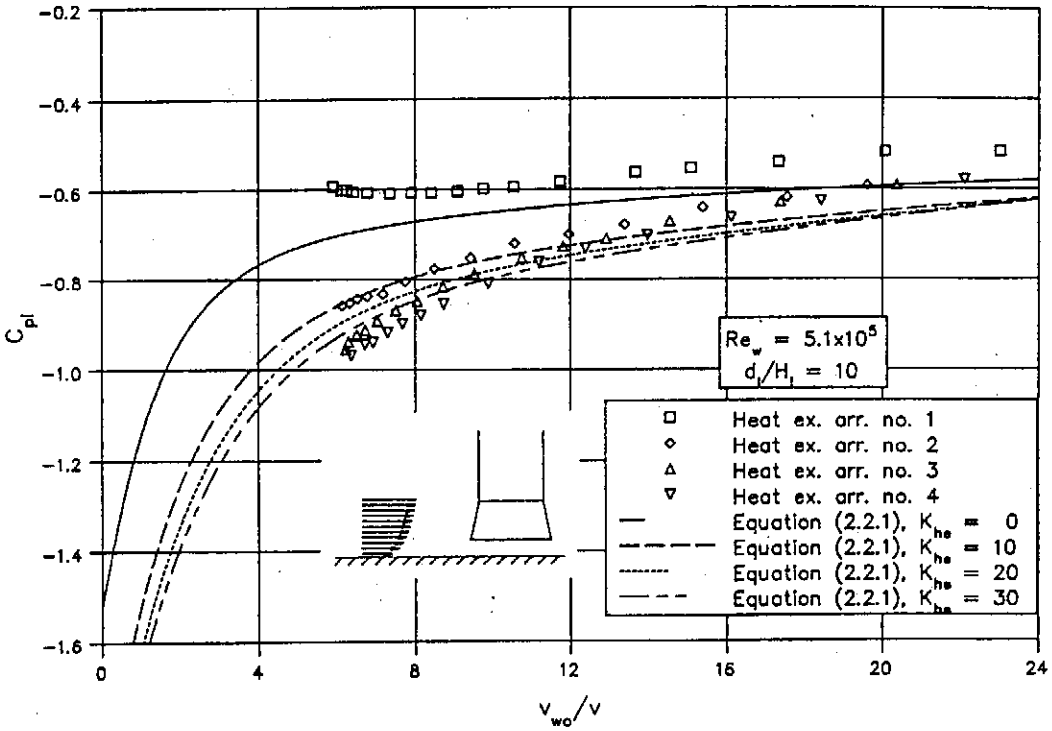

(b)

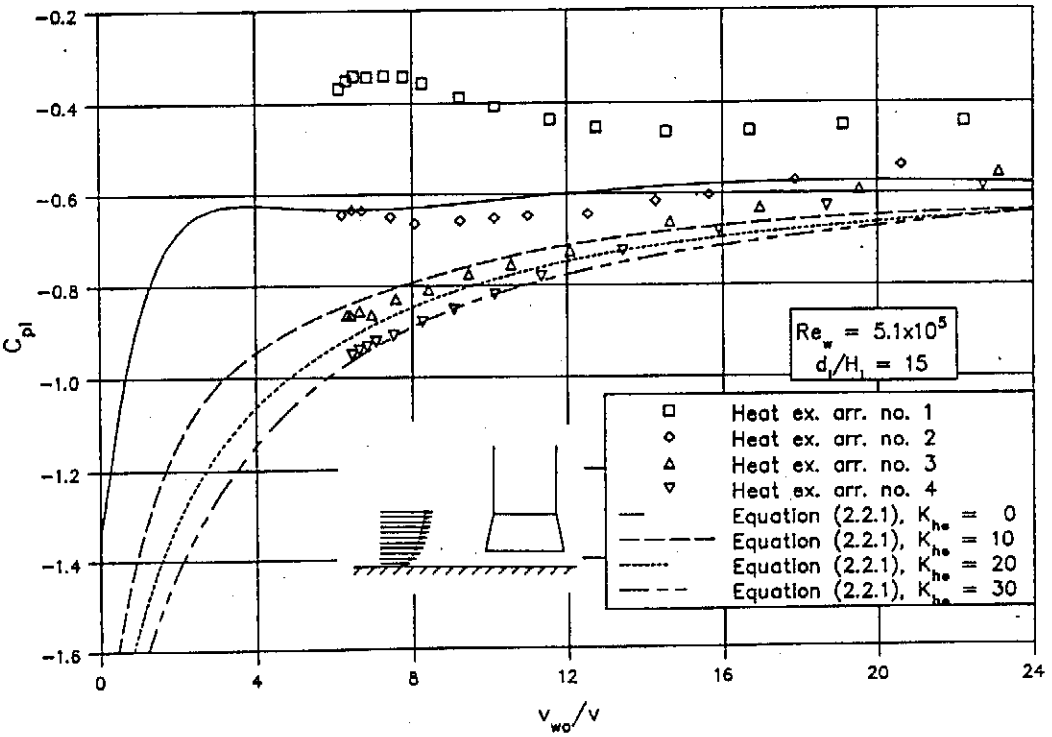

(c)

Figure 2.2.11: C_{pi} for a conical cooling tower with a wind profile.

The introduction of tower supports below the heat exchangers causes significant changes in the value of the inlet pressure coefficient. In figure 2.2.12, C_{pi} is shown as obtained with the model of the tower supports as discussed in appendix D installed in the inlet of the cylindrical tower model. If the values of the inlet pressure coefficient in the figure are compared with those shown in figure 2.2.5a, it is found that the tower supports cause a reduction of approximately 50% in the value of C_{pi}.

In figure 2.2.13 C_{pi} is shown for a conical tower model for different values of the d_i/H_i ratio and K_{he} values. If compared with the results in the previous figure, it is found that the shape of the tower inlet has very little effect on C_{pi} once the supports are installed. Furthermore it can be seen in figure 2.2.13 that although there is still a tendency for the tower to become more sensitive to cross-winds as the K_{he} value of the heat exchanger increases, the relative change in the value of C_{pi} is much less than that which was found for a tower without supports.

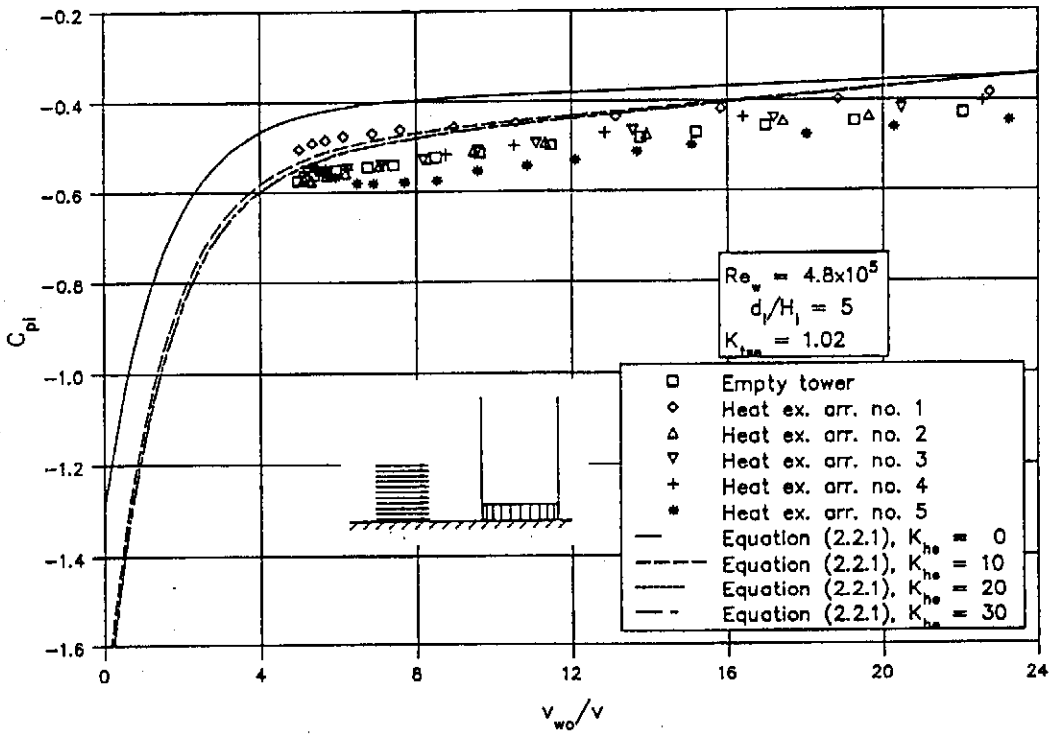

Figure 2.2.12: Inlet pressure coefficient for a cooling tower with tower supports.

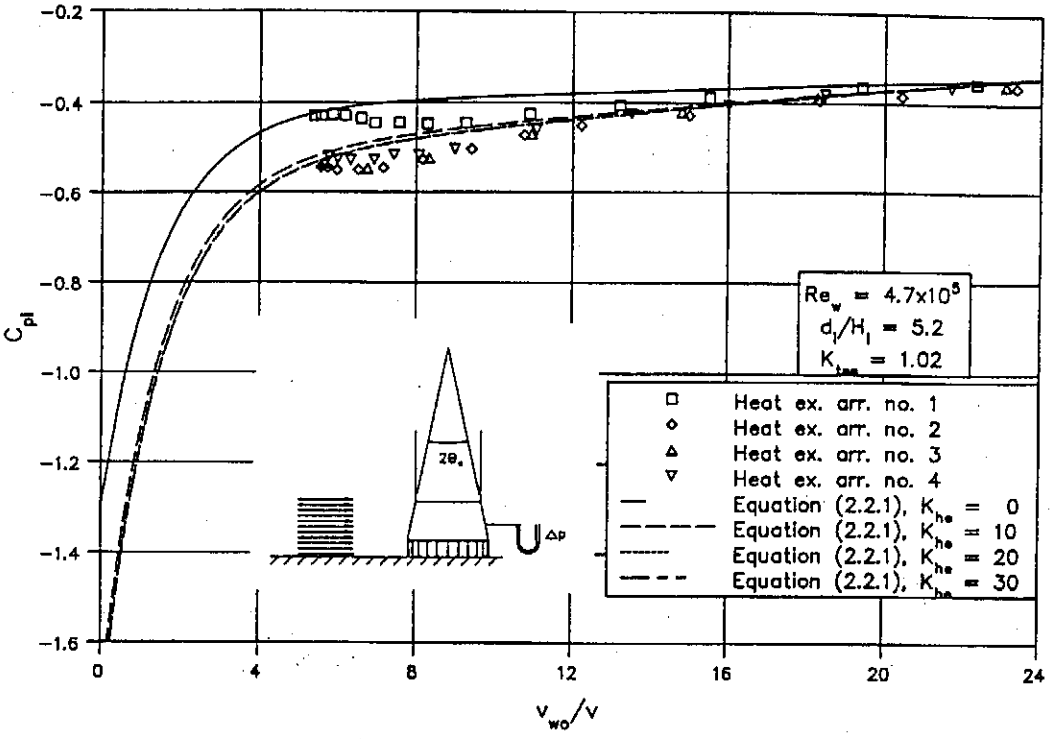
C_{pl}
V_{wo}/V
Re_w = 4.7x10^5
d_l/H_l = 5.2
K_{tse} = 1.02
Heat ex. arr. no. 1
Heat ex. arr. no. 2
Heat ex. arr. no. 3
Heat ex. arr. no. 4
Equation (2.2.1), K_{he} = 0
Equation (2.2.1), K_{he} = 10
Equation (2.2.1), K_{he} = 20
Equation (2.2.1), K_{he} = 30
$2\theta_e$
Δp

(a)

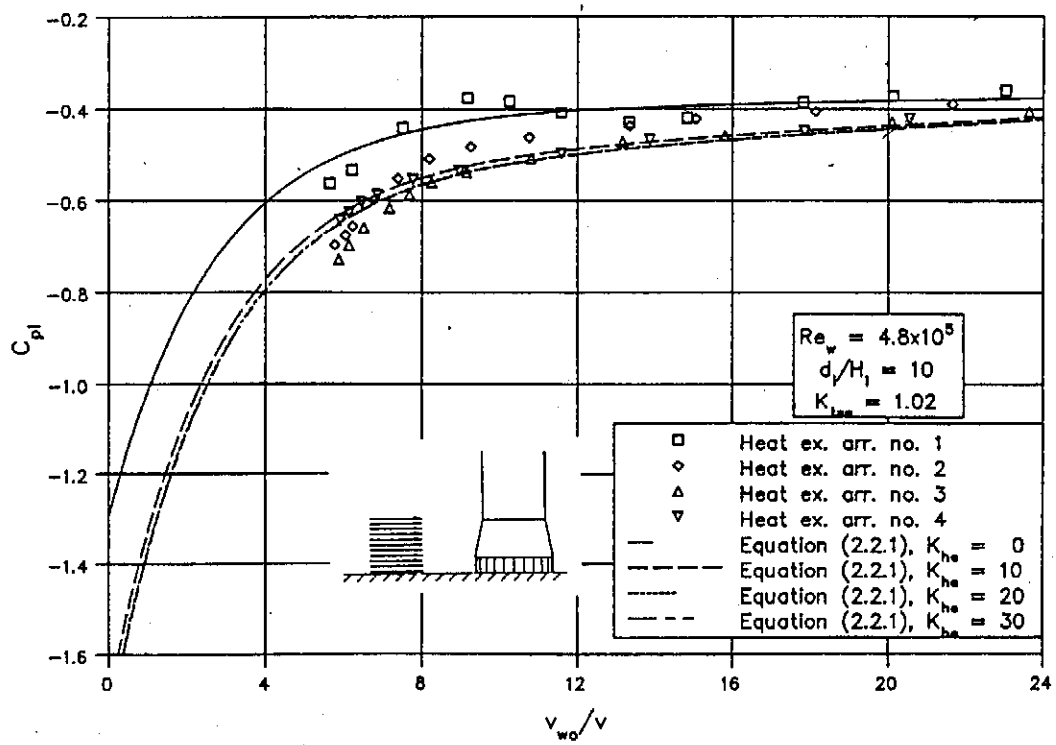
C_{pl}
V_{wo}/V
Re_w = 4.8x10^5
d_l/H_l = 10
K_{tse} = 1.02
Heat ex. arr. no. 1
Heat ex. arr. no. 2
Heat ex. arr. no. 3
Heat ex. arr. no. 4
Equation (2.2.1), K_{he} = 0
Equation (2.2.1), K_{he} = 10
Equation (2.2.1), K_{he} = 20
Equation (2.2.1), K_{he} = 30

(b)

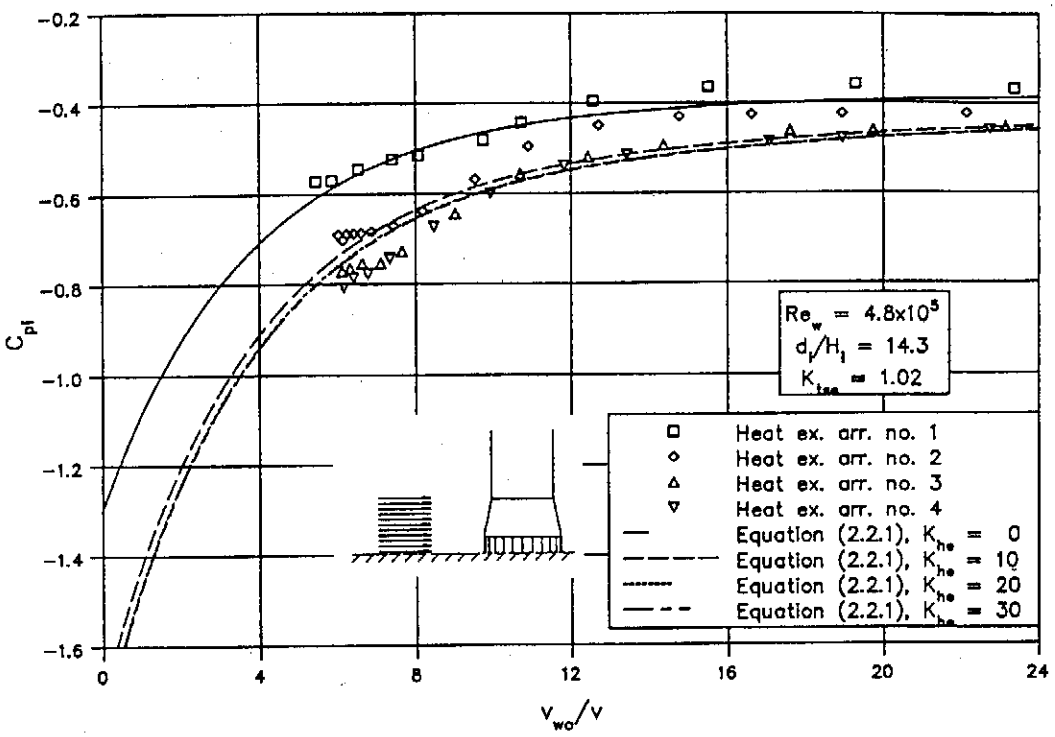

(c)

Figure 2.2.13: Inlet pressure coefficient for a conical tower with tower supports.

In figure 2.2.14 C_{pi} for the same tower geometry as that in figure 2.2.13 is shown for different wind Reynolds numbers. If the wind velocity is reduced, the value of C_{pi} will be influenced by two different counteracting effects. On the one hand the wind Reynolds number effect shown in figure E.3 will tend to cause an increase in the value of C_{pi}. The effect of the latter however is expected to be small according to figure 2.2.6. On the other hand the air velocity across the tower supports will also be less for lower wind velocities. The number of tower supports used in the model were calculated for the maximum wind Reynolds number in appendix D. Since the drag coefficient of a cylinder increases for a reduction in the Reynolds number, fewer tower supports should be used for smaller Reynolds numbers to keep the pressure loss coefficient of the supports in the model similar to that in the full scale tower. The results shown in figure 2.2.14 were obtained with the same support arrangement, therefore the slight reduction in the value of C_{pi} for smaller Reynolds numbers could be caused by the increase in the drag coefficients of the supports.

With the tower supports installed at the tower inlet, it is found that the wind profile has almost no effect on the value of C_{pi}. In figure 2.2.15 C_{pi} as obtained for a d_i/H_i ratio of 5 is shown with the relative high wind velocity at the outlet again being used as the reference. According to the latter it would seem as if the inlet pressure coefficient is not affected by the wind

velocity over the tower inlet height only, but also by the wind velocity at higher elevations. Figure 2.2.16 shows C_{pi} as obtained with a wind profile and different Reynolds numbers.

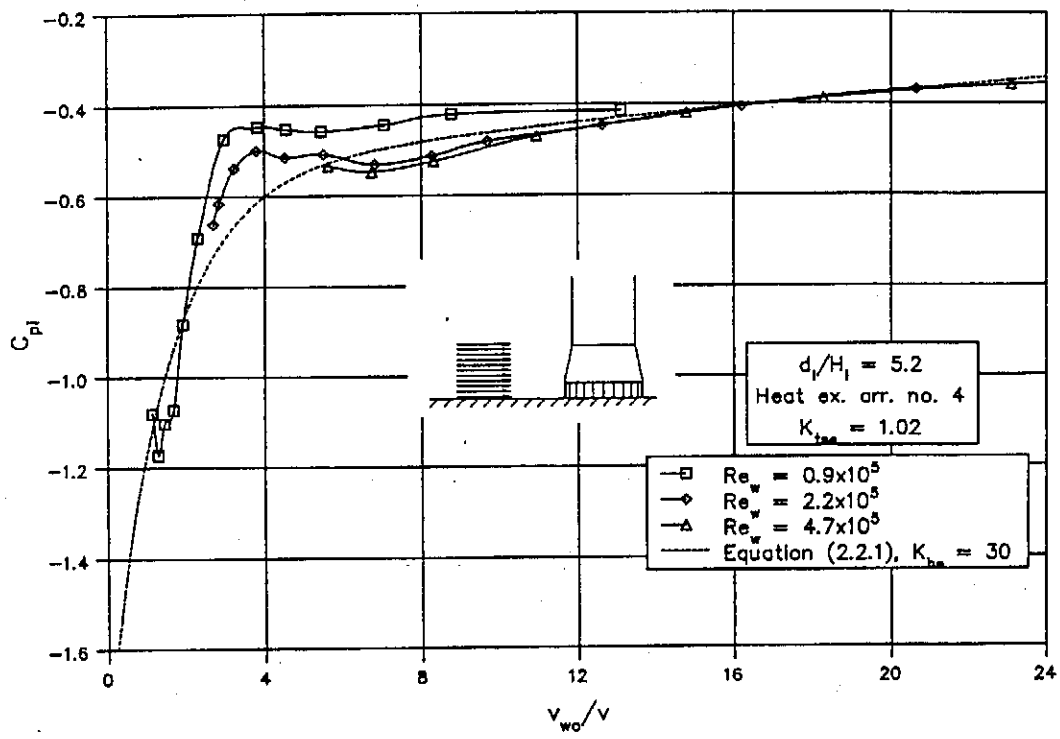

(a)

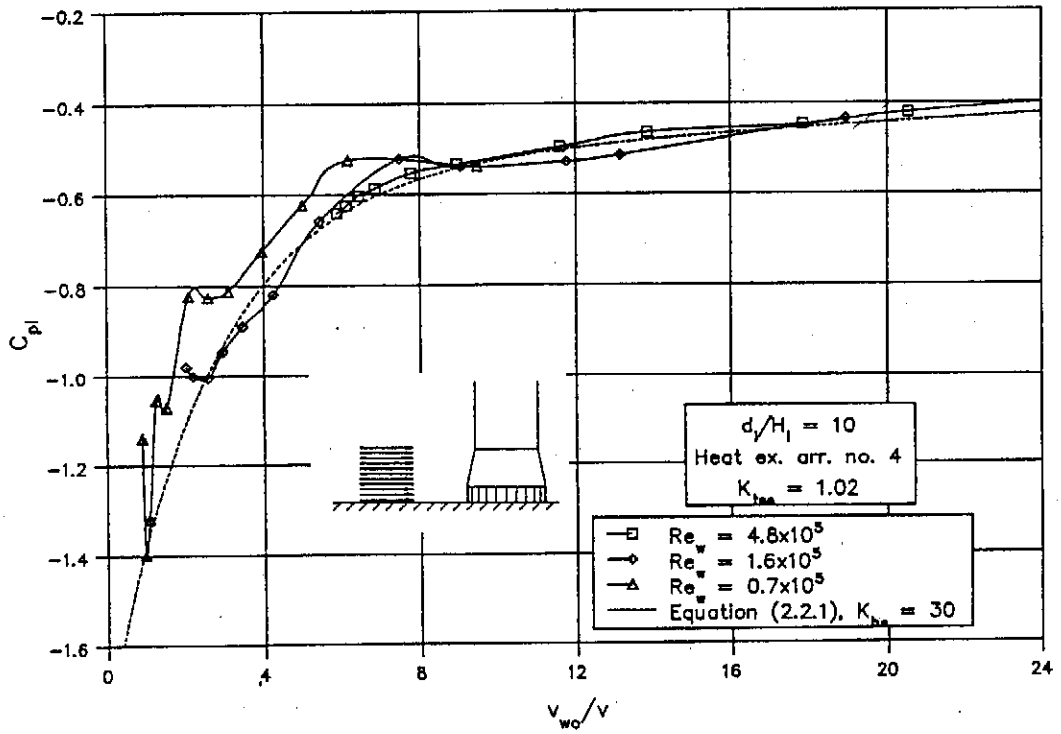

(b)

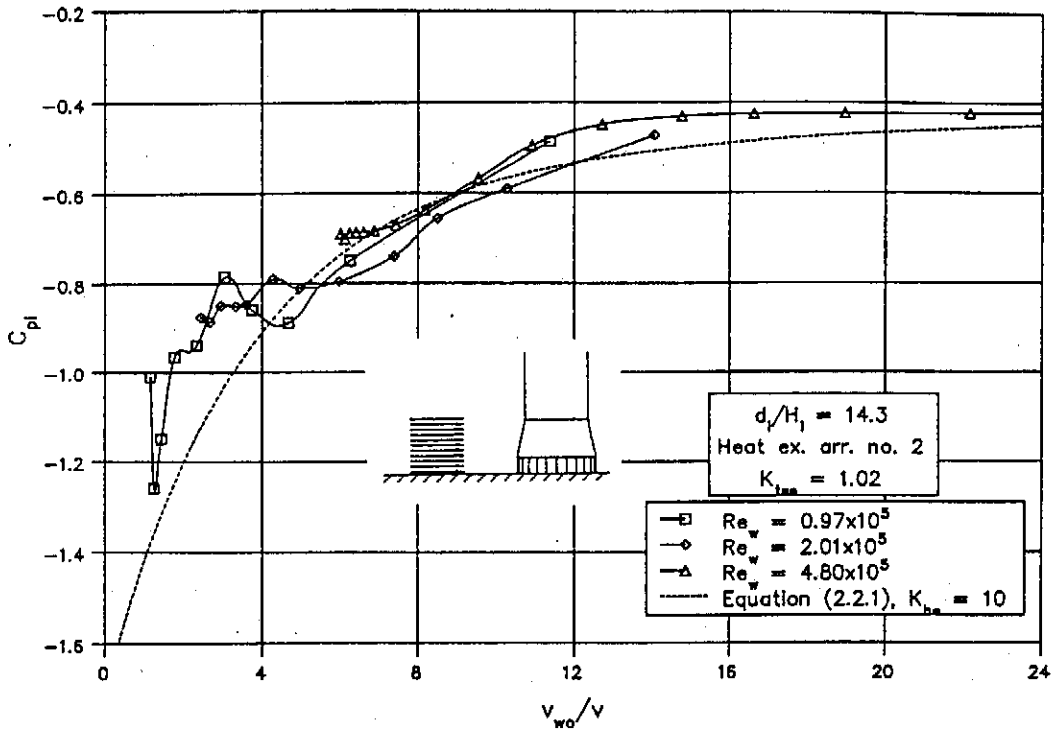

(c)

Figure 2.2.14: Inlet pressure coefficients of conical tower for different wind Reynolds numbers.

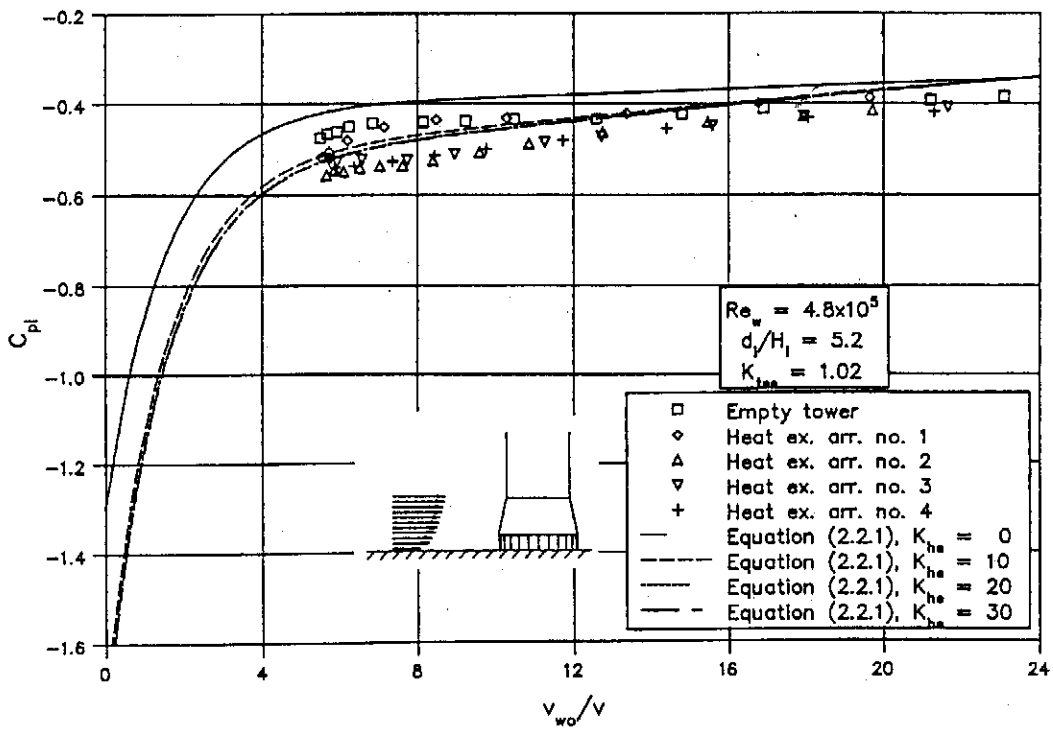

Figure 2.2.15: Inlet pressure coefficient with a wind profile.

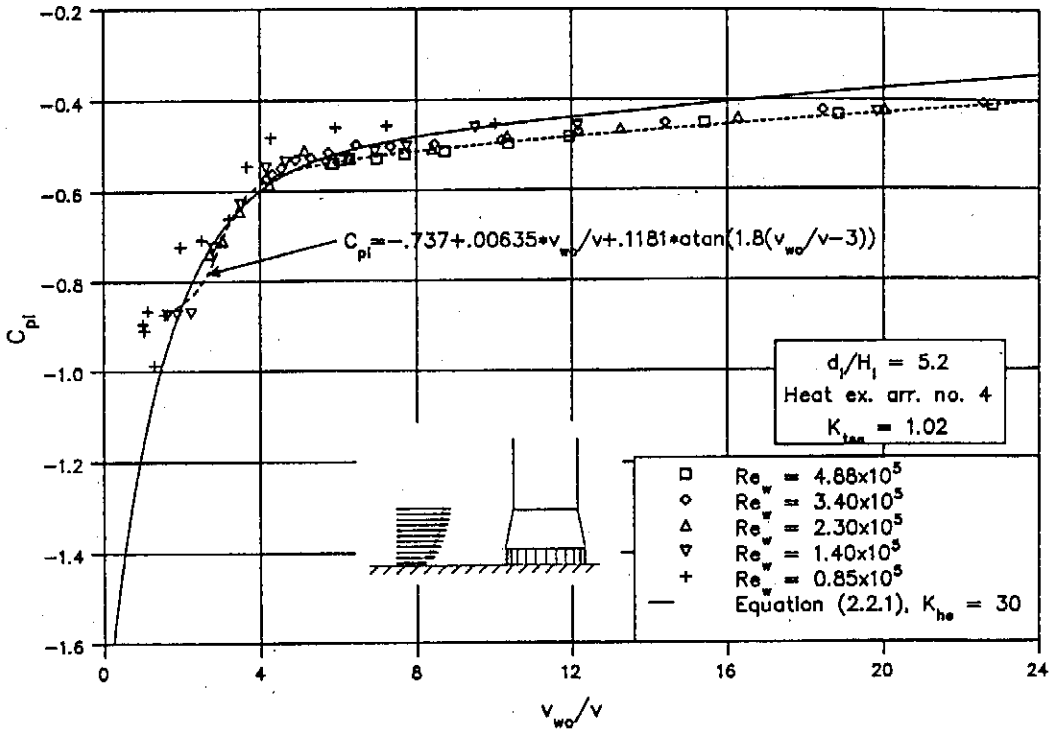

Figure 2.2.16: C_{pi} with a wind profile and different wind Reynolds numbers.

Due to the complex interrelation between the different parameters on the value of C_{pi} as discussed above, it is impossible to find a simple empirical correlation for C_{pi}. If it is accepted that the influence of the tower supports, form of the wind profile and the taper angle of the tower shell on the value of C_{pi} vary linearly between the values for which the tests were done, equation (2.2.1) is proposed for cylindrical shaped tower supports.

$$C_{pi} = \left[-0.57 + 0.0503 \left[\frac{v_{wo}}{v}\right]^{0.8} \left[\frac{d_i}{H_i}\right]^{-0.64} - 1.2 \,/\, \exp\left[2.4 \left[\frac{v_{wo}}{v}\right] \left[\frac{d_i}{H_i}\right]^{-0.8}\right]\right]$$

$$\times \left[1 - \left\{\frac{0.0067}{\exp\left(0.2\ K_{he}\right)}\right\}\left\{40 - 6\left[\frac{v_{wo}}{v}\right]\left[\frac{d_i}{H_i}\right]^{-0.8}\right\}\right]$$

$$+ \left[\left[-0.6 + 0.01\left[\frac{d_i}{H_i}\right] + \left\{-0.65 + 0.06\left[\frac{d_i}{H_i}\right] + 0.1K_{he}\right.\right.\right.$$

$$x \left[0.23 - 0.039\left[\frac{d_i}{H_i}\right] + 0.001\left[\frac{d_i}{H_i}\right]^2 \right] x\ 0.054\left[24 - \frac{v_{wo}}{v}\right]\Bigg]$$

$$+ \sin\left\{\frac{v_{wo}}{v} / \left[1 + \frac{0.17 v_{wo}}{v}\right]\right\} / \exp\left\{\frac{v_{wo}}{7\,v} + 0.2\left[15 - \frac{d_i}{H_i}\right] + \frac{K_{he}}{20}\right\}\Bigg]$$

$$x \left(1 - 0.978 K_{tse}\right)\left\{1 - \left(0.003 \times 2\theta_c + 2b + 0.027 \times 2\theta_c \times b\right)\right\} \qquad (2.2.1)$$

for $\quad 5 \le \frac{d_i}{H_i} \le 15\ ,\ 0 \le K_{he} \le 30$

$$0 \le \frac{v_{wo}}{v} \le 24\ ,\ 0 \le b \le 0.2$$

$$0 \le 2\theta_c \le 24^\circ\ ,\ 0 \le K_{tse} \le 1.02$$

The wind velocity, v_{wo}, in equation (2.2.1) refers to the wind velocity at the tower outlet height of the cooling tower while K_{he} is the value of the pressure loss coefficient of the heat exchangers obtained at an arbitrary Ry value of 200×10^3. The effective pressure loss coefficient of the tower supports, K_{tse}, is defined as the sum of the K_{ts} values of the different rings of supports based on the circumferential inlet area of the cooling tower. Furthermore it should be noted that C_{pi} in equation (2.2.1) is based on the wind velocity at the tower outlet height, v_{wo}. This equation is compared to the experimental results in all the appropriate preceding figures.

As the value of K_{tse} approaches the upper limit of 1.02, the second term in equation (2.2.1) reduces to zero and therefore C_{pi} becomes independent of the wind profile and the contraction angle of the cooling tower shell. The results in figures 2.2.12, 2.2.13 and 2.2.15 furthermore suggest that for high values of K_{tse}, C_{pi} also becomes independent of the pressure loss coefficient for sufficiently high K_{he} values. Therefore equation (2.2.1) is also applicable to cooling towers with K_{he} values higher than 30 provided that K_{tse} approaches 1.02.

Similar tests were also performed to determine the inlet pressure coefficient of a cooling tower with the finned tubes arranged round the circumference of the tower as shown in figure 1.1.2(a). For this layout the air which passes through the heat exchangers is directed in a normal direction.

This arrangement of the heat exchangers were modelled with metal rings cut from a 1 mm steel sheet as shown in figure 2.2.17. One mm washers are used to space the rings with a pitch of two mm with eight bolts being used to fasten the rings. Due to the size of the model, the A-frames usually found in practice could not be modelled properly. In an attempt to model the latter, vertical slots were cut in the rings, see figure 2.2.17, in which metal plates can be fitted to direct the entering flow in a radial direction. By adding screens, the heat exchanger pressure loss coefficient can be varied with the results shown in figure 2.2.18. Tests were only performed with a cylindrical cooling tower model without any supports installed in the tower inlet. The results of the tests are shown in figure 2.2.19 for three different heat exchanger arrangements. For sufficiently high K_{he} values the vertical plates used to simulate the A-frames have an insignificant effect on the inlet pressure coefficient. Furthermore C_{pi} is found to become independent of K_{he} for high values of the latter which is also true for a horizontal arrangement. If the C_{pi} values shown in figure 2.2.19 obtained for a d_i/H_i ratio of 5 is compared to that shown in figure 2.2.12 for a horizontal arrangement, the vertical arrangement appears, as far as the inlet pressure coefficient is concerned, to be less sensitive to a cross-flow as also suggested by Völler [85VO1].

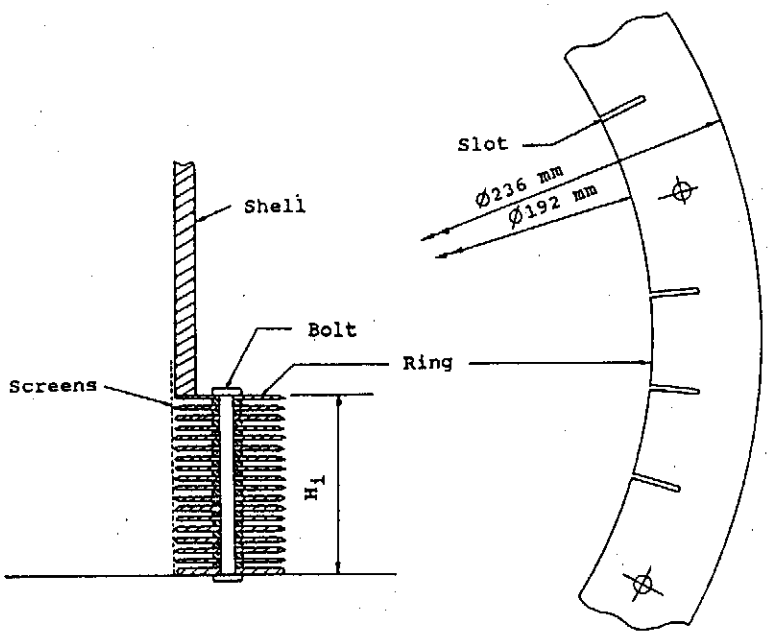

Figure 2.2.17: Model of the vertical heat exchanger arrangement.

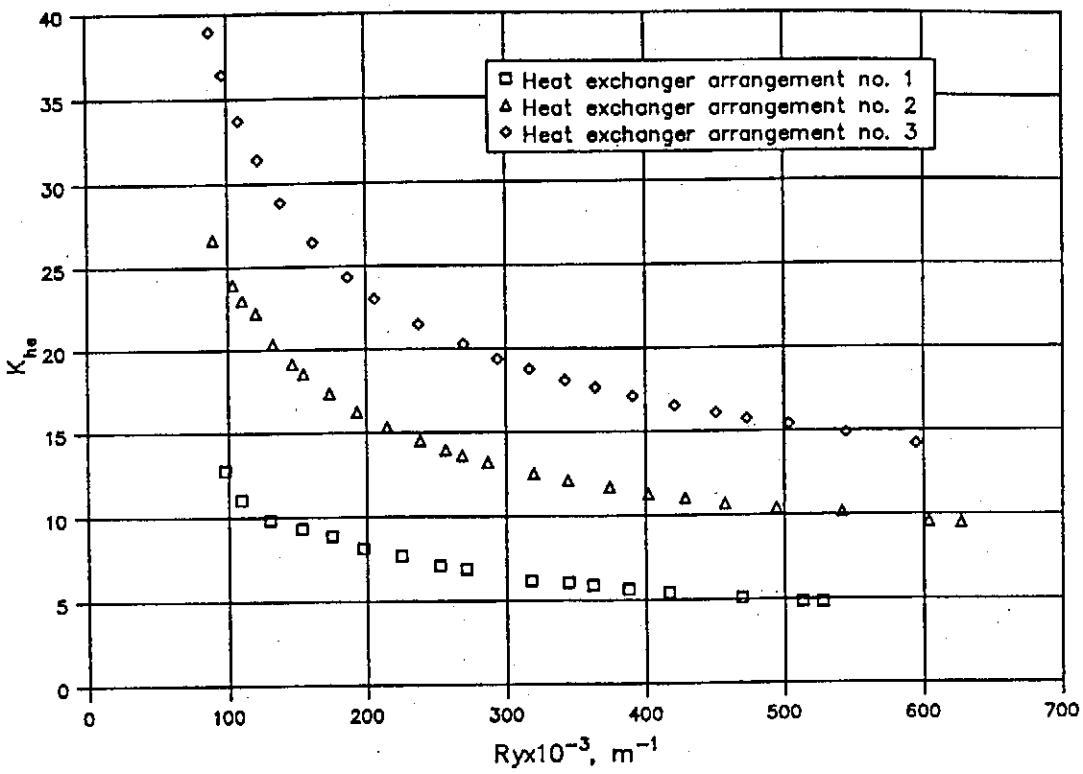

Figure 2.2.18: K_{he} values for the vertical heat exchanger arrangement.

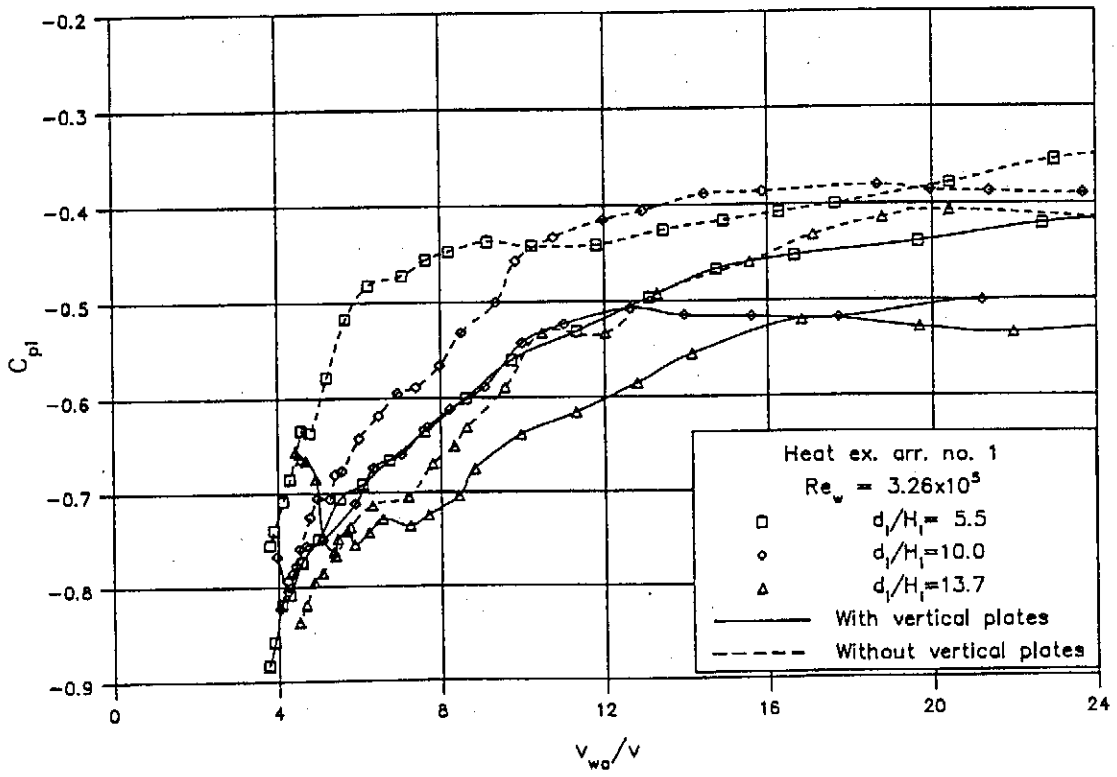

(a)

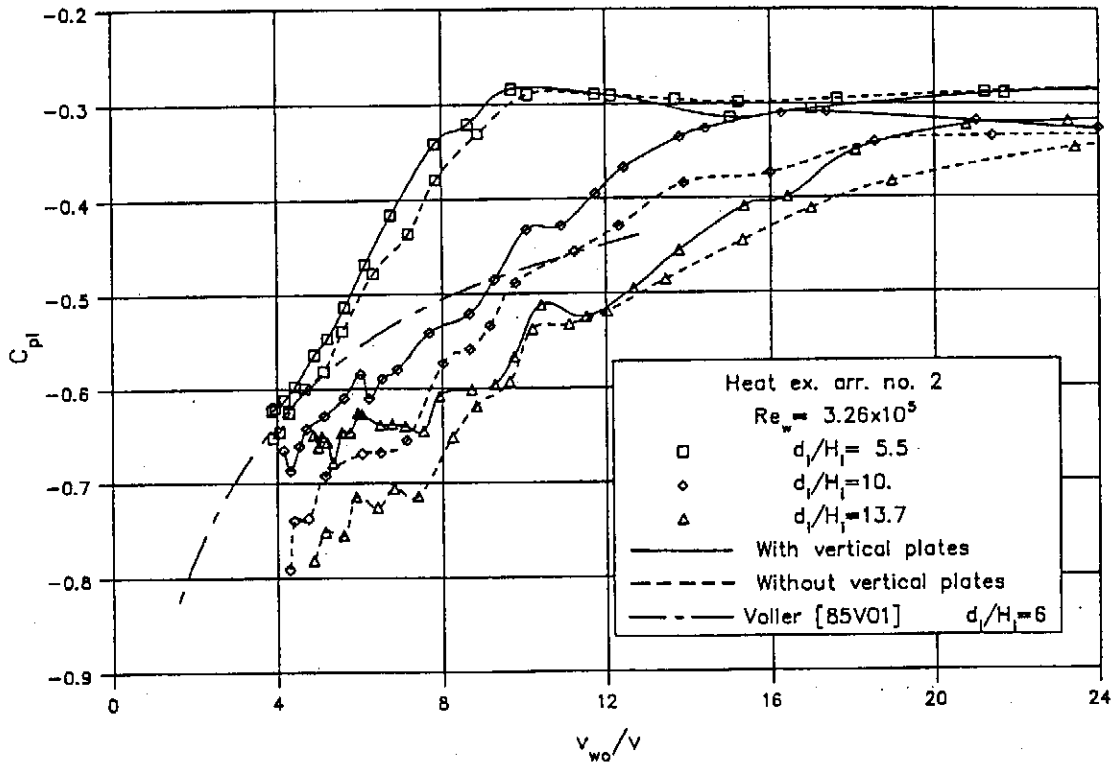

(b)

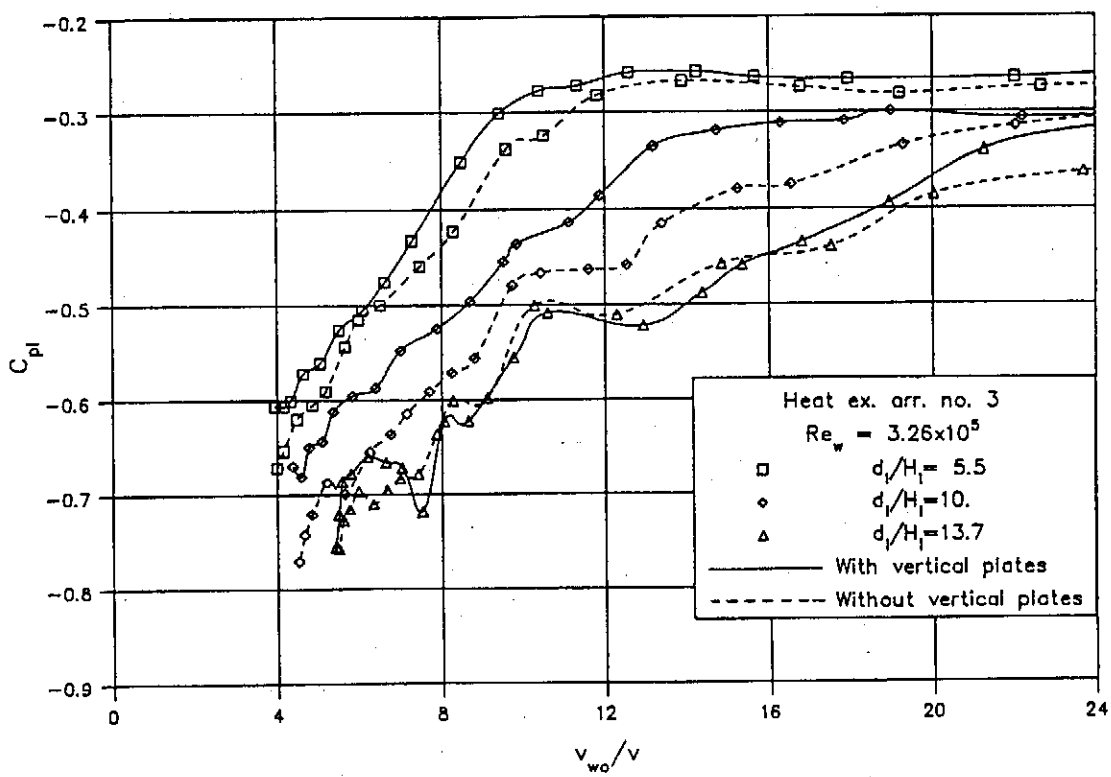

(c)

Figure 2.2.19: Inlet pressure coefficient for a vertical arrangement of the heat exchangers.

2.3: Velocity distribution through a horizontal heat exchanger arrangement in a cooling tower subjected to a cross-wind.

As a result of a cross-wind, the velocity distribution through the heat exchangers is distorted [85VO1]. In the present investigation the velocity distribution through the heat exchangers was only determined for a horizontal arrangement. The cylindrical tower model was used in all the tests with the tower supports installed in the inlet of the tower. The axial velocity distribution through the bundle was measured by arranging four total pressure tubes approximately 20 mm above the heat exchangers in such a way that the representative cross-sectional flow area was the same for each tube. Due to symmetry the velocity distribution was only measured in one half of the model.

The mean mass flow through the tower as calculated from the measured velocities should agree with the mass flow determined by the flow nozzle. The discrepancy between the two mass flow rates as calculated by the two methods vary between -5 and 5% for all the tests. This can be attributed to experimental inaccuracies. Figure 2.3.1 shows the ratio of the local air velocity to the mean air velocity through the heat exchangers, v_l/v, for six values of the relative wind velocity.

The results suggest that as the wind velocity increases, the flow through the bundle becomes increasingly more non-uniform with the maximum air velocity on the lee side of the tower. On the upstream side, the air flow through the bundles decreases due to the formation of a separated flow pattern below the heat exchangers. Smoke was used to visualize the velocity distribution inside the tower and for very high wind velocities flow recirculation was observed with air from inside the model flowing through the heat exchanger to return through the bundles further downstream. Flow patterns similar to those shown in the figure were also observed for d_i/H_i ratios of 10 and 15.

The flow pattern as measured is completely different to that suggested by Witte [83WI1]. According to his proposal the maximum air velocity should be found at the upstream side of the tower.

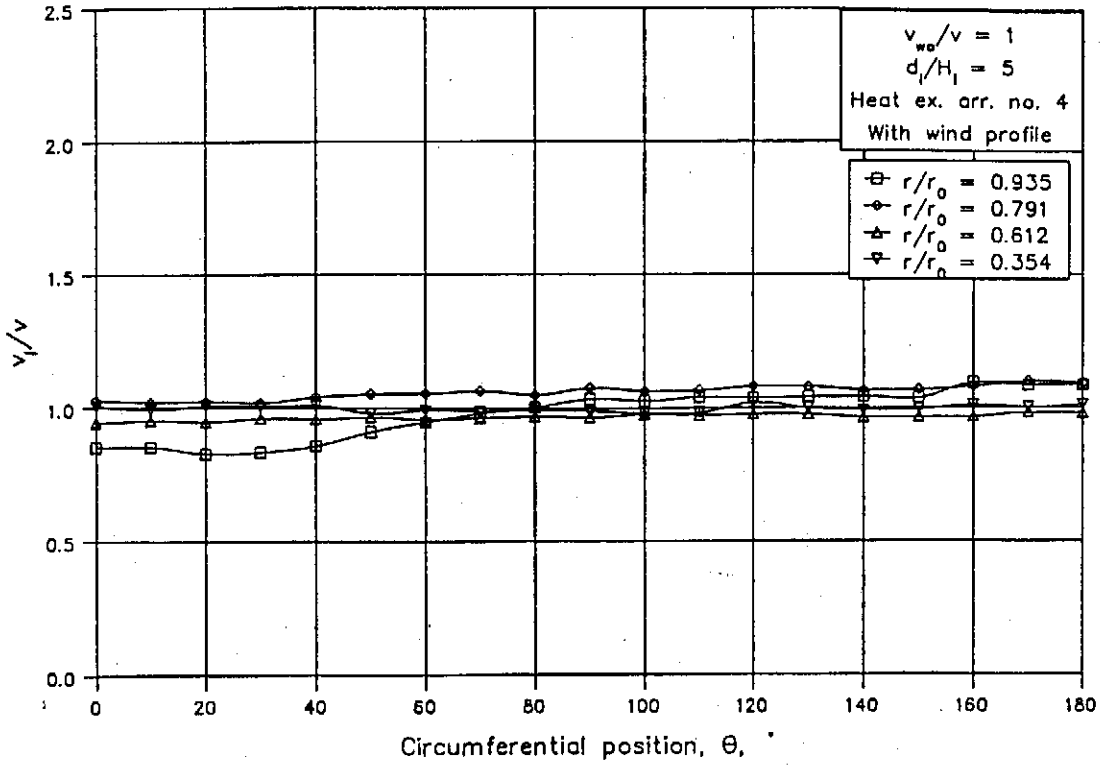
v_{wo}/v = 1
d_1/H_1 = 5
Heat ex. arr. no. 4
With wind profile
r/r_0 = 0.935
r/r_0 = 0.791
r/r_0 = 0.612
r/r_0 = 0.354
v_1/v
Circumferential position, θ,

(a)

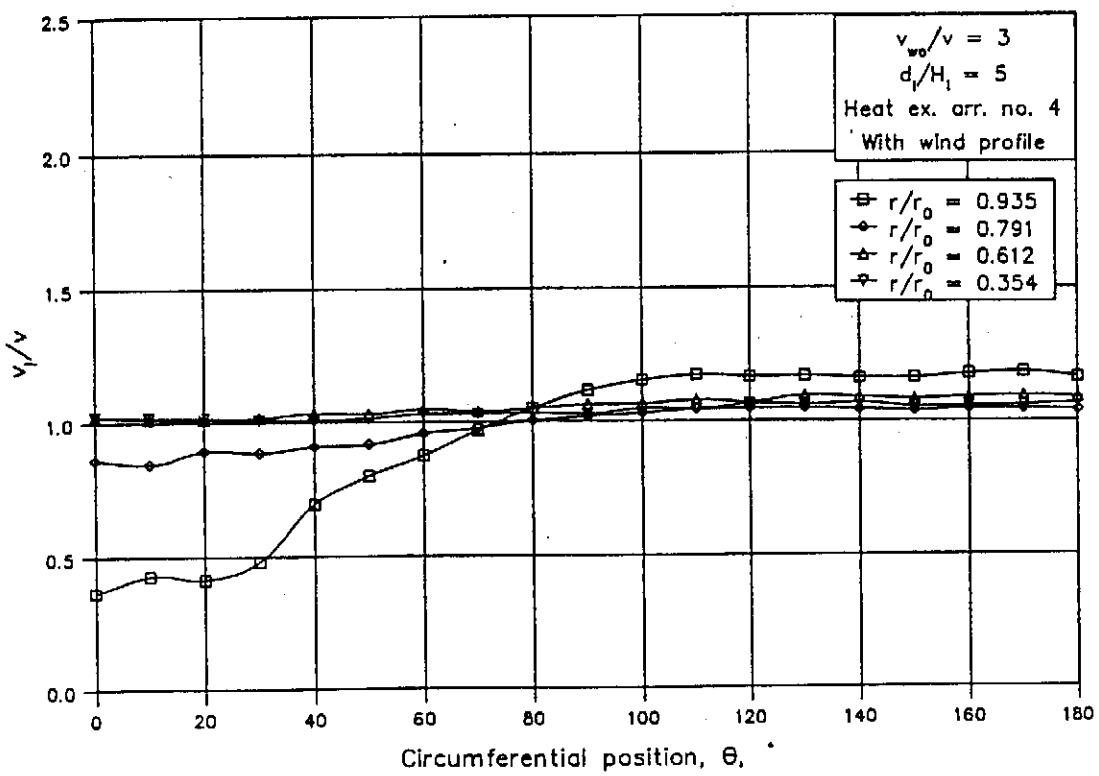
v_{wo}/v = 3
d_1/H_1 = 5
Heat ex. arr. no. 4
With wind profile
r/r_0 = 0.935
r/r_0 = 0.791
r/r_0 = 0.612
r/r_0 = 0.354
v_1/v
Circumferential position, θ,

(b)

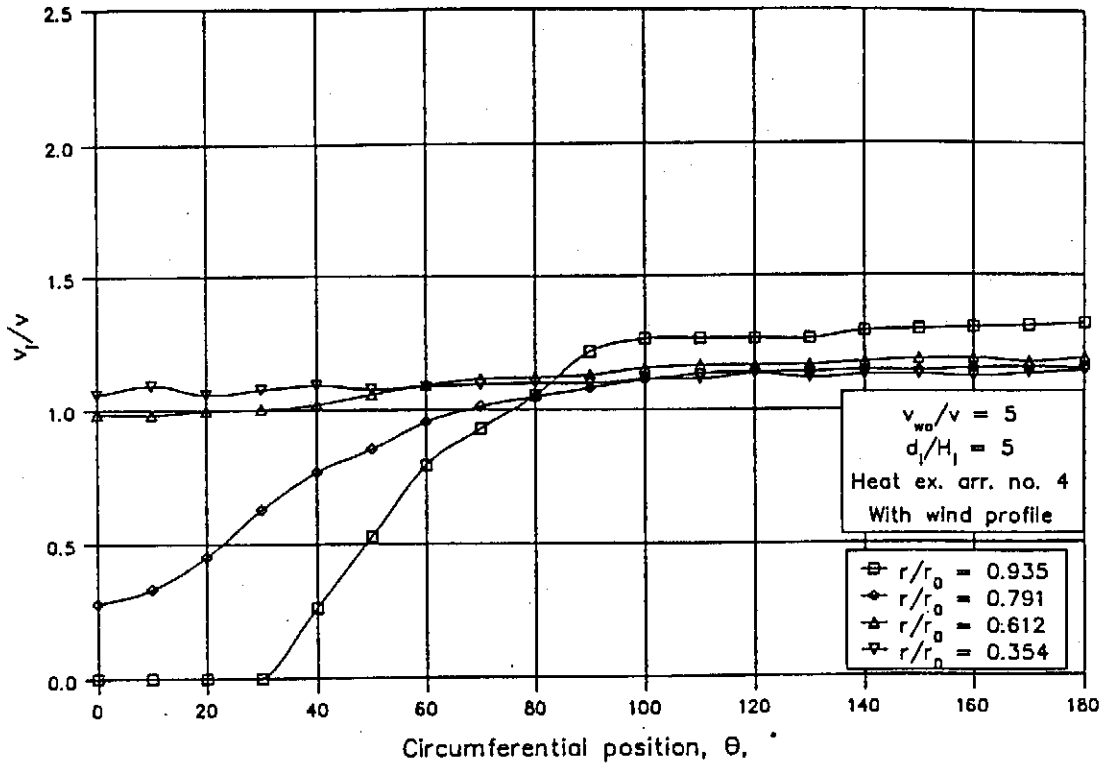
2.5
2.0
1.5
1.0
0.5
0.0
v_l/v
0
20
40
60
80
100
120
140
160
180
Circumferential position, θ,
v_{wo}/v = 5
d_l/H_l = 5
Heat ex. arr. no. 4
With wind profile
r/r_0 = 0.935
r/r_0 = 0.791
r/r_0 = 0.612
r/r_0 = 0.354

(c)

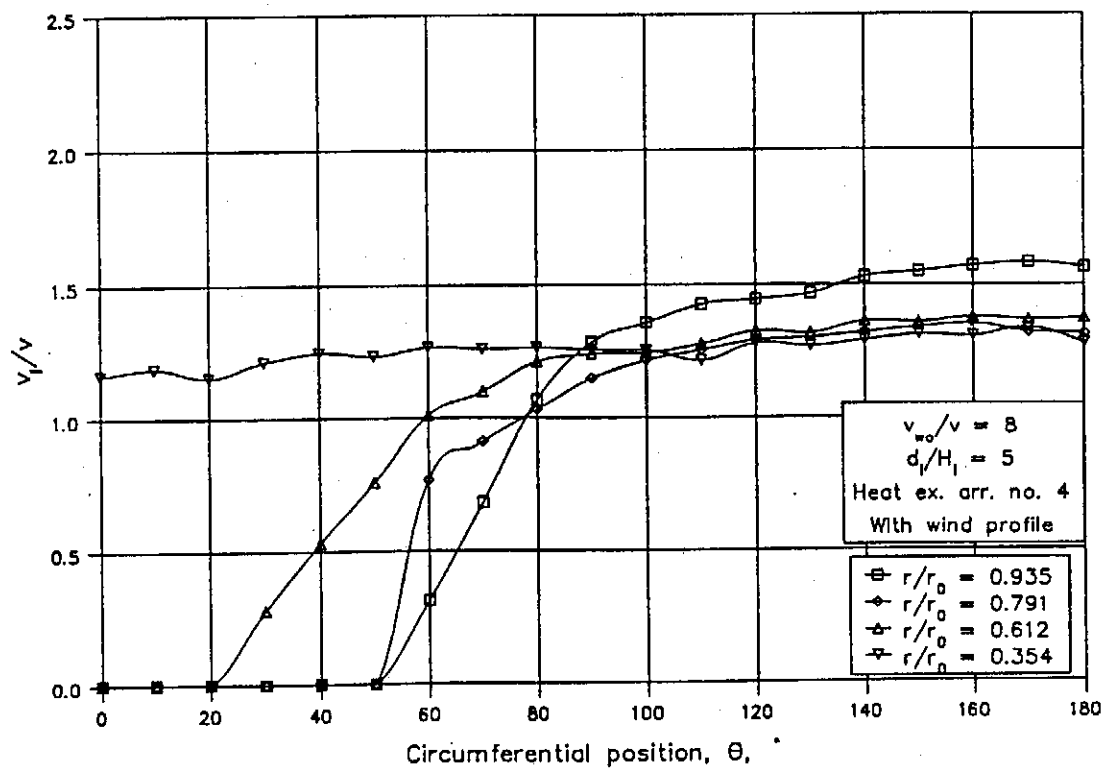
2.5
2.0
1.5
1.0
0.5
0.0
v_l/v
0
20
40
60
80
100
120
140
160
180
Circumferential position, θ,
v_{wo}/v = 8
d_l/H_l = 5
Heat ex. arr. no. 4
With wind profile
r/r_0 = 0.935
r/r_0 = 0.791
r/r_0 = 0.612
r/r_0 = 0.354

(d)

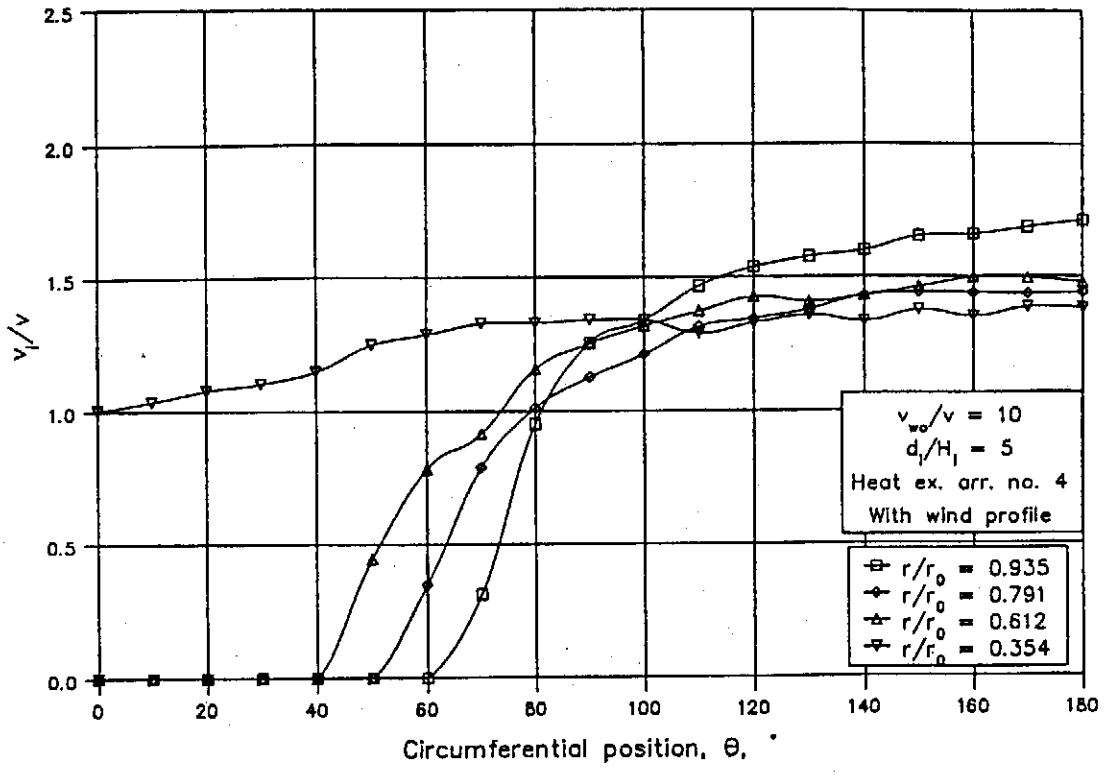

(e)

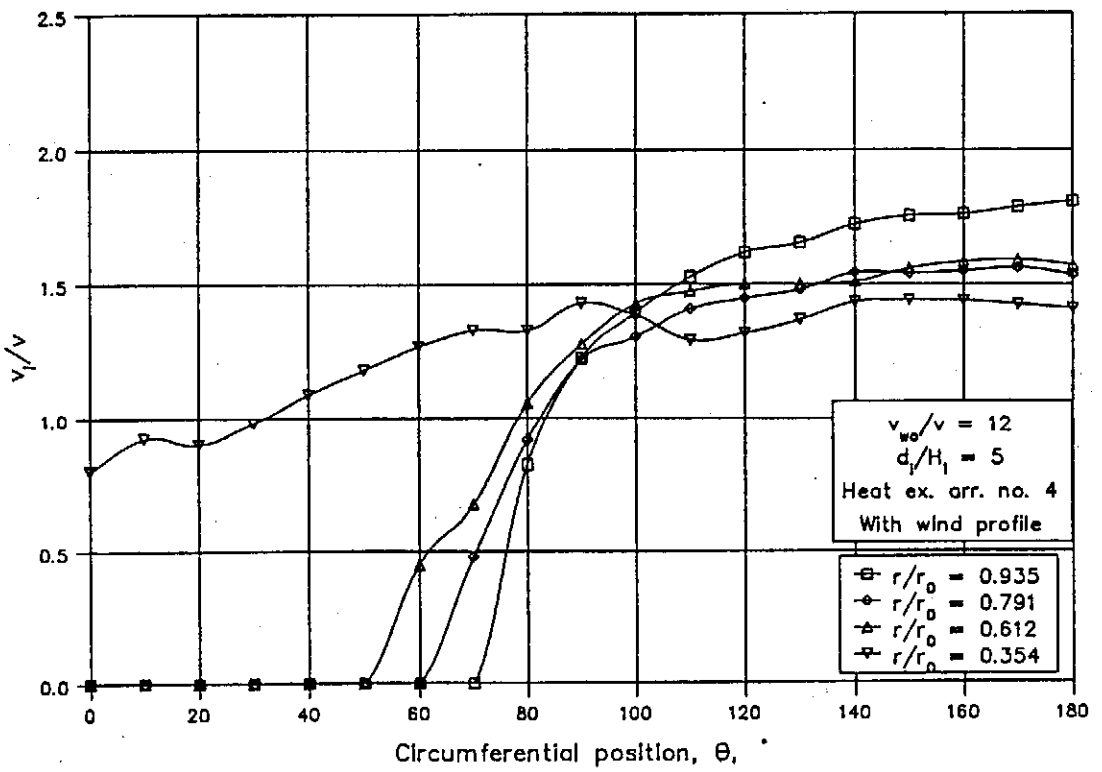

(f)

Figure 2.3.1: Velocity distribution through horizontal heat exchanger.

By using the kinetic energy coefficient defined in equation (A.1.3), the corresponding values of α can be calculated with the results shown in figure 2.3.2. In contrast with the inlet pressure coefficient, the wind profile causes a slight improvement in the velocity distribution through the heat exchanger. It was furthermore found that the cylindrical tower supports have no influence on the velocity distribution.

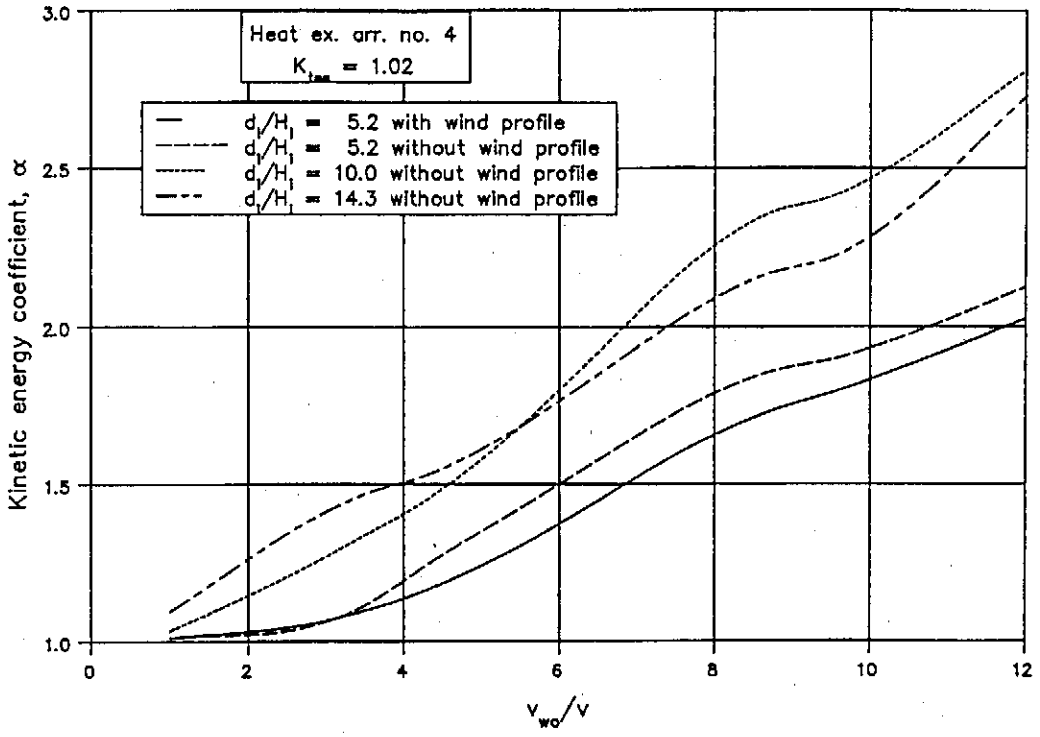

Figure 2.3.2: α for the velocity profile in the tower.

The distorted flow pattern through the finned tube heat exchangers will influence the heat transfer characteristics of the heat exchanger. For a uniform air velocity distribution the heat transfer rate in a cross-flow finned tube heat exchanger with two or more tube passes (essentially counterflow), commonly found in dry-cooling towers, can be approximated by

$$Q \approx v_{he}\rho_a A_{fr} c_{pa}(T_{wi} - T_{ai})\epsilon \qquad (2.3.1)$$

where v_{he} is the mean air velocity based on the frontal area of the heat exchangers with the effectiveness, ϵ, given by Holman [81HO1] for a counterflow geometry. If the air velocity through the heat exchangers is distorted, the reduced effective heat transfer rate is found by introducing a correction factor such that

$$Q_e = \alpha_Q\, Q \text{ where } \alpha_Q = \int_{A_{fr}} v_l \rho_a c_{pa} \epsilon \, dA_{fr}/(v\rho_a A_{fr} c_{pa}\epsilon) \qquad (2.3.2)$$

where v_l is the local air velocity through the heat exchanger. The heat transfer correction factor is a function of the overall heat transfer coefficient of the heat exchangers which may be approximated by

$$UA = a_{UA} Ry^{b_{UA}}$$

As the value of b_{UA} increases an increase in the value of α_Q is found. The exponent b_{UA} is a characteristic of the type of heat exchanger that is used, however, for the finned tube heat exchangers commonly found in dry-cooling towers the value of b_{UA} is in the order of 0.45. Based on the measured velocity distribution through the horizontal heat exchanger, α_Q was calculated for different relative wind velocities and is shown in figure 2.3.3. The following empirical relation is recommended for design purposes within the limits specified below and is compared to the experimental results in figure 2.3.3.

$$\alpha_Q = \left\{ 1 - \frac{\left[\frac{v_{wo}}{v}\right]^{3.6} \exp\left[-\frac{v_{wo}}{3.75v}\right] v^{0.576}}{3561} \right\}$$

$$x \left[0.98 + 0.02 \left\{ \exp\left[5.2 - \frac{d_i}{H_i}\right] + \exp\left[-\frac{v_{wo}}{v}\right] \right\} \right]$$

$$-(1.5 - 0.05K_{he}) \, x \left[\left\{ 0.013 - 0.0048\left[\frac{d_i}{H_i}\right] + 0.000302\left[\frac{d_i}{H_i}\right]^2 \right\} \right.$$

$$+ \left\{ 0.0134 - 0.00129\left[\frac{d_i}{H_i}\right] + 0.000038\left[\frac{d_i}{H_i}\right]^2 \right\} x \left[\frac{v_{wo}}{v}\right]$$

$$\left. + \left\{ 0.0035 + 0.00206\left[\frac{d_i}{H_i}\right] - 0.000085\left[\frac{d_i}{H_i}\right]^2 \right\} \sin\left[\frac{v_{wo}}{1.9v}\right] \right]$$

$$- \left[0.0053 - \frac{K_{he}}{9182}\right](11.26 - 25.64 b_{UA})\frac{v_{wo}}{v} \qquad (2.3.3)$$

for $5.2 \leq \frac{d_i}{H_i} \leq 15$, $10 \leq K_{he} \leq 30$, $0 \leq \frac{v_{wo}}{v} \leq 12$

$0 \leq b \leq 0.2$, $0 \leq K_{tse} \leq 1.02$, $0.4 \leq b_{UA} \leq 0.5$

$1 \leq v \leq 4$ m/s

Note that if $\alpha_Q > 1$ in the above equation a value of $\alpha_Q = 1$ is assumed.

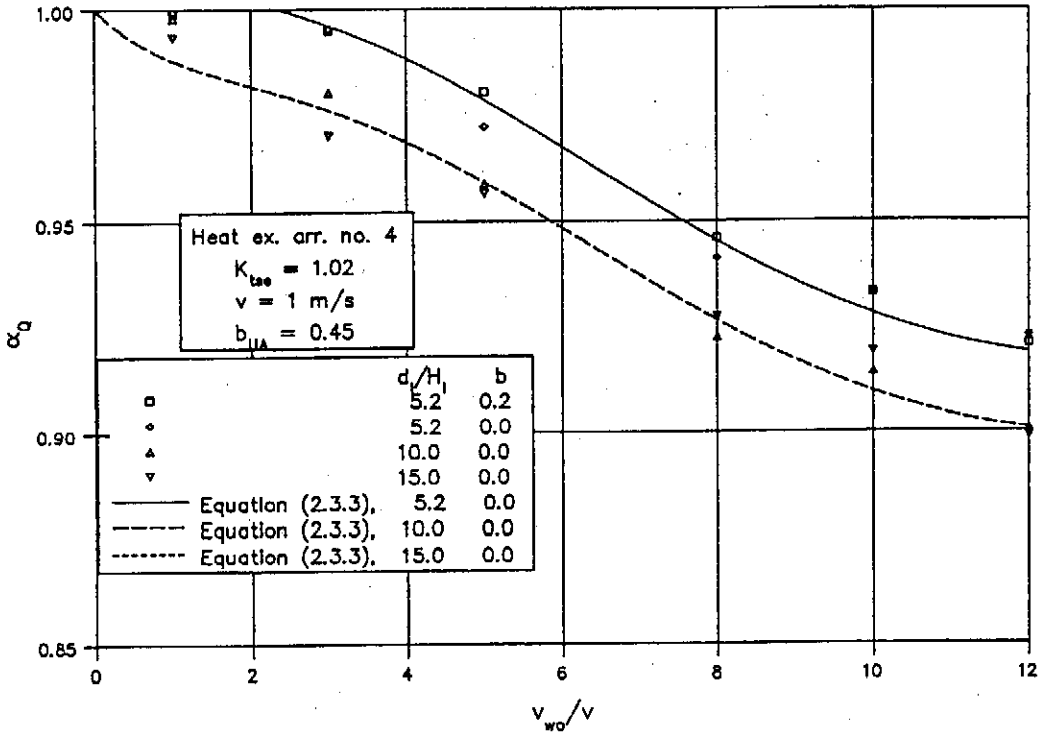

Figure 2.3.3: α_Q for a horizontal heat exchanger arrangement.

As discussed in Appendix B, the maximum air velocity through the bundles is needed when using the experimental data to predict the wind influence on the amount of heat rejected by the cooling tower. For that purpose it would be convenient to have an empirical relation giving the maximum air velocity in terms of the independent variables. Based on the measurements, equation (2.3.4) is proposed and is shown in figure 2.3.4.

$$\frac{v_{max}}{v} = 1.014 - 0.0095\left[\frac{d_i}{H_i}\right] + 0.0014\left[\frac{d_i}{H_i}\right]^2$$

$$+\left\{-0.1265 + 0.0509\left[\frac{d_i}{H_i}\right] - 0.00245\left[\frac{d_i}{H_i}\right]^2\right\}\frac{v_{wo}}{v} \times (1 - 0.26b)$$

$$+\left[-.362 + .0865\left[\frac{d_i}{H_i}\right] - 0.00321\left[\frac{d_i}{H_i}\right]^2\right.$$

$$\left.+\left\{0.288 - .0572\left[\frac{d_i}{H_i}\right] + 0.00242\left[\frac{d_i}{H_i}\right]^2\right\}\frac{v_{wo}}{v}\right]\left(1.5 - 0.05K_{he}\right) \qquad (2.3.4)$$

for $5.2 \le \frac{d_i}{H_i} \le 15$, $10 \le K_{he} \le 30$, $0 \le K_{tse} \le 1.02$

$$0 \le \frac{v_{wo}}{v} \le 12 \text{ , } 0 \le b \le 0.2$$

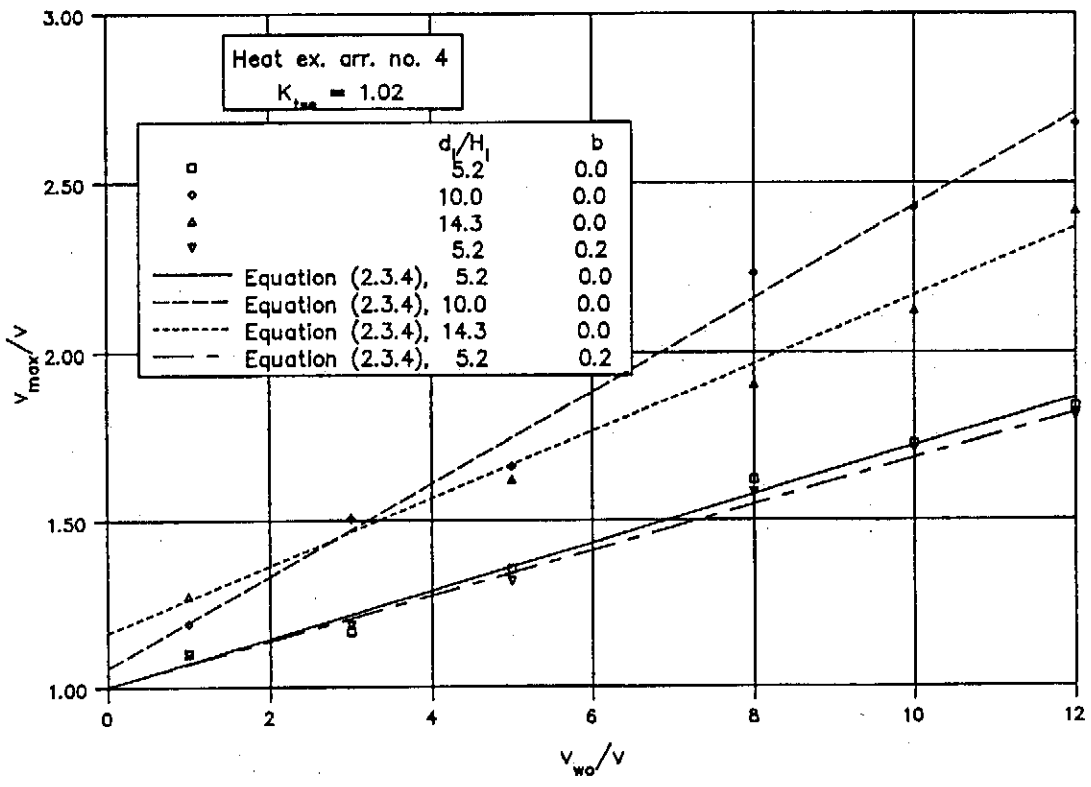

Figure 2.3.4: v_{max}/v for large K_{he} values.

Similar measurements were also made for a smaller K_{he} values. Figure 2.3.5 shows the velocity distribution as measured for a d_i/H_i ratio of 14.7 with the corresponding α_Q in figure 2.3.6. The flow distortion found in figure 2.3.5(a) is mainly due to the separated flow pattern below the heat exchangers as shown by Geldenhuys [86GE1].

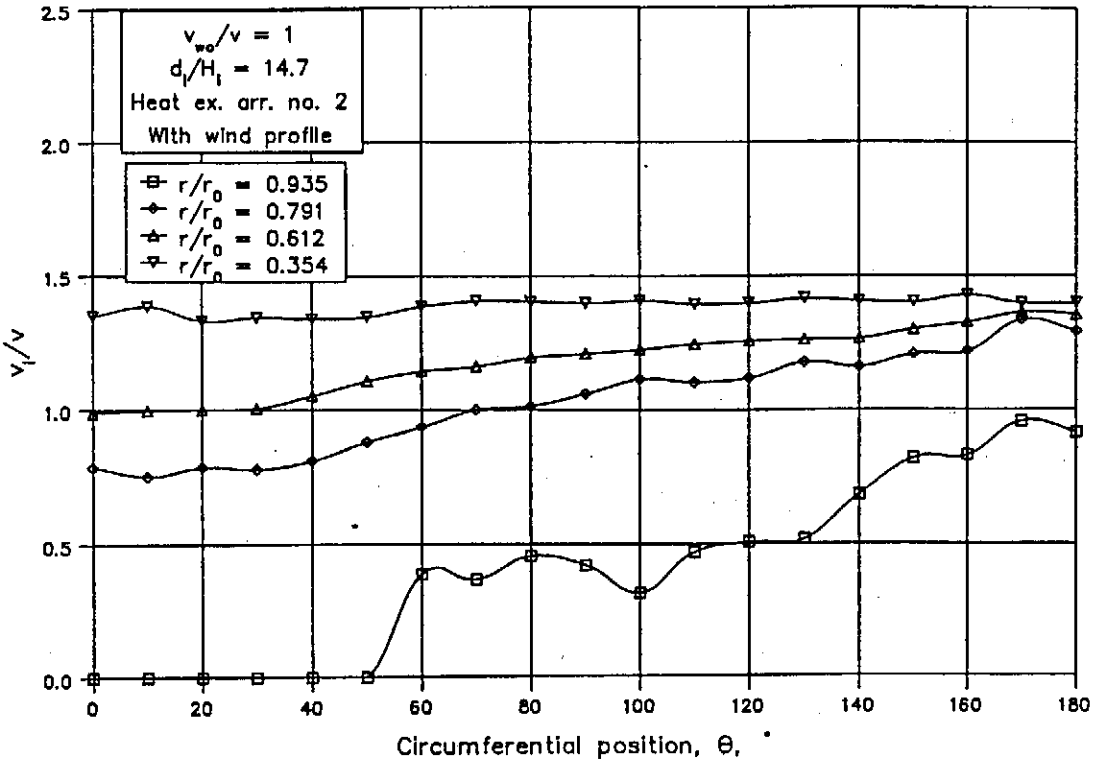

(a)

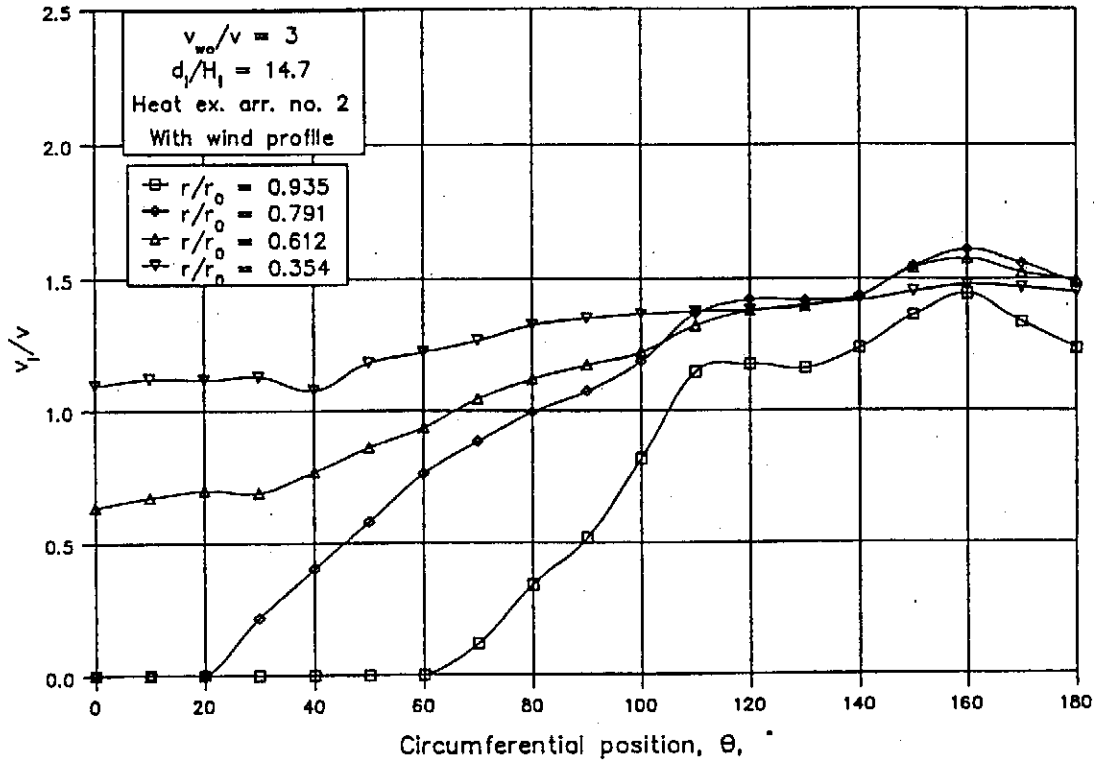

(b)

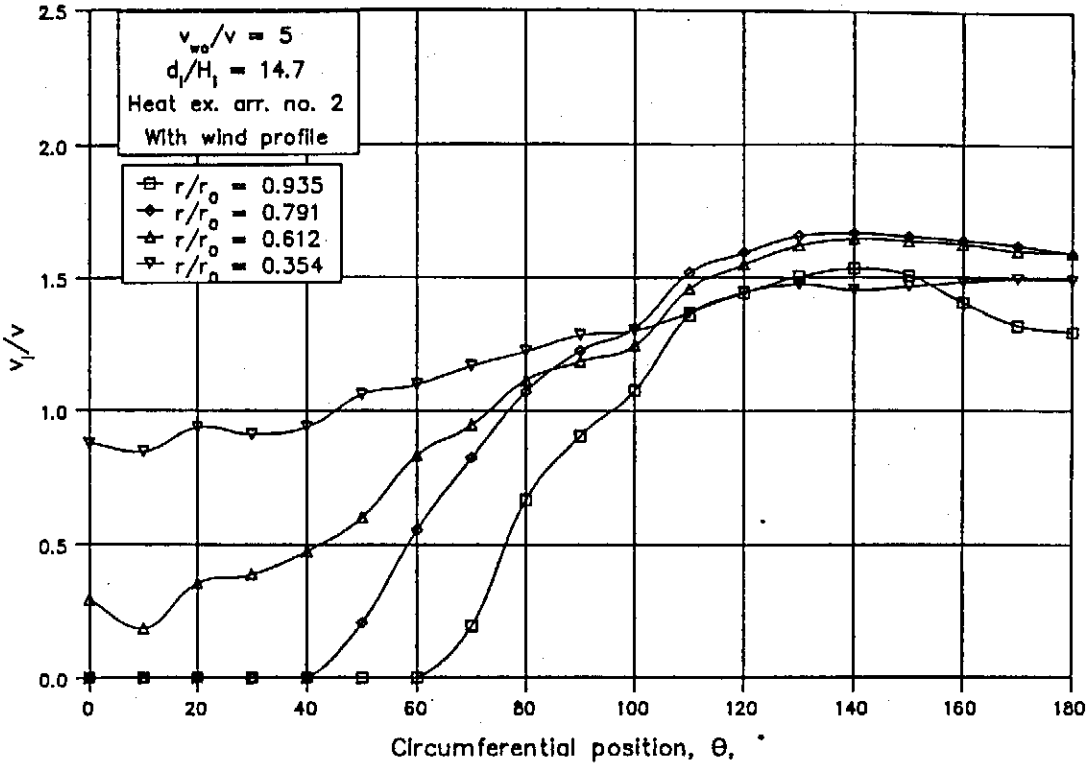
v_{wo}/v = 5
d_i/H_i = 14.7
Heat ex. arr. no. 2
With wind profile
r/r_o = 0.935
r/r_o = 0.791
r/r_o = 0.612
r/r_o = 0.354
v_i/v
Circumferential position, θ,

(c)

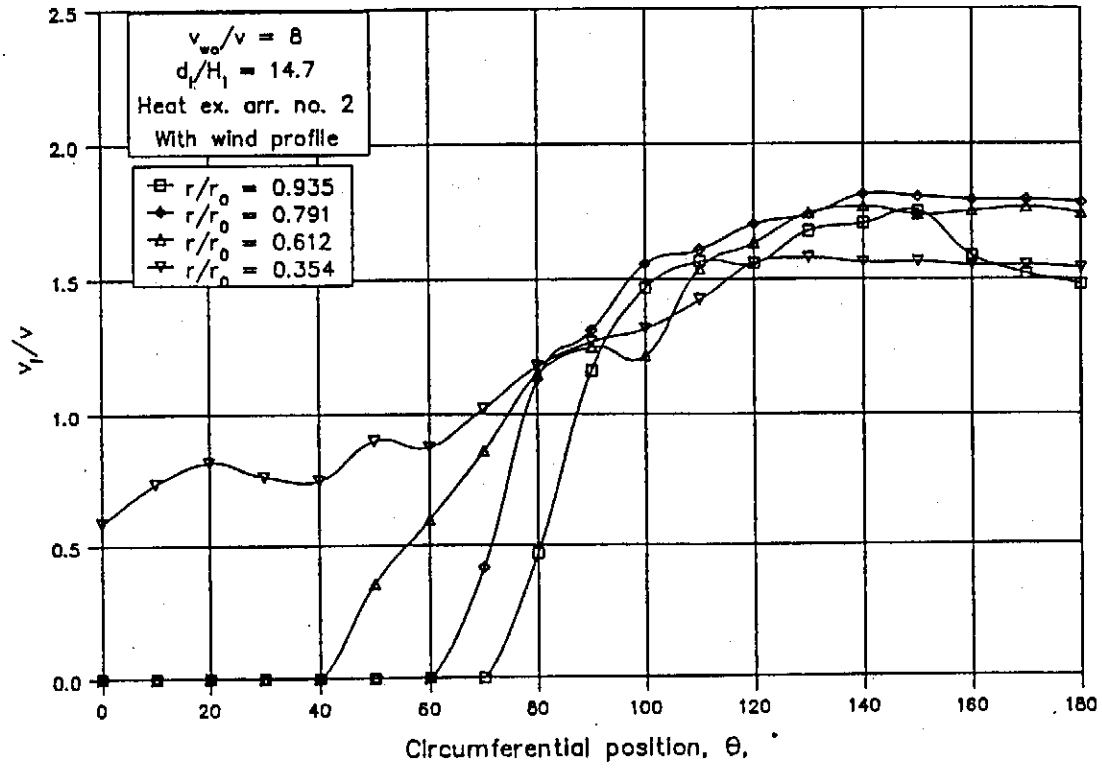
v_{wo}/v = 8
d_i/H_i = 14.7
Heat ex. arr. no. 2
With wind profile
r/r_o = 0.935
r/r_o = 0.791
r/r_o = 0.612
r/r_o = 0.354
v_i/v
Circumferential position, θ,

(d)

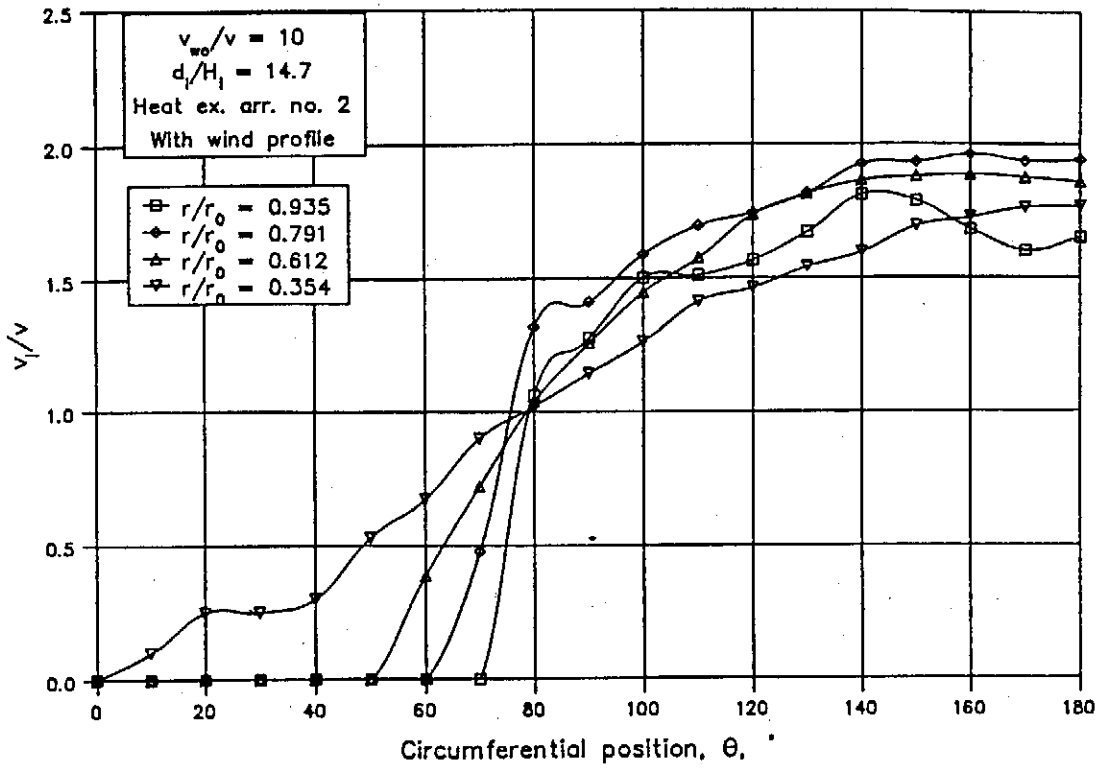

(e)

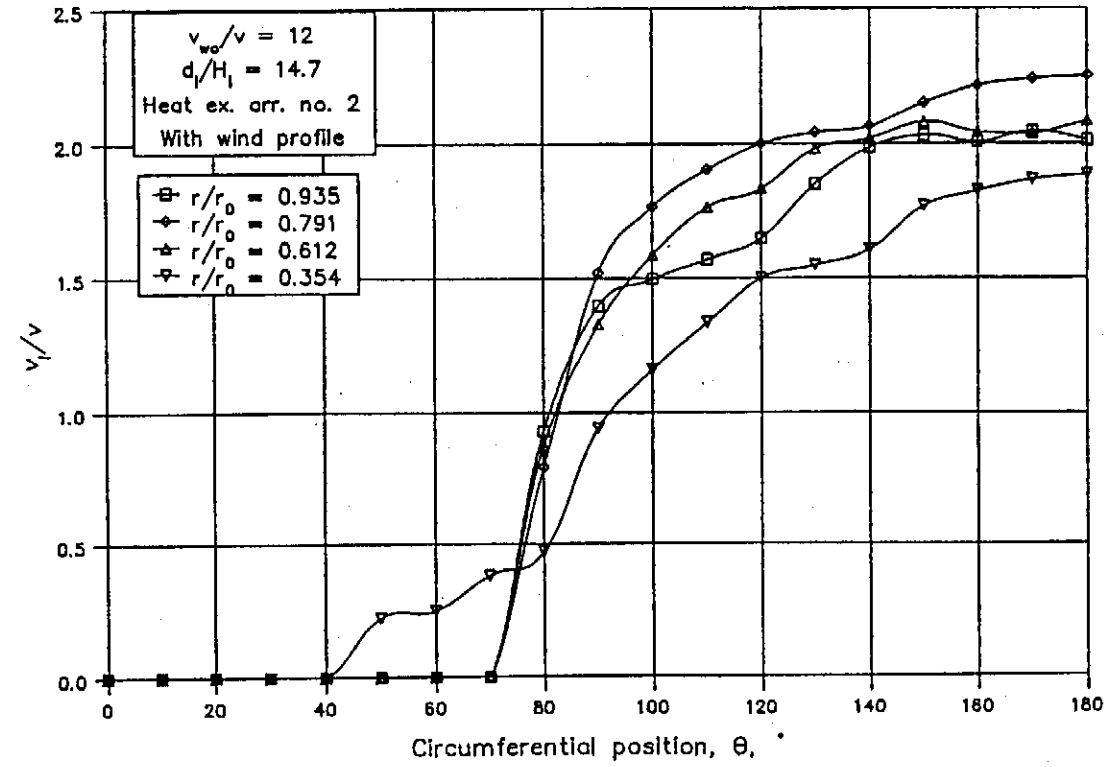

(f)

Figure 2.3.5: Velocity distribution for cooling tower with a small K_{he} values.

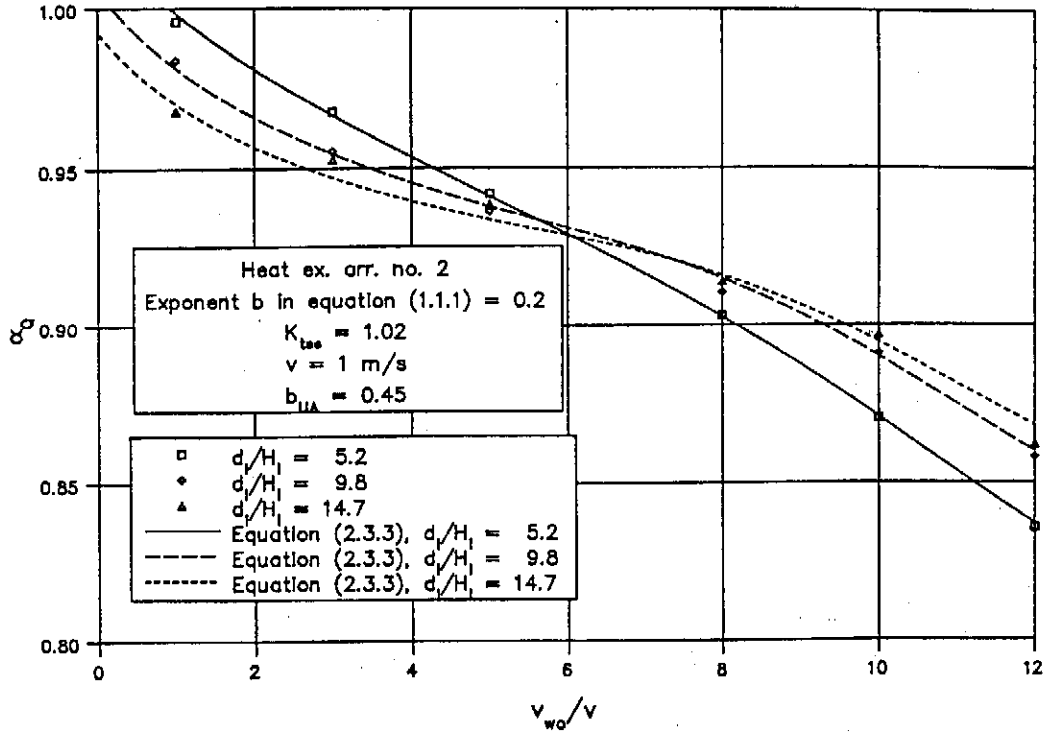

Figure 2.3.6: α_Q for a tower with a small value of the heat exchanger loss coefficient.

In figure 2.3.7 equation (2.3.4) is compared to the experimental results obtained for small K_{he} values.

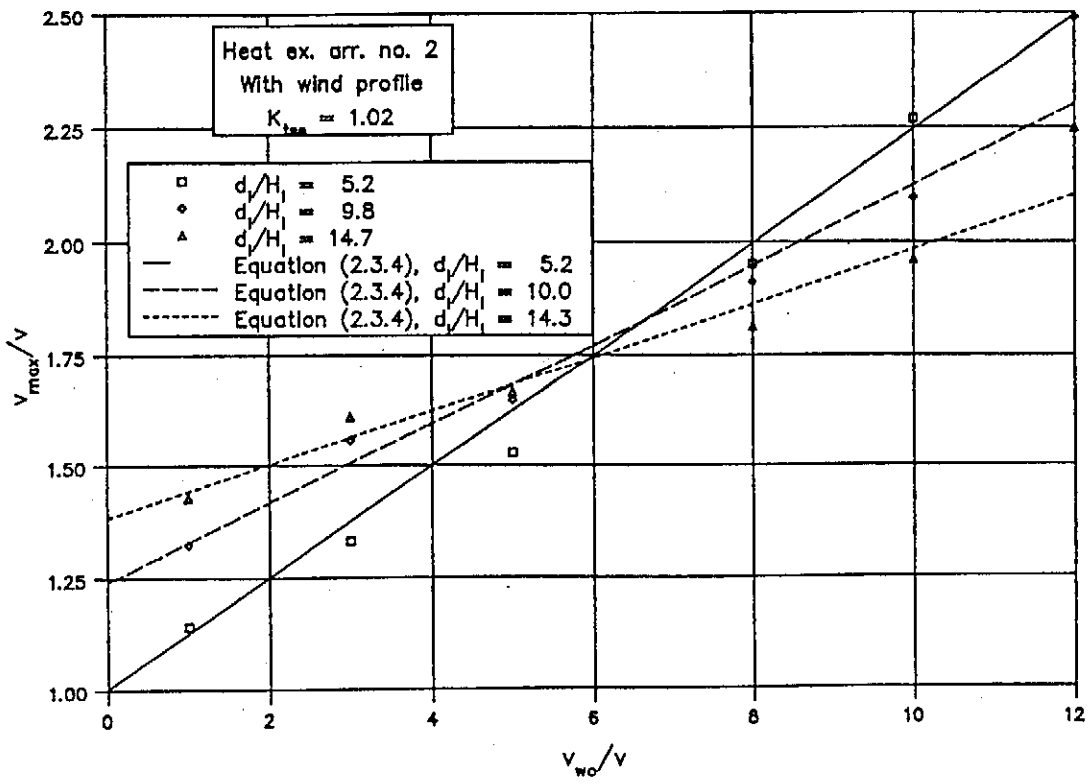

Figure 2.3.7: v_{max}/v for small K_{he} values.

The velocity distribution through a vertical arrangement of the heat exchangers was not determined in the present investigation, primarily due to the difficulties involved in modelling the A-frames. It is expected that the wind will cause a severely distorted flow distribution through the A-frames, especially for the bundles positioned at the flanks of the tower. [77MA1]. Christopher [69CH1] performed measurements on the dry-cooling tower of the Rugeley power station with such a heat exchanger arrangement. His survey revealed that the deterioration brought about by the wind was mainly due to the blanketing of the downstream coolers of those A-fames suffering from tangential wind components. Therefore more model tests are recommended to determine the velocity distribution through the A-frames before the wind effect on such a dry-cooling tower can be predicted.

2.4: Pressure coefficients for a cylindrical cooling tower outlet.

The wind effect at the outlet of the cooling tower has been studied by a number of investigators [72EC1, 79DI1, 80BO1, 82BU1, 82CH1, 82RU1, 83BU1, 85VO1]. In the present study the wind effect on only a cylindrical cooling tower outlet was studied by using the same tower model. A few mesh layers were placed one diameter from the outlet edge of the model to simulate the heat exchangers.

An initial test was performed with no flow in the model with the static pressure inside the tower being measured for different wind velocities. The outlet pressure coefficient as defined in equation (2.1.1) obtained for this test is shown in figure 2.4.1.

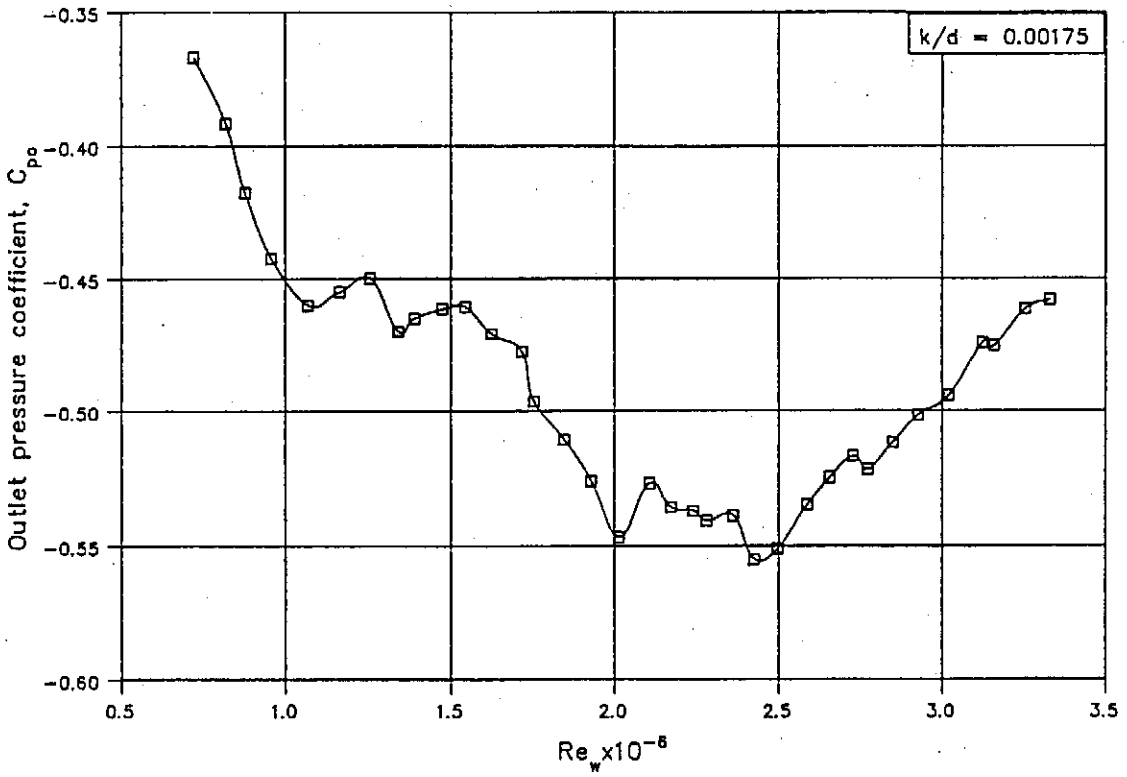

Figure 2.4.1: Outlet pressure coefficient with no flow in tower.

By varying the air speed inside the model, the outlet pressure coefficient was determined for different values of the relative wind velocity with the results shown in figure 2.4.2. The increase in the value of C_{po} as the wind Reynolds number decreases is due to the influence of the wind Reynolds number and is in agreement with the results shown in figure 2.4.1. The data obtained at the maximum wind Reynolds number for a cylindrical tower outlet, i.e. with the outlet to throat area ratio, A_o/A_t, equal to 1, are correlated by equation (2.4.1) and is also shown in figure 2.4.2 in its range of applicability. By using data for divergent and convergent outlet shapes as published by Völler [85VO1], the equation for a cylindrical tower outlet was

extended to be applied for other shapes as well within the limits as specified.

$$C_{po} = -0.405 + 1.07\left[\frac{v_{wo}}{v}\right]^{-1}\left[\frac{A_o}{A_t}\right]^{-1.65} + 1.8\log_{10}\left\{\left[\frac{v_{wo}}{2.7v}\right]\left[\frac{A_o}{A_t}\right]^{1.65}\right\}$$

$$x\left\{\left[\frac{v_{wo}}{v}\right]\left[\frac{A_o}{A_t}\right]^{1.65}\right\}^{-2} + \left\{-1.04 + 1.702\left[\frac{A_o}{A_t}\right] - 0.662\left[\frac{A_o}{A_t}\right]^2\right\} x \left[\frac{v_{wo}}{v}\right]^{-0.7} \quad (2.4.1)$$

for $\quad 1.8 \le \frac{v_{wo}}{v} \le 24 \quad$ if $\frac{A_o}{A_t} = 1$

$$1.8 \le \frac{v_{wo}}{v} \le 12 \quad \text{if} \quad \frac{A_o}{A_t} \ne 1$$

$$0.893 \le \frac{A_o}{A_t} \le 1.232$$

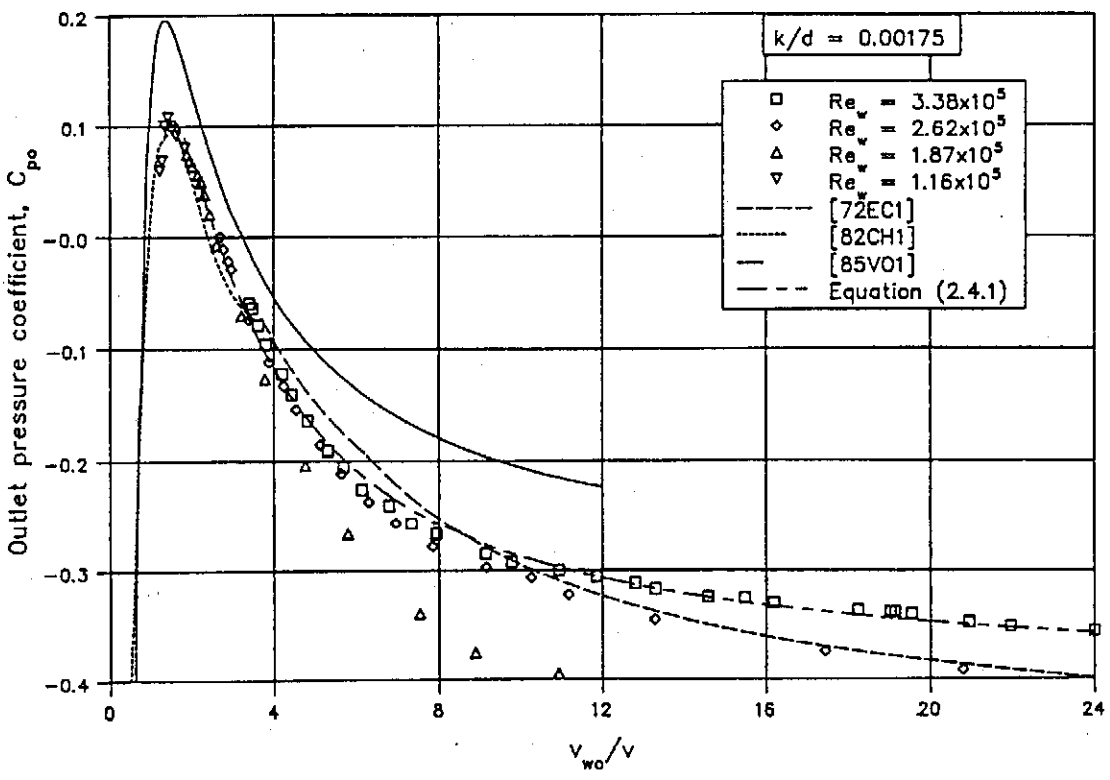

Figure 2.4.2: C_{po} for a cylindrical cooling tower outlet.

The effect of the cooling tower shell on the outlet pressure coefficient was determined by attaching a steel ring onto the outlet of the model. The inner diameter of the ring was equal

to the outlet diameter of the tower while the outer diameter was 112% larger. The situation is therefore similar to that of a jet issuing into a free stream. The results are shown in figure 2.4.3 and are compared with that of Dibelius [79DI1] who did a theoretical analysis for a similar configuration. The results suggest that the static pressure distribution round the outside of the shell tends to decrease the static pressure inside the tower and will therefore increase the tower draft.

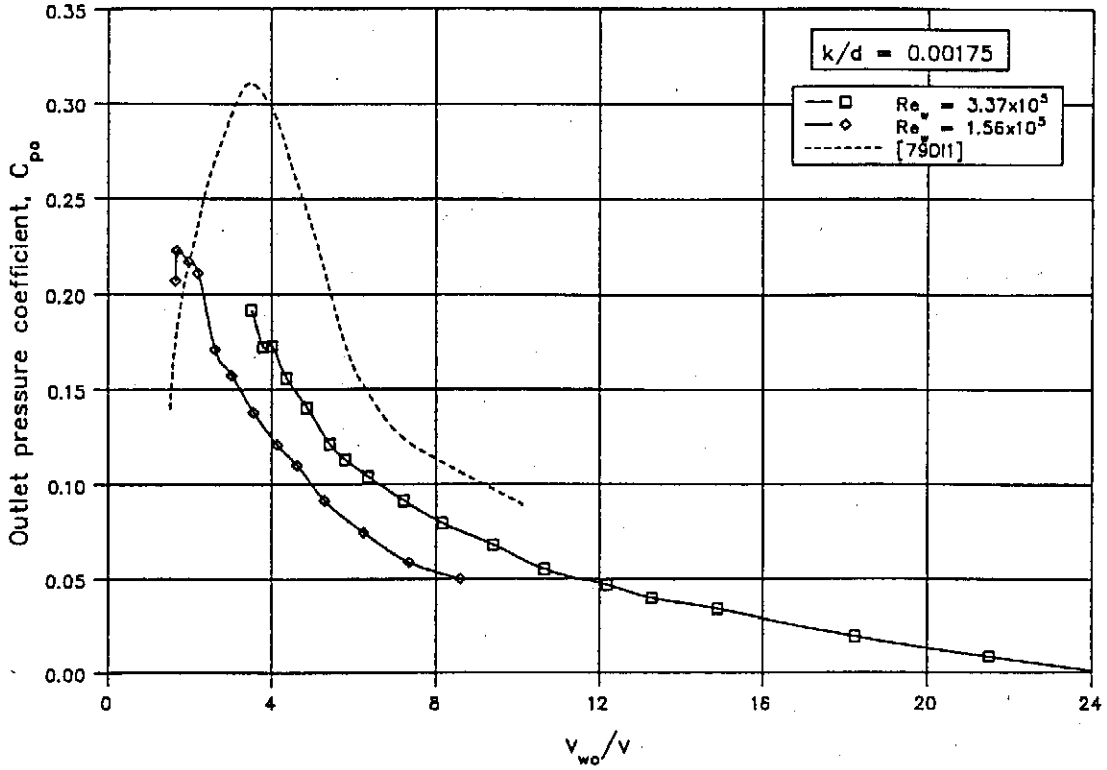

Figure 2.4.3: Outlet pressure coefficient for a jet issuing in a free stream.

With isothermal model tests, the effect of the wind on the inlet and outlet of the tower is normally tested separately and it is assumed that the wind effect on the tower outlet is independent of that at the inlet and vice versa. In section 2.3 it is shown that the wind effect at the inlet causes a non-uniform velocity distribution in the tower. A similar velocity distribution was modelled with the aid of a flow resistance with a non-uniform loss coefficient placed one diameter from the outlet edge inside the model with the resultant velocity distribution shown in figure 2.4.4. It is found however, that this velocity distribution has no effect on the outlet pressure coefficient. By visualizing the flow in the tower with smoke, it was furthermore found that the wind effect on the outlet of the tower has very little effect on the flow pattern in the tower [85VO1], thus it is unlikely that the former will have any effect on the inlet. Buxmann [86BU1] and Ruscheweyh [82RU1] investigated the influence of the tip shape of the tower on the tower draft and both found that for high wind speeds a divergent outlet shape has the most favourable characteristics.

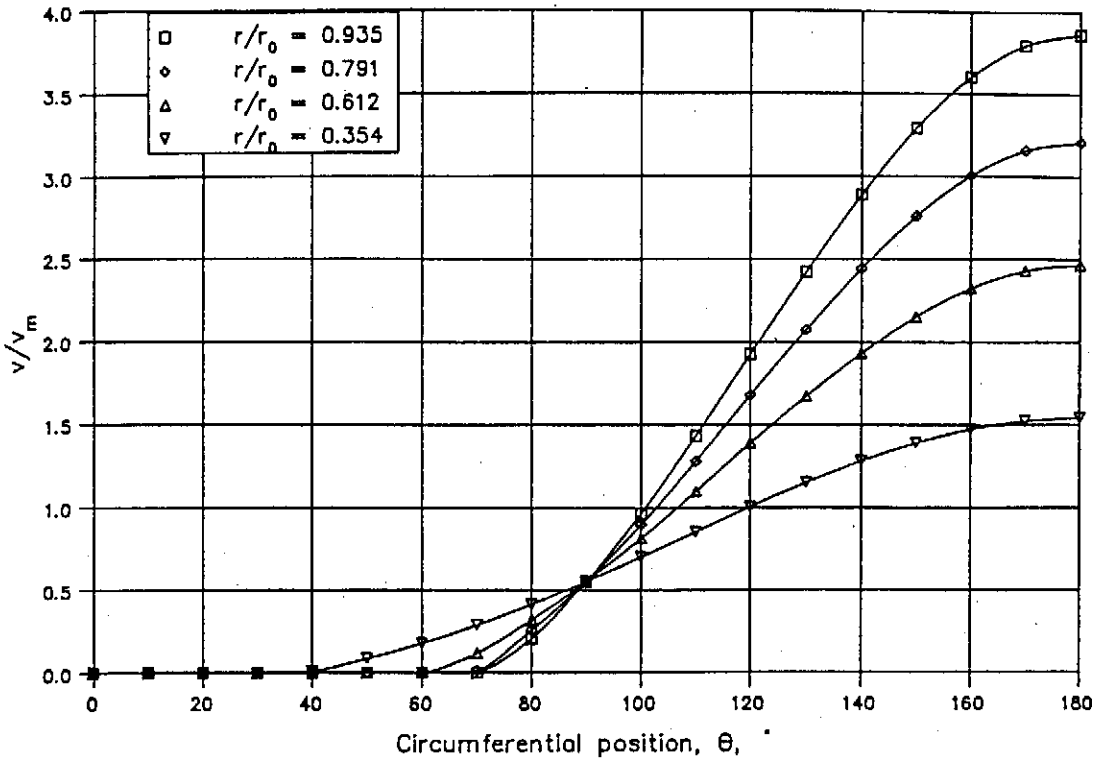

Figure 2.4.4: Velocity distribution inside tower above the non-uniform flow resistance.

2.5: Prediction of the wind effect on a cooling tower with a horizontal arrangement of the heat exchangers.

By using the results obtained with the experimental tests, the rise of the outlet water temperature of a cooling tower for a given heat rejection rate can be calculated for different wind speeds. For this purpose, equations (2.2.1), (2.3.3), (2.3.4) and (2.4.1) were employed in a computer program, NCHOR, which was developed to determine the operating point of any given cooling tower with a horizontal arrangement of the heat exchangers. This is accomplished by following an iterative procedure to obtain the value of the air mass flow rate through the tower that will satisfy both the energy and draft equations. With a known air mass flow rate and rise in the air temperature, the heat rejection rate of the tower can be calculated. If however, the amount of heat rejected by the tower has to be kept constant for different atmospheric conditions, the corresponding water inlet temperature can also be obtained with the program. This is done by introducing another iterative procedure using an interval halving search method for finding the correct water inlet temperature.

In the computer program the wind effects on the energy and draft equations is considered separately. For any given air mass flow rate, m_a, through the tower, the energy transferred to the air stream is calculated by

$$Q_a = m_a \, c_{pa34} \, \Delta T_a \, \alpha_Q = m_a \, c_{pa34} \, (T_{a4} - T_{a3}) \, \alpha_Q \qquad (2.5.1)$$

with the air velocity and the air outlet temperature, T_{a4}, considered to be uniform. By applying equation (2.3.3) the reduction in the efficiency of the heat exchanger due to the velocity distribution is calculated.

In Appendix B two different proposals are made for calculating the air outlet temperature to be used in the draft equation but they will not be repeated here. It should be noted that the air temperature used in the draft equation will always be less than the air outlet temperature which satisfies the energy equation where a uniform velocity profile through the heat exchanger was assumed.

By using the above mentioned computer code, the wind influence on a natural draft hyperbolic concrete cooling tower was calculated for different wind speeds with the results shown in figure 2.5.1. The following data is also available.

Ambient conditions:

Air temperature at ground level	T_{a0}	= 15.6 °C
Wetbulb temperature at ground level	T_{wb}	= 0°C (essentially dry air)
Atmospheric pressure at ground level	p_{a0}	= 84600 N/m^2

Ambient temperature gradient, -0.00975 K/m from ground level.

Cooling tower specifications:

Tower height	H_5	= 120 m
Tower inlet height	H_3	= 13.67 m
Tower inlet diameter	d_3	= 78.3233 m
Tower outlet diameter	d_5	= 58.0 m
Inlet taper angle of tower	$2\theta_c$	= 20 °
Number of tower supports	n_{ts}	= 60
Length of tower supports	l_{ts}	= 15.79 m
Diameter of tower supports	d_{ts}	= 0.5 m
Drag coefficient of tower supports	C_{Dts}	= 2.0
Effective pressure loss coefficient of tower supports	K_{tse}	= 1.0

Finned tube bundle specifications:

Hydraulic diameter of tube	d_e	= 0.0216 m
Relative surface roughness	ϵ/d_e	= 5.24x10^{-4}
Inside area of tube / unit length	A_{ti}	= 0.0679 m
Inside cross-sectional flow area	A_{ts}	= 3.664x10^{-4} m^2
Length of finned tube	L_t	= 15 m
Number of tube rows	n_r	= 4
Number of tubes per bundle	n_{tb}	= 154
Number of water passes	n_{wp}	= 2
Number of bundles	n_b	= 142
Total frontal area of bundles	A_{fr}	= 4818.06 m^2
Ratio of minimum to free stream flow area	σ	= 0.433

The loss coefficient for isothermal normal flow conditions across the heat exchanger bundles can be expressed as:

$$K_{he} = 1383.94795\ Ry^{-0.332458} \qquad (2.5.2)$$

The overall heat transfer coefficient of the heat exchangers is approximated by

$$UA = a_{UA} Ry^{0.46} \tag{2.5.3}$$

The characteristic heat transfer parameter, as defined by Kröger [86KR1], is given by

$$Ny = 383.61731\ Ry^{0.523761} \tag{2.5.4}$$

It is assumed that the wind profile can be described by the power law, with the exponent b in equation (1.1.1) equals to 0.2. The amount of heat rejected by the tower is kept constant at a value of 354.39 MW for all wind speeds while the water mass flow rate through the tower, m_w = 4390 kg/s. In appendix G a complete sample calculation is done for a wind speed of 6 m/s at a height of 10 m AGL for both perfect and no mixing of the air in the tower.

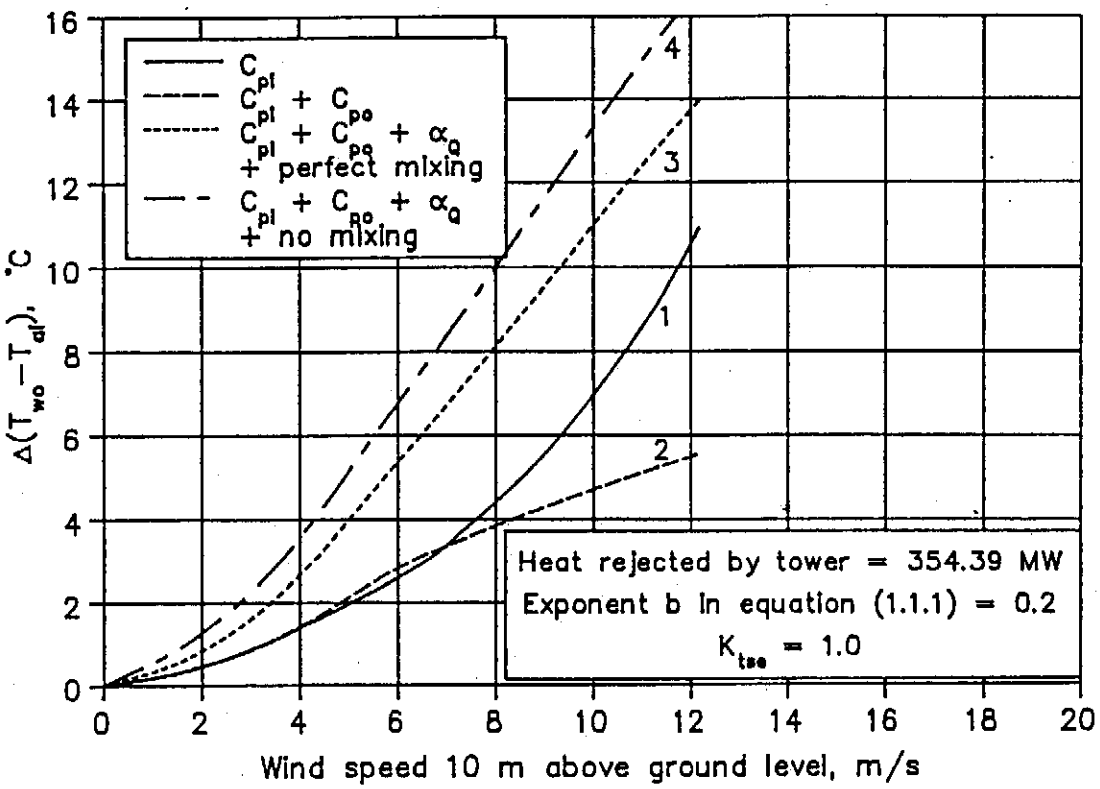

Figure 2.5.1: Rise in the approach temperature of a tower as a function of the wind velocity 10 m AGL.

The curves shown in figure 2.5.1 can be compared with similar results as presented by Buxmann [86BU1]. With the first curve shown in the figure, only the suction effect of the wind on the tower inlet was considered. As the wind speed increases the wind effect on the

inlet causes the available tower draft to reduce and therefore the approach temperature of the tower increases to maintain the same heat rejection rate of the tower.

With the second curve, the wind effect on the tower outlet is also included. For wind speeds higher than 7 m/s the wind has a favourable effect on the tower and therefore the rise in the approach temperature of the tower reduces while for wind speeds between 4 and 7 m/s the tower performance decreases.

In the third and fourth curve, the non-uniform velocity profile through the heat exchangers is also included which causes a reduction in the effectiveness of the heat exchangers as well as a non-uniform temperature distribution in the tower. In the third curve the air is assumed to be perfectly mixed while in the fourth curve no mixing is assumed with the correct solution for the problem being somewhere between the two.

In figure 2.5.2 the same lines shown in the previous figure are based on the wind velocity measured at the tower outlet height. Because the wind velocity increases for an increase in height, the tower appears to be less sensitive to cross-winds when the rise of the approach temperature is shown as a function of the wind speed at higher elevations.

In figure 2.5.3 the ratio of the average air mass flow through the tower with wind to the mass flow rate without wind is shown for different wind speeds. The figure shows that the reduction in the mean air mass flow rate through the tower is primarily due to the suction effect of the wind on the inlet.

Significant changes in the wind effect on the tower are found for a variation in the tower height. Due to the additional draft, higher towers tend to be less affected by cross-winds than those with a smaller height. Figure 2.5.4 shows the change in the approach temperature for a constant wind speed and water mass flow rate as a function of the tower height. The cooling capacity of the tower was kept at a constant value of 354.39 MW by varying the initial water temperature for each value of the tower height.

Further calculations revealed that for the heat exchangers arranged horizontally (no A-frames) in the inlet cross-section of the tower, the wind influence on the tower increases for an increase in the heat rejection rate of the tower as shown in figure 2.5.5.

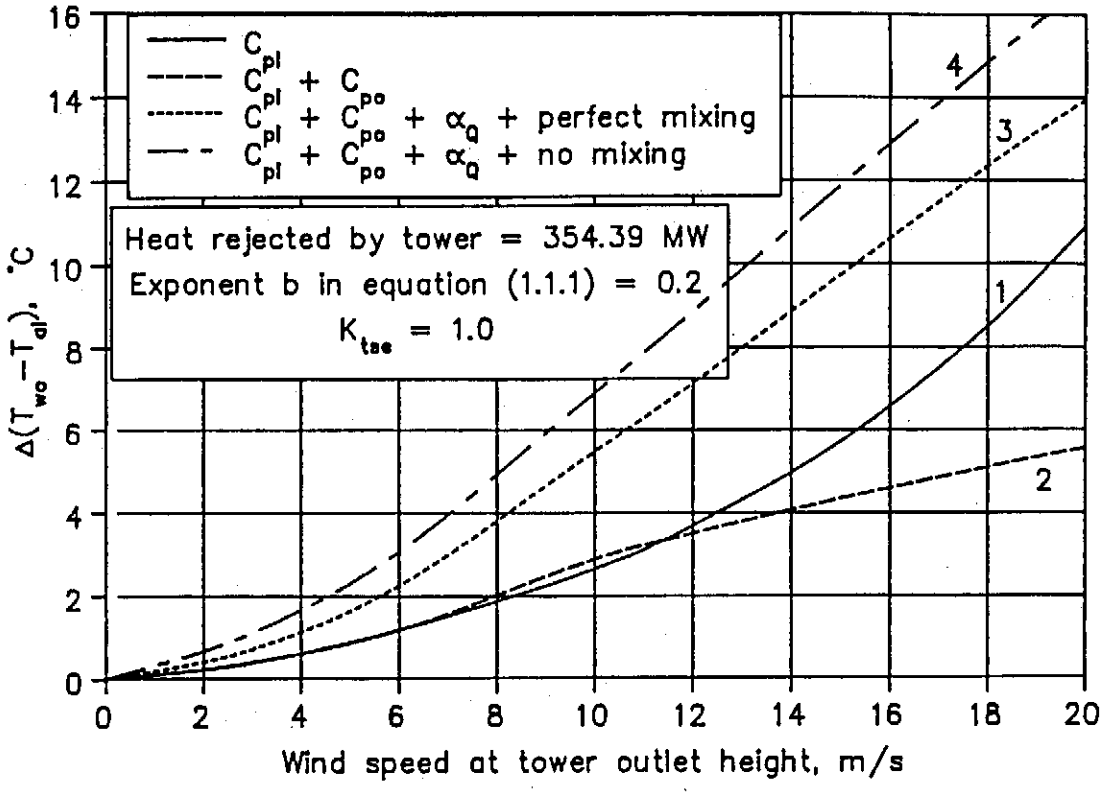

Figure 2.5.2: Rise in the approach temperature of a tower as a function of the wind velocity at the tower outlet height.

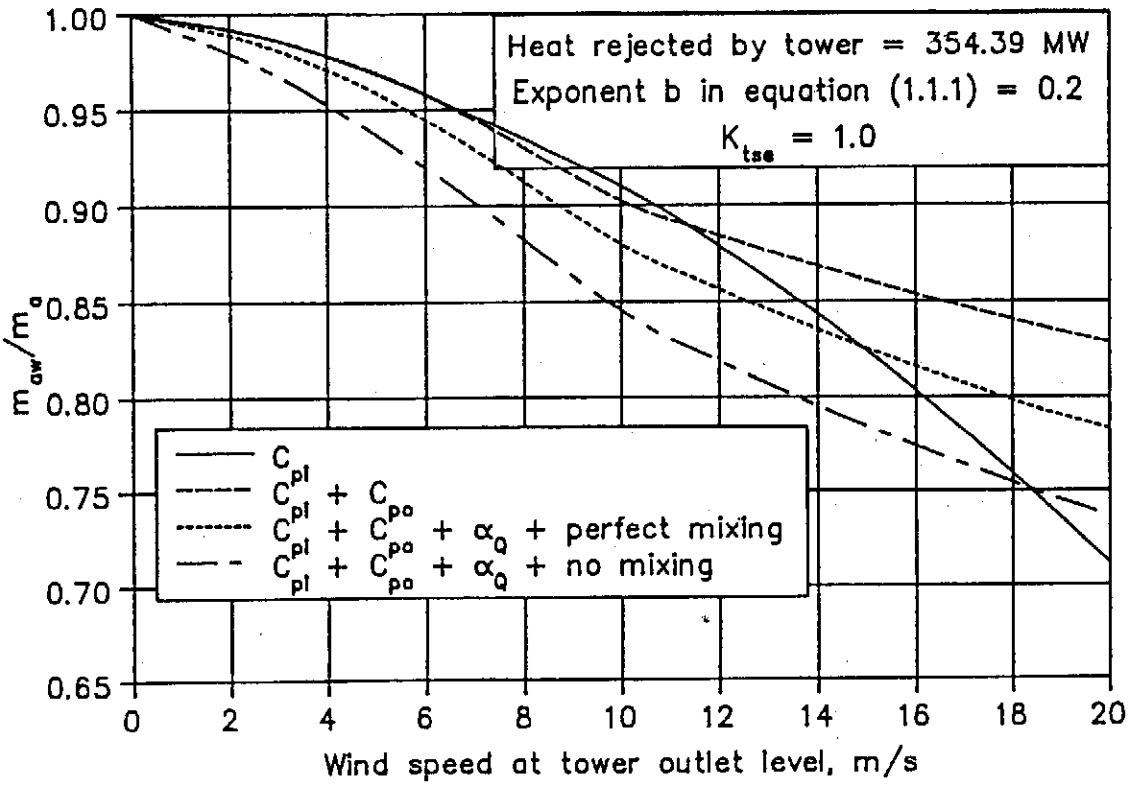

Figure 2.5.3: Reduction of the mean air mass flow rate through the tower as a result of the wind.

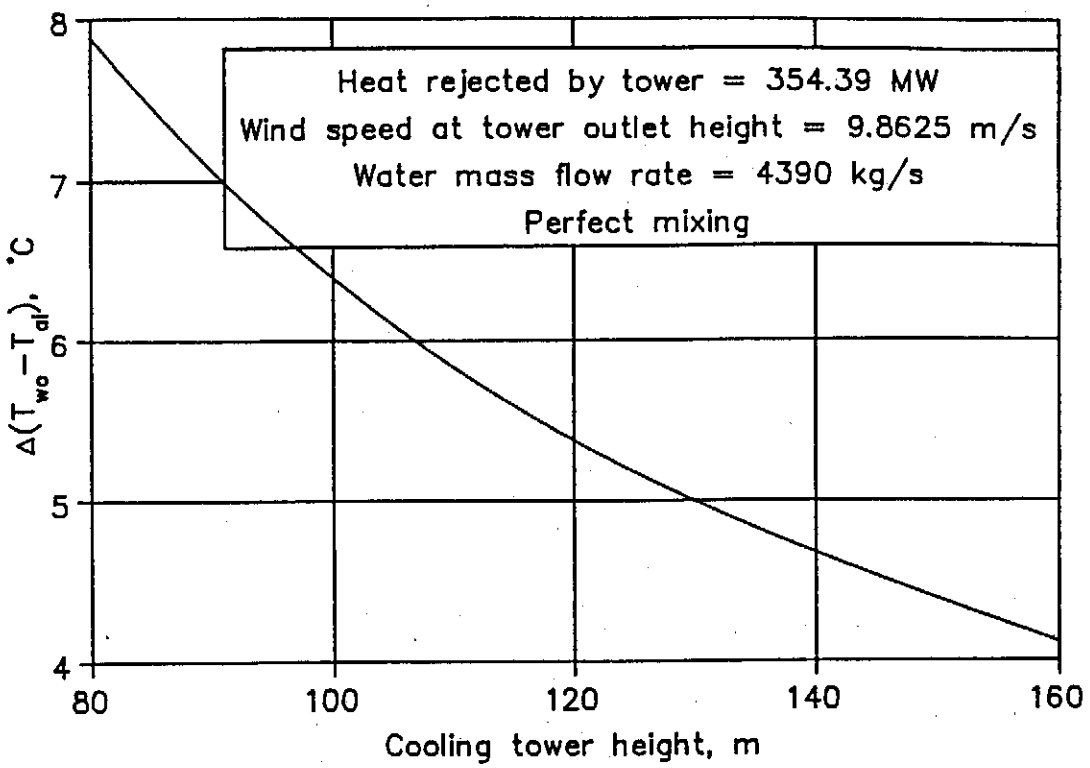

Figure 2.5.4: Increase in the approach temperature as a function of the tower height.

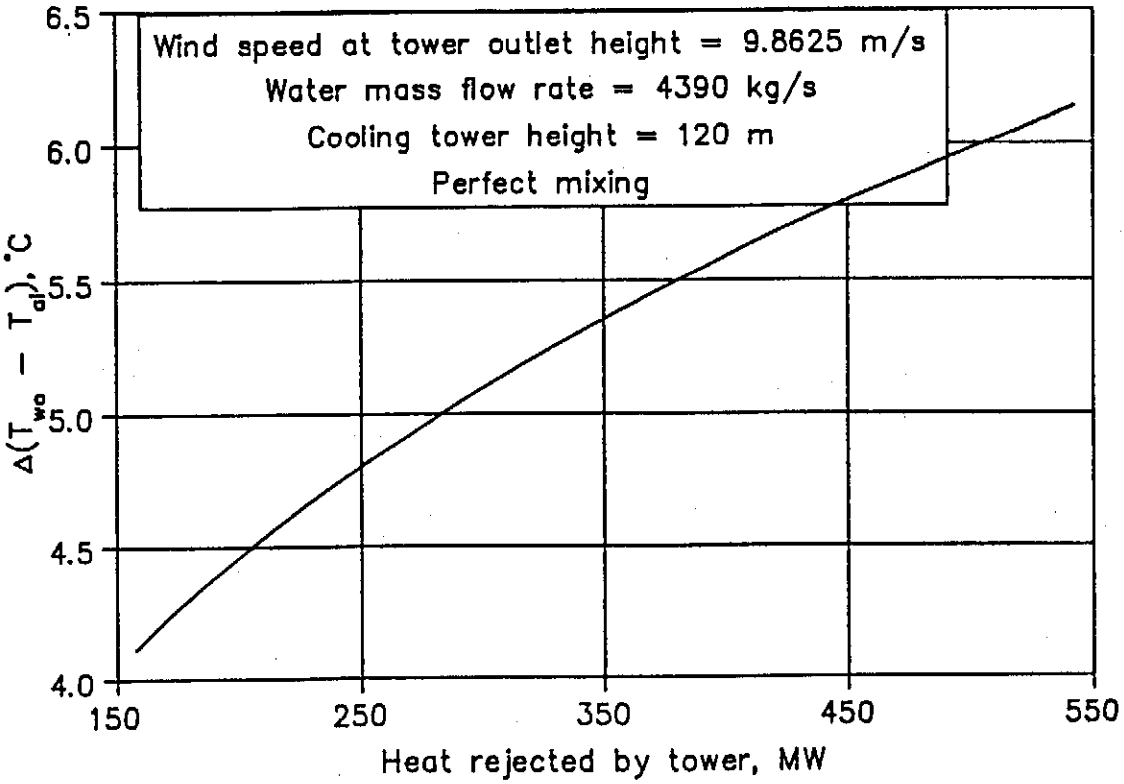

Figure 2.5.5: Variation in the approach temperature as a function of the heat rejected by the tower.

2.6: The effect of various windbreaking devices on the wind influence on the performance of a dry-cooling tower.

According to the results obtained in model tests, the greatest action of the wind on a natural draft cooling tower is the suction effect at the inlet of the tower. The latter tends to decrease the tower draft and therefore reduces the mean air mass flow through the tower. Thus, in an attempt to reduce the negative action of the wind on a tower, it will be most profitable to install windbreak devices in the inlet of the tower. The latter have to be positioned in such a way that the dynamic pressure of the incoming wind is used to increase the static pressure below the heat exchanger and thereby counteract the effect of the separation region.

The first arrangement which was tested was essentially that of the Grootvlei 5 tower but the A-frames were not represented. In this tower the heat exchangers in a horizontal arrangement are installed on two different elevations with the deltas in the centre of the tower positioned approximately five meters below the rest of the bundles. The ratio of the frontal area of the bundles on the lower elevation to the total frontal bundle area of all the heat exchangers in the tower is approximately 0.32. In the model this arrangement was modelled by means of a circular piece of honeycomb, 20 mm thick and 113 mm in diameter, positioned below the screen layers.

In figure 2.6.1 the inlet pressure coefficient of this arrangement is given for different wind Reynolds numbers. In comparison with that shown in figure 2.2.15, it is found that the latter arrangement causes a reduction of roughly 20% in the value of C_{pi}.

In figure 2.6.2 the velocity distribution through the heat exchangers as measured in the model is shown. For higher values of the relative wind velocities, the favourable effect of this arrangement of the heat exchangers in the upwind side of the tower can clearly be seen, while almost no change in the velocity distribution is observed in the lee side of the tower if compared to the results shown in figure 2.3.1. In figure 2.6.3 the heat transfer correction factor, α_Q, is shown as obtained with and without a wind profile.

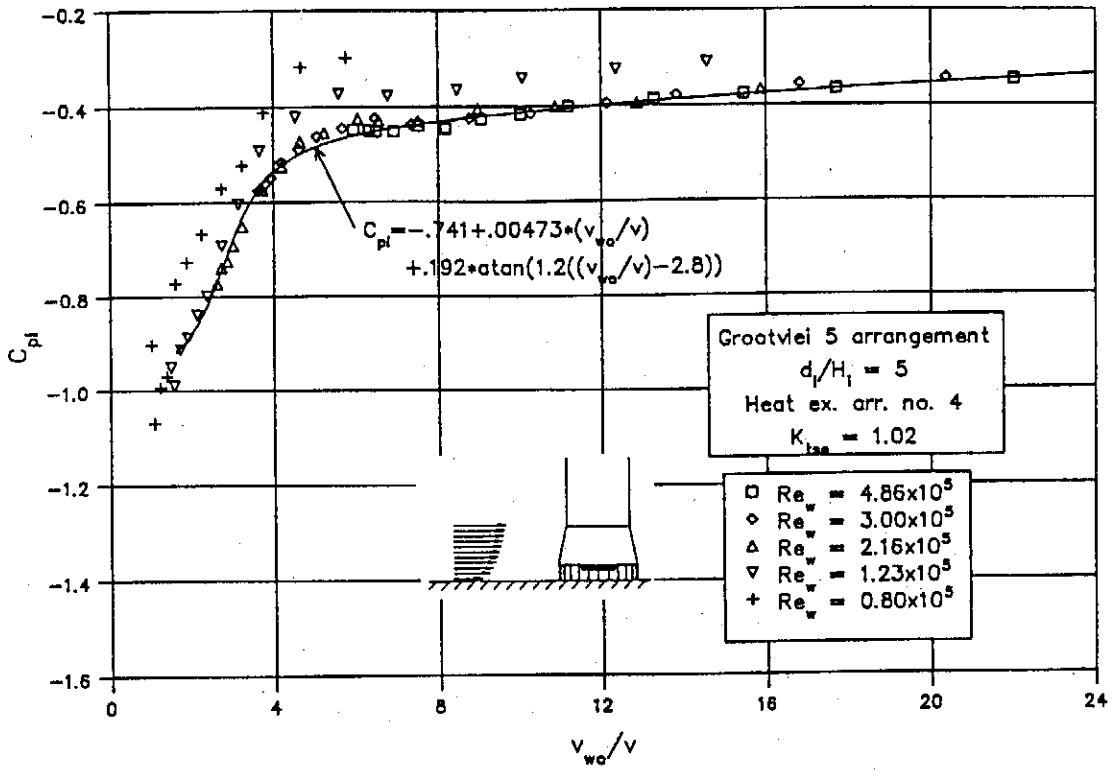

Figure 2.6.1: C_{pi} for the Grootvlei 5 tower.

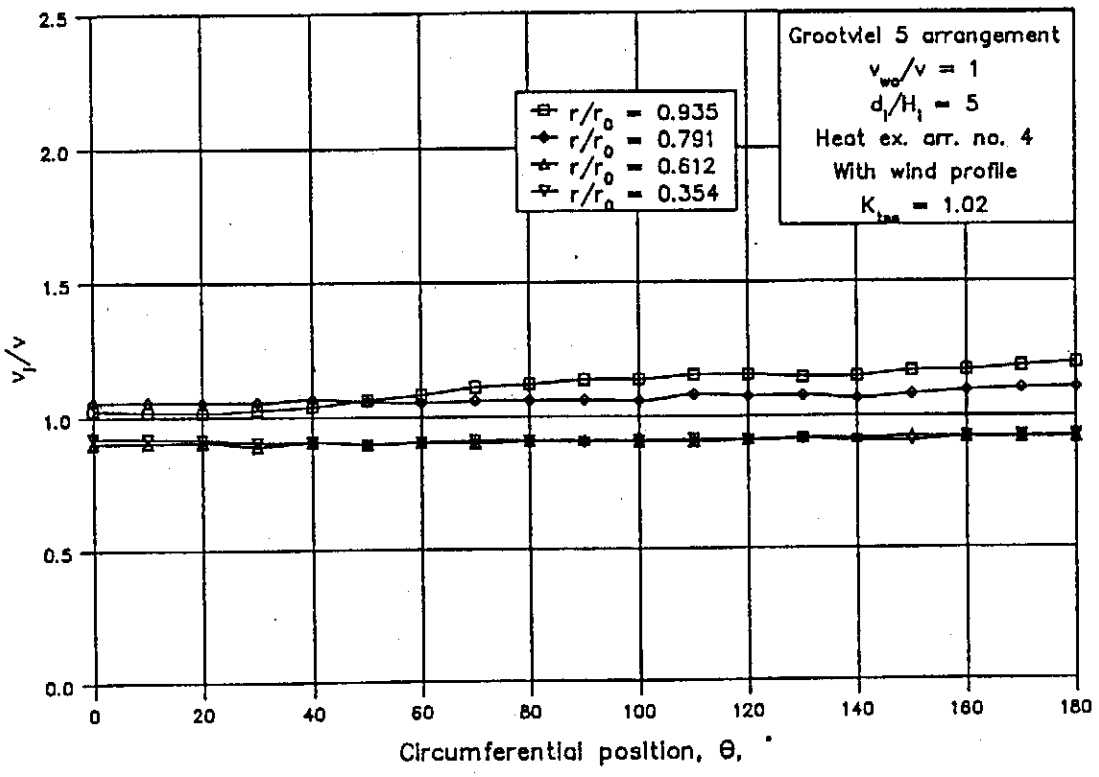

(a)

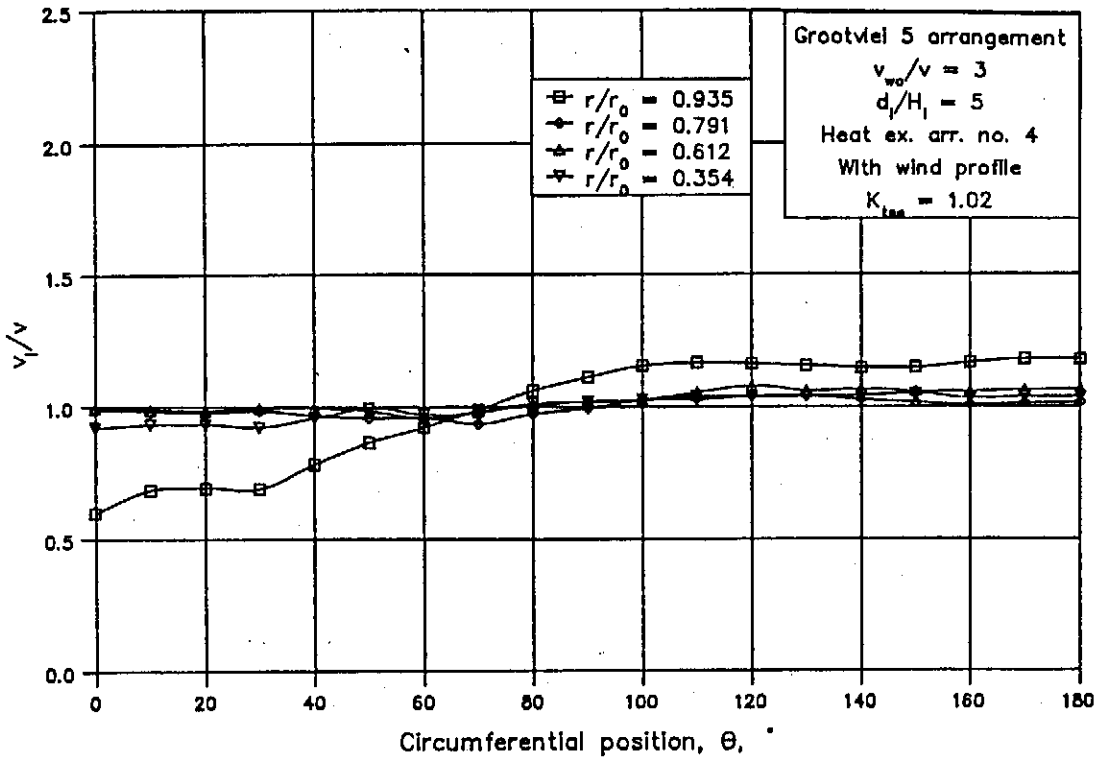
Grootviel 5 arrangement
v_{wo}/v = 3
d_i/H_i = 5
Heat ex. arr. no. 4
With wind profile
K_{tke} = 1.02
r/r_o = 0.935
r/r_o = 0.791
r/r_o = 0.612
r/r_o = 0.354
v_i/v
Circumferential position, θ, °

(b)

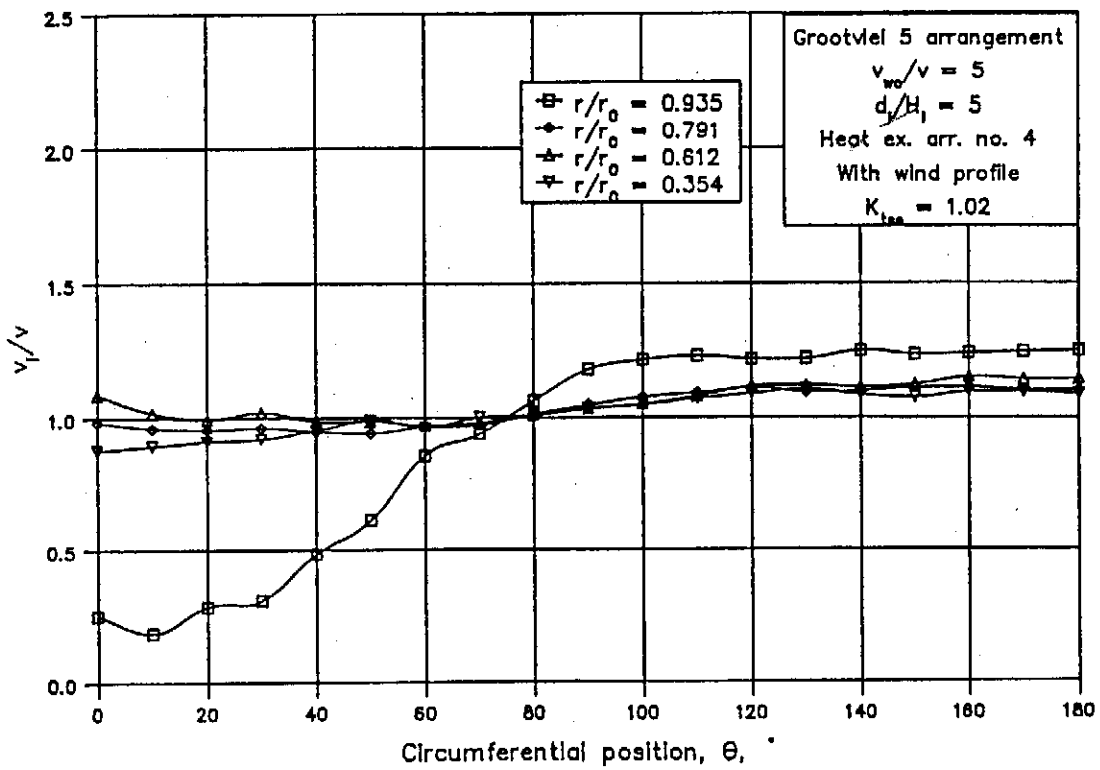
Grootviel 5 arrangement
v_{wo}/v = 5
d_i/H_i = 5
Heat ex. arr. no. 4
With wind profile
K_{tke} = 1.02
r/r_o = 0.935
r/r_o = 0.791
r/r_o = 0.612
r/r_o = 0.354
v_i/v
Circumferential position, θ, °

(c)

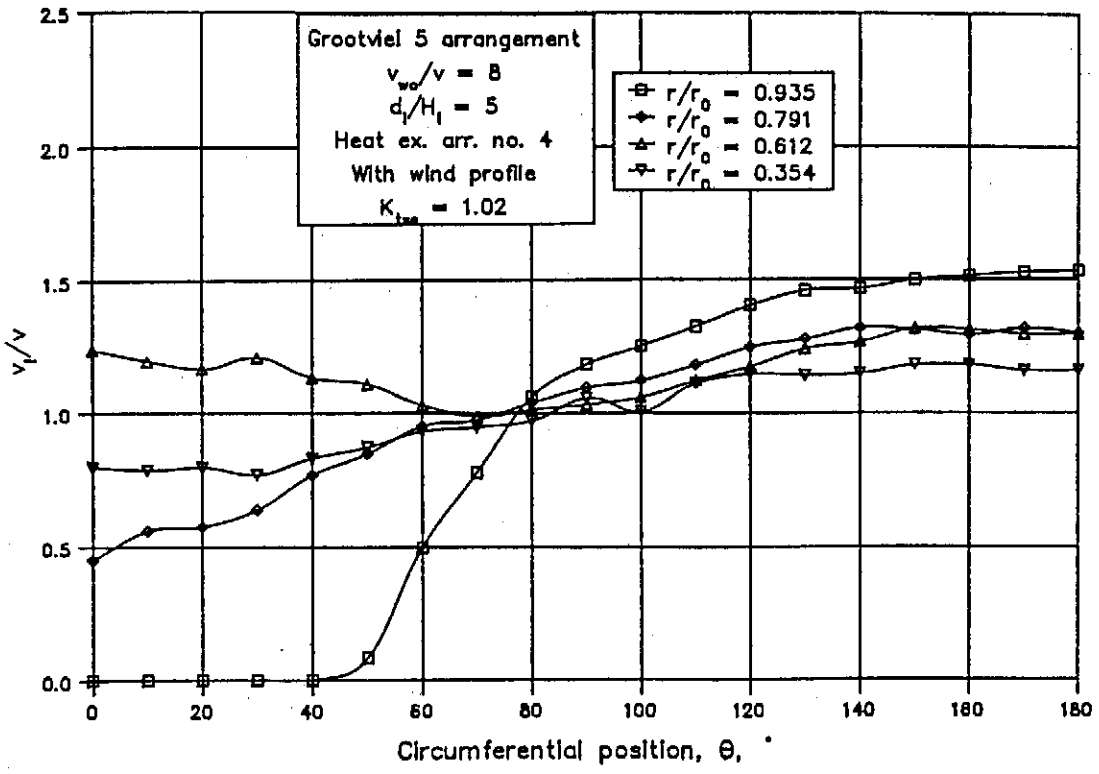
Grootviel 5 arrangement
v_{wo}/v = 8
d_l/H_l = 5
Heat ex. arr. no. 4
With wind profile
K_{tsa} = 1.02
r/r_o = 0.935
r/r_o = 0.791
r/r_o = 0.612
r/r_o = 0.354
v_l/v
Circumferential position, θ, °

(d)

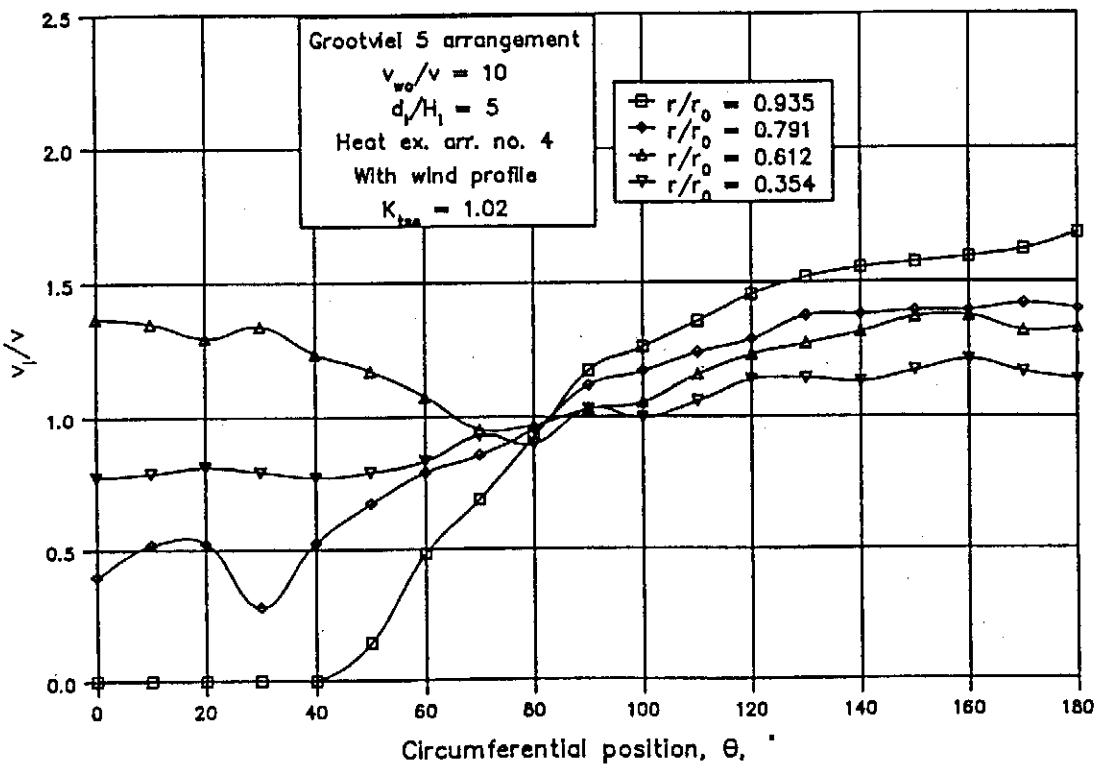
Grootviel 5 arrangement
v_{wo}/v = 10
d_l/H_l = 5
Heat ex. arr. no. 4
With wind profile
K_{tsa} = 1.02
r/r_o = 0.935
r/r_o = 0.791
r/r_o = 0.612
r/r_o = 0.354
v_l/v
Circumferential position, θ, °

(e)

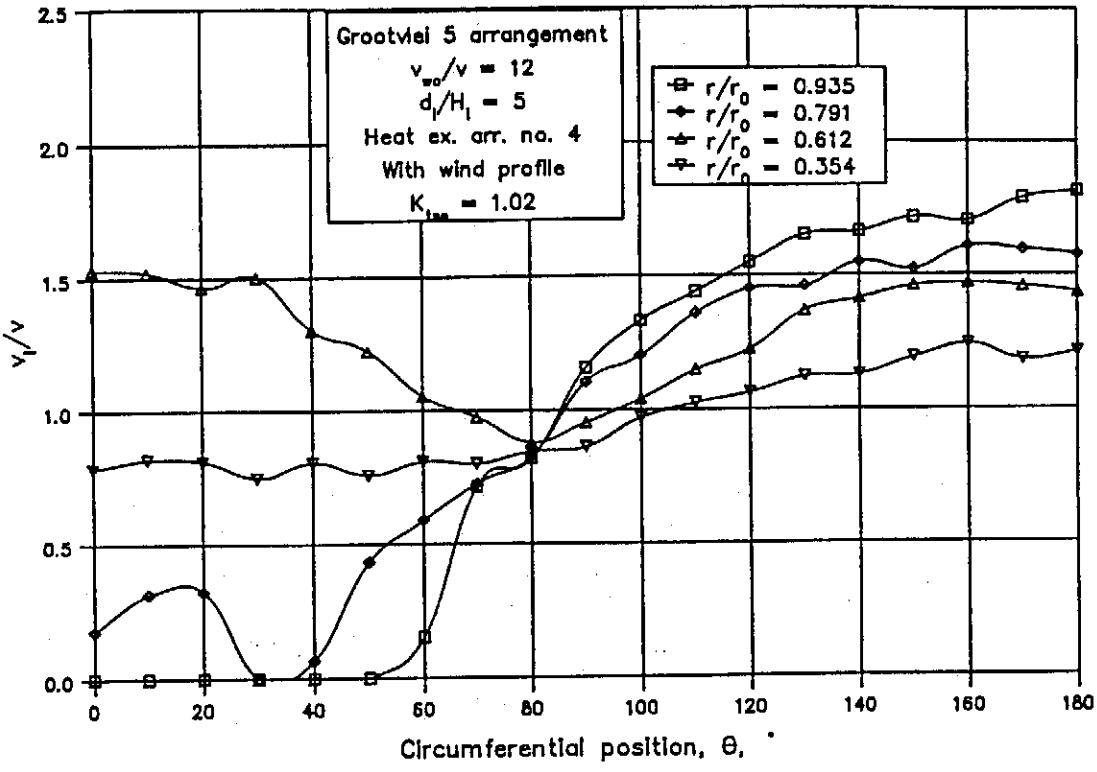

(f)

Figure 2.6.2: Velocity distribution through the heat exchanger of the Grootvlei 5 tower.

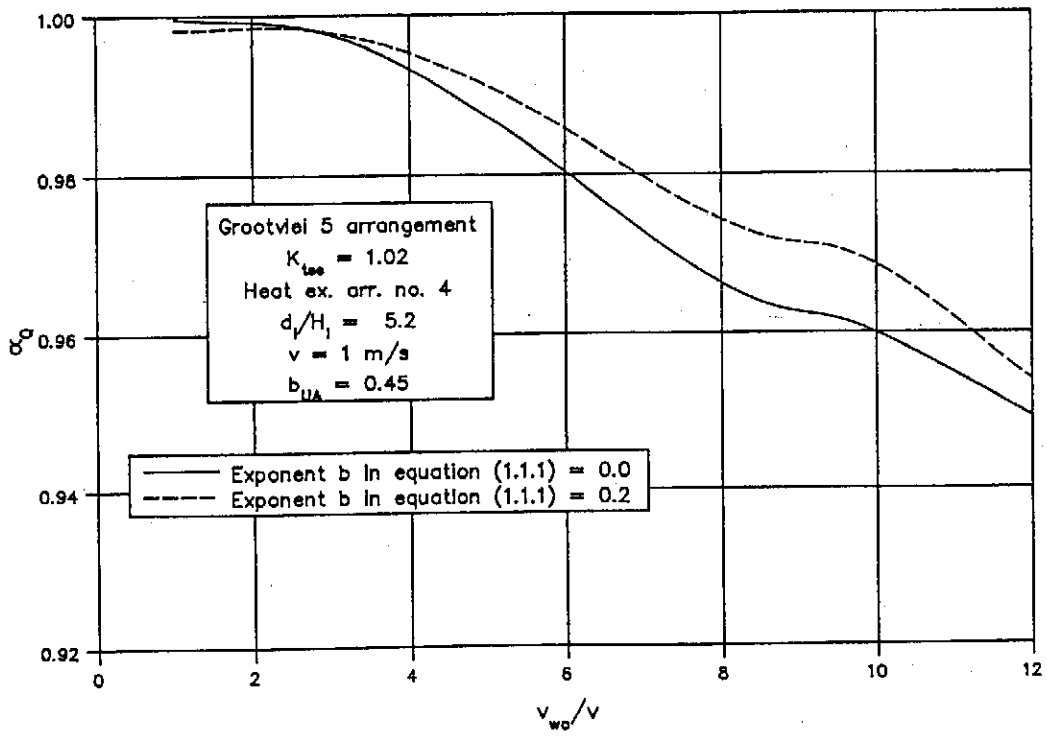

Figure 2.6.3: α_Q for the Grootvlei 5 tower.

Another arrangement which was investigated is that of a solid cylinder positioned below the horizontal heat exchangers in the centre of the tower. The diameter of the cylinder was 45% of the inlet diameter of the tower with the height of the cylinder being equal to the inlet height of the model. In this case only part of the horizontal inlet cross-section of the tower is available for the instalment of bundles. The inlet pressure coefficient for the latter arrangement is shown in figure 2.6.4 and if compared to that shown in figure 2.2.15, a reduction of almost 30% in the value of C_{pi} is observed. The velocity distribution for different relative wind velocities is shown in figure 2.6.5 with the corresponding heat transfer correction factor in figure 2.6.6. It is found that the presence of the cylinder partly counteracts the effect of the separation region on the upstream side of the tower and the velocity distribution through the heat exchangers becomes more uniform.

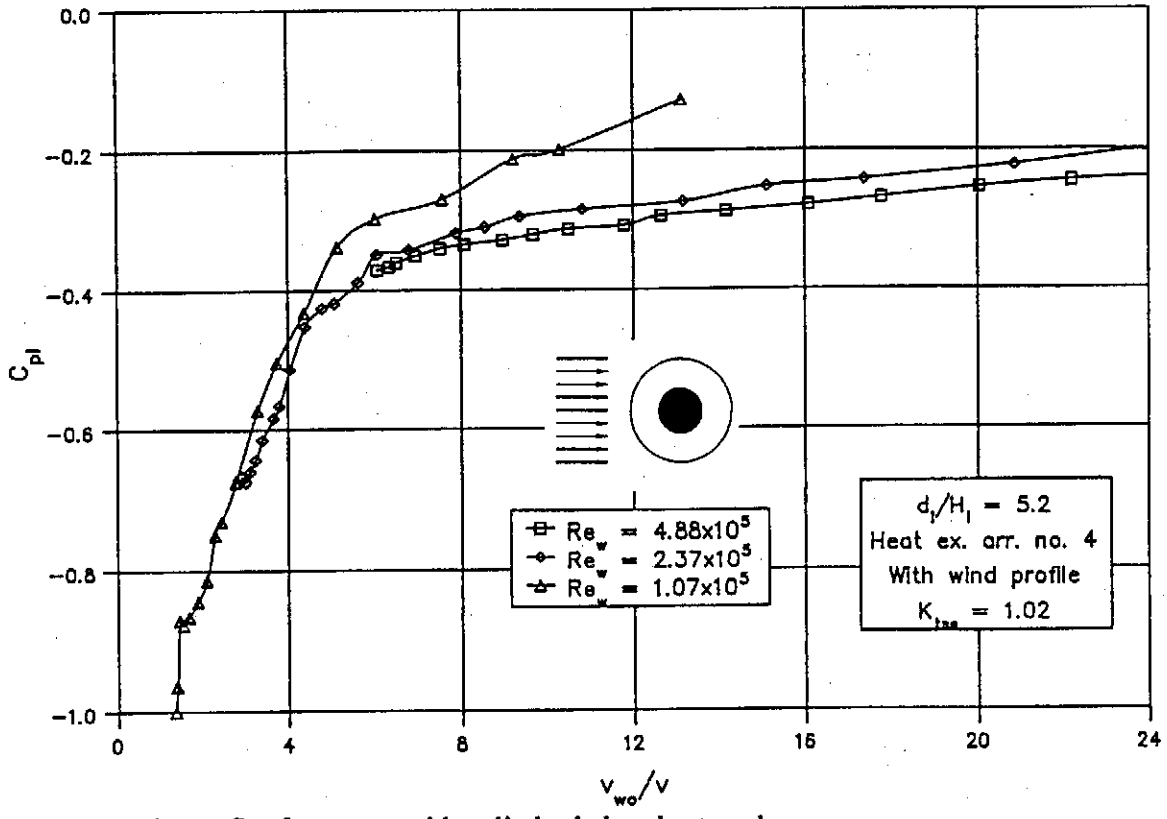

Figure 2.6.4: C_{pi} for tower with cylinder below heat exchangers.

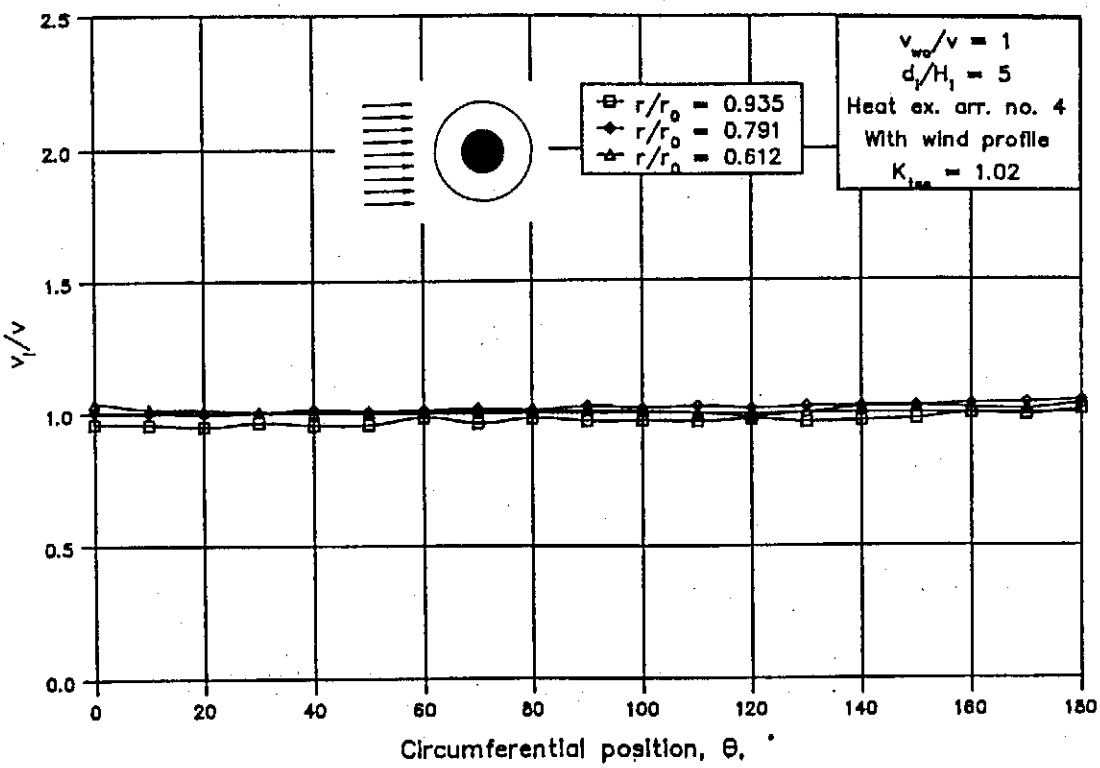
v_{wo}/v = 1
d_1/H_1 = 5
Heat ex. arr. no. 4
With wind profile
K_{1ex} = 1.02
r/r_0 = 0.935
r/r_0 = 0.791
r/r_0 = 0.612
v_1/v
Circumferential position, θ, °

(a)

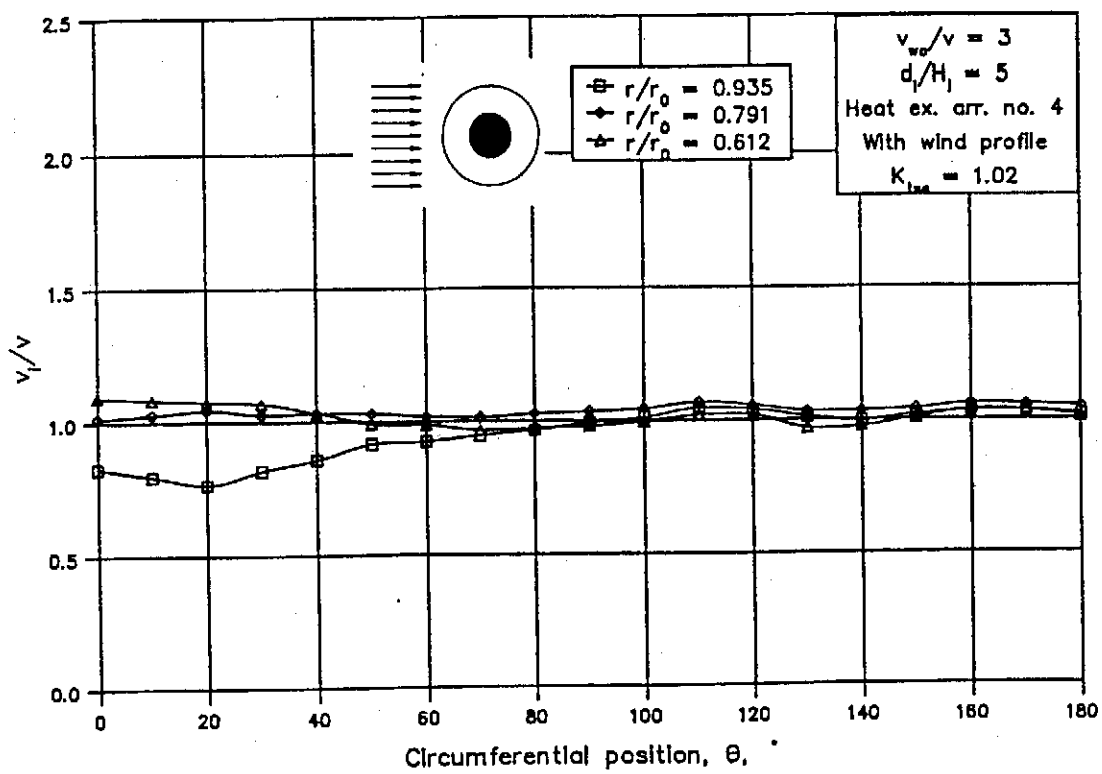
v_{wo}/v = 3
d_1/H_1 = 5
Heat ex. arr. no. 4
With wind profile
K_{1ex} = 1.02
r/r_0 = 0.935
r/r_0 = 0.791
r/r_0 = 0.612
v_1/v
Circumferential position, θ, °

(b)

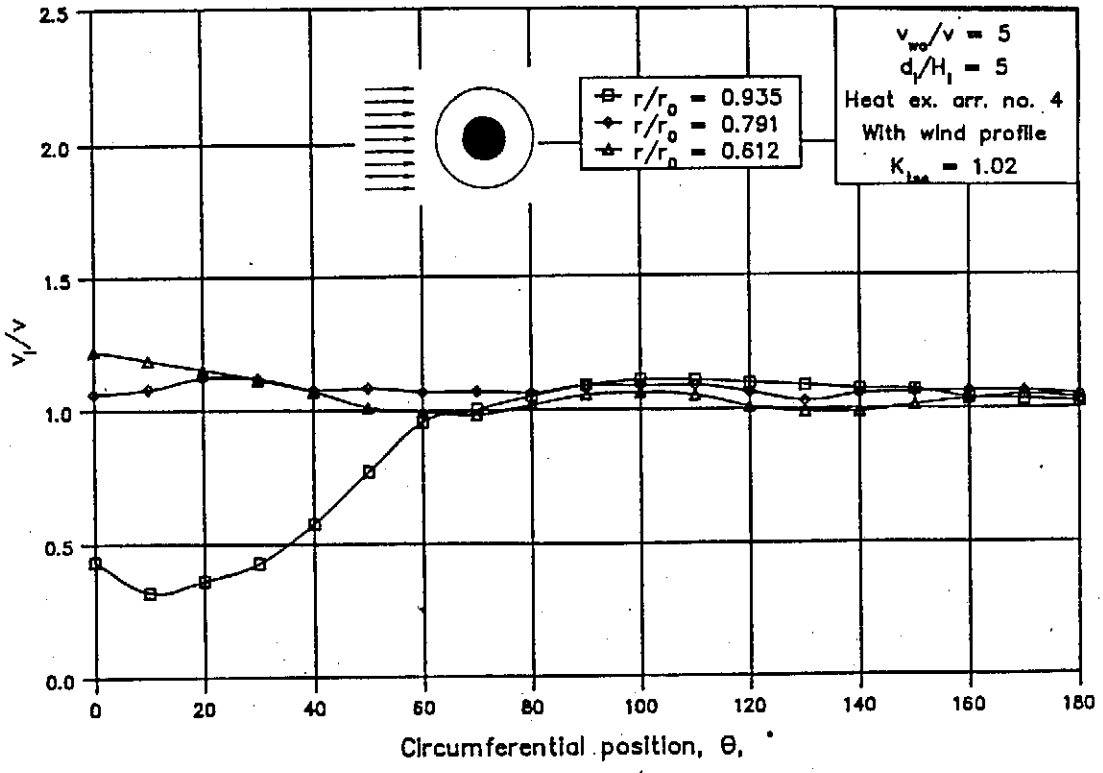
v_{wo}/v = 5
d_i/H_i = 5
Heat ex. arr. no. 4
With wind profile
$K_{t,ex}$ = 1.02
r/r_o = 0.935
r/r_o = 0.791
r/r_o = 0.612
v_i/v
Circumferential position, θ, °

(c)

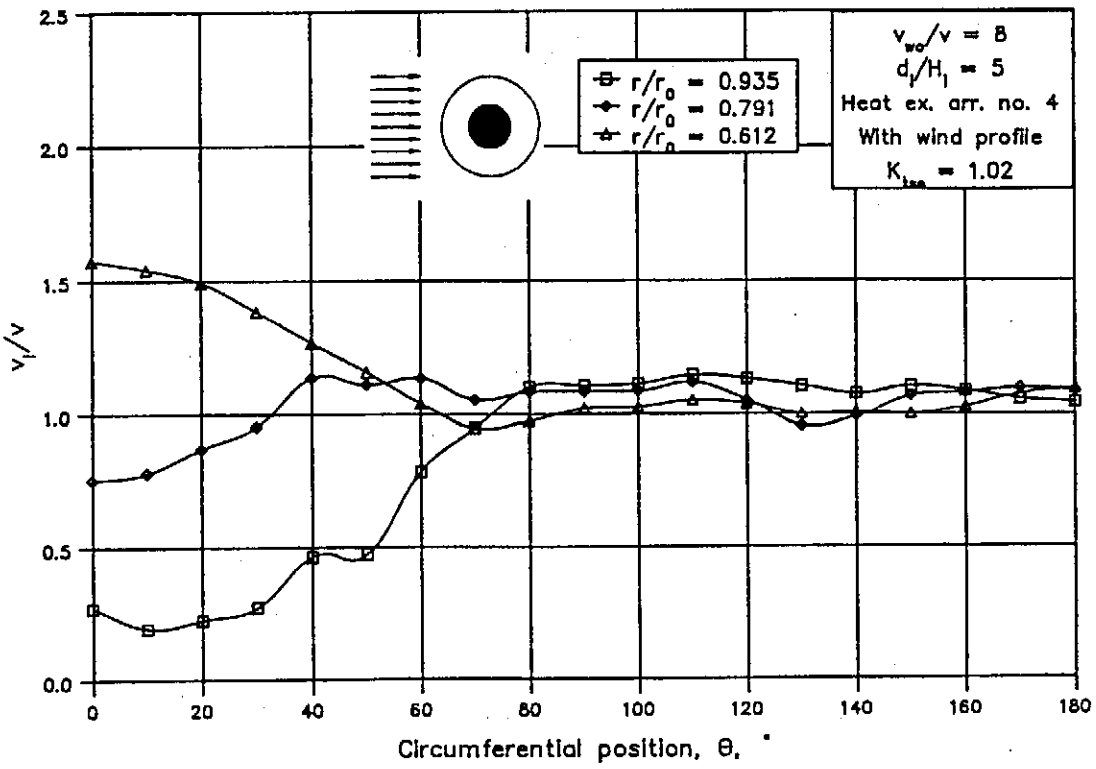
v_{wo}/v = 8
d_i/H_i = 5
Heat ex. arr. no. 4
With wind profile
$K_{t,ex}$ = 1.02
r/r_o = 0.935
r/r_o = 0.791
r/r_o = 0.612
v_i/v
Circumferential position, θ, °

(d)

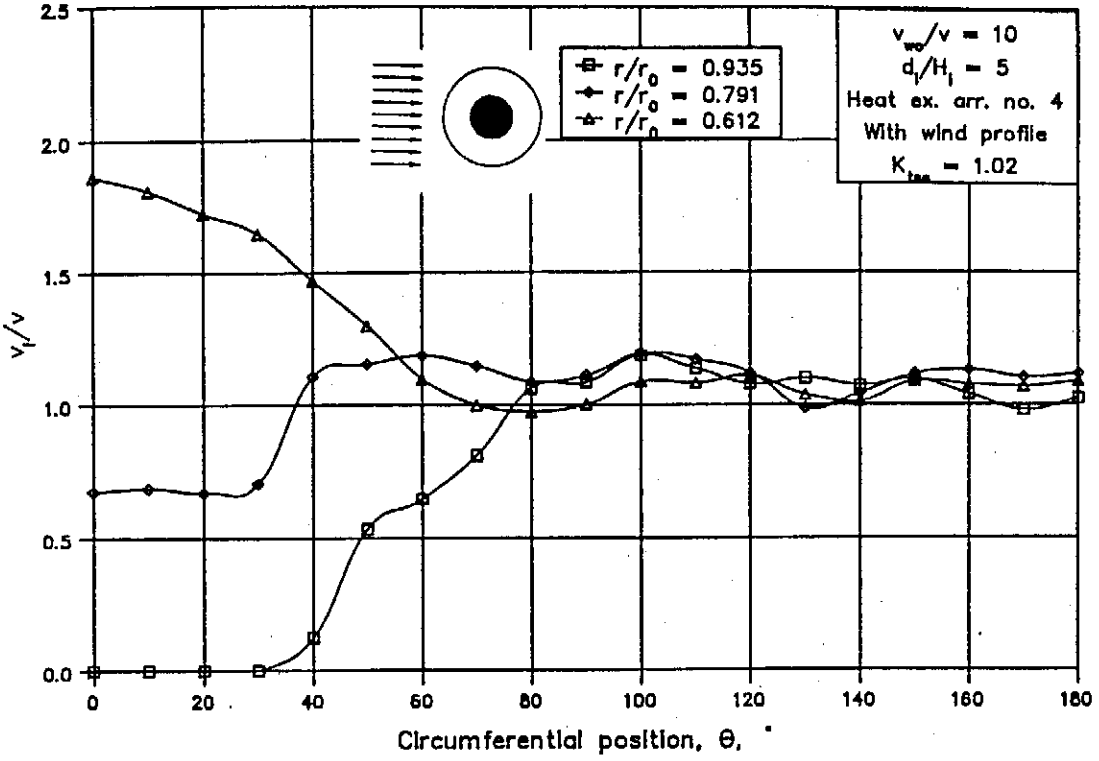

(e)

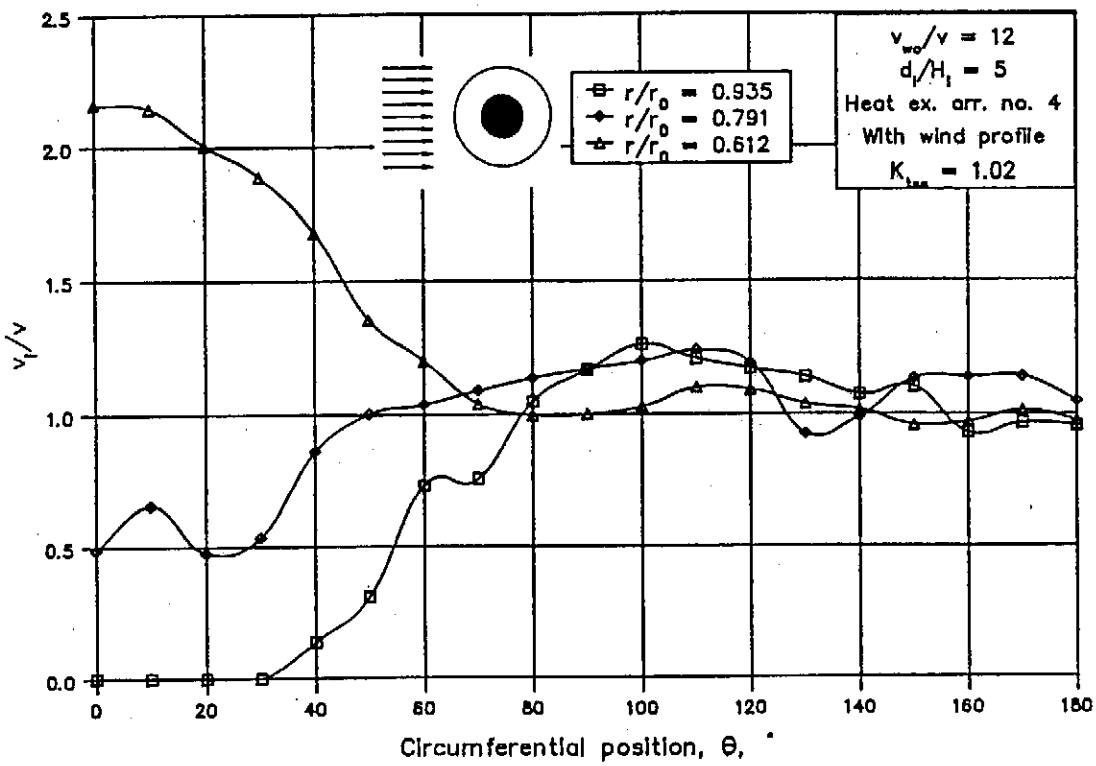

(f)

Figure 2.6.5: Velocity distribution through the heat exchanger with a cylinder positioned below it.

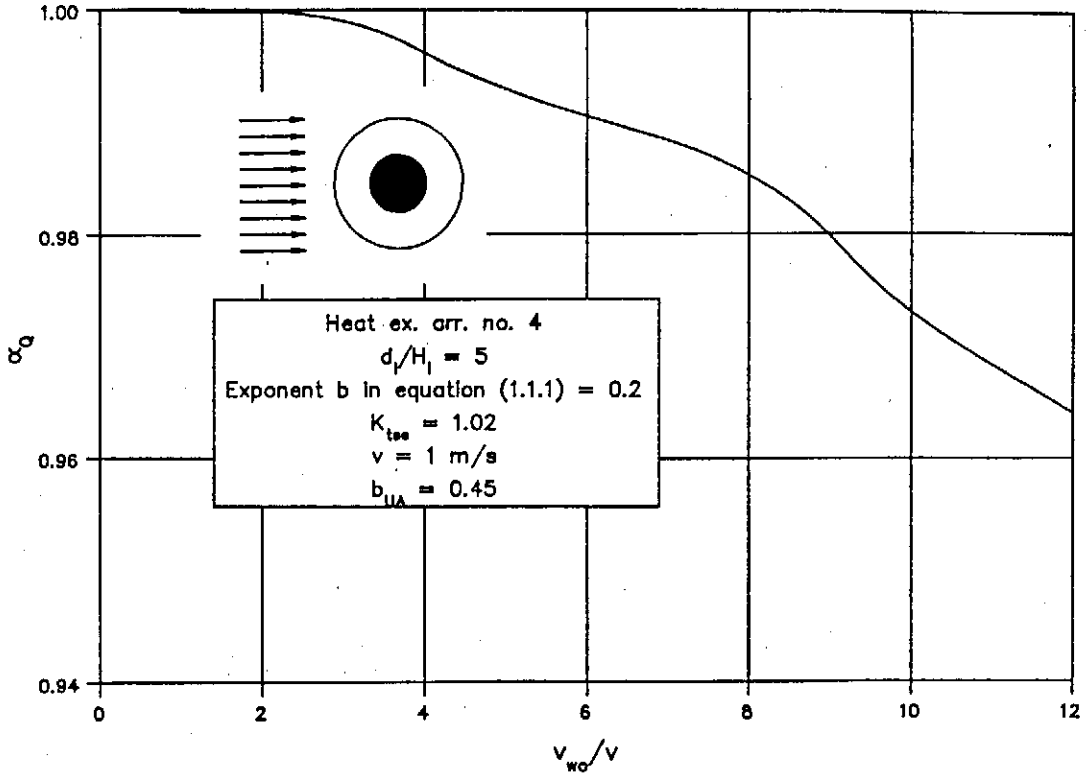

Figure 2.6.6: α_Q for a tower with a cylinder placed below the horizontal heat exchanger.

Further tests revealed that the introduction of windbreak walls under the horizontal heat exchanger causes significant changes in both the value of the inlet pressure coefficient as well as the velocity distribution through the heat exchangers. The height of the walls, arranged in the form of a X, was equal to the inlet height of the tower while the length of the walls was the same as that of the tower diameter. All the tests were performed for a d_i/H_i ratio of 5 and with the horizontal heat arrangement no. 4 (see figure A.1.5) with a fairly high value of the pressure loss coefficient. The tests were furthermore repeated with solid windbreak walls as well as two porous walls having pressure loss coefficients, K_{wall1} and K_{wall2}, as shown in figure 2.6.7. The pressure loss coefficients are based on the normal air velocity through the walls.

It was found that with the present heat exchanger arrangement the windbreak wall with the higher pressure loss coefficient offers the most favourable characteristics. It is however expected that the latter is not only a function of the pressure drop coefficient of the windbreak walls but is also dependent on the ratio of the K_{he} value of the heat exchangers to that of the wall. Thus for towers with lower K_{he} values, the pressure drop coefficient of the walls should be correspondingly less.

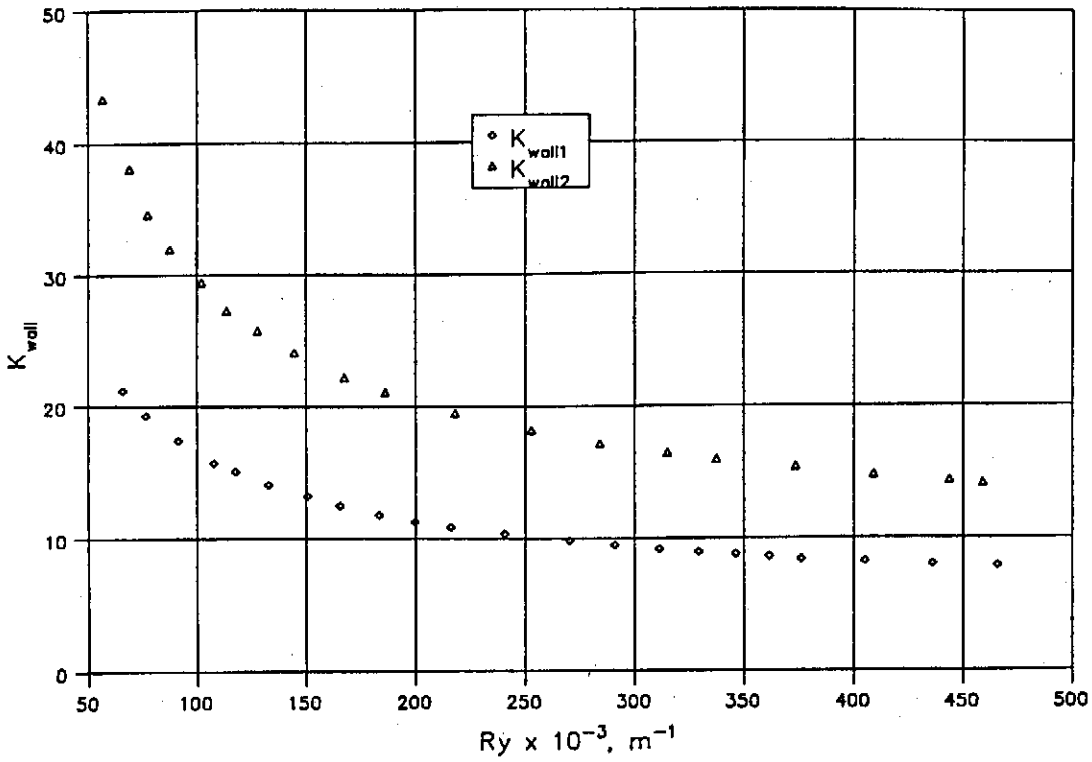

Figure 2.6.7: Windbreak wall pressure loss coefficient.

C_{pi} as obtained with the windbreak wall, K_{wall1}, installed below the heat exchangers is shown in figure 2.6.8 for two different wind directions with respect to the wall. If compared to the results shown in figure 2.2.15, it is found that this geometry causes a reduction of roughly 60% in the value of C_{pi}. The heat transfer correction factor is shown in figure 2.6.9, also for two wind directions.

The inlet pressure coefficient with a windbreak wall, K_{wall2},installed below the heat exchangers is shown in figure 2.6.10. The dimensionless velocity distribution through the horizontal heat exchangers is given in figures 2.6.11 and 2.6.12 with the corresponding heat transfer correction factor shown in figure 2.6.13. The results suggest that the wall below the heat exchangers causes the region of separated flow in the upstream side of the tower under the heat exchangers to diminish considerably. In the lee side of the walls, an almost uniform velocity profile is obtained which is roughly equal to that of the mean air velocity in the inlet cross-section of the tower. Recirculation of the air in the downstream part of the tower as suggested by Blanquet [86BL1] was not found in the present model.

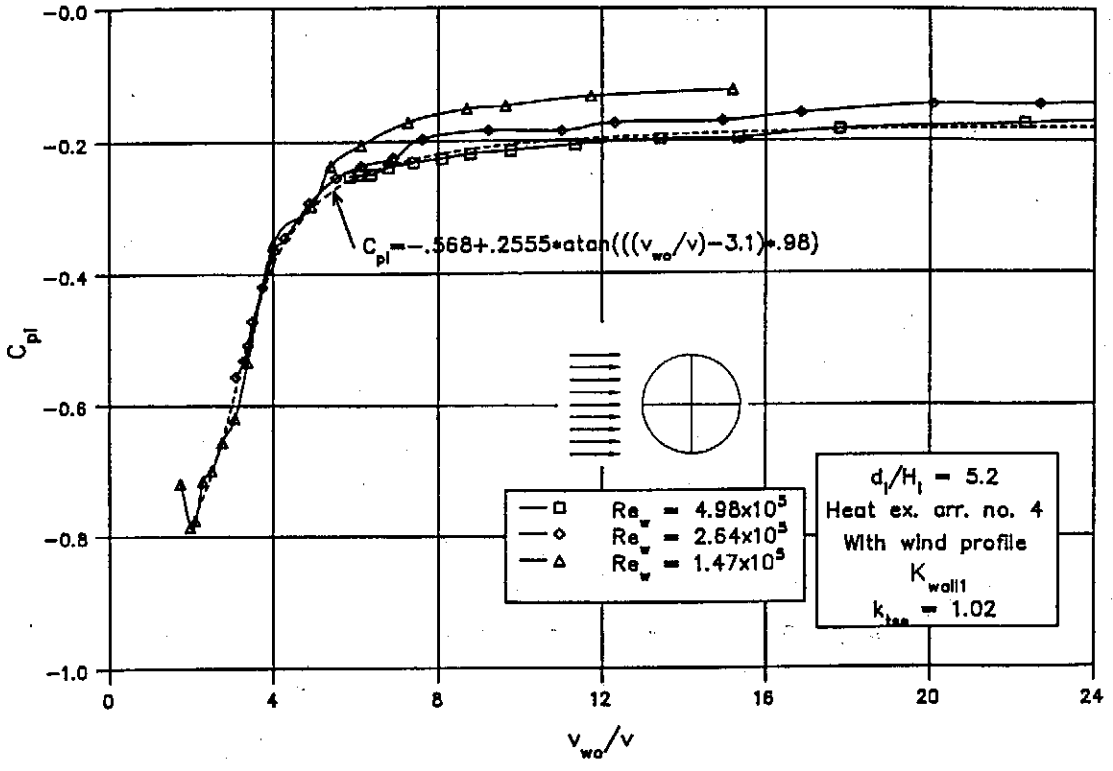

(a)

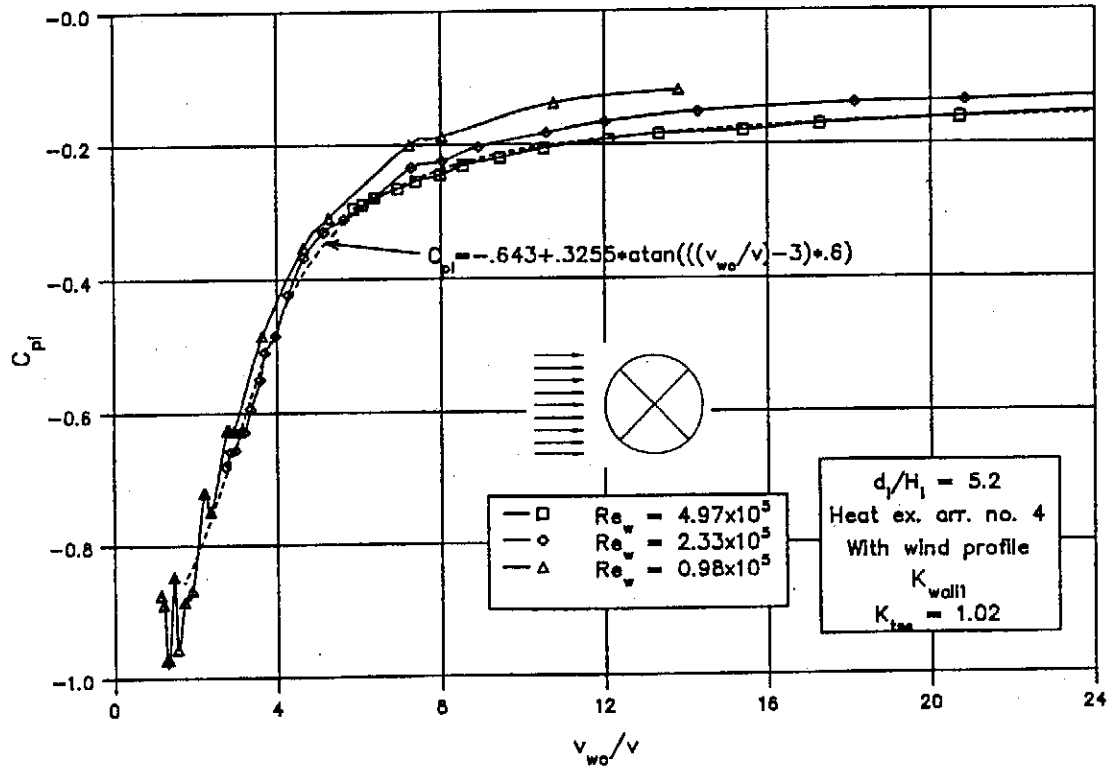

(b)

Figure 2.6.8: C_{pi} with windbreak walls, K_{wall1}.

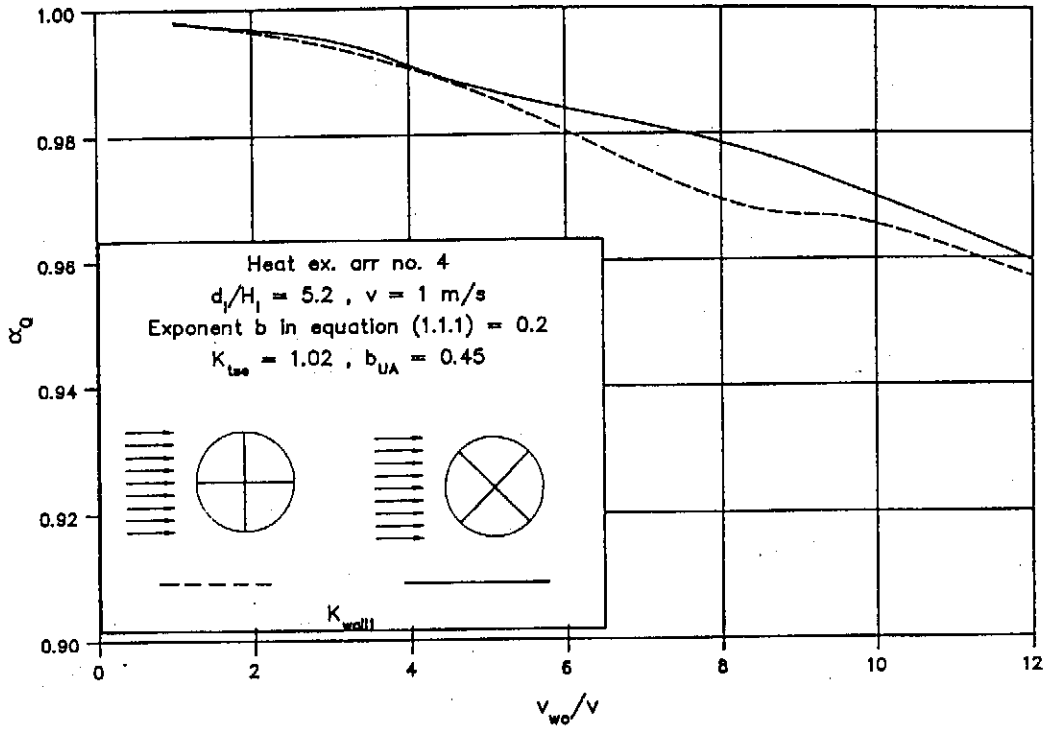

Figure 2.6.9: α_Q with windbreak walls, K_{wall1}.

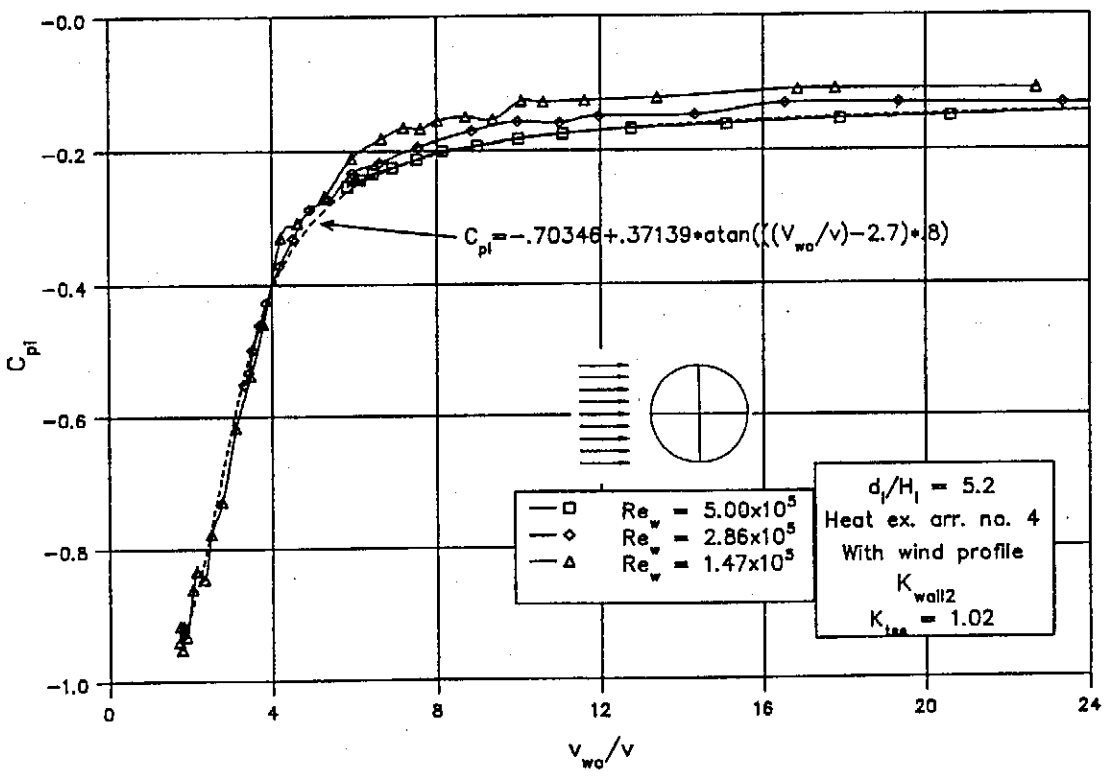

(a)

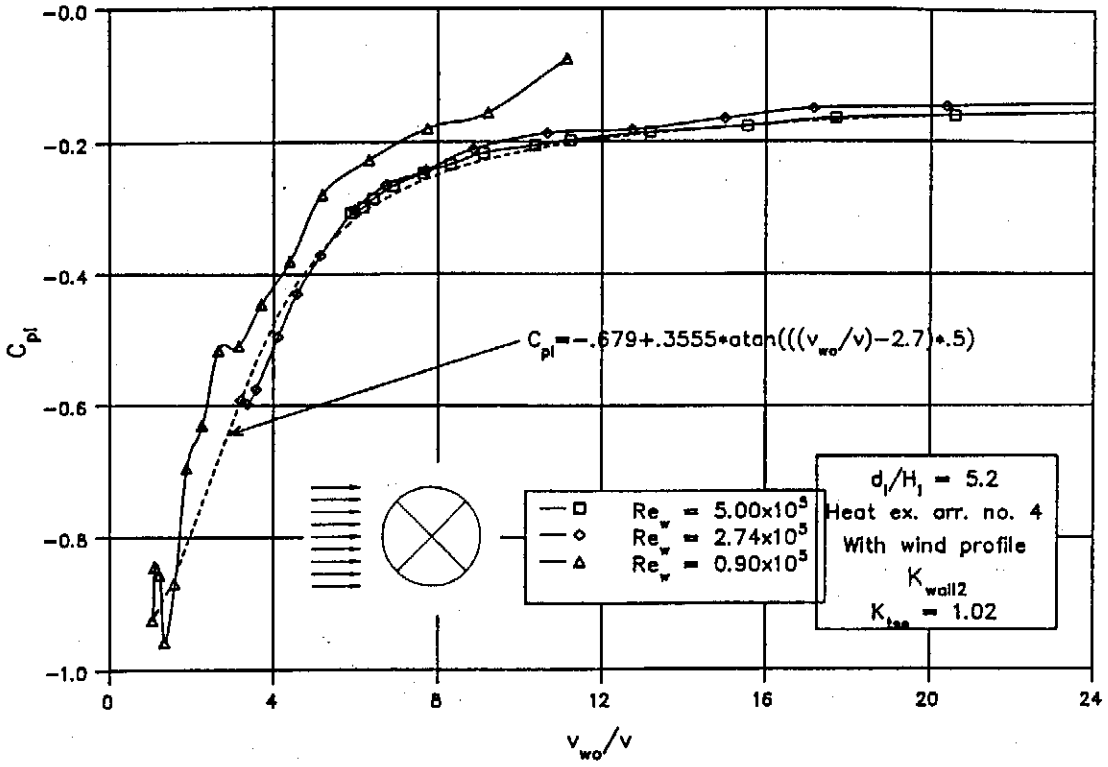

(b)

Figure 2.6.10: C_{pi} with windbreak walls, K_{wall2}.

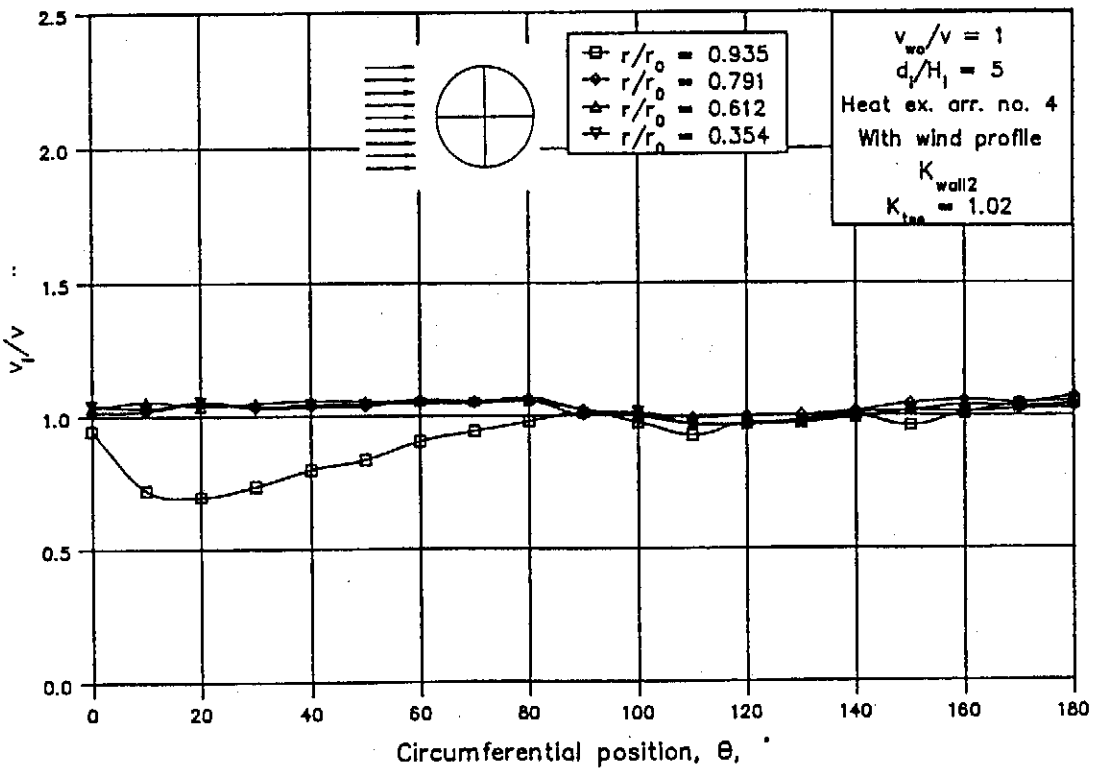

(a)

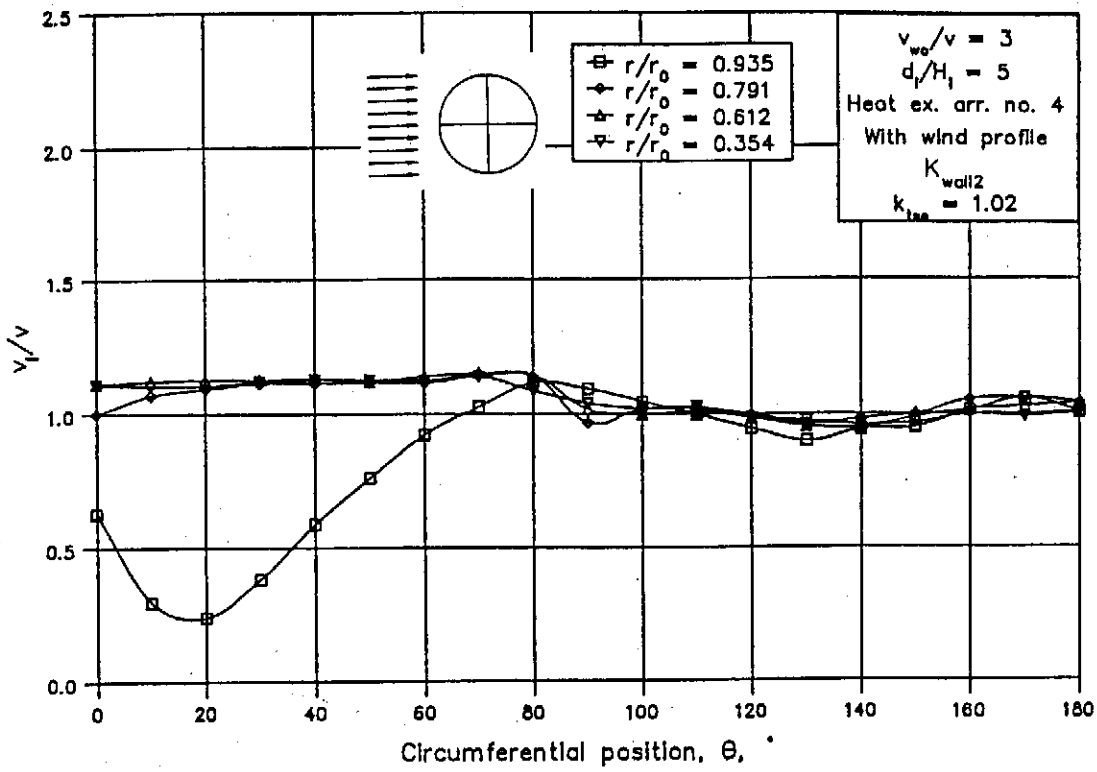
r/r_o = 0.935
r/r_o = 0.791
r/r_o = 0.612
r/r_o = 0.354
v_{wo}/v = 3
d_i/H_i = 5
Heat ex. arr. no. 4
With wind profile
K_{wall2}
k_{tse} = 1.02
v_i/v
Circumferential position, θ,

(b)

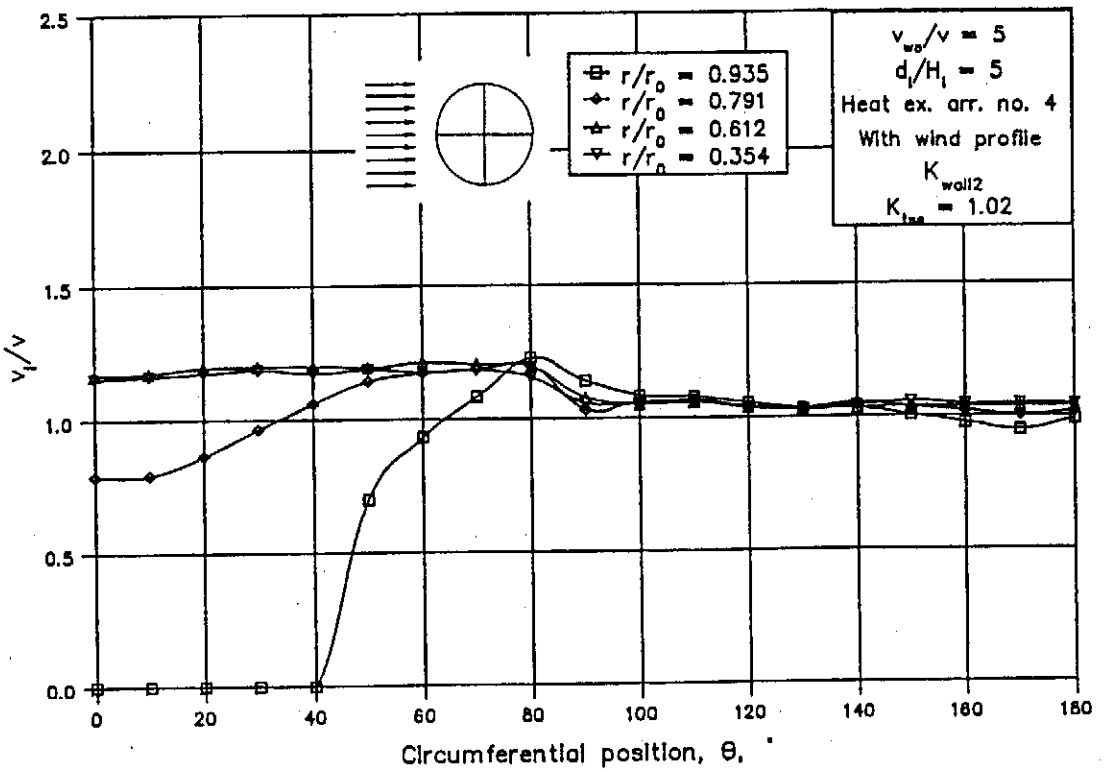
r/r_o = 0.935
r/r_o = 0.791
r/r_o = 0.612
r/r_o = 0.354
v_{wo}/v = 5
d_i/H_i = 5
Heat ex. arr. no. 4
With wind profile
K_{wall2}
K_{tse} = 1.02
v_i/v
Circumferential position, θ,

(c)

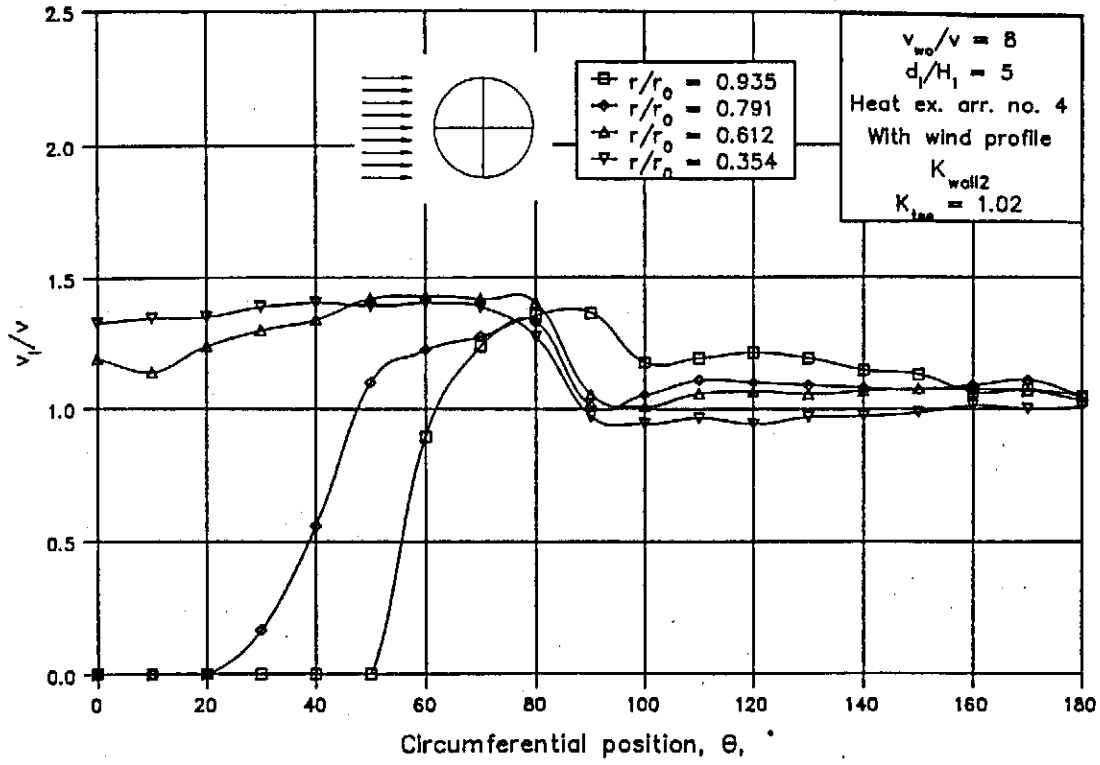
v_{wo}/v = 8
d_1/H_1 = 5
Heat ex. arr. no. 4
With wind profile
K_{wall2}
K_{tee} = 1.02
r/r_o = 0.935
r/r_o = 0.791
r/r_o = 0.612
r/r_o = 0.354
v_1/v
Circumferential position, θ, °

(d)

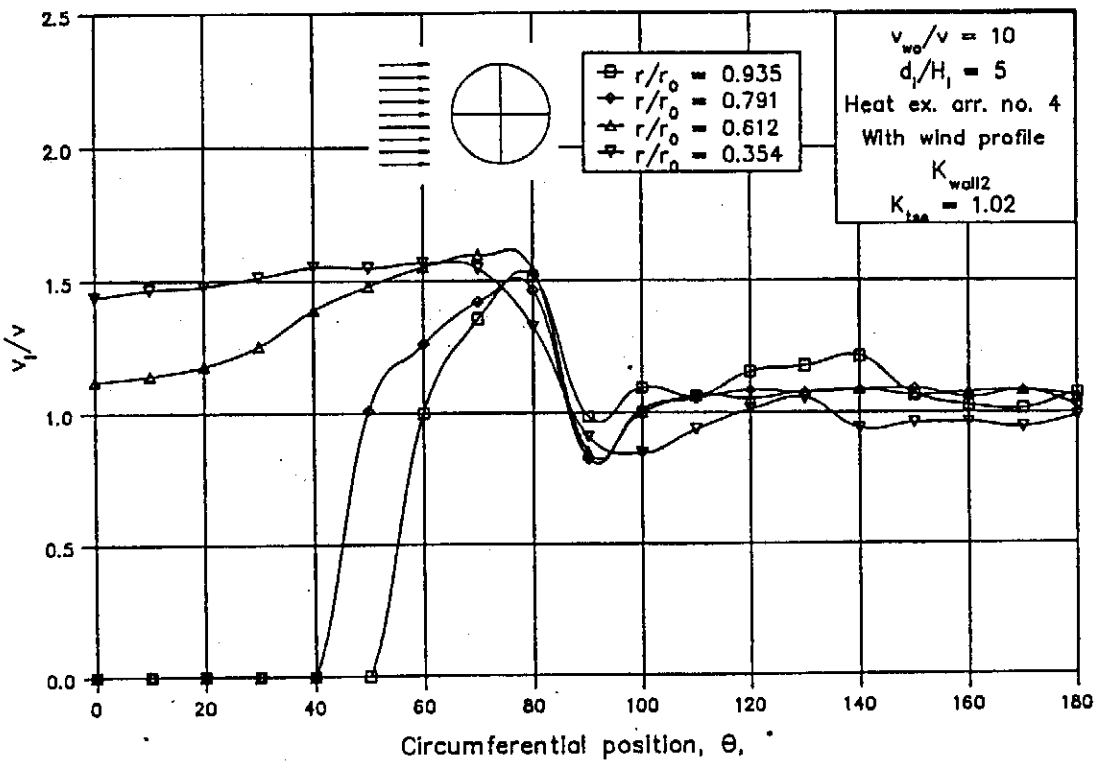
v_{wo}/v = 10
d_1/H_1 = 5
Heat ex. arr. no. 4
With wind profile
K_{wall2}
K_{tee} = 1.02
r/r_o = 0.935
r/r_o = 0.791
r/r_o = 0.612
r/r_o = 0.354
v_1/v
Circumferential position, θ, °

(e)

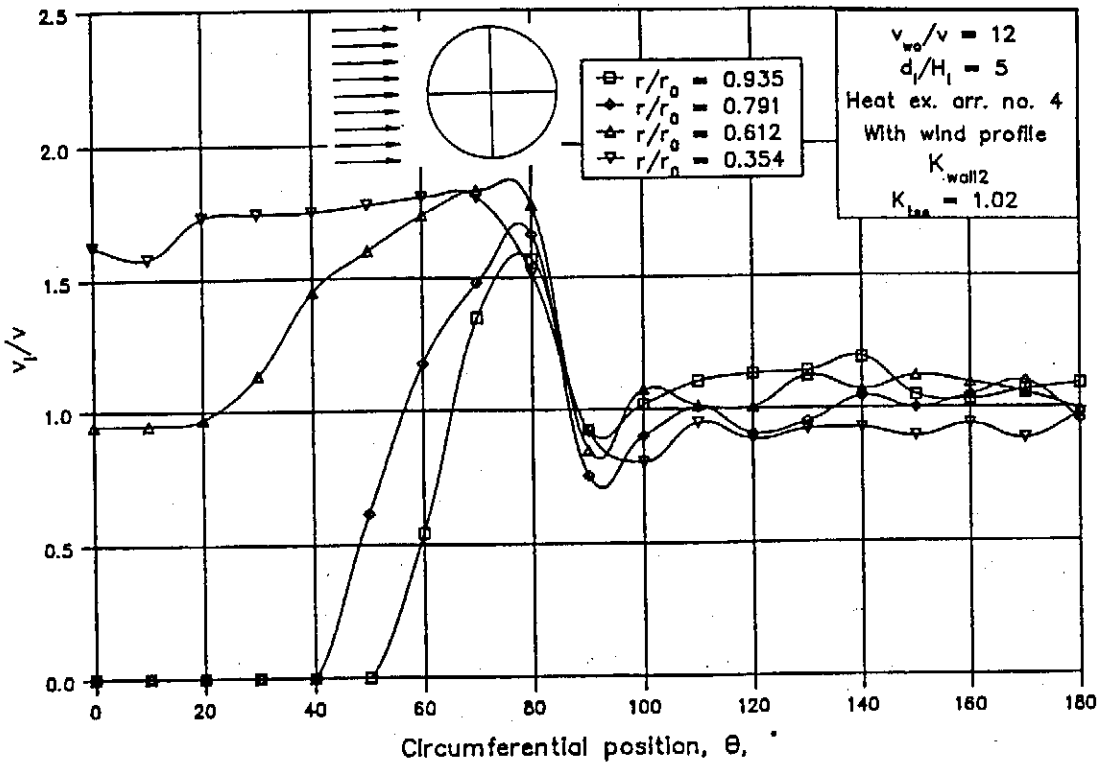

(f)

Figure 2.6.11: Velocity distribution with windbreak wall, K_{wall2}.

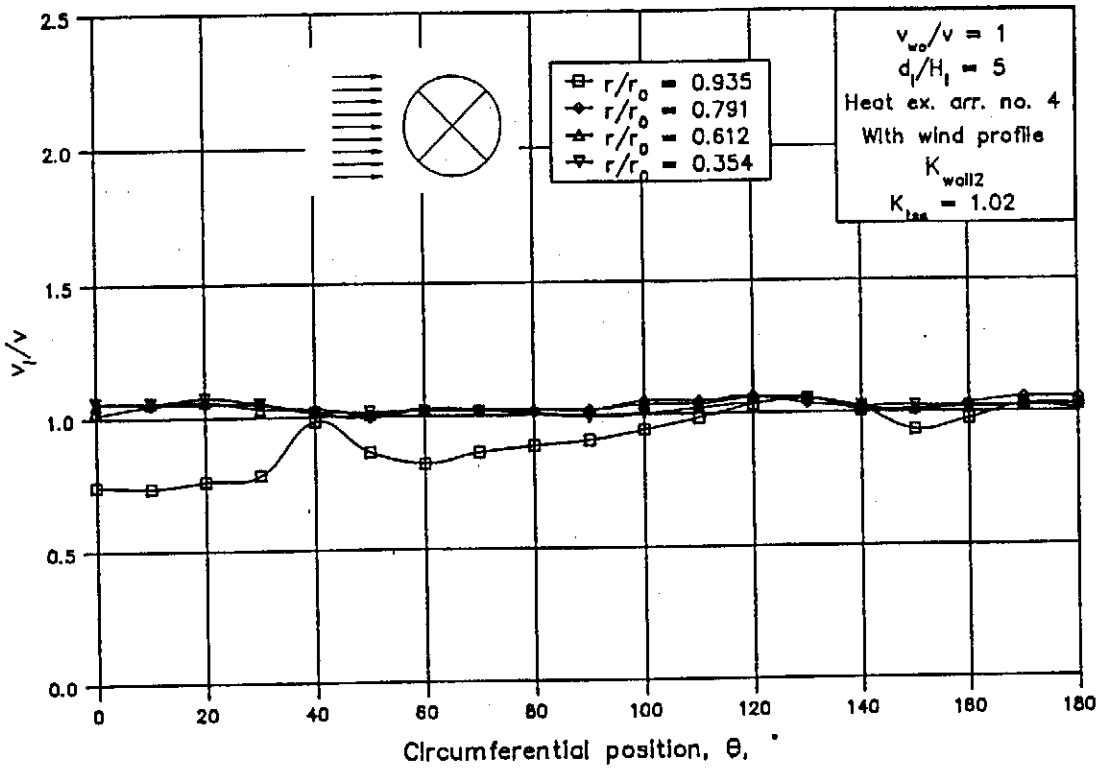

(a)

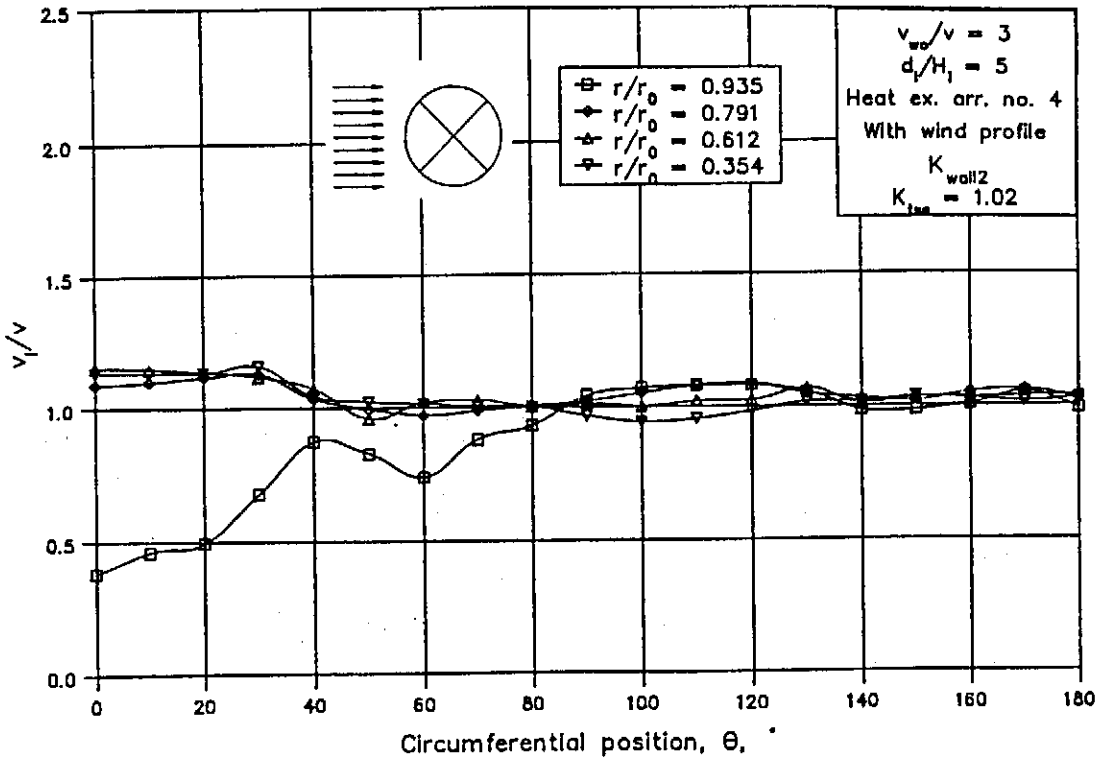
v_{wo}/v = 3
d_i/H_i = 5
Heat ex. arr. no. 4
With wind profile
K_{wall2}
K_{tee} = 1.02
r/r_o = 0.935
r/r_o = 0.791
r/r_o = 0.612
r/r_o = 0.354
v_i/v
Circumferential position, θ, °

(b)

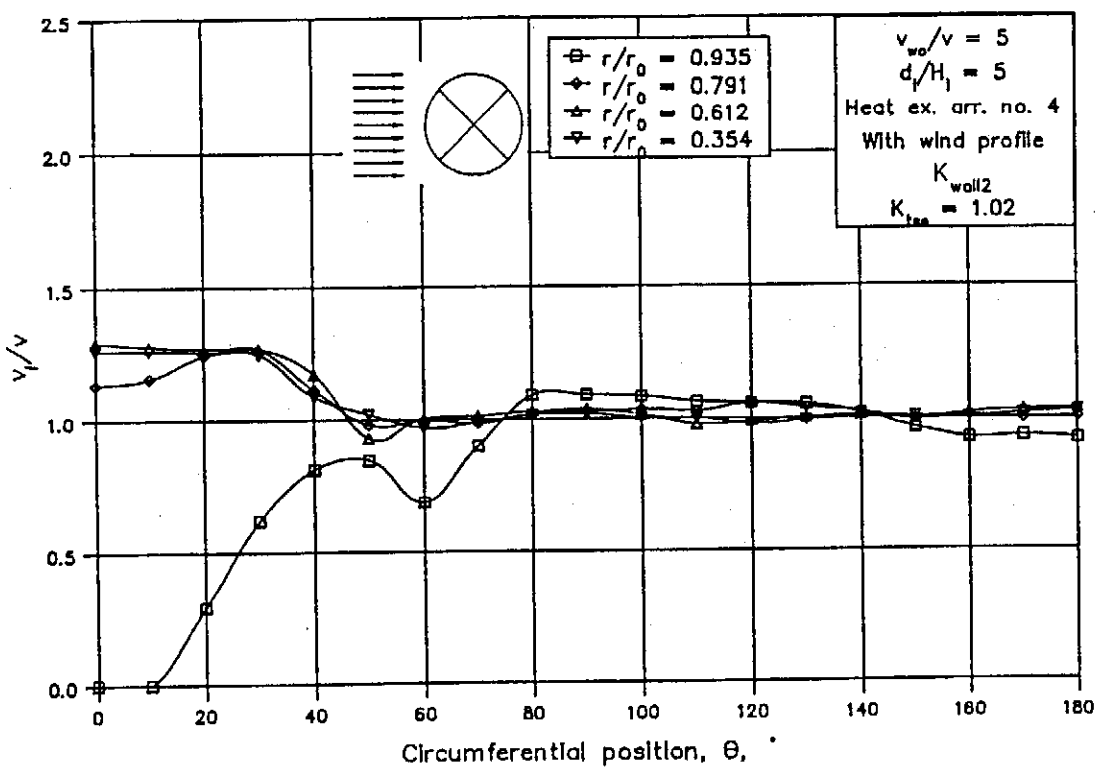
v_{wo}/v = 5
d_i/H_i = 5
Heat ex. arr. no. 4
With wind profile
K_{wall2}
K_{tee} = 1.02
r/r_o = 0.935
r/r_o = 0.791
r/r_o = 0.612
r/r_o = 0.354
v_i/v
Circumferential position, θ, °

(c)

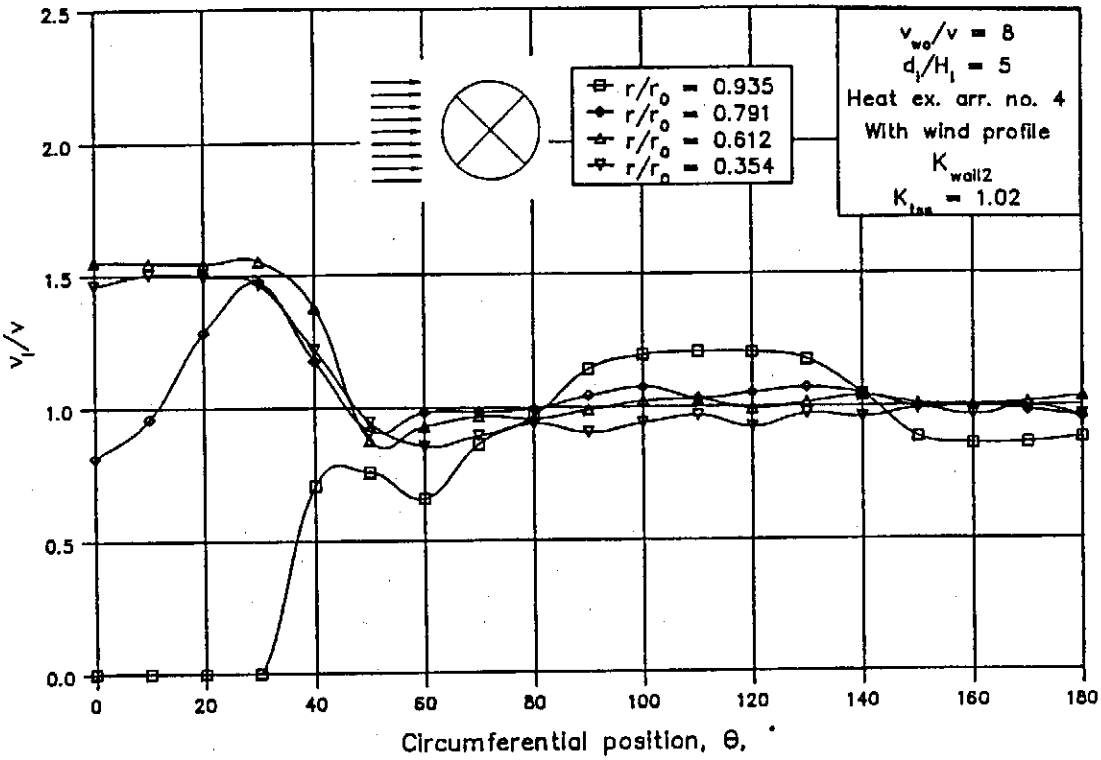
v_{wo}/v = 8
d_i/H_i = 5
Heat ex. arr. no. 4
With wind profile
K_{wall2}
K_{tan} = 1.02
r/r_o = 0.935
r/r_o = 0.791
r/r_o = 0.612
r/r_o = 0.354
v_i/v
Circumferential position, θ, °

(d)

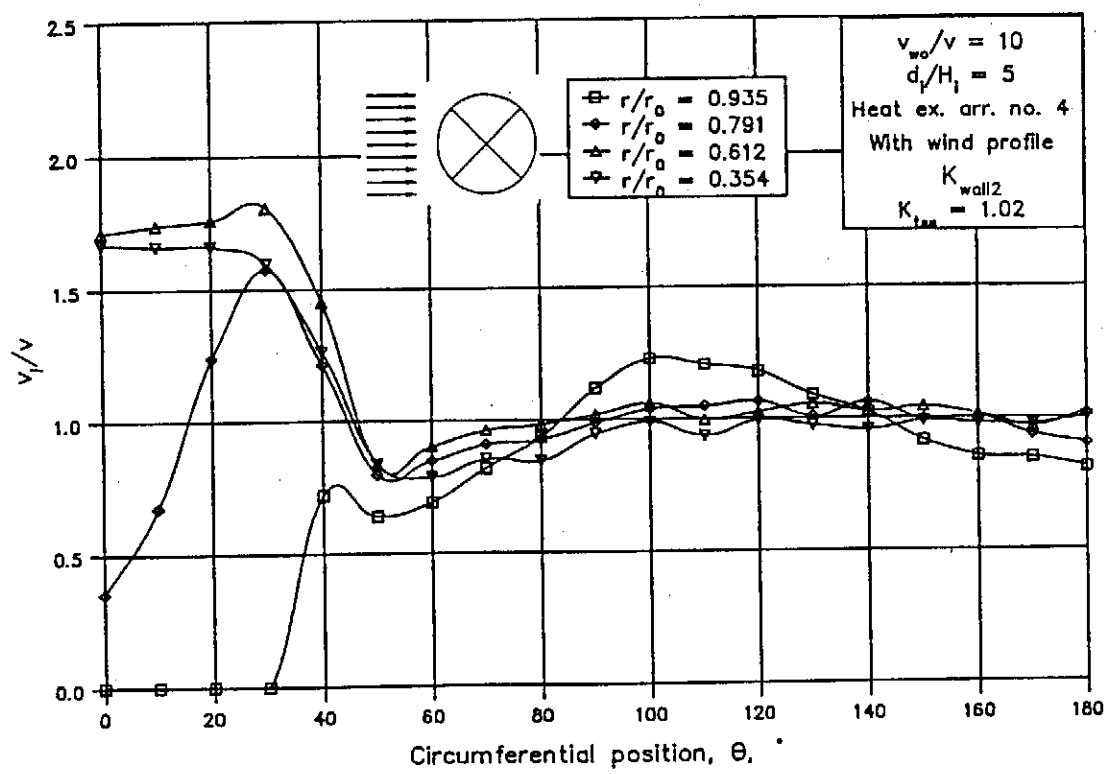
v_{wo}/v = 10
d_i/H_i = 5
Heat ex. arr. no. 4
With wind profile
K_{wall2}
K_{tan} = 1.02
r/r_o = 0.935
r/r_o = 0.791
r/r_o = 0.612
r/r_o = 0.354
v_i/v
Circumferential position, θ, °

(e)

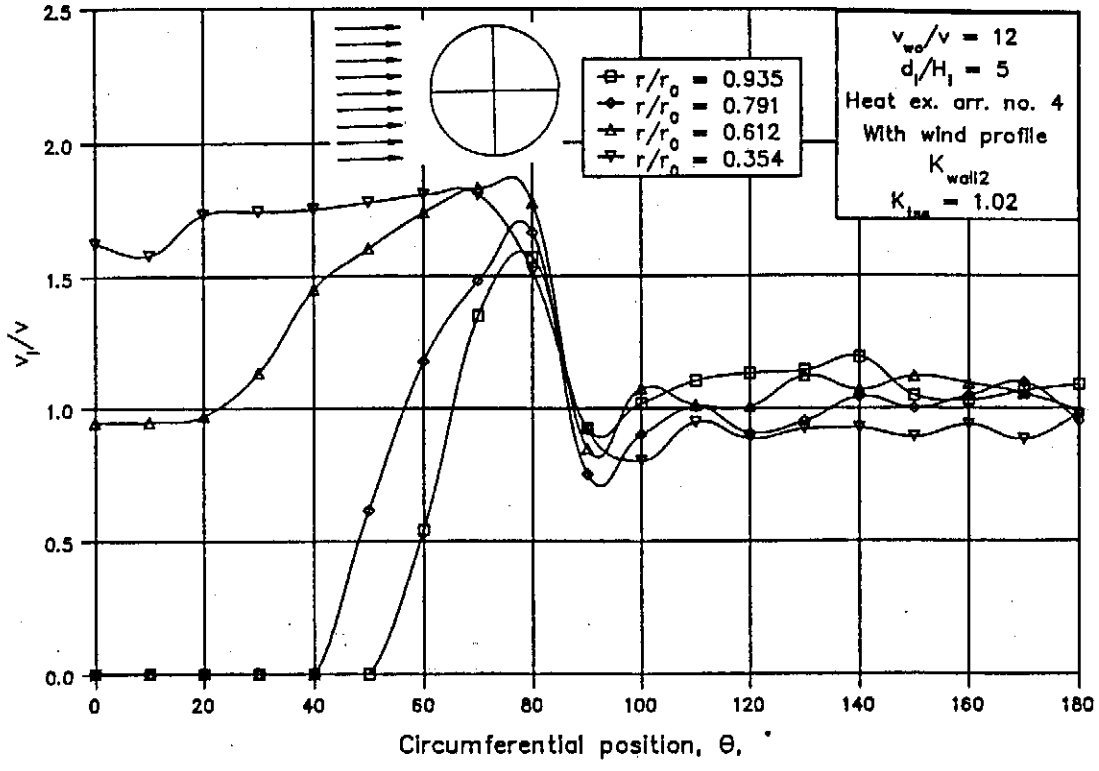

(f)

Figure 2.6.12: Velocity distribution with windbreak wall, K_{wall2}.

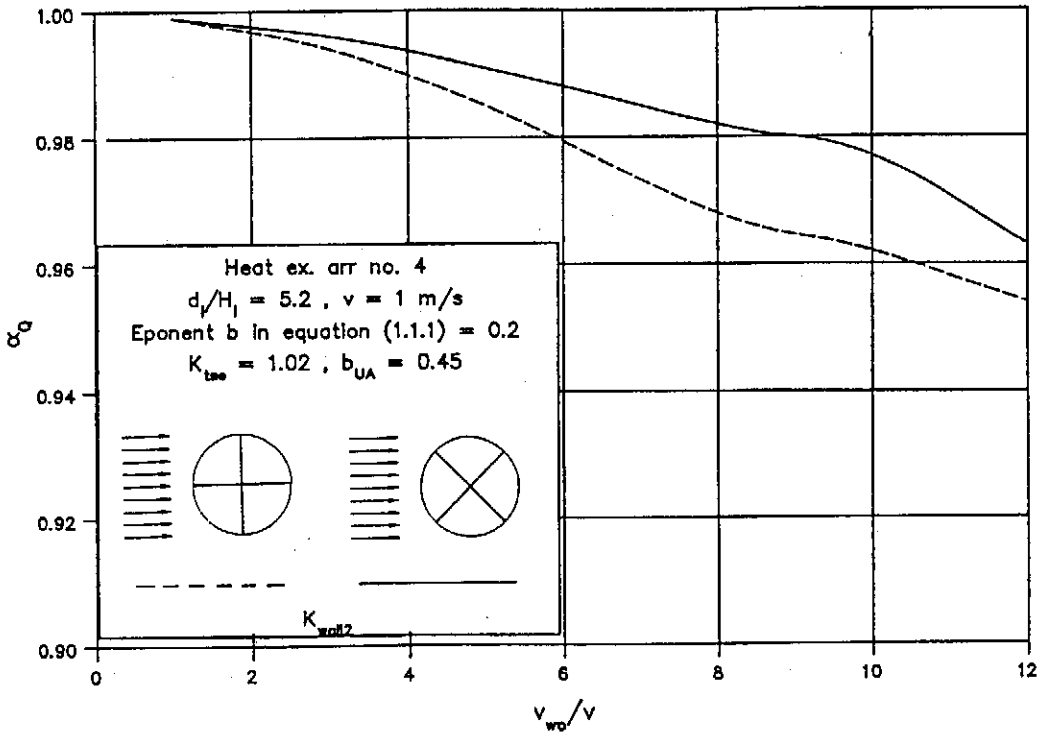

Figure 2.6.13: α_Q with windbreak wall, K_{wall2}.

The results shown in the figures above can be used to calculate the rise in the approach temperature of a tower with windbreak walls installed under the heat exchangers. The data of the tower used in the calculations was the same as that used in section 2.5.

The results of the present calculations, shown in figure 2.6.14, indicate that the windbreak walls cause significant reductions in the wind influence on the performance of a natural draft tower. For a wind velocity at the tower outlet of 20 m/s, the increase in the approach temperature of the tower is found to be 4 °C to maintain the heat rejection rate of the tower, while for the case without any windbreak walls a temperature increase of 14 °C (see figure 2.5.2) was required for the same wind velocity.

Since the walls have no effect on the operation of the tower in windless conditions, the erection of walls below the heat exchangers of a dry-cooling tower proves to be an effective method to diminish the wind influence on such a tower. Conversely Sabaton [82SA1] found that the instalment of similar walls in a wet tower is not beneficial.

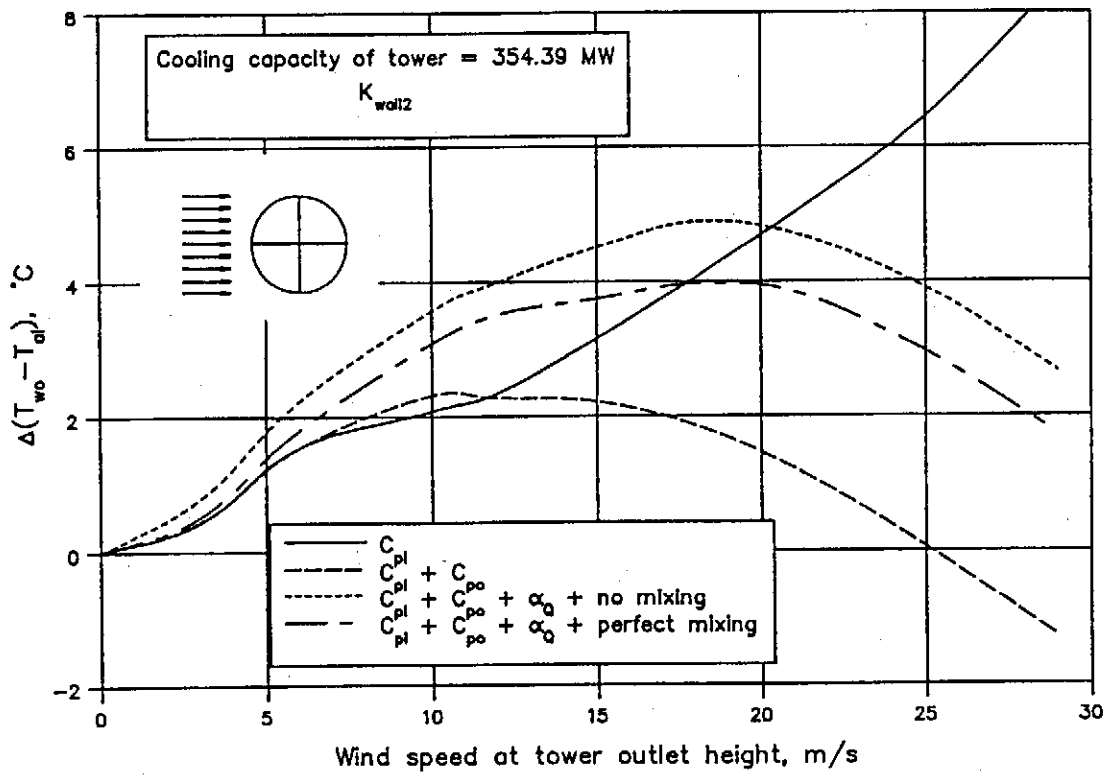

Figure 2.6.14: Rise in the approach temperature of a tower with windbreak walls installed below the heat exchangers.

In figures 2.6.15 and 2.6.16 the inlet pressure coefficient and α_Q are shown for the case where solid windbreak walls are installed below the heat exchangers.

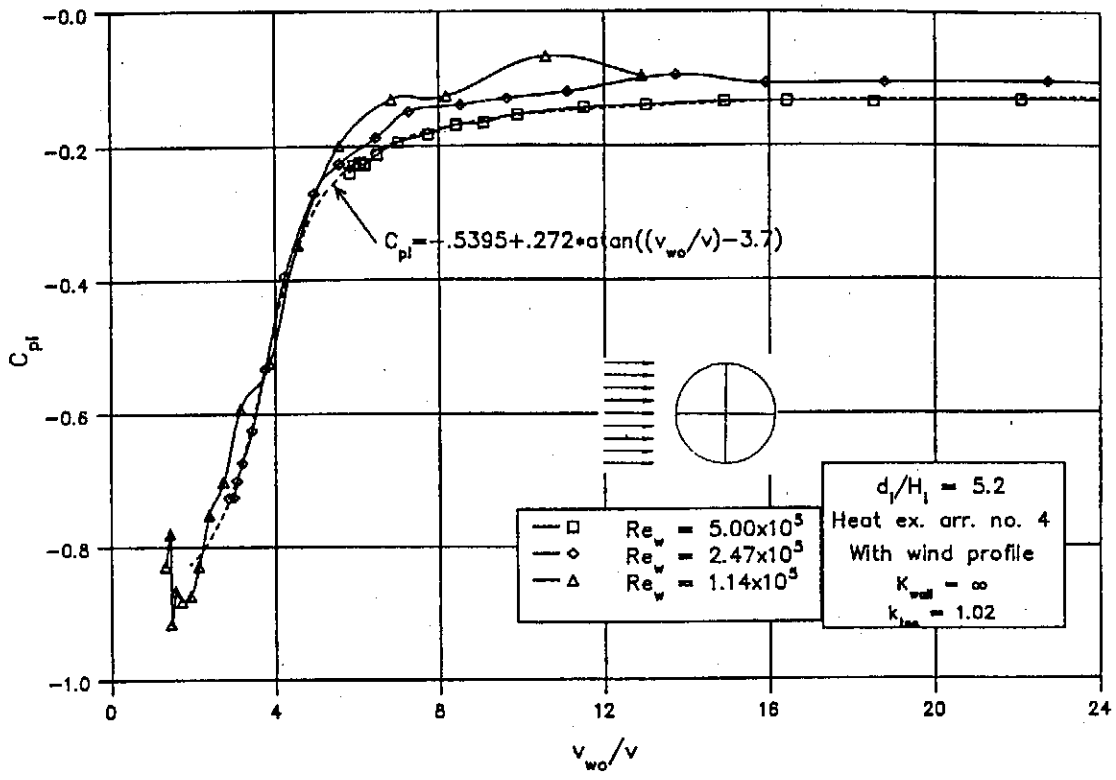

(a)

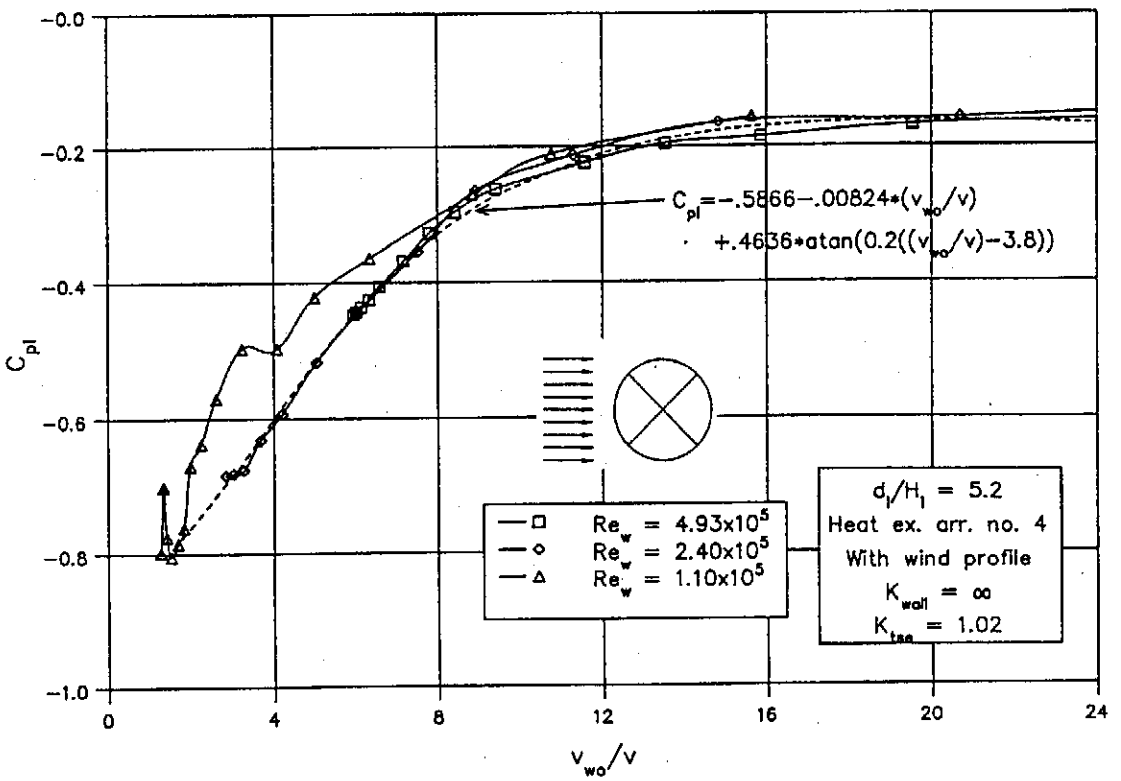

(b)

Figure 2.6.15: C_{pi} with windbreak wall, $K_{wall} = \infty$.

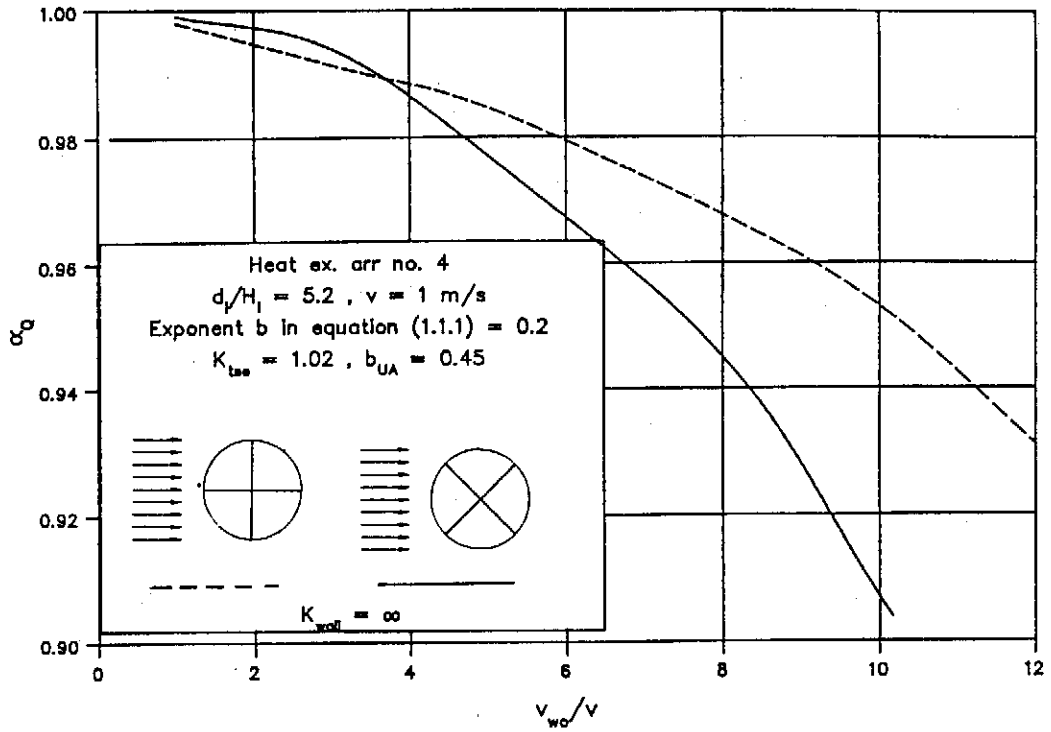

Figure 2.6.16: α_Q with windbreak walls, $K_{wall} = \infty$.

2.7: Conclusions

By means of model tests the influence of cross-winds on the performance of natural draft dry-cooling towers has been studied and most of the objectives listed in section 2.1 have been reached. The results can be summarized as follows:

1. By applying a solid blockage correction factor the effective wind velocity across the tower models was calculated and the blockage effect on the experimental results was found to be negligible.

2. Due to difficulties involved in modelling the heat exchangers, the wind effect on a tower with a vertical heat exchanger arrangement could not be solved by means of model tests. The problem is however addressed in chapter 4.

3. In the present study the finned tube heat exchangers were simulated with mesh layers in series with honeycomb. It was however found that heat exchangers with a relatively high pressure loss coefficient can correctly be modelled only with a number of mesh layers.

4. In the absence of tower supports and for large values of the d_i/H_i ratio the inlet pressure coefficients are found to be strongly dependent on the pressure loss coefficient of the heat exchangers. Such towers become more to winds for an increase in the K_{he} value of the heat exchangers. The wind effect on towers with small d_i/H_i values is in contrast almost independent of the pressure loss coefficient of the bundles.

   Once tower supports are installed in the tower the wind effect is much less influenced by the K_{he} value of the heat exchangers and the tower performance generally becomes less sensitive to the wind for a reduction in the K_{he} value of the heat exchangers. For large values of the pressure loss coefficient of the tower supports, C_{pi} is independent of K_{he} for sufficiently large values of the latter.

5. For large values of the pressure loss coefficient of the tower supports the wind effect on the tower decreases for a reduction in the d_i/H_i ratio of the tower.

   If no tower supports are installed in the inlet, the absolute value of C_{pi} reduces for a reduction in the d_i/H_i ratio of the tower for large K_{he} values while the opposite is true for

smaller values of the heat exchanger pressure loss coefficient.

6. The introduction of tower supports in the tower inlet causes a significant reduction in the wind effect on the performance of a tower. The resistance exerted by the supports on the air flow tends to reduce the incoming wind speed below the heat exchangers with a corresponding rise in the static pressure in this region. The latter will cause an increase in the mean air mass flow rate through the tower and therefore also enhance the heat rejection rate of the tower.

7. The form of the approaching wind profile has a very small effect on the wind influence on the tower provided that the pressure loss coefficient of the tower supports is sufficiently large. With no tower supports, the wind effect on the tower increases as the wind profile becomes more uniform.

8. The air velocity distribution through the heat exchangers becomes increasingly more non-uniform for an increase in the wind velocity. A deterioration in the velocity distribution is also observed for an increase in the d_i/H_i ratio of the tower and also for a reduction in the pressure loss coefficient of the heat exchangers.

9. It was found that the wind effect on the outlet of the tower is independent of the velocity distribution formed in the tower inlet during windy periods.

10. Significant reductions in the wind effect of the tower are achieved by installing windbreak walls in the base of the tower below the horizontally arranged heat exchangers.

If the size of most available wind tunnels is considered, cooling tower models of a scale much larger than 1:100 cannot be employed without the results being seriously affected by solid blockage effects. Furthermore is it impossible to satisfy both the Reynolds number and the densimetric Froude number in a single model test while the amount of information that can be gathered by means of experimental techniques is also limited. Therefore full scale measurements and a numerical analysis are employed in chapters 3 and 4 respectively to clarify further aspects of the problem.

CHAPTER 3

Full scale measurements on a natural draft dry-cooling tower.

3.1: Introduction.

During July and August 1990, full scale measurements were performed on one of the natural draft dry-cooling towers of the Kendal power station, which is presently under construction, in South Africa. The purpose of the measurements were to determine the effect of atmospheric variations on the performance of the cooling tower.

The Kendal power station will at completion be the world's largest indirect dry-cooled power station and has 6 x 686 MW turbines. Each unit is provided with a hyperbolic concrete natural draft cooling tower to cool the water in the cooling circuit. Although the 6 cooling towers had already been erected before the experiments, only the first two units of the power station were operational at that stage. The measurements were performed on the cooling tower of the first unit which was commissioned about two years prior to the tests. A few initial runs of short duration were done on unit two, but for most of the time during the test period, only unit one was in operation.

The position of the various power station structures are shown on a ground plan in figure 3.1.1. The power station is located approximately 90 km east of Johannesburg on the Transvaal Highveld, in a grassland with few trees. The main farming activity in the region is maize production. Except for the power station buildings and cooling towers, no other major structures exist in the immediate vicinity of the station.

The concrete cooling towers of the power station are each 165 m high with an inlet diameter of 144.5 m while the diameter at the tower outlet is 101.1 m. X-shaped columns are used to support the shell with further details of the support arrangement given in table D.1. Finned tube heat exchangers, in the form of A-frames with an apex angle of 60°, are arranged radially in the base of the tower as shown in figure 3.1.2. The total length of the tubes used in one of the towers is 1980 km. Hot water from the surface condenser flows in 3.1 m diameter ducts to and from the tower.

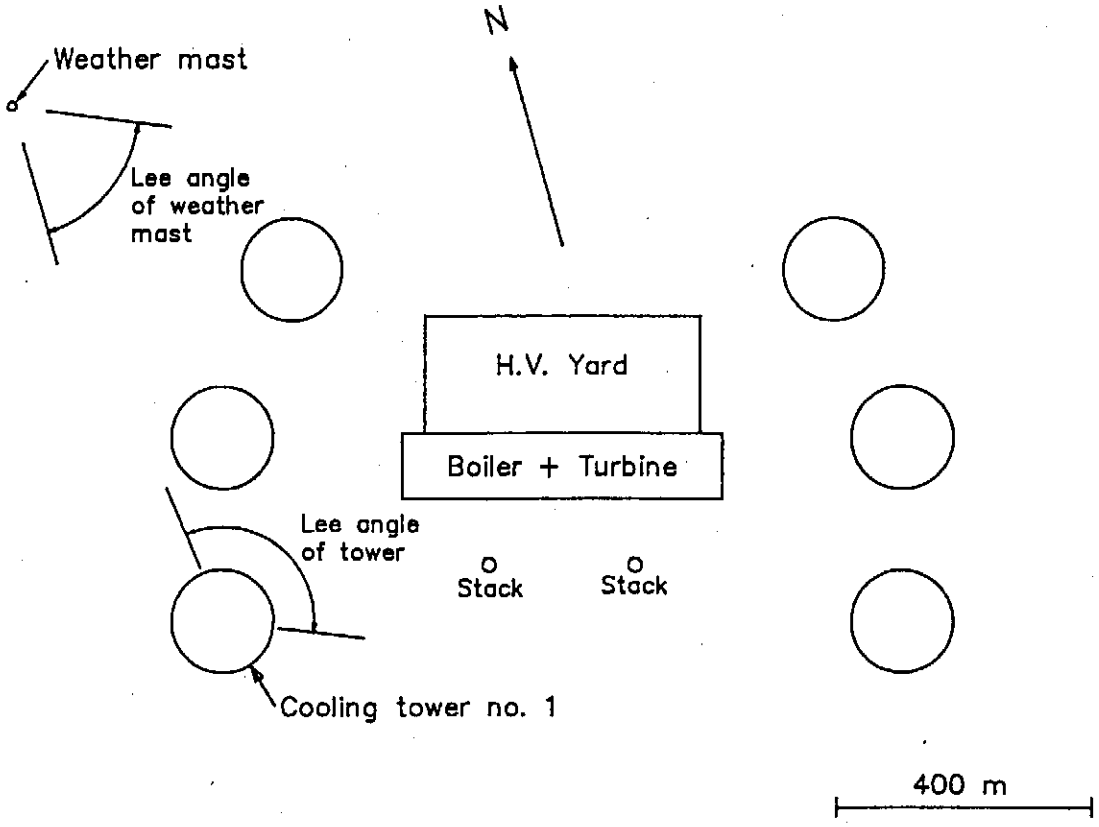

Figure 3.1.1: Ground plan of power station.

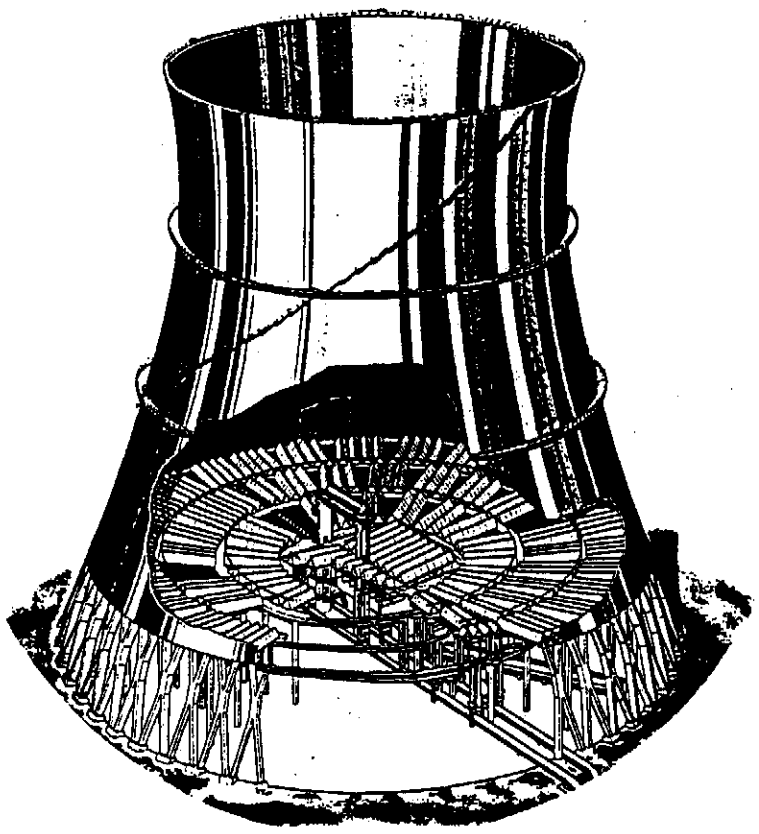

Figure 3.1.2: Kendal cooling tower.

The 500 heat exchanger bundles in the tower are divided into 11 cooling sectors with the number of bundles in each sector indicated in brackets in figure 3.1.3. The sectors are controlled from the control room and can be closed individually with a maximum of four sectors closed. Once a sector is closed, the cooling water is immediately drained and the finned tubes are filled with nitrogen gas.

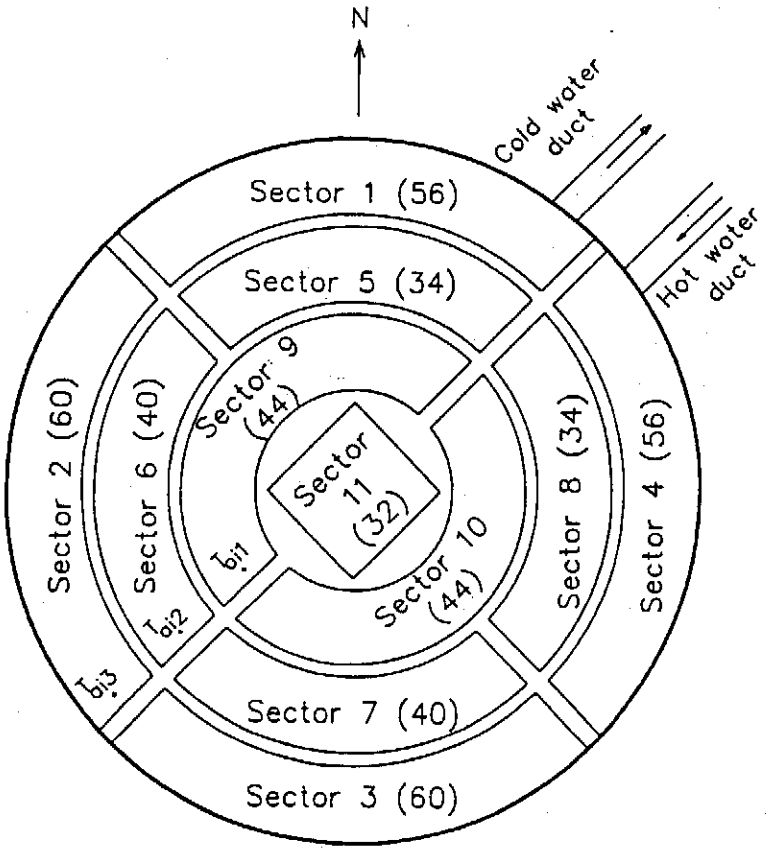

Figure 3.1.3: Cooling sectors in the tower.

3.2: Instrumentation.

During the tests the ambient meterological conditions were obtained from a 96 m high weather mast erected by ESKOM, 700 m north of the cooling tower under consideration as shown in figure 3.1.1. The dry-bulb air temperature is measured at 1.2, 2.5, 5, 10, 20, 40, 65 and 96 m above ground level (AGL). Anemometers positioned at 10, 20, 40, 65, and 96 m measured the three-dimensional wind velocity profile while the barometric pressure at ground level is also measured. The data was recorded 24 hours a day and is stored every six minutes on tape.

In order to investigate the influence of atmospheric variations like cross-winds and vertical temperature distributions, instrumentation was installed in the cooling tower to measure the air and water temperatures and velocities. All the data was logged continually, 24 hours a day, for almost two months to obtain the variation of all the dependent variables in relation to the atmospheric variations.

Three unshielded cromel-alumel thermocouples, T_{ai1}, T_{ai2} and T_{ai3}, were used to measure the temperature of the air entering the heat exchangers. The thermocouples were positioned approximately 1.5 meter below sectors 9, 6 and 2 respectively on the south-west-side of the tower (see figure 3.1.3). These thermocouples were heated due to radiation from the heat exchangers. The difference between the thermocouple temperature and the temperature of the air is given by the following relation.

$$T_{thermocouple} - T_{ai} = 0.01\ (T_{wo} - T_{ai})$$

Four shielded thermocouples, suspended from two cables strung across the outlet of the tower, measured the air outlet temperature. The cables, placed across the tower outlet during erection, can be pulled right down to the heat exchanger elevation and can be raised again from the outside of the tower. These thermocouples were positioned approximately 110 m above the heat exchangers in the throat of the tower as shown in figure 3.2.1 (Approximately 30 m below tower outlet edge). The thermocouple sensing tips were surrounded by reflective radiation shields as protection from the sun.

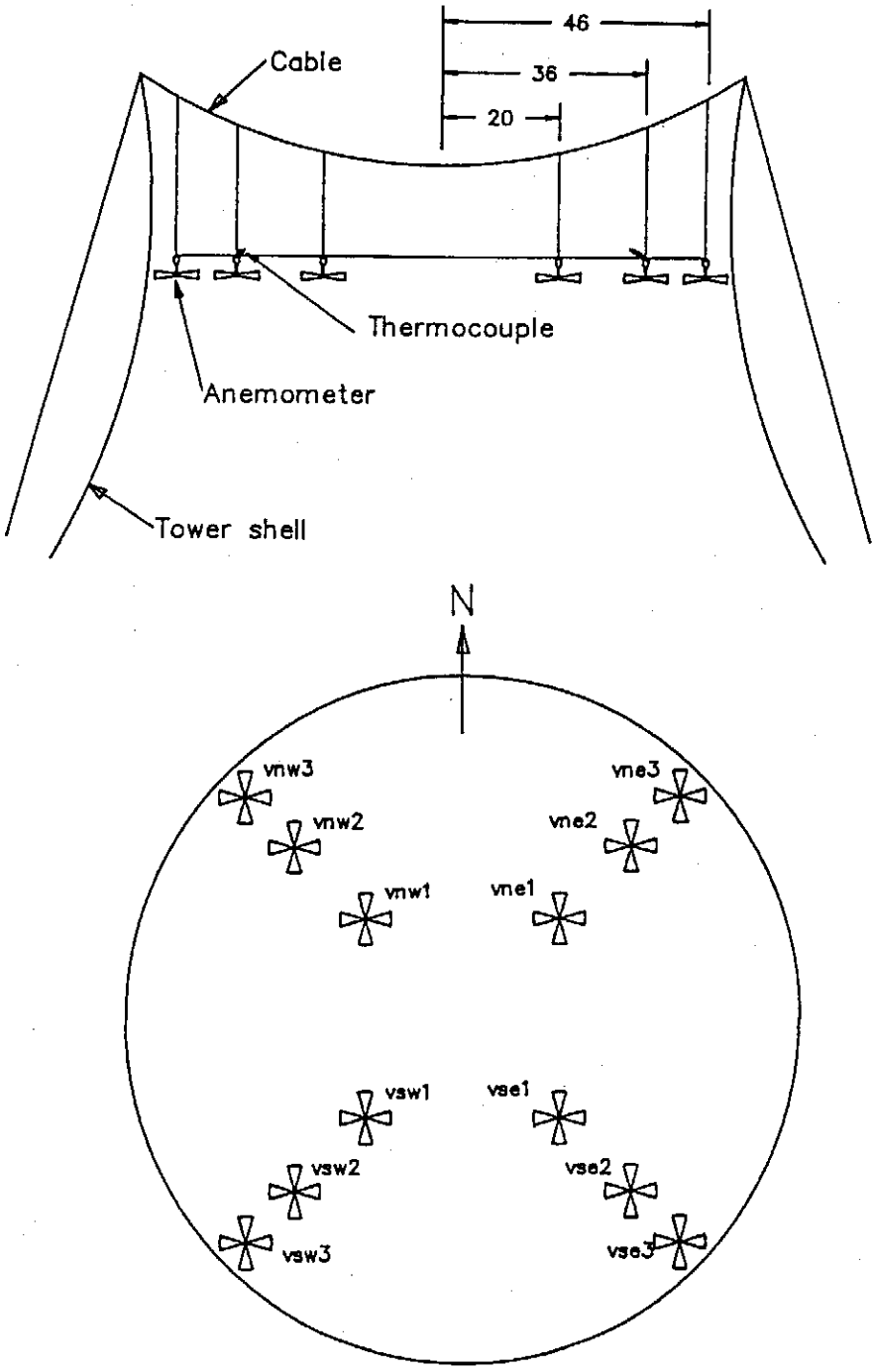

Figure 3.2.1: Position of thermocouples and anemometers in throat of tower.

A further twelve anemometers were placed at the same elevation for measuring the air velocity in the tower as also shown in figure 3.2.1. The anemometers were positioned in such a way that the representative cross-flow area for each of the anemometers was approximately the same. The first anemometer in the north-east-side of the tower, vne1, was damaged during instalment, and therefore the air velocity in this position was not measured. Before the tests, the anemometers were calibrated individually in a wind tunnel under normal flow conditions and

the relationship between the anemometer output voltage and the air velocity for each anemometer was obtained. The response of one of the anemometers as shown in figure 3.2.2 is correlated by a linear function.

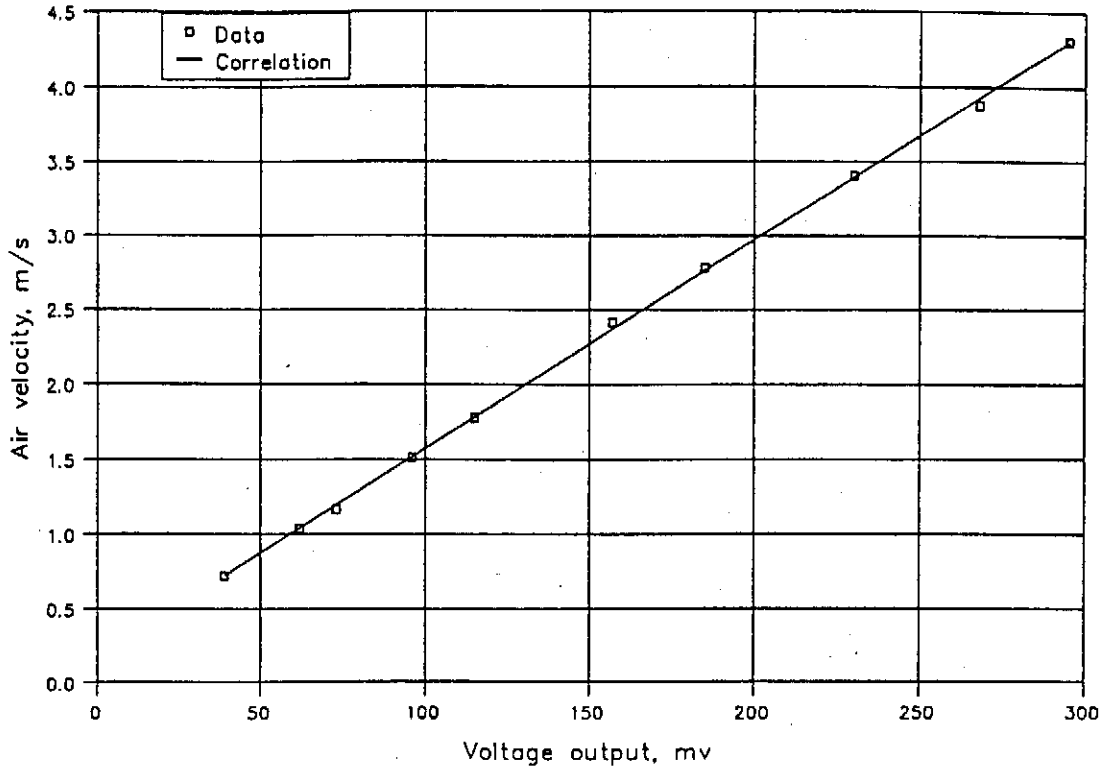

Figure 3.2.2: Response of anemometer.

The water in the cooling circuit is circulated by three parallel connected circulating pumps. Although the total water mass flow rate in the cooling circuit is logged on an hourly basis in the control room, the flow rate through each of the cooling sectors is not known. It is therefore assumed that the ratio of the water mass flow rate in each sector to the total mass flow rate is proportional to the ratio of the number of bundles in the sector to the total number of bundles in the tower.

Because holes could not be drilled in the pipe walls, cromel-alumel thermocouples were attached to the outer surface of the water ducts. Thereafter the sensing tips of the thermocouples were insulated from the surroundings by means of a 250 mm diameter foam cone. In this way the duct wall temperature was measured which is, for all practical purposes, equal to the water temperature in the duct.

The water inlet temperature, which is the same for the different cooling sectors, was measured

with the aid of two thermocouples, T_{wi1} and T_{wi2}, located on the main hot water duct from the condenser. The water outlet temperature from each sector was similarly measured, by placing thermocouples on the outlet pipe of each sector, approximately two metres above the connection to the main water return duct.

The outputs of all the thermocouples and anemometers were collected with the aid of a DIGISTRIP III data logger. The internal ice reference point and standard thermocouple function for cromel- alumel thermocouples of the data logger were used to convert the thermocouple outputs to temperatures in degrees Celsius. Prior to the experiments, the internal reference point of the data logger was calibrated for each thermocouple by using crushed ice. The maximum deviation from zero was found to be less than $\mp$ 0.2 °C.

A complete set of data was recorded each ten seconds and transmitted to a computer. A Turbo Pascal program was employed to receive the data set and the air velocities in the different positions in the throat were calculated by applying the calibration functions of the different anemometers. Furthermore the temperature readings of the thermocouples were corrected by adding the calibration constants. The data received every ten seconds were integrated over periods of five minutes to obtain mean values, whereupon these were stored on disk.

3.3: General discussion of the data.

The general procedure adopted in analyzing the test results was to graph all the observations against a time base to obtain an overall picture of the trends of the dependent variables. An hourly log of the generator output of unit one during the test period was provided by the control room. Most of the time the output of the generator was kept constant round about 500 MW, but occasionally the output was increased to 660 MW as shown in figure 3.3.1. In figure 3.3.2 the corresponding average temperature values as measured in the cooling tower are plotted. As expected, the change in turbine output has a noticeable effect on the water and air temperatures in the cooling tower. In figure 3.3.3 the air velocities in the south-east and south-west-side of the tower throat are also shown for the same time period. A rise in the water temperature in the tower will result in a rise in the air temperature in the tower. The latter will cause an increase in the tower draft and therefore a higher air mass flow rate through the tower.

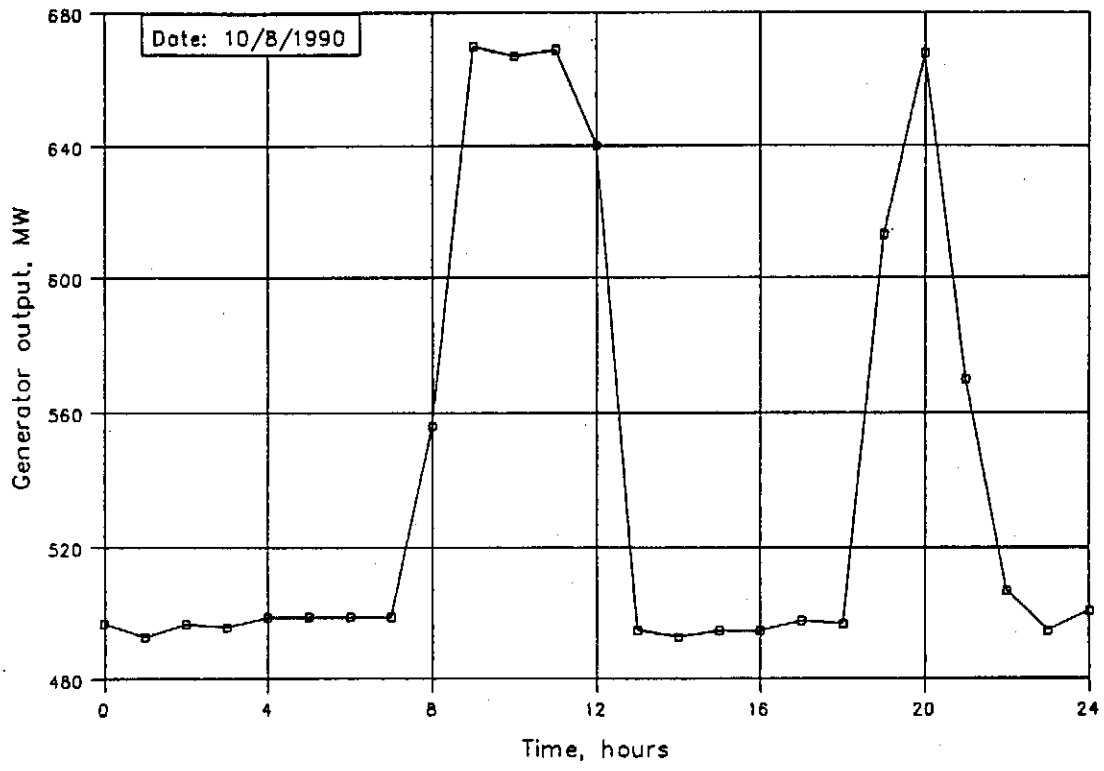

Figure 3.3.1: Turbine output of unit one.

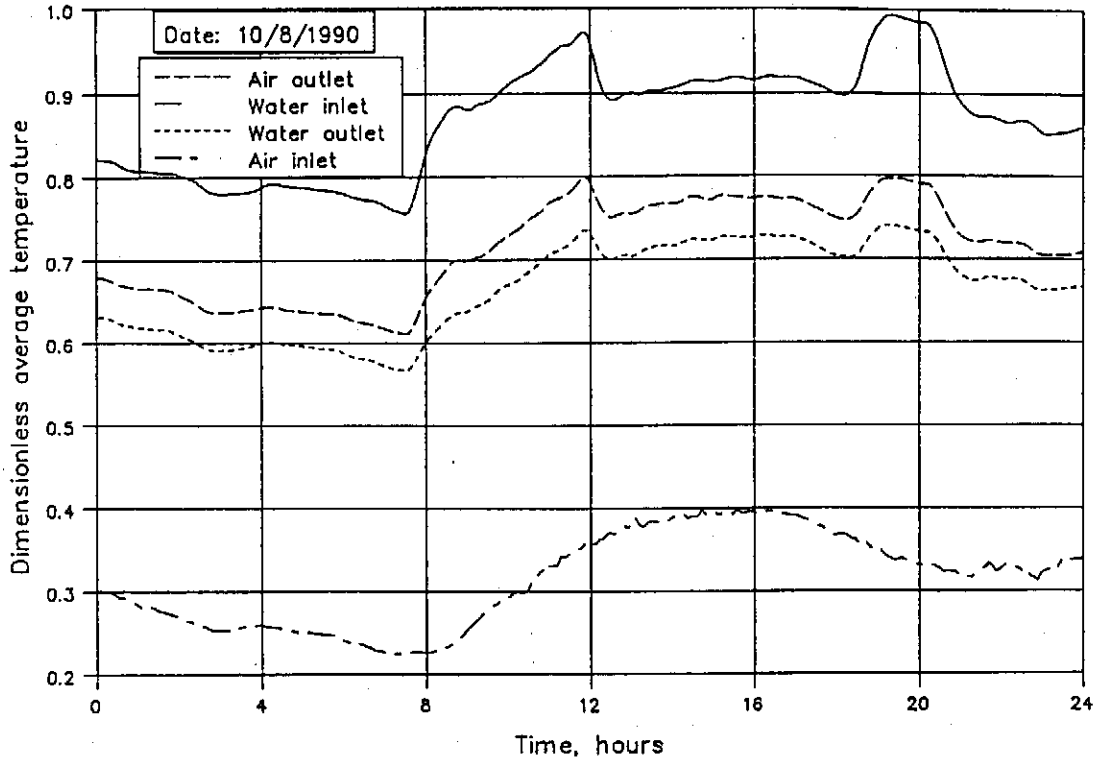

Figure 3.3.2: Average temperatures in the cooling tower.

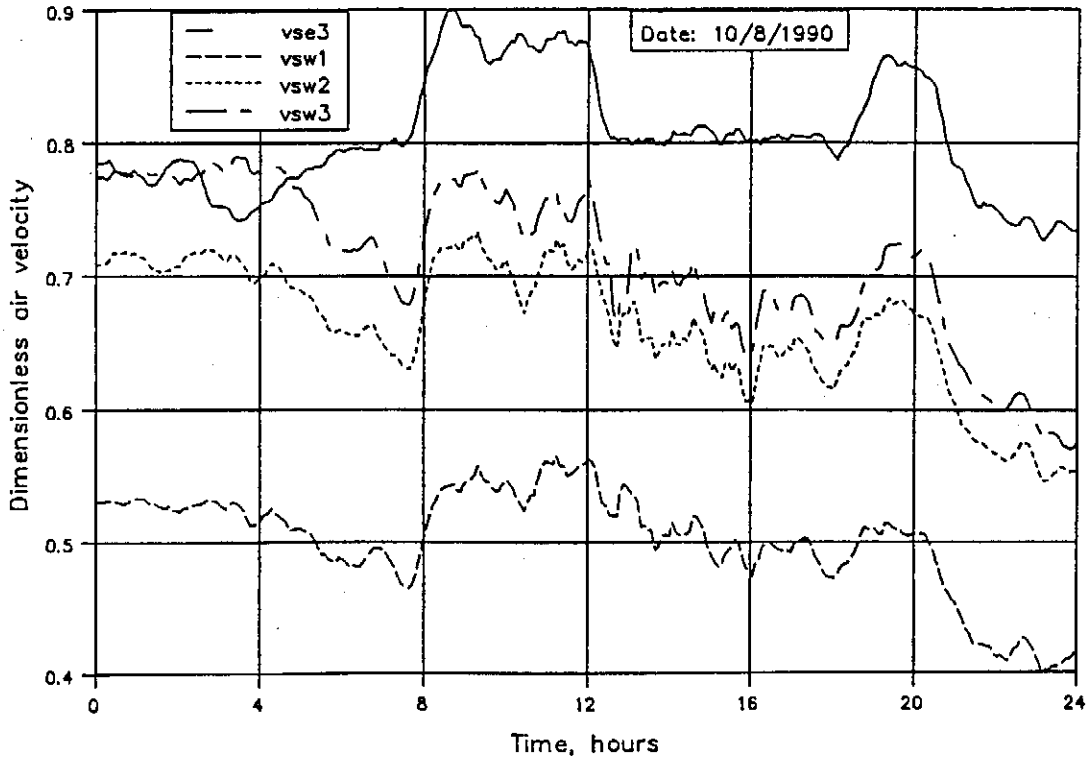

Figure 3.3.3: Air velocities in the tower throat.

Because the experiments were designed to investigate only the effect of atmospheric variations on the tower performance, it is desirable that all the other independent variables, like the turbine output, should be kept at a constant value. Therefore the data obtained for a turbine output of 500 MW and 660 MW are considered separately.

The water mass flow rate through the tower as logged in the control room was for all practical purposes kept constant at 16826 kg/s through the entire test period.

The wind velocity distribution and the wind direction at different heights above ground level are shown in figures 3.3.4 and 3.3.5 respectively for 19-20/8/1990. For relatively high wind velocities, the wind directions on the five elevations above ground level were practically the same while more scatter in the wind direction is observed for smaller wind velocities.

For the correct interpretation of the measurements, it is important that the wind speed and the direction as measured at the weather mast and that which acts upon the cooling tower is the same and that the approaching wind profile is not disturbed. If the wind direction is between 15 degrees west of north and 25 degrees south of east, the cooling tower is positioned in the lee side of the other power station buildings and the wind profile will be disturbed. The latter is shown in figure 3.1.1 as the lee angle of the tower. Although the correct wind speed will be measured at the weather mast for the wind direction mentioned above, the data cannot be used to predict the wind speed at the tower.

On the other hand, for any wind direction between 20 degrees south of east to 10 degrees west of south, the wind speed which is measured at the tower will be essentially undisturbed, but in this case the weather mast is on the lee side of the buildings. Incorrect wind velocities will therefore be indicated by the anemometers on the mast. In figure 3.1.1 above mentioned direction is shown as the lee angle of the weather mast.

For this reason only the data for wind directions between 15 degrees west of north and 10 degrees west of south was used. The rest of the data had to be rejected owing to uncertainties in the value of the wind speed at the tower.

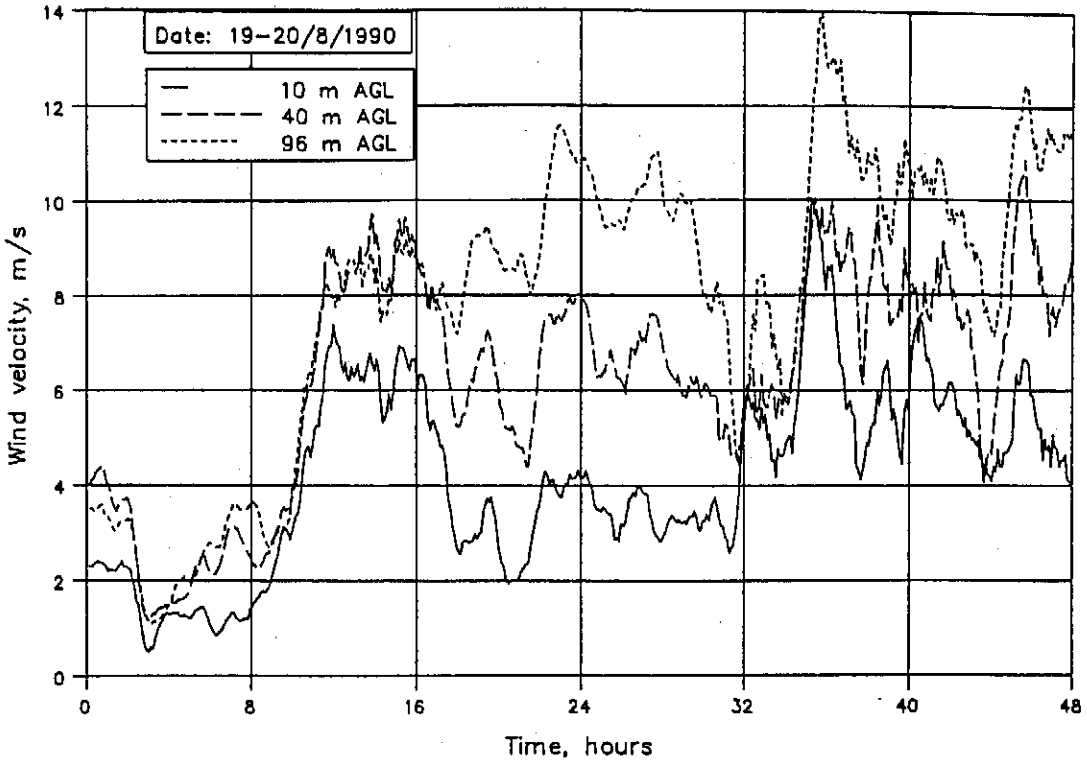

Figure 3.3.4: Wind speed at different elevations.

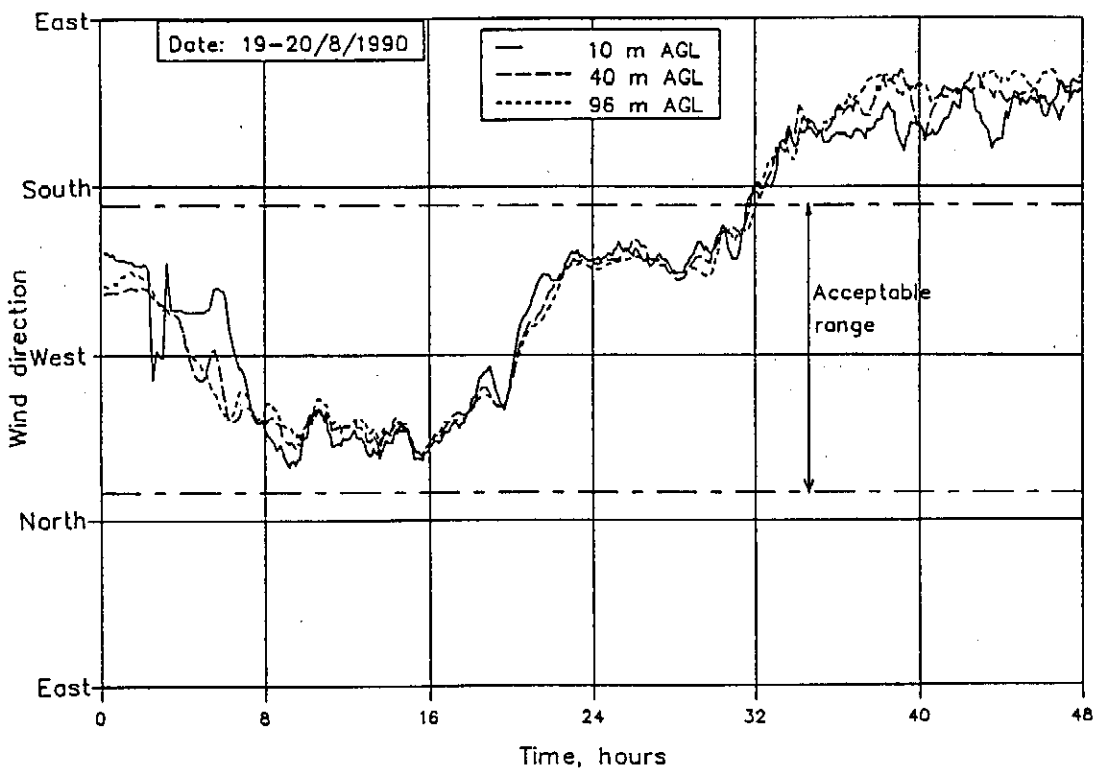

Figure 3.3.5: Wind direction at different elevations.

In figures 3.3.6 and 3.3.7 the vertical wind velocity and temperature distribution are shown for the days 15/8/1990 and 16/8/1990. The inversion layer which formed near the ground surface during the night is clearly visible in figure 3.3.6. During the day the air near the ground is heated and will tend to rise due to buoyancy effects and the air in the surface layer is thus effectively mixed. Due to the corresponding momentum transfer, a uniform velocity profile will be obtained while a surface boundary layer is formed during the night as shown in figure 3.3.7. If the wind profile is described by a power law, as defined in equation (1.1.1), the exponent b can be calculated for the velocity distribution shown in figure 3.3.7. The results are shown in figure 3.3.8. The data in the figure suggests that the value of the exponent, b, can vary from approximately zero during the day to values as high as 1.2 during the night. The value of 0.2 as recommended by VDI 2049 [78VD1] for cooling tower measurements seems therefore to be applicable during the day only.

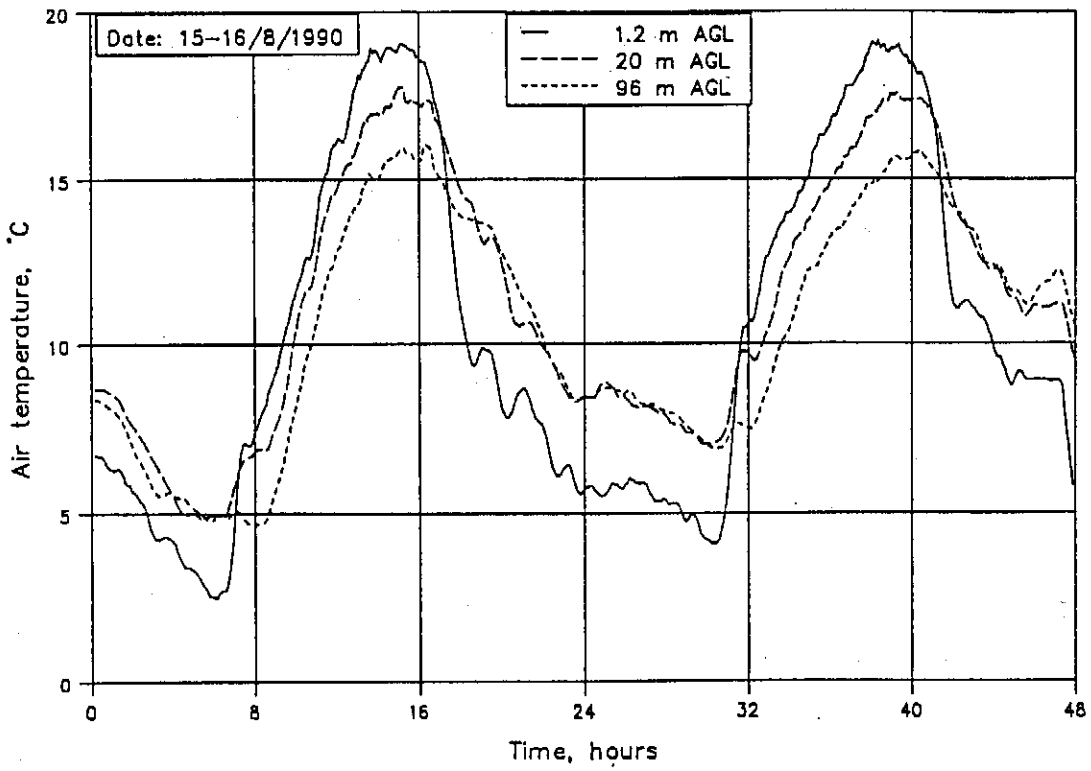

Figure 3.3.6: Temperature distribution.

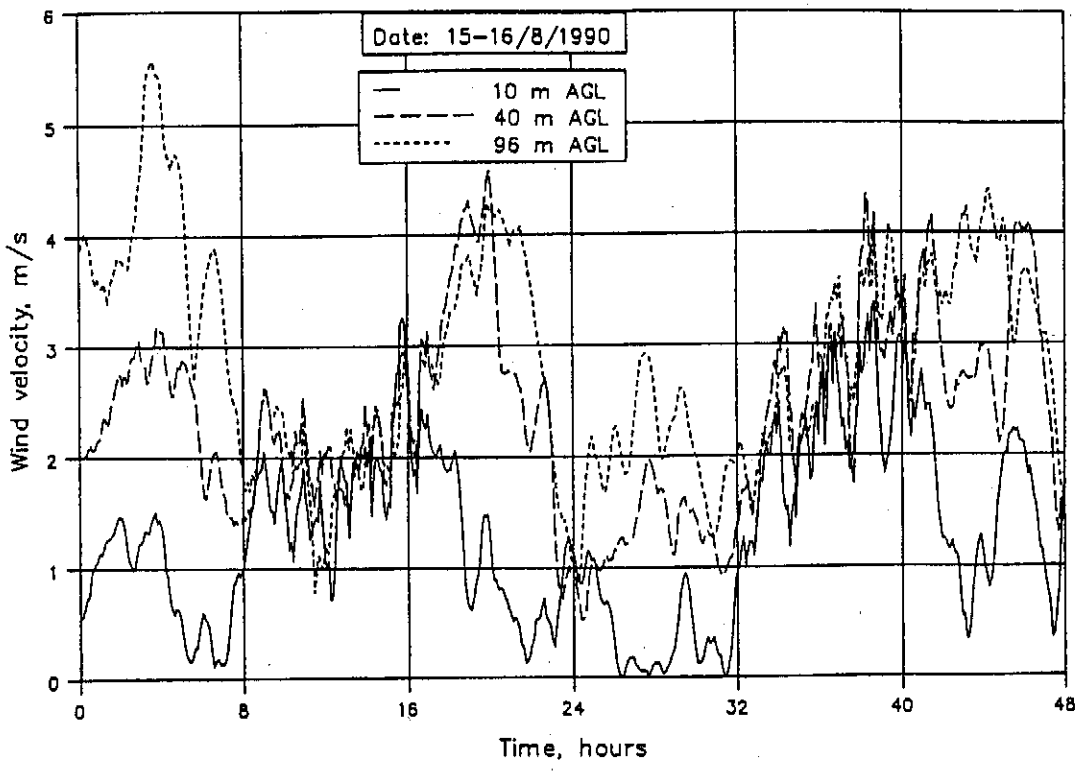

Figure 3.3.7: Wind velocity distribution.

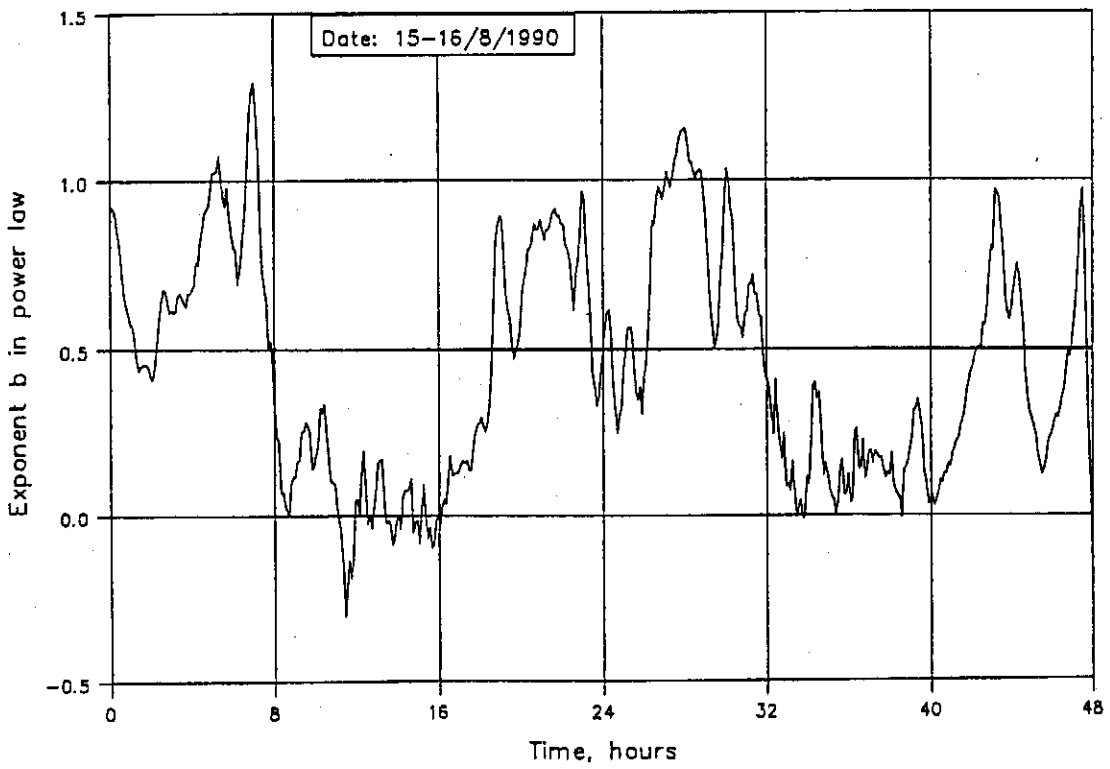

Figure 3.3.8: Exponent b in power law.

In figure 3.3.9 the temperature difference between 5 m and 96 m above ground level is shown as a function of the wind speed at 96 m above ground level. It is obvious that there is no relationship between the inversion strength and the wind speed and that relatively strong inversions are observed even at high wind velocities.

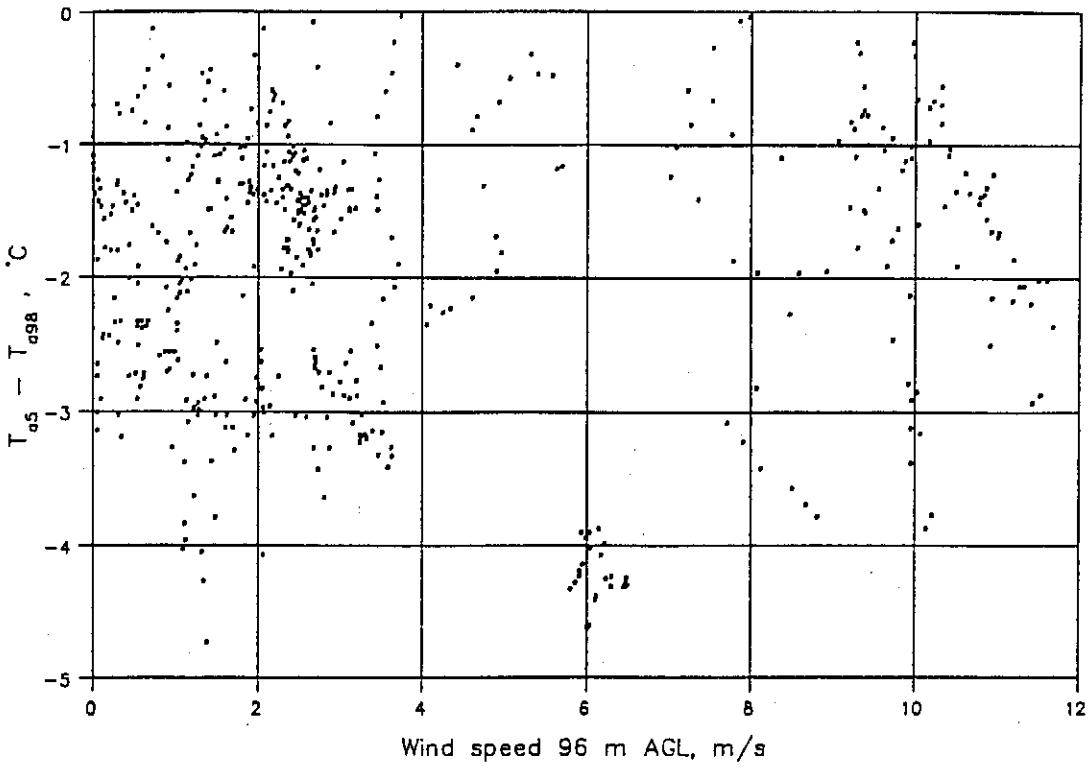

Figure 3.3.9: Relationship between inversion strength and wind speed.

The air inlet temperatures measured by the three air inlet thermocouples, T_{ai1}, T_{ai2}, and T_{ai3}, were for all practical purposes always the same. This leads to the conclusion that the air which enters the cooling tower is either thoroughly mixed or most is drawn from essentially the same elevation. In figure 3.3.10 the temperature of the air which enters the heat exchangers and the air temperatures as measured on the weather mast are shown for 9/8/1990. For this particular day the wind speed almost never exceeded 3 m/s. The results in the graph suggest a good agreement between the temperature of the air which enters the heat exchanger and the air temperature at higher elevations and therefore it appears as if very little of the air from low elevations enters the tower [82GR1]. Due to adiabatic compression, the air from higher elevations which enters the tower will be heated which might be an explanation for the high air temperature in the tower inlet during the night.

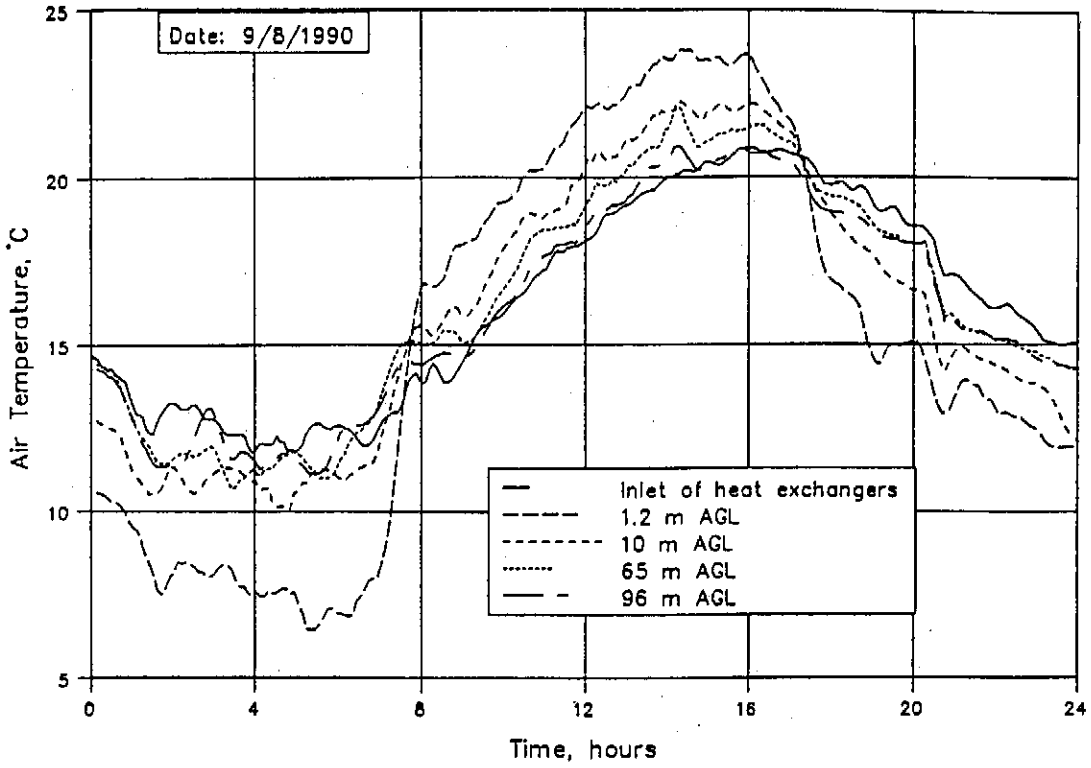

Figure 3.3.10: Air temperature in tower inlet v. the air temperature at weather mast.

On a few occasions during the two months while the tests were in progress, one or more of the cooling sectors in the tower were closed for a period of time. Although interesting air velocity profiles were measured in the tower, the rest of the data obtained in those periods had to be rejected.

Due to the thermal inertia of the cooling system, the correct procedure to follow would be that measurements on the tower are only made after all the independent variables are constant for at least a long enough period of time to let the dependent variables stabilize. Because of the unstable character of the wind both in speed and direction and the continuous variation in the air temperature during the day, the above mentioned conditions were never met during the test period.

In figures 3.3.11, 3.3.12 and 3.3.13 the water outlet temperature, air outlet temperature and air velocities in the tower are shown for a few hours as measured on the 9/7/1990. During this time sector 8 was closed for about 55 minutes. Because the water in the sector is immediately drained when the sector is closed, the temperature of the air leaving the particular bundle will within a few seconds be equal to the air inlet temperature. This will cause an abrupt change in the operating conditions of the tower and the temperature of the water in the cooling system

will increase until a new operating point is reached. The results shown in the three figures, as based on five minute observation periods, show that a new operating point is reached within 30 minutes after the bundle was closed as shown in figure 3.3.11.

The parameters of the cooling circuit are such that water in the circuit completes the cycle approximately every 9 minutes. If it is assumed that the heat rejected in the condenser is constant and not a function of the cooling water temperature, the water inlet temperature of the cooling tower will therefore not change within nine minutes after an abrupt change in the operating conditions of the tower. This process will be repeated until the system stabilizes at a new operating point. Because both the air and water flow through the tower in less than 1.5 minutes, the cooling tower, if considered on its own, will reach a stable operating point in probably less than nine minutes after a change in the water inlet temperature of the tower. Thus the situation will be found where the cooling tower operates at a temporary stable condition while the cooling system has not yet reached its new operating point. Therefore the measurements performed on the tower will not be much affected by an instability in the cooling system. Furthermore, changes in the independent variables like wind speed or air temperature very seldom occur instantaneously and therefore the cooling system will tend to stabilize in a much shorter time period, as in the case of an abrupt change like the closing of a cooling sector.

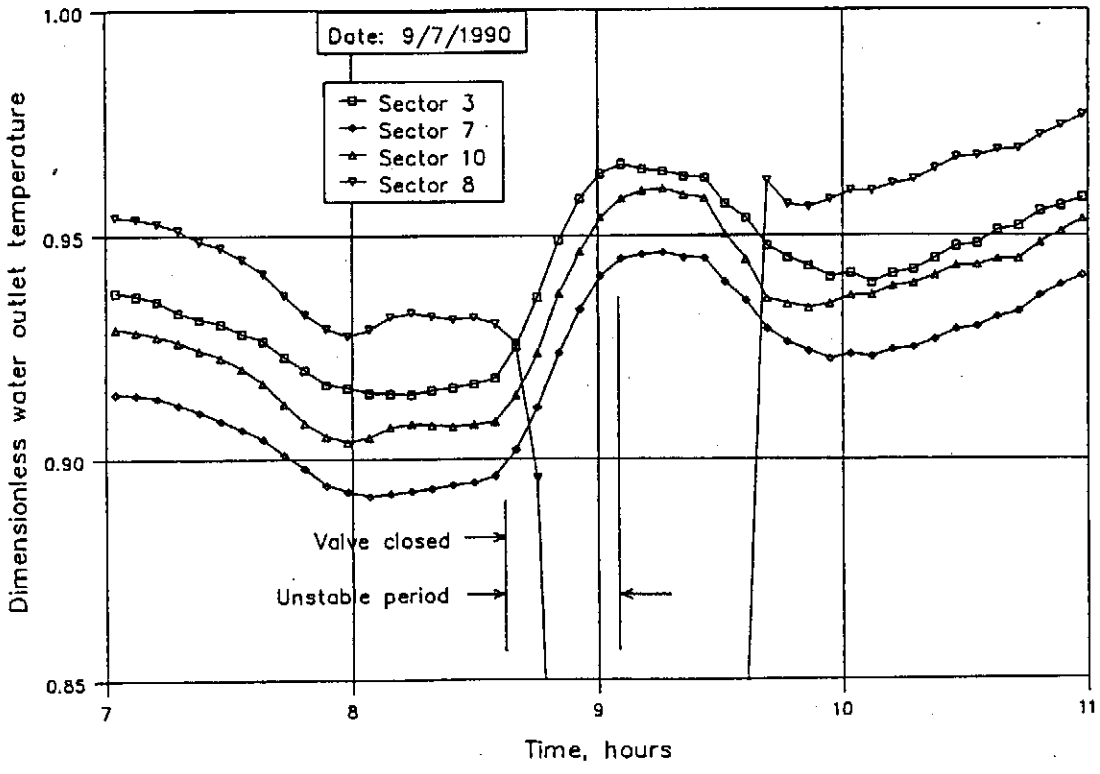

Figure 3.3.11: Water outlet temperature on 9/7/1990.

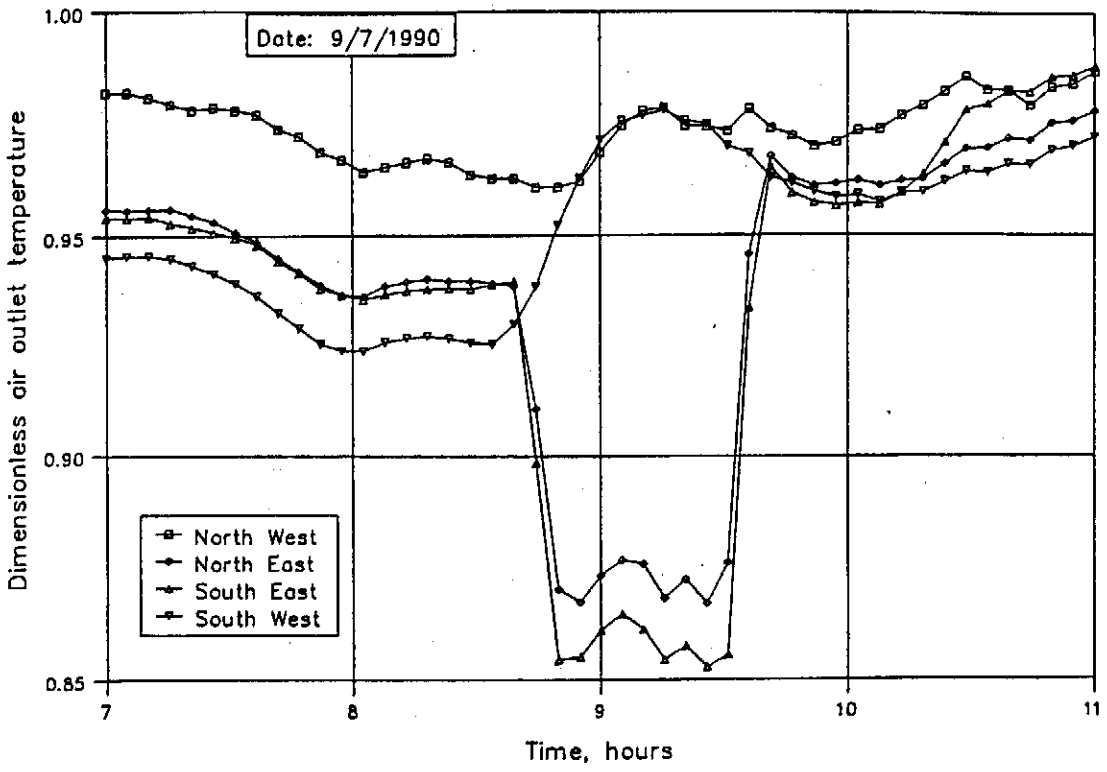

Figure 3.3.12: Air outlet temperatures on 9/7/1990.

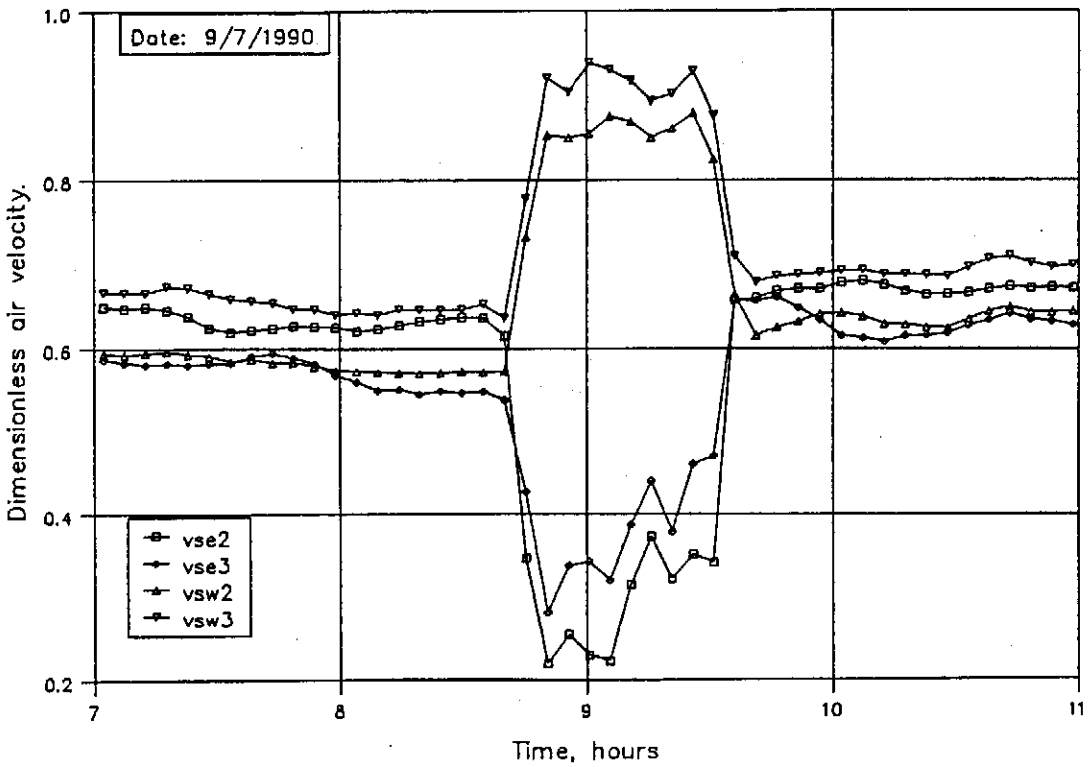

Figure 3.3.13: Air velocities in the tower throat as measured on 9/7/1990.

Due to the nature of the measurements, it will be practically impossible to make allowance for the thermal inertia of the cooling system for each variation in the value of the independent variables. Although the latter may cause scatter in the data, no serious errors are expected in the light of the preceding discussion.

3.4: Influence of the wind on the performance of the dry-cooling tower.

The influence of a cross-wind on a cooling tower is best illustrated by graphing all the independent and dependent variables for the same time period. In figure 3.4.1 the generator output, ambient air temperature, wind speed, wind direction, water outlet temperature, air outlet temperature and air velocity distribution in the tower throat are shown respectively as measured on 18-19/7/1990. The measurements of this particular time period were chosen because at 20:00 on the 18/7/1990 an almost instantaneous change in the wind direction from NW to SW occurred, which had a significant influence on the values of the dependant variables. As the measurements based on five minute observation time periods proved to be too spiky for qualitative analysis, the curves were smoothed by converting the data to a fifteen-minute average base.

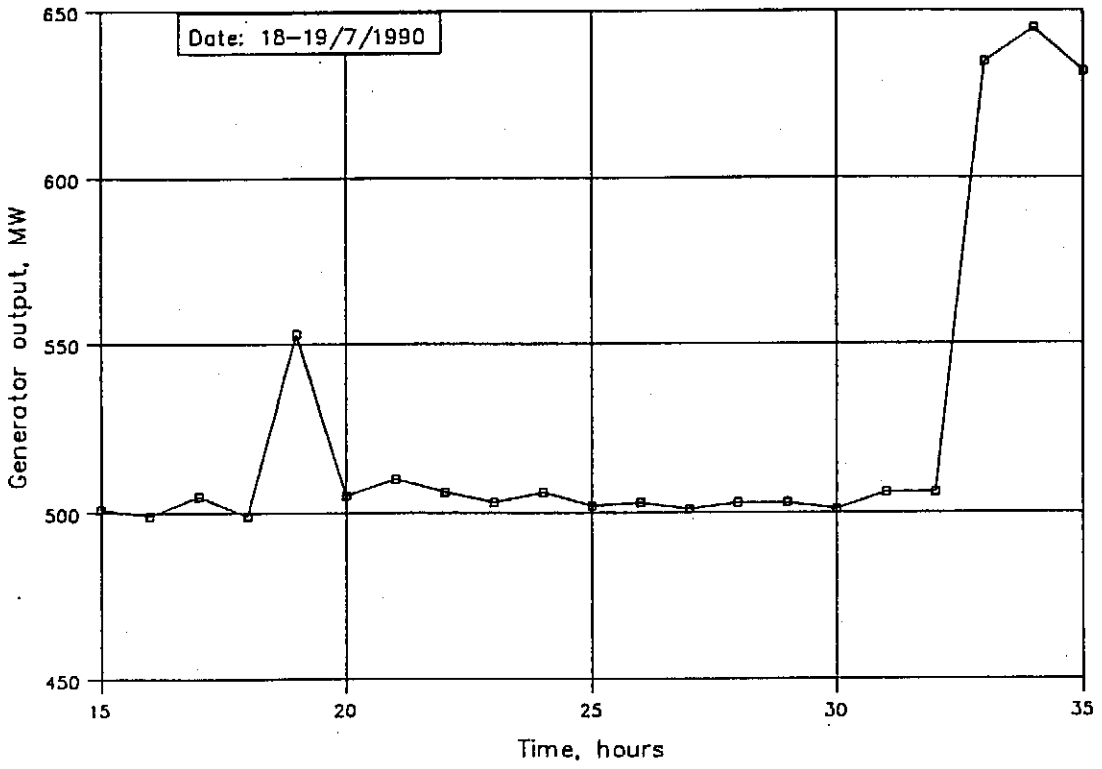

Figure 3.4.1a: Generator output of unit one.

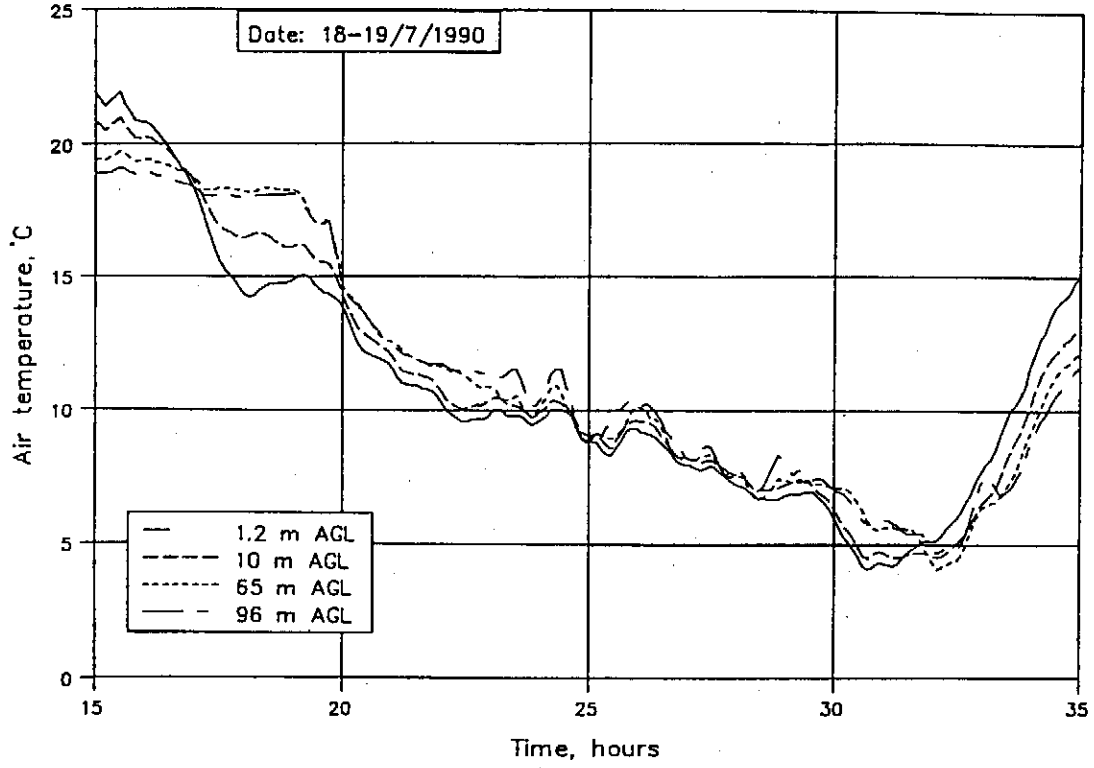

Figure 3.4.1b: Air inlet temperature as measured on weather mast.

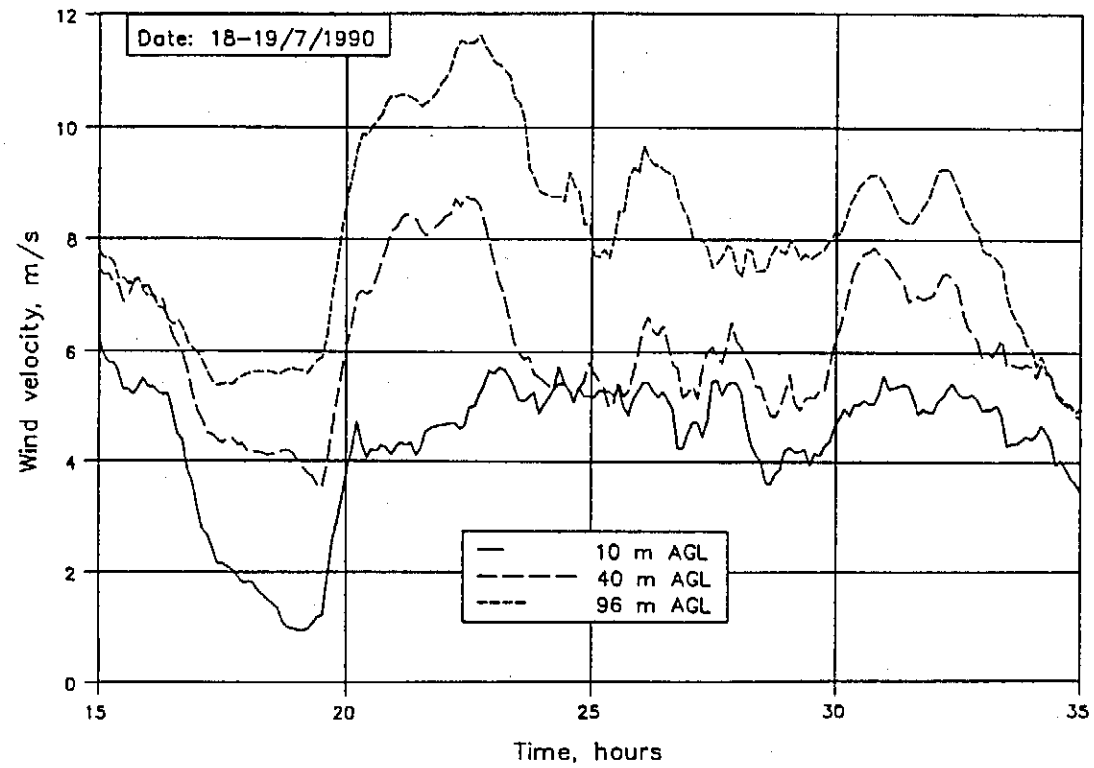

Figure 3.4.1c: Wind speed as measured on weather mast.

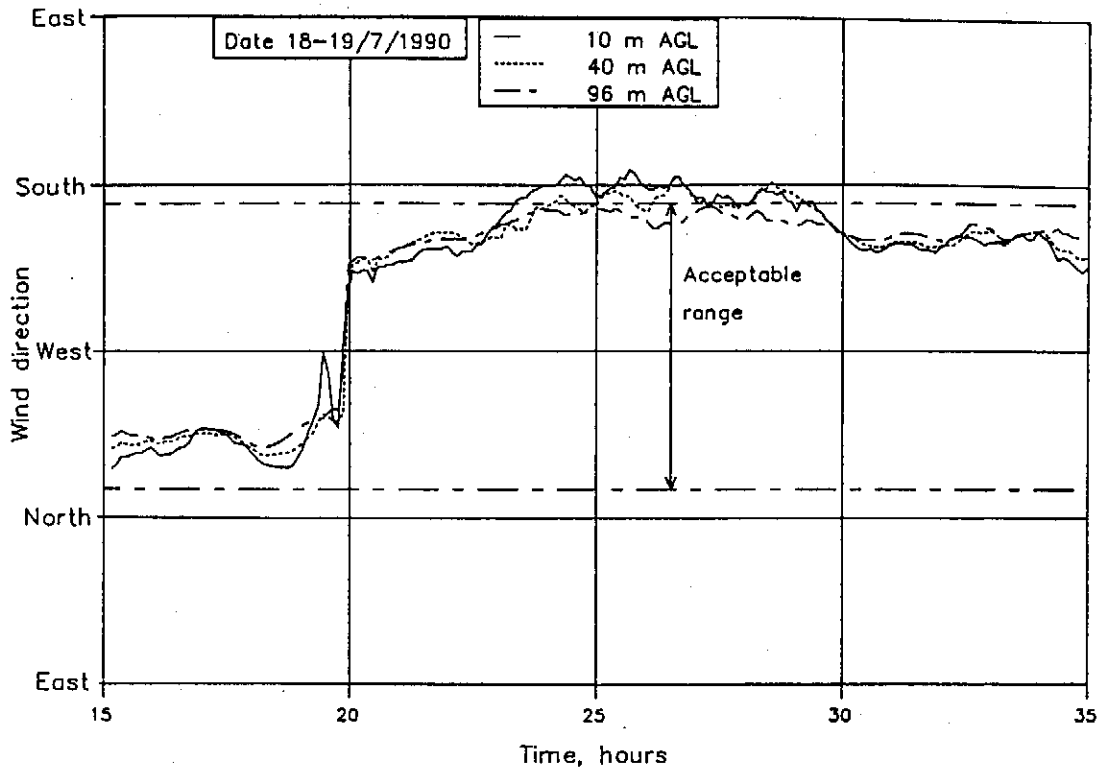

Figure 3.4.1d: Wind direction.

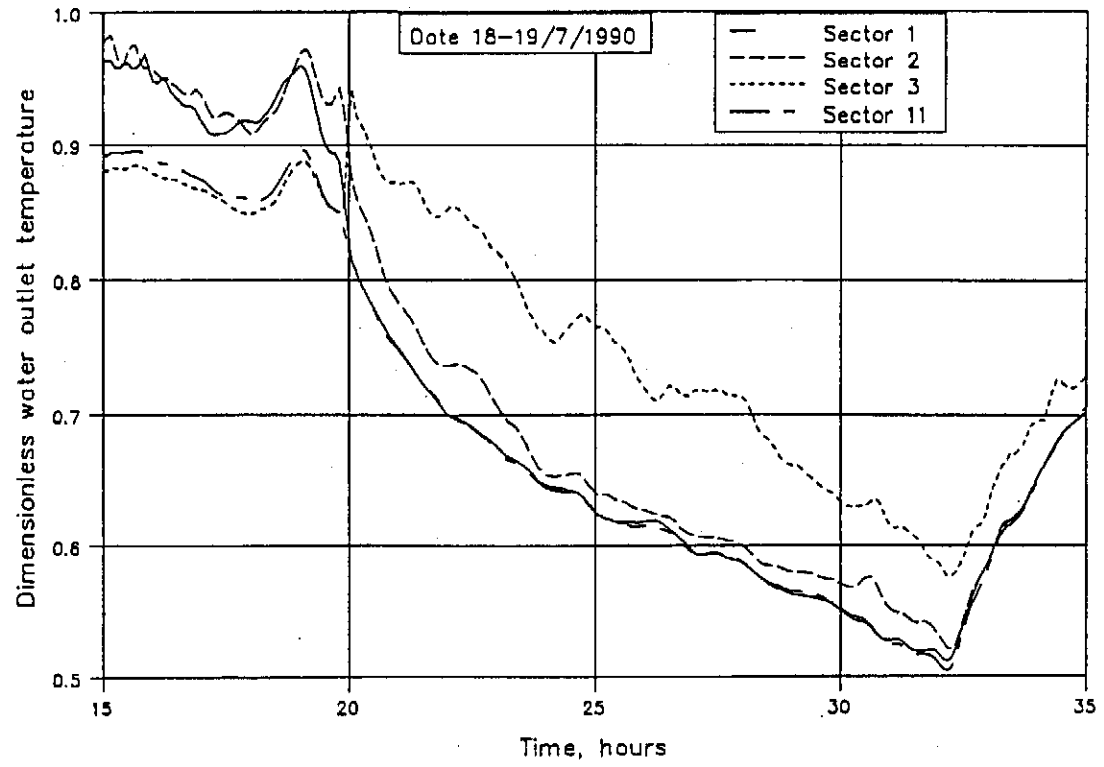

Figure 3.4.1e: Water outlet temperature.

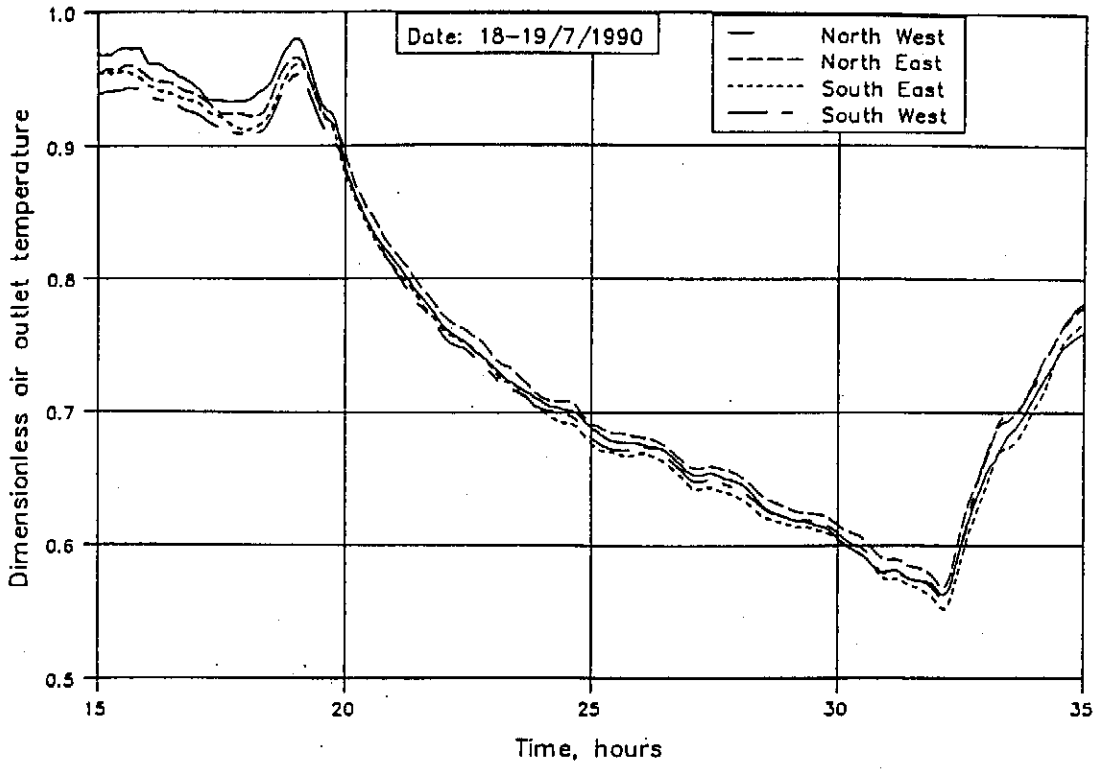

Figure 3.4.1f: Air outlet temperature as measured in tower throat.

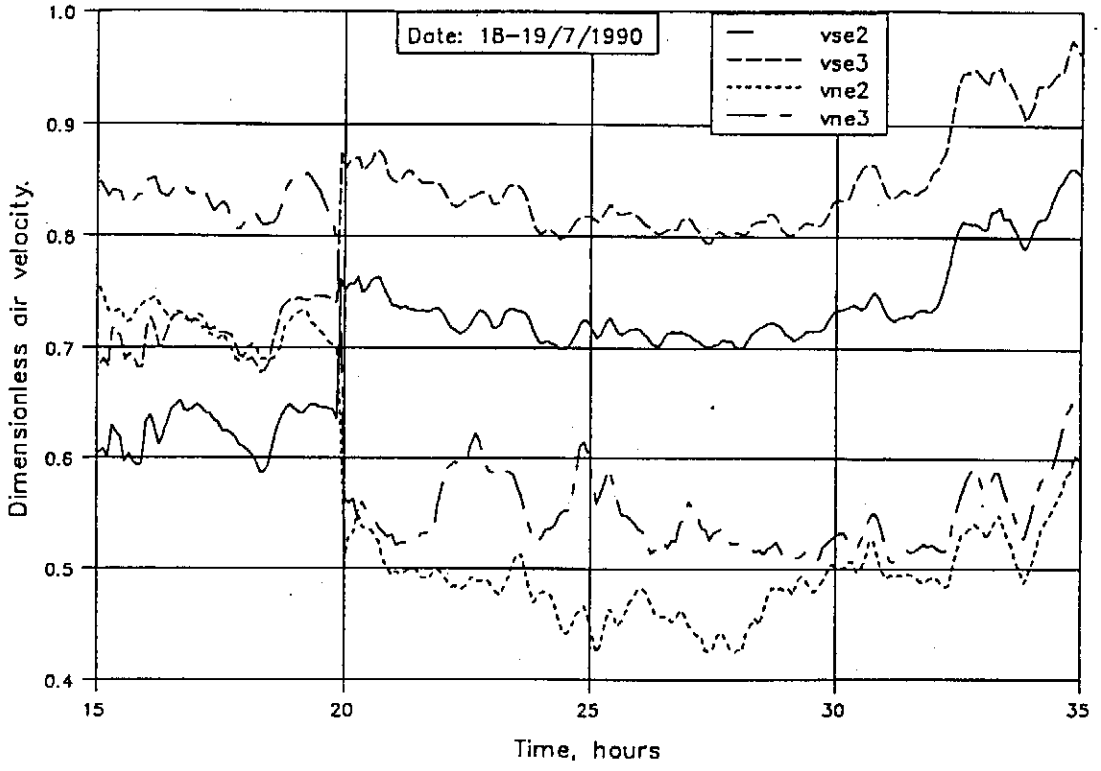

Figure 3.4.1g: Air velocity as measured in tower throat.

The rise in the water and air outlet temperature on 18/7/1990, 18:00 and 19/7/1990, 8:00 is caused by the increase in the turbine output during these periods. The latter is in agreement with the results shown in figure 3.3.1 to 3.3.3.

As expected, the variation in the air and water outlet temperatures follow the trend of the air inlet temperatures closely. The influence of a cross-wind on the performance of a dry-cooling tower is normally expressed in terms if the rise in the approach temperature of the tower for a fixed heat rejection rate of the tower as a function of the wind speed, where the approach temperature is defined as the difference in the mean water outlet temperature and the mean air temperature entering the bundles.

Before the rise in the approach temperature of a cooling tower can be calculated, a reference approach temperature has to be found. The latter is defined as the approach temperature of the tower without atmospheric disturbances like a cross-wind, temperature inversions or rain. Obviously, these ideal atmospheric conditions were never found during the two months of the test period, therefore the reference approach temperature of the cooling tower is considered to be the approach temperature as obtained for a cross-wind speed, 96 m above ground level, of less than 2 m/s together with a temperature gradient between zero and 2 °C. All the measurements made during the test period with atmospheric conditions which satisfy the limits mentioned above, are shown in figure 3.4.2 as a function of the air inlet temperature. No explanation could be found for the scatter in the data, since the latter is neither a function of the wind velocity, temperature gradient or the output of the turbine. The turbine output for the data shown in the figure was ca. 500 MW which corresponds with a cooling tower output of ca. 650 MW. The reference approach temperature appears to be a function of the air inlet temperature which is caused by the variation of the heat transfer properties of the air and cooling water.

The water outlet temperature for a few of the cooling sectors in the tower is shown in figure 3.4.1e. On the 18/7/1990 before 20:00 the water outlet temperatures of sector 1 and 2 are shown to be noticeably higher than the outlet temperatures of the rest of the sectors. The wind direction during that time, as shown in figure 3.4.1d was NW and therefore, according to figure 3.1.3, sectors 1 and 2 were positioned in the upstream side of the tower. This was always found to be the case, i.e. the sectors in the upstream side of the tower are the worst affected by cross-winds. The latter is confirmed by observing the rise in the water outlet temperature of sector 3 on 18/7/1990, 20:00 which occurred simultaneously with the change in wind

direction from NW to SW. At the same time the water outlet temperature of sector 1 dropped to the approximately the same value of the water outlet temperature of sector 11. Although a similar temperature drop was found in sector 2, the latter was still slightly affected by the wind. It is furthermore found that the cooling sectors arranged round the circumference of the tower namely sectors 1, 2, 3 and 4 (see figure 3.1.3) are the worst affected by the wind. Sectors 5 to 11, positioned nearer to the centre of the tower, proved to be much less sensitive to cross-winds.

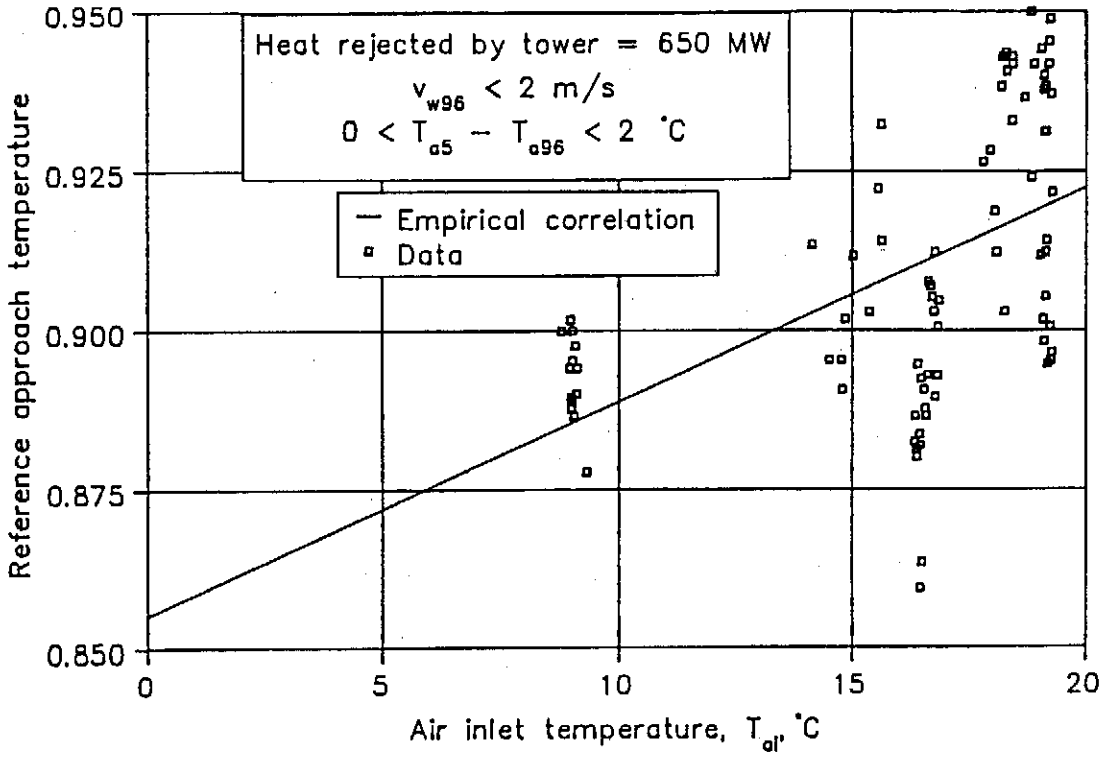

Figure 3.4.2: Reference approach temperature of the tower.

The air temperature distribution in the tower throat, shown in figure 3.4.1f is almost uniform during the entire period shown in the figures and is therefore not affected by the wind. This is in agreement with the results reported by Van der Walt [76VA1] who performed similar measurements on a dry-cooling tower of the Grootvlei power station.

As shown in figure 3.4.1g the wind has also an effect on the air velocity distribution in the tower. On 18/7/1990 before 20:00, the air velocity in the SE-side of the tower throat was the highest and a sudden drop in the air velocity on that side of the tower is observed simultaneously with the change in the wind direction while the air velocity in the NE-side of the tower increased. The highest air velocity was always found in the lee side of the tower.

By using the experimental results which satisfy the conditions as discussed in section 3.3, the influence of cross-winds on the performance of the cooling tower of the Kendal power station can be obtained. In figure 3.4.3 the increase in the approach temperature of the cooling tower is given as a function of the wind speed as measured 96 m above ground level. All the observations shown in the figure were made for a turbine output of ca. 500 MW while roughly 650 MW was dissipated by the tower. Furthermore, the difference in the air temperature between 5 and 96 m above ground level was above zero, in other words most of the observations in the figure were made during the day. During the night temperature inversions are formed as shown in figure 3.3.9, and it was not possible to distinguish the individual influences of the two atmospheric variations. With the wind profile described by the power law, the exponent b was calculated for the observations shown in the figure. The average value of b during the day was found to be equal to 0.16. Based on the results shown in figure 3.4.3, the rise in the approach temperature of the cooling tower as a function of the wind speed is correlated by equation (3.4.1)

$$\Delta(T_{wo} - T_{ai}) = 0.07335\ v_{w96} + 0.027396\ v_{w96}^2 \qquad (3.4.1)$$

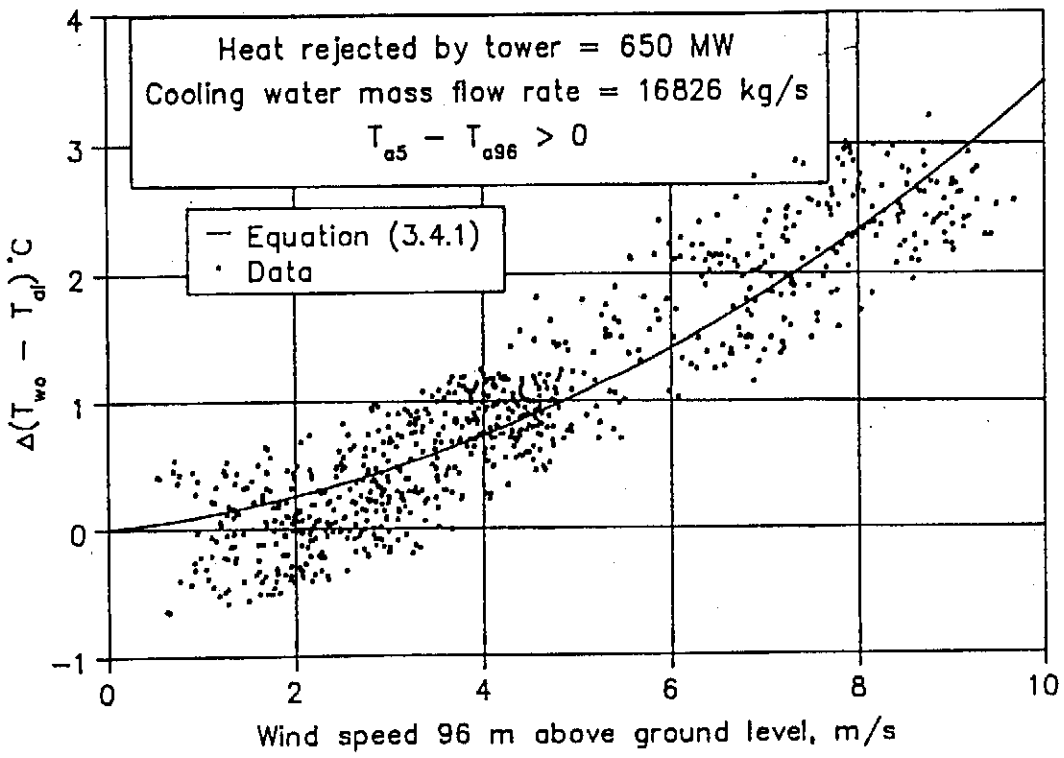

Figure 3.4.3: Wind effect on tower based on the wind speed as measured 96 m AGL.

Though some of the scatter in the data could be caused by the thermal inertia of the cooling system, no other cause for the scatter could be found since the latter is not a function of any of the independent variables.

In figure 3.4.4, the results in figure 3.4.3 are based on the wind speed measured 10 m AGL. A prominent difference between the results shown in the previous two figures, is that considerably more scatter in the data is found when the observations are based on the wind speed as measured close to the ground surface. The same tendency was also observed by Bourillot [80BO1] who used the wind speed at the tower outlet as reference since it leads to the lowest result dispersion. Although one is inclined to accept that the latter is caused by instabilities in the surface layer, this could not be confirmed by the measurements. Observations made for a turbine output of ca. 650 MW with a corresponding heat rejection rate of 860 MW in the tower are shown in figure 3.4.5 with equation (3.4.1) also shown. The results clearly suggest that as the heat rejection rate of the tower increases, the tower becomes less sensitive to cross-winds, which is in agreement with similar observations reported by Markòczy [77MA1] for a tower with a vertical arrangement of the heat exchangers.

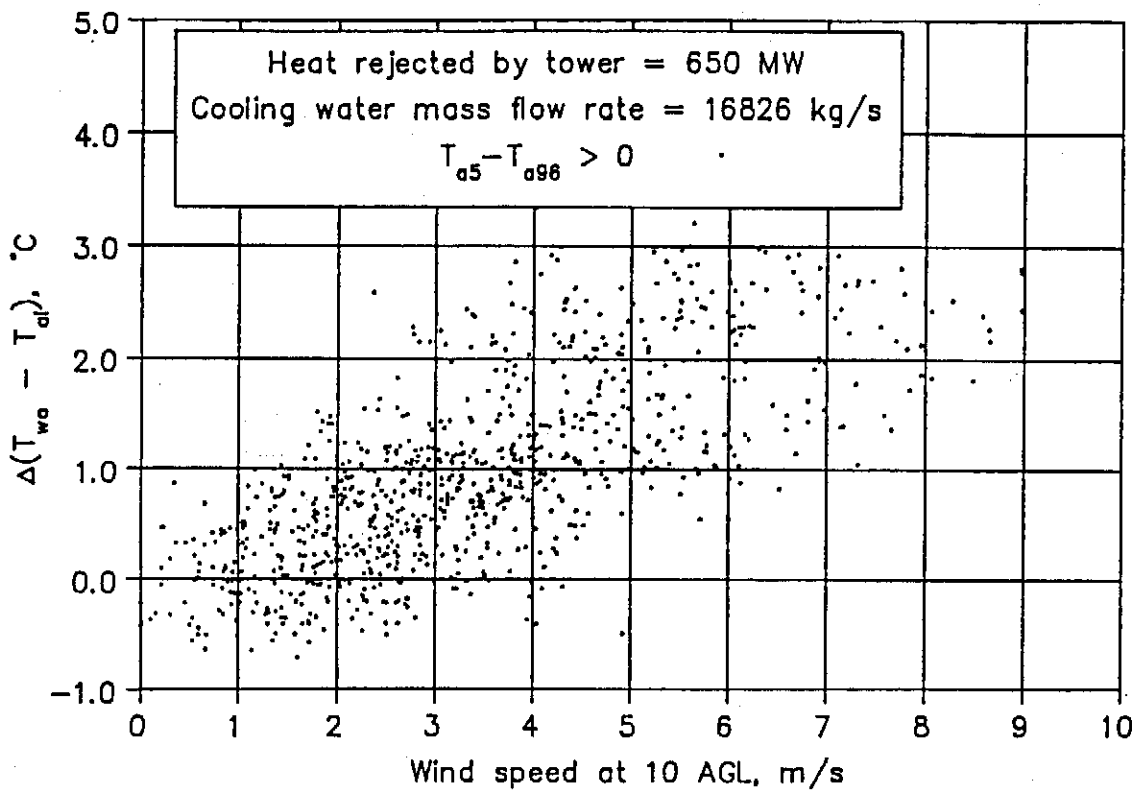

Figure 3.4.4: Wind effect on cooling tower based on the wind speed 10 m AGL.

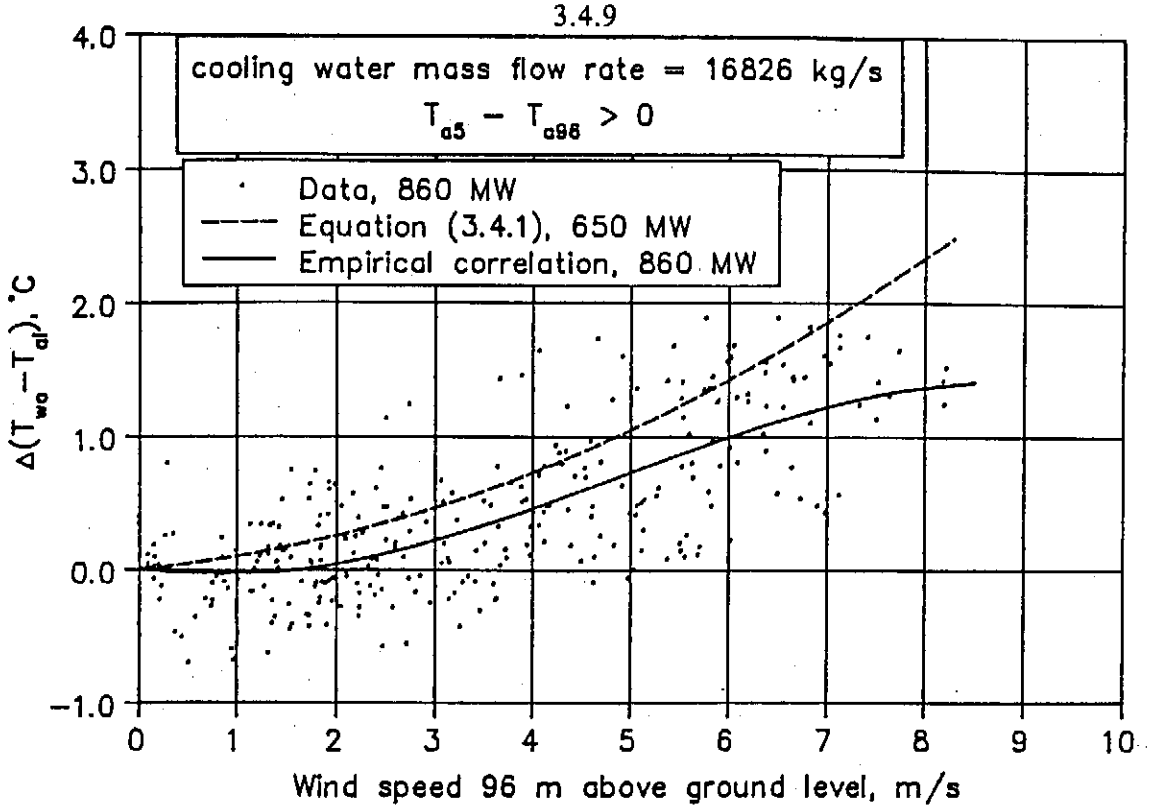

Figure 3.4.5: Wind effect on tower based on the wind speed as measured 96 m above ground level.

During the night temperature inversions are formed which will also have an effect on the performance of the tower, therefore it is not possible to distinguish the individual effects of the wind and inversion on the approach temperature. However, if it is assumed that the wind effect on the approach temperature as given by equation (3.4.1) is still applicable during the night, the latter can be used to obtain the effect of the temperature inversions on the performance of the tower. This was done by calculating the expected rise in the approach temperature for each of the observations made during the night according to equation (3.4.1) and subtract the latter from the measured rise in the approach temperature of the tower. In figure 3.4.6 the change in the approach temperature of the tower is shown as a function of the difference between the air temperature at 5 and 96 meter above ground level as measured on the weather mast. For all the observations in the figure the wind speed at 96 m above ground level was less than 9 m/s. The results suggest that much more scatter in the data is found in the measurements made during the night and that the tower is very little affected by the inversions. It should be emphasised that the approach temperature is defined as the difference between the water outlet temperature and the temperature of the air which enters the bundles and not the air temperature as measured on the weather mast.

If the approach temperature is defined as the difference between the mean water outlet

temperature and the air temperature as measured 5 m AGL on the weather mast, an almost linear relationship is found between the rise in the approach temperature of the tower and the inversion strength as shown in figure 3.4.7. If the air temperature at a lower elevation, say 1.2 m, was used, an even greater gradient will be found. It is therefore very important that field tests on cooling towers should be thoroughly documented, to avoid erroneous interpretation of the data.

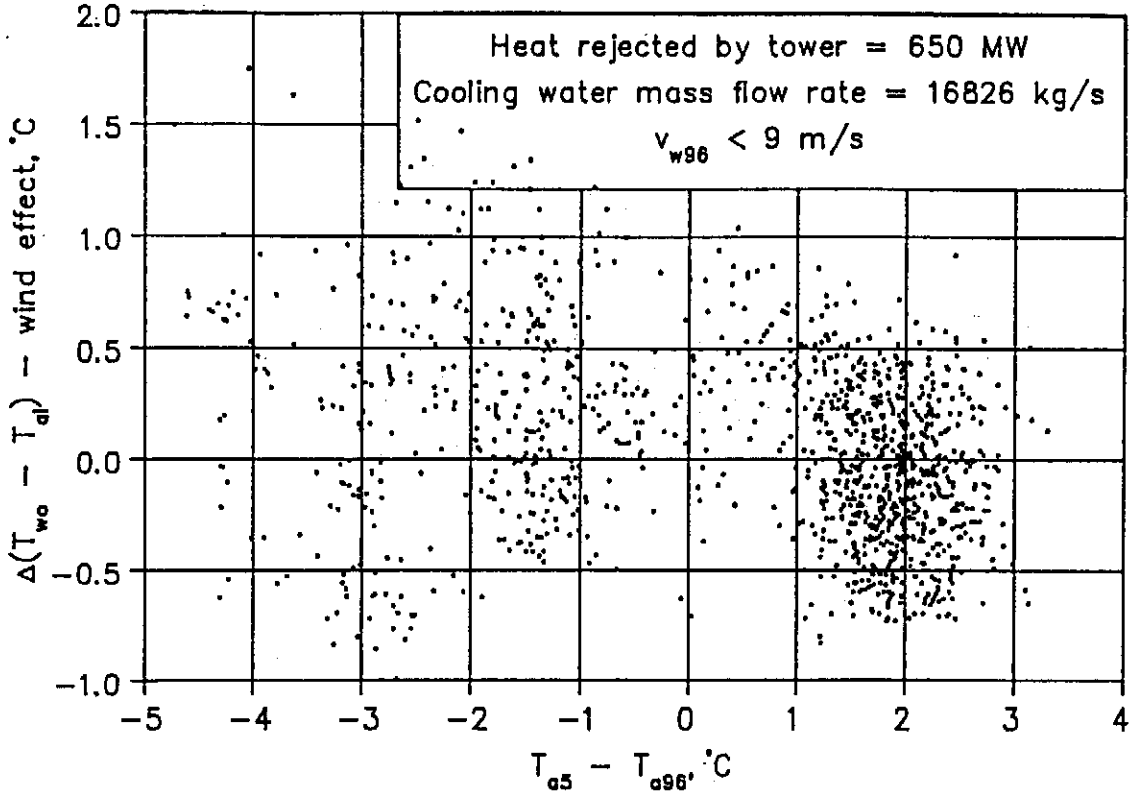

Figure 3.4.6: Approximate effect of temperature inversions on the approach temperature of the tower.

The mean air mass flow rate through tower was obtained by integrating the readings of the eleven anemometers positioned in the tower throat. In figure 3.4.8 the ratio of the air mass flow rate with wind to the mass flow rate without wind is shown as a function of the wind speed measured 96 m AGL. The results clearly indicated a reduction in the air mass flow rate through the tower for increasing wind speeds as also observed by Grange [82GR1] for a tower with a vertical arrangement of the heat exchangers. By applying equation (A.1.3), the kinetic energy coefficient was calculated for the air velocity distribution as measured in the tower throat. The results are shown in figure 3.4.9 as a function of the relative wind speed.

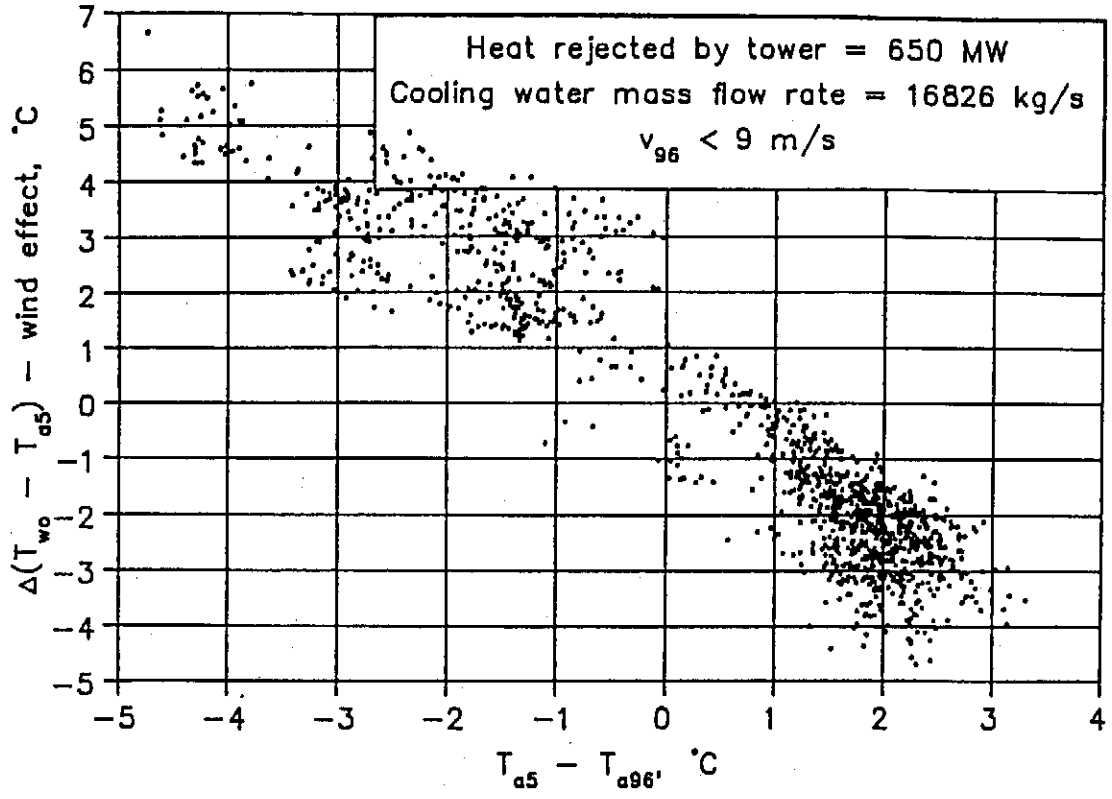

Figure 3.4.7: Effect of inversions on the approach temperature of the tower when based on the air temperature 5 m AGL.

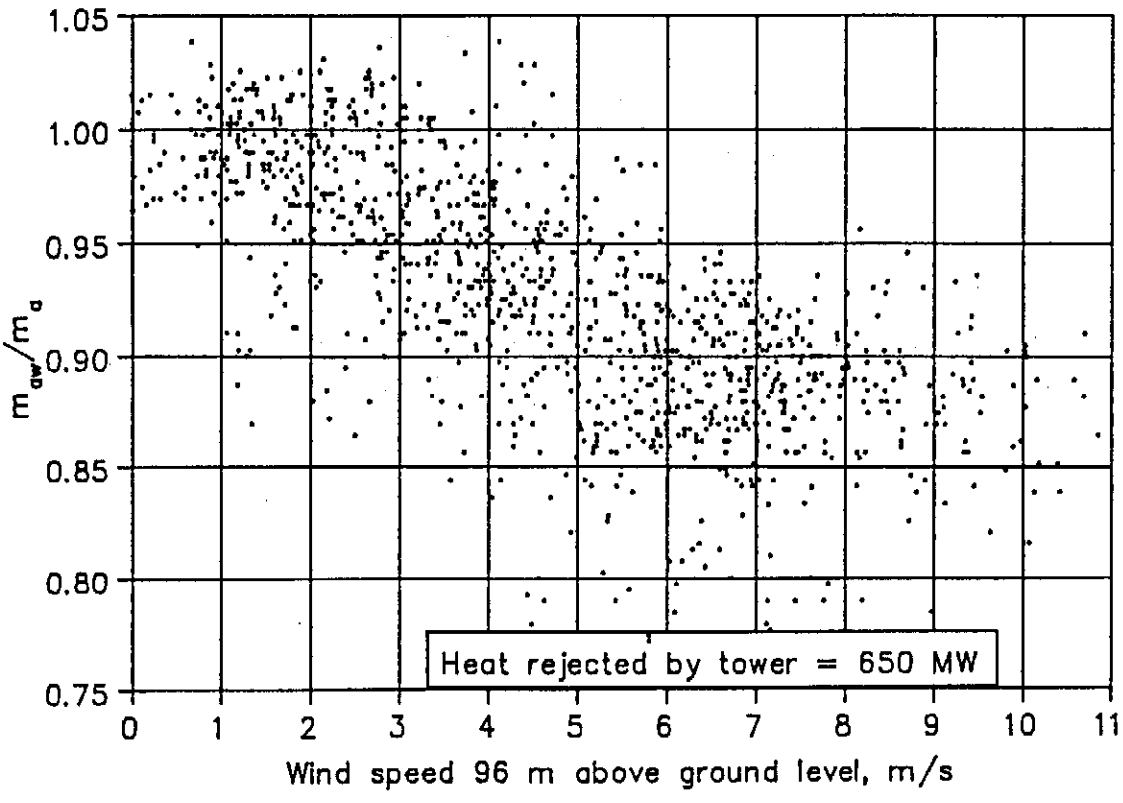

Figure 3.4.8: Mean air mass flow through the tower as a function of the wind speed.

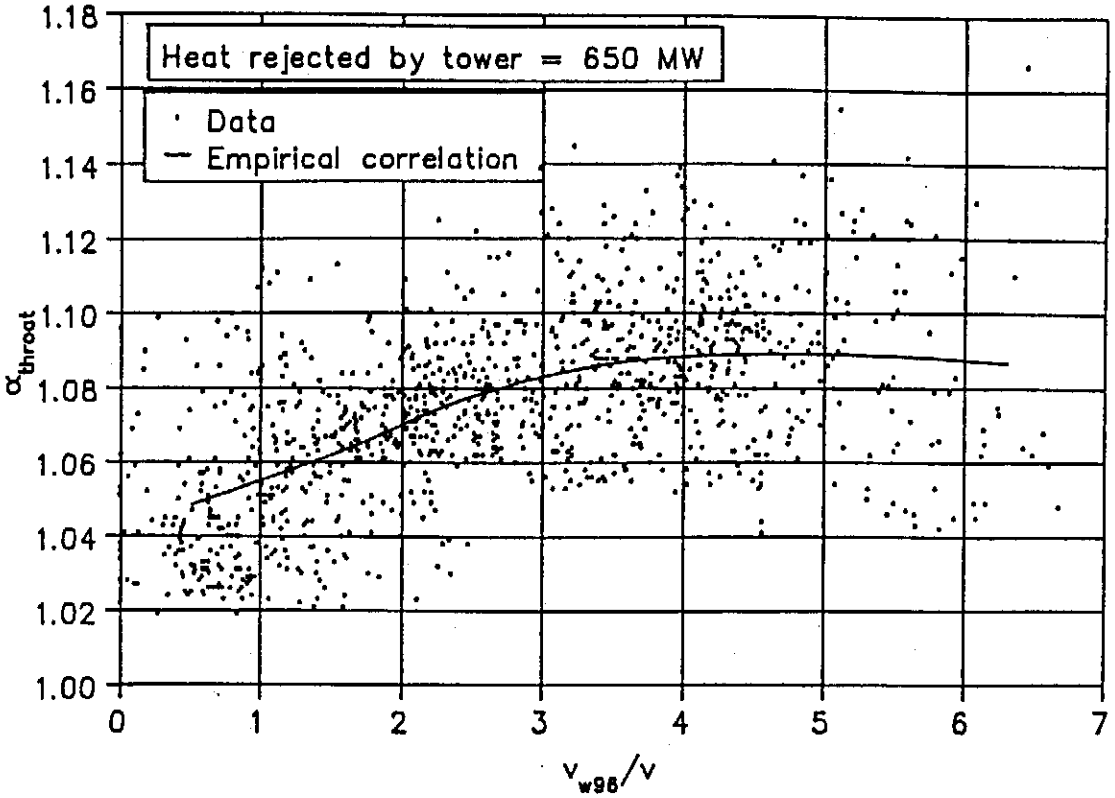

Figure 3.4.9: Kinetic energy coefficient in tower throat.

3.5: Conclusions

The effect of cross-winds on the performance of a representative natural draft dry-cooling tower was investigated by means of full scale measurements. The main findings of the measurements, as discussed in the preceding sections, may be summarised as follows:

1. The vertical temperature distribution has a strong influence on the wind velocity profile in the surface boundary layer. During daytime an almost uniform wind profile is found due to effective mixing in the unstable surface boundary layer. During the night when a stable inversion layer is formed near the ground surface an almost linear wind profile is obtained.

2. No relationship between the wind speed and inversion strength was found and strong inversions were observed at high wind speeds.

3. The mean temperature of the air entering the heat exchangers corresponds to the air temperature measured 96 m above ground level on the weather mast. It therefore appears that most of the air entering the cooling tower is drawn from elevations higher than the inlet height of the cooling tower.

4. Vertical temperature inversions, which usually form during the night, have almost no effect on the performance of the cooling tower.

5. As the wind speed increases the mean air mass flow rate through the tower decreases with a corresponding reduction in amount of heat rejected by the tower.

6. A reduction in the wind effect on the tower is found if the heat rejection rate of the tower is increased.

7. Much more scatter is found in the results when the observations are based on the wind velocity measured near the ground surface in comparison with the scatter found when the wind velocity 96 m above ground level is used as reference.

8. The performance of the heat exchangers on the upstream side of the tower is affected the most by the wind.

9. The maximum air velocity in the tower throat is always found on the lee side of the tower.

10. As the wind speed increases, the air velocity distribution in the tower becomes increasingly more non-uniform.

Since the experimental results, shown in chapter 2, were obtained for a tower with a horizontal heat exchanger arrangement (no A-frames), the full scale measurements cannot be used to evaluate the results of the model tests. It is however worth while to take note of the similarities and differences between the results obtained with the two methods.

1. The experimental procedure and the full scale measurements both indicate a reduction in the heat rejection rate of the tower if the wind speed increases, compare figures 2.5.2 and 3.4.3.

2. Both methods show a reduction in the mean air mass flow rate through the tower as the wind speed increases (see figures 2.5.3 and 3.4.8).

3. The full scale measurements indicate that the heat exchangers on the upstream side of the cooling tower are most affected by a cross-flow. The air velocity distribution measured through the heat exchangers in the model also shows a reduction in the air mass flow rate through the heat exchangers on the upstream side of the tower (see figure 2.3.1).

4. Tests performed on the scale model show that the air velocity distribution through the tower becomes increasingly more non-uniform as the wind speed increases (see figure 2.3.2) which is in agreement with full scale observations shown in figure 3.4.9.

5. Figure 2.5.5 predicts an increase in the wind effect on the performance of a tower if the heat rejection rate of the tower is increased which is in direct contrast with the results obtained on the full scale tower shown in figure 3.4.5.

Numerical simulations are free from many of the constraints imposed on experimental and full scale methods and can provide values for all the relevant variables throughout the entire domain of interest. In the following chapter a numerical procedure is employed to investigate the influence of A-frames and tower supports on the performance of a dry-cooling tower during wind periods.

CHAPTER 4

Prediction of the wind effect on a natural draft dry-cooling tower by using numerical methods.

4.1: Introduction.

Radosavljevic [88RA1] used the general purpose computer code PHOENICS to predict the internal and external aerodynamics and thermal flow field of a natural draft wet cooling tower in a cross-wind. By following a similar approach the wind effect on a natural draft dry-cooling tower was studied in the present investigation.

A three dimensional model of a dry-cooling tower, similar to the towers erected at the Kendal power station, was used in the analysis. Due to symmetry only one half of the tower and the immediate surroundings were considered. Obstacles such as pipes, tanks and their structural supports located on the ground under the heat exchangers in practical cooling towers are not considered in the present model. In a dry-cooling tower, heat is transferred from the water in the finned tubes to the cold ambient air by convection. Since the water is not in direct contact with the air, no mass transfer is involved in the cooling process. It is therefore only necessary to solve the appropriate differential equations for the air. It is furthermore assumed that the problem is time independent, which is actually not true since vortices are shed in a Kármán vortex street on the downstream side of the cooling tower with a frequency which is dependent on the Reynolds number. By solving the problem as a steady one, a potential type flow is forced around the cylindrical cooling tower which will affect the pressure distribution around the outer surface of the tower shell. As discussed in Appendix E, the latter has a noticeable influence on the static pressure inside the tower and therefore also on the air mass flow rate through the tower.

If the flow instabilities exterior to the tower have to be represented, it would be necessary to employ a time-dependent solution with a much finer grid which will drastically increase the computational time. It was therefore decided, that for the purpose of the present investigation, the computer time will be used more effectively by doing more runs with a somewhat coarser grid for different tower geometries, which can be used for comparative purposes.

For a steady, single-phase problem PHOENICS provides solutions to the discretized form of

sets of differential equations of the form

$$\text{div}(\rho v\phi - \Gamma_\phi \text{ grad } \phi) = S_\phi \qquad (4.1.1)$$

where $\rho v\phi$ represents the convection term, Γ_ϕ grad ϕ the diffusion term and ρ, v, Γ_ϕ, S_ϕ are the density, velocity vector, exchange coefficient and source rate per unit volume respectively for the dependent variable ϕ. The dependent variables solved for the present problem were the static air pressure, p1, the three air velocity components in the tangential, u1, radial, v1, and vertical, w1, directions and the air temperature, h1.

Body-fitted coordinates, which almost coincide with polar coordinates, were used to define the shape of the tower shell with an inlet height of 24.5 m and outlet height of 165 m. The hyperbolic shape of the tower was approximated by a conical inlet section, with a cone apex angle of 26° and a cylindrical outlet section. The three-dimensional solution domain was divided into 4920 cells with six cells along the X_θ, 20 cells along the Y_r and 41 cells along the Z coordinate axes respectively. X_θ was measured in radians and represents angular position, while Y_r and Z were measured in metres and represent radial distance and height above ground level respectively. The grid was found to be fine enough to obtain a grid independent solution. The grid in the first and last X_θ-plane and the first Z-plane are shown in figure 4.1.1 with the cartesian coordinate indices also indicated. To simulate the interaction between the flow fields inside and outside the tower, the outer limits of the computational domain had a total height of 240 m with a 217.6 m radius. The Q1 instruction file which is read by the pre-processor is attached as Appendix I in which all the main settings are shown.

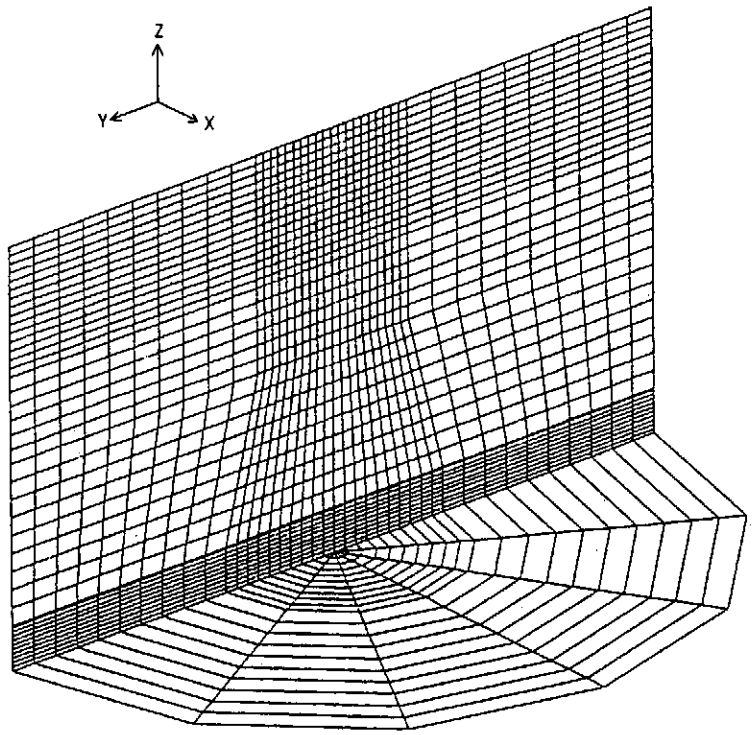

Figure 4.1.1: Grid distribution.

4.2: Sources and boundary conditions.

Calculations were done for both a uniform and a non-uniform wind profile with the wind entering the computational domain from the positive Y-direction as shown in figure 4.2.1. In the case of a uniform wind velocity, the velocity components u and v in the X and Y-directions were calculated by using the GXBFC subroutine for any wind velocity v_w. The form of the wind profile for a non-uniform velocity distribution was approximated by the power law, equation (1.1.1), and special GROUND coding was needed to calculate the velocity components at the inlet of the domain. The velocity component in the X_θ-direction, u1, for any given wind velocity was calculated by

$$u1 = v_w \sin\theta \left[\frac{z}{z_{ref}}\right]^b \qquad (4.2.1)$$

where z is the height above ground level of the cell under consideration, z_{ref} is the tower outlet height and b is the exponent in the power law. θ represents the angular position of the element as shown in figure 4.2.1.

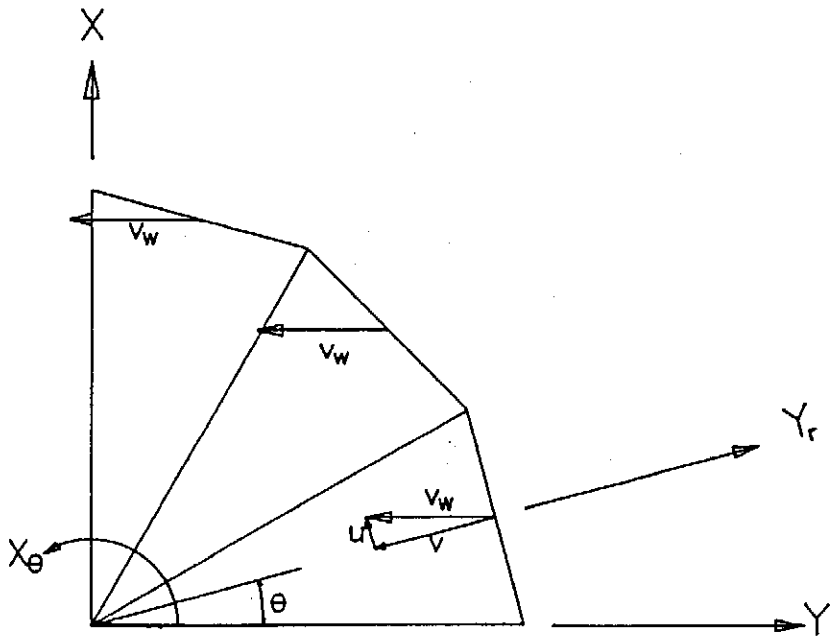

Figure 4.2.1 Components of entering wind profile.

For the Y_r-direction the component was similarly calculated i.e.

$$v1 = v_w \cos\theta \left[\frac{z}{z_{ref}}\right]^b \qquad (4.2.2)$$

A printout of the GROUND subroutine containing all the additional coding is shown in Appendix J. No-slip boundary conditions were specified at the ground level and the tower shell while no heat and mass flux was allowed through the tower wall. "Open" boundary conditions were specified at the exit of the computational domain at the top and the lee side. This was based on the assumption that the flow could be considered to be fully developed. Buoyancy forces were represented as sources in the momentum equations for w1 by

$$S_w = (\rho - \rho_{ref})\, g\, V \qquad (4.2.3)$$

where ρ is the air density of the warm air inside the tower, g is the gravitational constant, 9.8 m/s^2, and V is the cell volume. Because gravitational body forces were not represented, the static air pressure and the ambient temperature over the height of the computational domain were constant. Thus, the reference air density, ρ_{ref}, of the cold ambient air was also constant over the entire computational domain. The dry-bulb air temperature of the incoming wind was specified as 287.15 K, which was used in all the calculations. Furthermore the air was assumed to be dry with the air density calculated by the ideal gas relation. With the reference atmospheric pressure specified as 83330 N/m^2, ρ_{ref} = 1.0108 kg/m^3. The laminar kinematic viscosity, υ, of the air was kept at a constant value of $1x10^{-3}$ m^2/s over the entire computational domain. The value of υ could be varied considerably without any significant changes in the amount of heat rejected in the tower. It was furthermore found that if the k-ϵ model was used to model the air turbulence, the amount of heat rejected in the tower increased by less than 0.3 %.

Resistances to the air flow, like the tower supports and the heat exchangers, were specified as sinks in the source terms of the momentum equations of the form

$$S_v = - K\, 0.5\, \rho\, |v|\, v \qquad (4.2.4)$$

where S_v is the source term, v the velocity vector while K is the pressure loss coefficient of the specific flow resistance. The pressure loss coefficient of the horizontal heat exchangers was specified as an effective pressure loss coefficient. The latter includes the pressure loss coefficient for normal flow, the inlet and outlet loss coefficients through the A-frames and the

contraction and expansion loss coefficients due to the fact that the entire inlet cross-section of the tower is not effectively covered with heat exchangers. Based on experimental data, K_{he} for the heat exchangers employed in the Kendal cooling towers is found to be a function of the mean approach velocity as shown in figure 4.2.2, and was correlated by a relation of the form

$$K_{he} = a\, v^b \tag{4.2.5}$$

where v is the vertical air velocity based on the inlet cross-section of the tower.

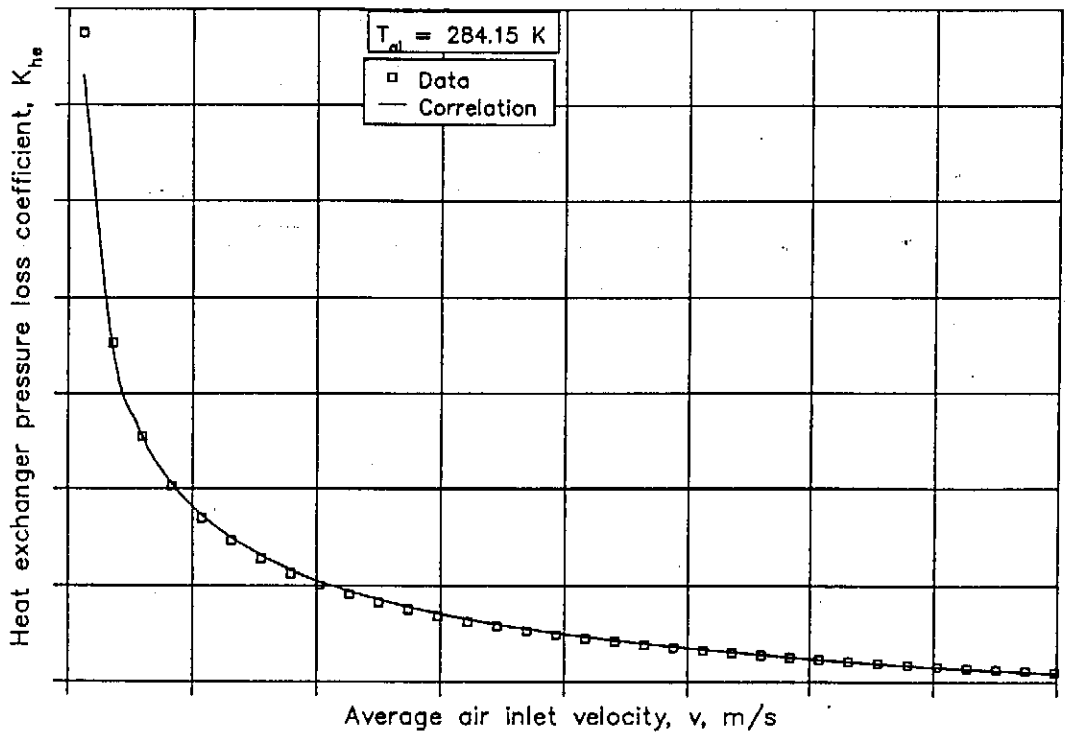

Figure 4.2.2: K_{he} for the heat exchangers in the Kendal tower.

In the PHOENICS model, the heat exchangers were confined to the first plane of cells in the tower inlet. Only the vertical velocity component, w, was allowed through the exchangers which is a reasonable assumption for the finned tube heat exchangers employed in the tower. The heat transfer characteristics of the particular heat exchanger bundles were determined experimentally. Based on the experimental data the air outlet temperature was determined for different air velocities and water inlet temperatures through the exchangers with the results correlated by a relation of the form:

$$T_{ao} = 273.15 + (a + b\,T_{wi}) + (c + d\,T_{wi} + e\,T_{wi}^2)\,v + (f + g\,T_{wi} + h\,T_{wi}^2)\,v^2 + (i + j\,T_{wi} + k\,T_{wi}^2)\,v^3 + l\,(T_{ai} - T_{airef})\,v \qquad (4.2.6)$$

T_{airef} is the reference air temperature of 287.15 K. The experimental data is compared to the correlation in figure 4.2.3 for an air inlet temperature of 287.15 K. The water mass flow rate through the tower was kept at a constant value of 16826 kg/s.

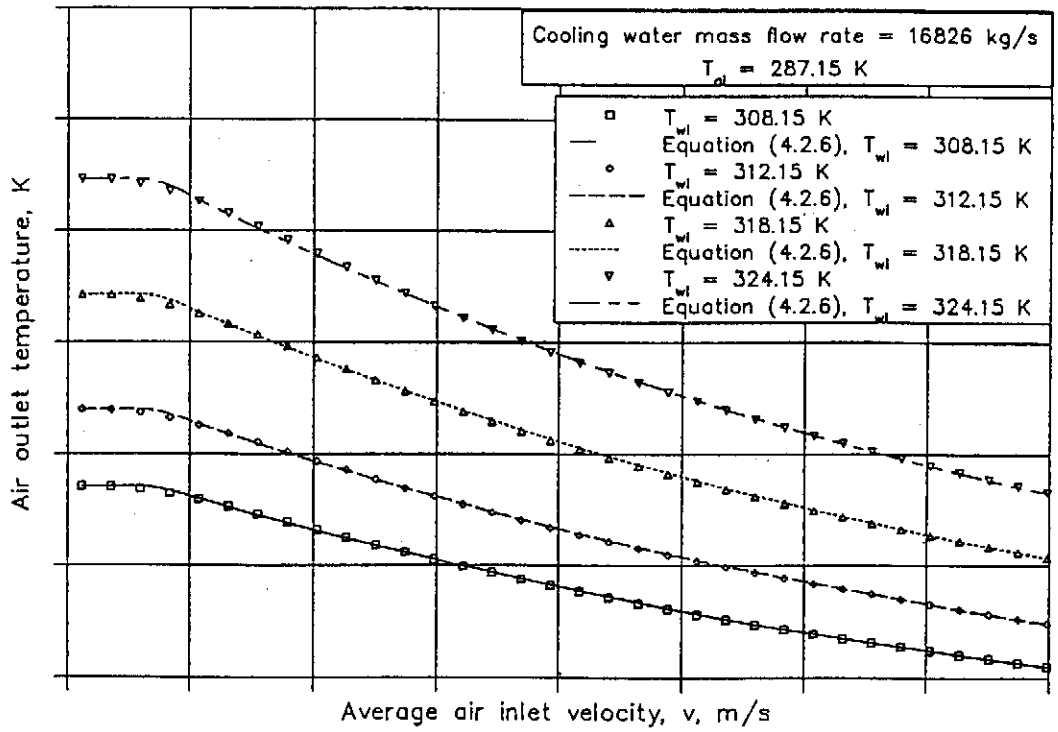

Figure 4.2.3: Air outlet temperature for different water inlet temperatures as a function of the vertical air velocity.

At high wind speeds a recirculation region is found on the upstream side of the tower, above the heat exchangers, with hot air flowing from the inside of the tower through the heat exchangers. As a result the air below the heat exchangers in this region is heated and the temperature of the air, T_{ai}, which enters the bundles further downstream is higher than the reference air temperature, T_{airef}. The outlet air temperature from these heat exchangers will therefore be correspondingly higher. For the known heat transfer characteristics of the heat exchangers employed in the Kendal cooling towers, the air outlet temperatures were calculated for different air inlet temperatures with the results shown in figure 4.2.4 and are compared to equation (4.2.6).

In the presence of a cross-wind the incidence angle of the approaching air flow to the tower supports varies circumferentially. Due to the lack of relevant information in the literature, experimental tests were performed to determine the pressure loss coefficient and the mean outlet flow angle for different incidence angles and Reynolds numbers.

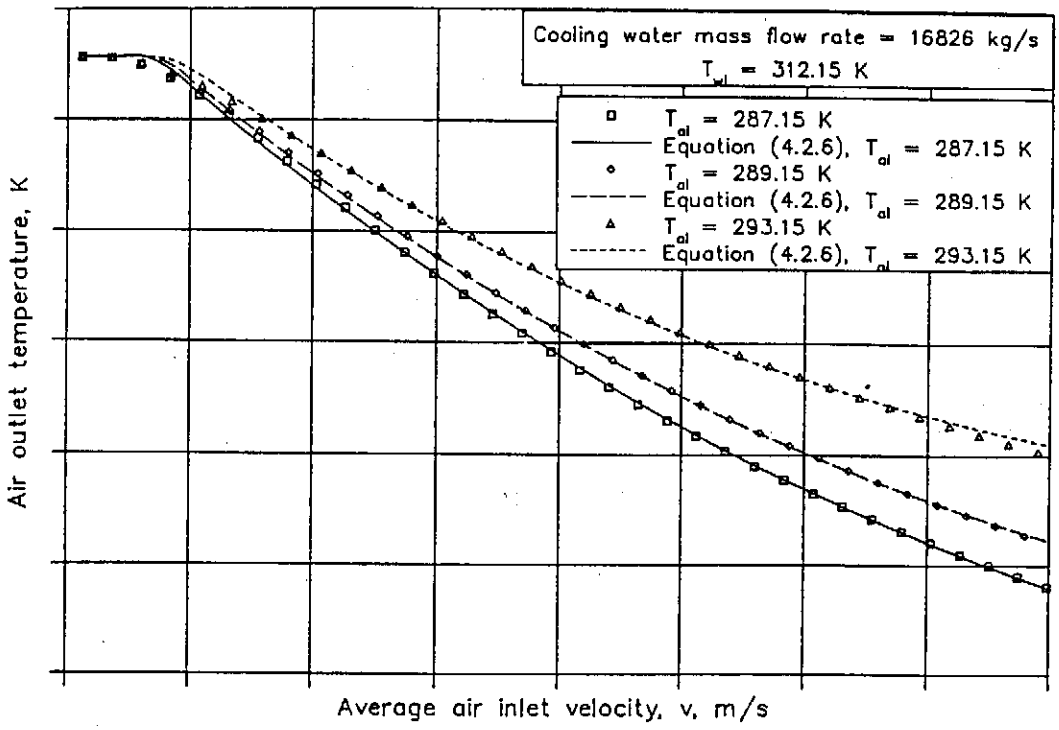

Figure 4.2.4: Air outlet temperature for different air inlet temperatures as a function of the vertical air velocity.

The tests were repeated for three different support arrangements, namely vertical round supports (see figure 4.2.6), vertical rectangular supports (see figure 4.2.7), and X-shaped supports as shown in figure 4.2.8. The latter are similar to the tower supports in the Kendal cooling towers as discussed in Appendix D. The supports were installed in a section which was coupled to the outlet of the wind tunnel as shown in figure C.2.1. The incidence angle ,θ , could be varied continuously from 90°, i.e. normal flow, to a minimum of approximately 15°. The air stream from the wind tunnel flows across the supports and discharges freely into the atmosphere. The mean outlet flow angle, ϕ, was determined with the aid of a woollen tuft. By measuring the difference between the static pressure upstream of the supports and the atmosphere, a support pressure loss coefficient was defined as

$$K_{ts} = \Delta p_{ts} / 0.5\rho v_{ts}^2 \qquad (4.2.7)$$

where Δp_{ts} is the difference in static pressure across the supports and the velocity v_{ts} is the air velocity normal to the support plane. The results are shown in figures 4.2.6 to 4.2.8 for different support arrangements and were found to be independent of the Reynolds number. Based on the experimental data, the following correlations were obtained for K_{ts} and ϕ for the different support arrangements and are compared to the experimental results in figures 4.2.6 to 4.2.9.

For the vertical round supports, figure 4.2.6, :

$$K_{ts} = -0.0958 + 0.02553\,\theta + 11.593/\exp(\theta/10) - 0.000168\,\theta^2 \qquad (4.2.8)$$

$$\phi = 14.79 + 0.8358\,\theta \qquad (4.2.9)$$

For the vertical rectangular supports, figure 4.2.7, :

$$K_{ts} = 2.42415 - 0.006169\,\theta - 0.00081993\,\theta^2 + 0.0000074336\,\theta^3 \qquad (4.2.10)$$

$$\phi = 71.93 + 0.0021869\,\theta^2 \qquad (4.2.11)$$

And for the X-shaped supports, figure 4.2.8, :

$$K_{ts} = 1 - 0.00567\,\theta - 0.000007866\,\theta^2 + 0.126594 \sin(4\theta) \qquad (4.2.12)$$

$$\phi = 21.9 + 0.75047\,\theta \qquad (4.2.13)$$

As indicated in Appendix D, is it possible to express K_{ts} approximately in terms of the drag coefficient, C_{Dts}. In table 4.2.1, the drag coefficient for the different support arrangements obtained experimentally for normal flow, $\theta = 90°$, is compared to the value of K_{ts} when based on the drag coefficient.

Table 4.2.1: Pressure loss coefficient of tower supports.

Support arrangement	K_{ts} Experimental	K_{ts} Based on C_{Dts}
Vertical round	0.841	0.362
Vertical rectangular	0.646	0.354
X-shaped	0.426	0.328

Due to the influence of the supports on each other, the experimental value of K_{ts} tends to be higher than that which is found when the supports are considered as an array of single bodies in a free stream. Further tests indicated that the drag coefficient of the supports can be used to calculate K_{ts} provided that the value of the support pitch to support diameter ratio is more than 15. The rings of tower supports to uphold the bundles in the present support arrangement (see figure D.1) all have support pitch to support diameter ratios of more than 16, and therefore the values of K_{ts}, as given in table D.2, for these supports need not be corrected. The effective pressure loss coefficient of the inner rings of supports as based on the inlet circumferential area of the tower is found to be 0.181.

In the PHOENICS model, the effect of the supports on the air flow was represented by flow resistances. These resistances were only applied on the ring of cells located in the vertical inlet cross-section of the tower, i.e. the cells directly below the inlet edge of the tower. Because PHOENICS provides solutions for the velocity components tangential, u, and normal, v, to the supports, the pressure loss coefficients have to be specified accordingly. The pressure loss coefficients in the direction tangential, K_{tsu}, and normal, K_{tsv}, to the array of supports were obtained by considering the change in fluid momentum as the air flows across the supports as shown schematically in figure 4.2.5. The array of supports are represented by an actuating plane across which the static pressure and flow direction of the fluid changes instantaneously while the control surfaces, 1 and 2, are selected so that they are normal to the flow direction. The air approaches the supports with an incidence angle θ and is discharged at an angle ϕ. Because of the conservation of mass, the velocity component normal to the supports, v_{ts}, is constant. Furthermore the static pressure upstream of the supports is assumed to be constant while the static pressure downstream of the supports is zero. The forces F_x and F_y represent the forces exerted by the supports on the air in the X and Y-directions respectively.

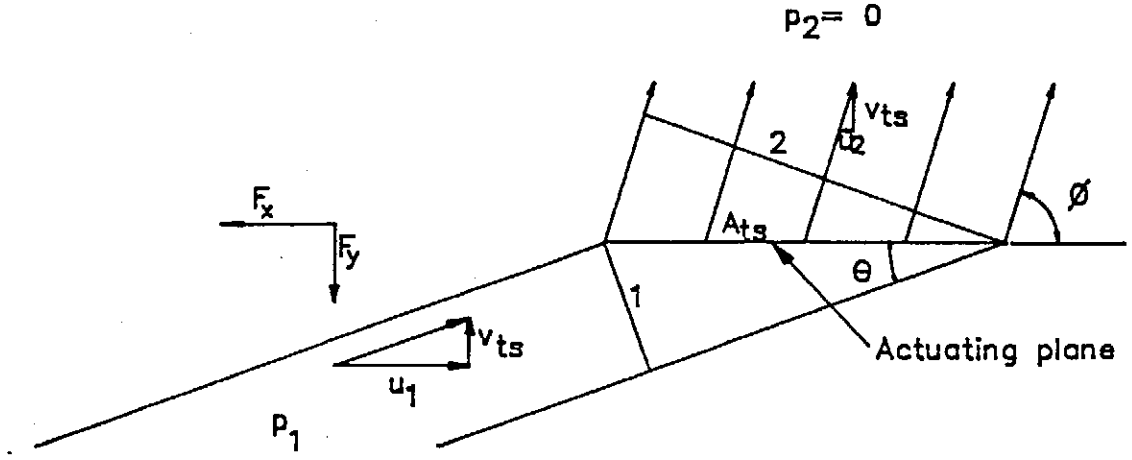

Figure 4.2.5: Inclined flow through array of tower supports.

Because the sum of the external forces on the body of fluid in a specific direction is equal to the change in momentum of the body in that direction, the following is found for the X-direction

$$p_1 A_{ts} \sin\theta \cos\theta - F_x = \rho Q (u_2 - u_1) \tag{4.2.14}$$

where Q is the volume flow rate of the flow, $A_{ts}\, v_{ts}$. If the force F_x is expressed in terms of a pressure loss coefficient, K_{tsu}, and substituted in equation (4.2.14), the following is found.

$$K_{tsu}\, 0.5\rho u_1^2\, A_{ts} = \rho v_{ts} A_{ts} u_1 - \frac{\rho v_{ts}^2 A_{ts}}{\tan\phi} + p_1 A_{ts} \sin\theta \cos\theta \tag{4.2.15}$$

where ϕ is the mean outlet flow angle for the particular support arrangement as shown in figure 4.2.9. Equation (4.2.15) may be re-written as:

$$K_{tsu} = \tan\theta \left[2 - \frac{2\tan\theta}{\tan\phi} + K_{ts} \sin^2\theta \right] \tag{4.2.16}$$

Similarly for the Y-direction:

$$K_{tsv} = K_{ts} \sin^2\theta \tag{4.2.17}$$

Equations (4.2.16) and (4.2.17) were employed in the GROUND subroutine, shown in Appendix J, to quantify the pressure loss coefficients of the tower supports in the X and Y-directions respectively with the incidence angle θ considered as the flow angle in the upstream cell. The value of the effective pressure loss coefficient of the inner rings of tower supports was added as a constant to K_{tsv}.

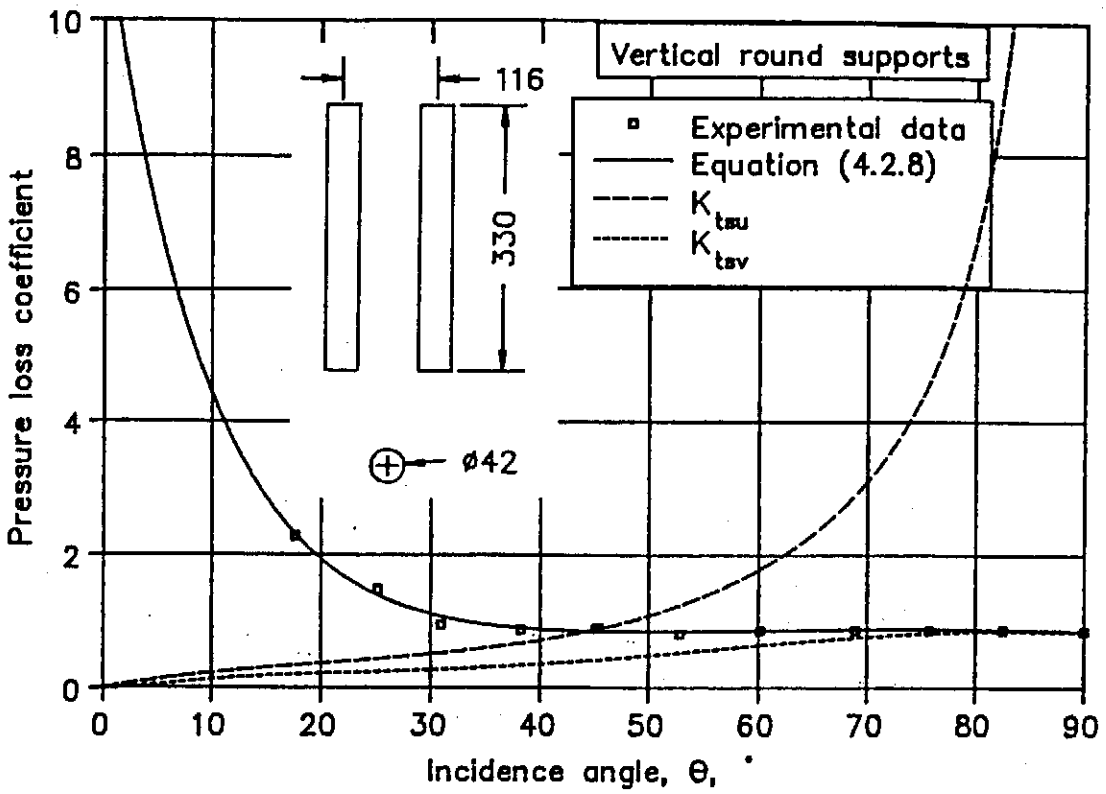

Figure 4.2.6: Pressure loss coefficient for vertical round tower supports.

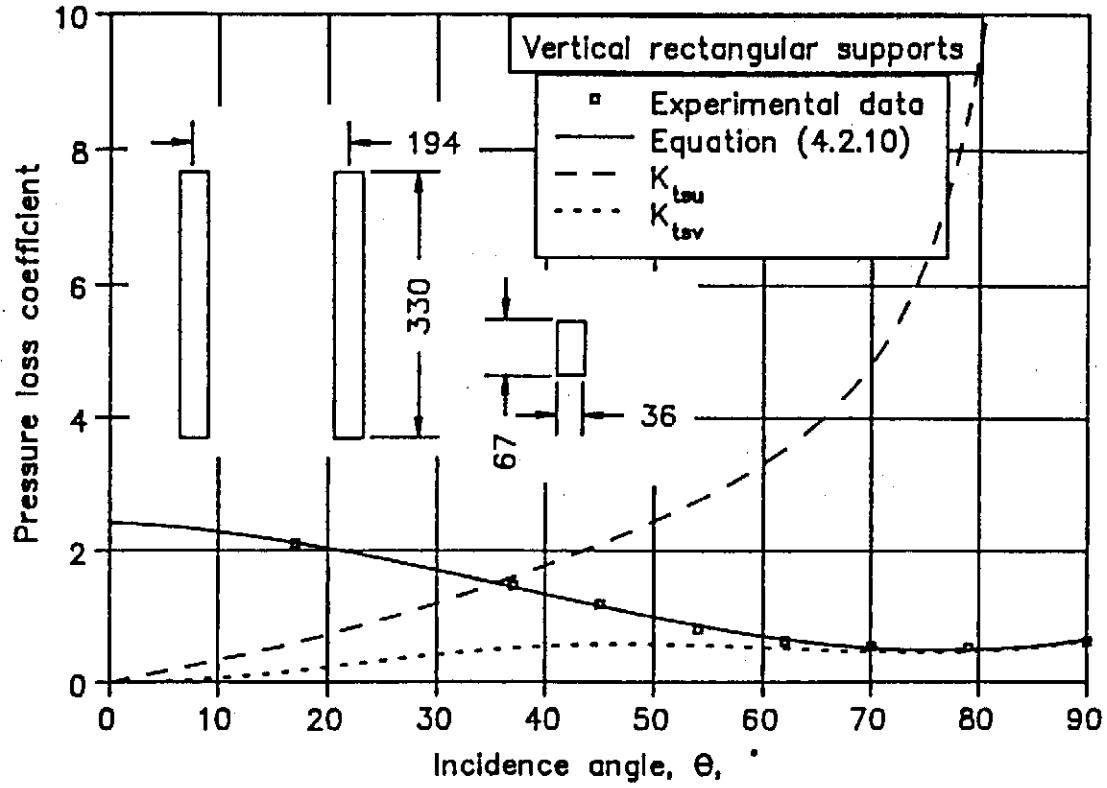

Figure 4.2.7: Pressure loss coefficient for vertical rectangular supports.

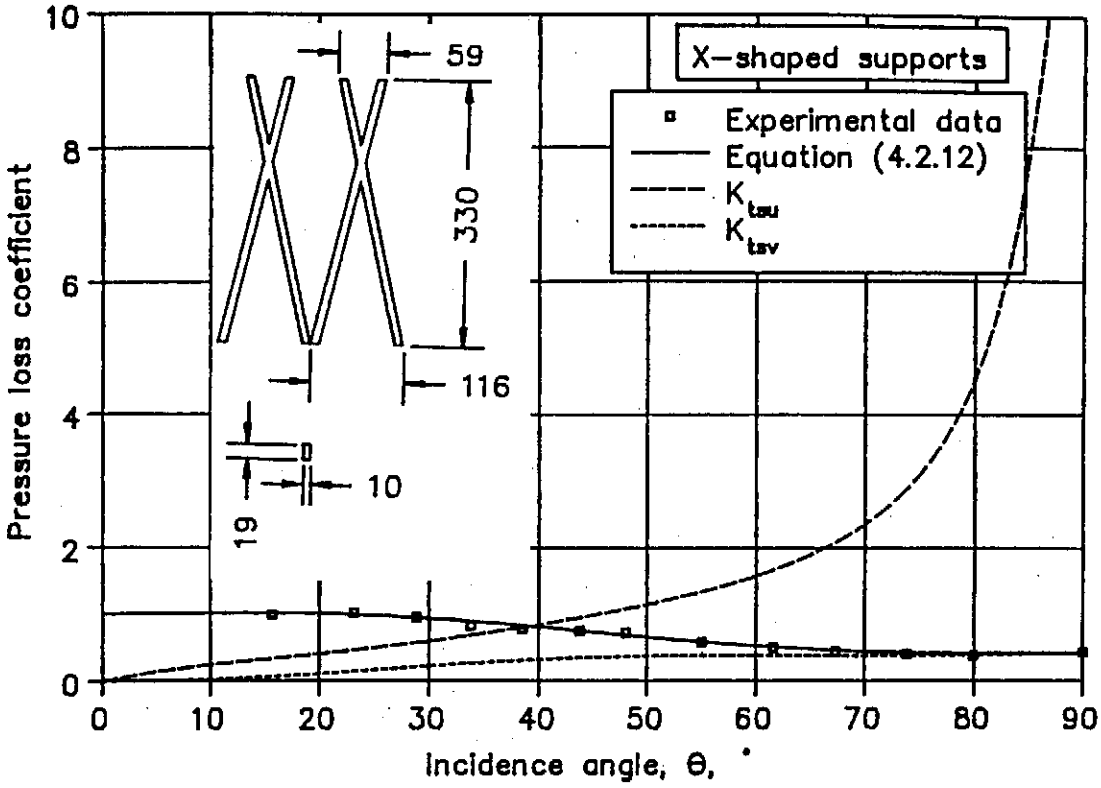

Figure 4.2.8: Pressure loss coefficients for X-shaped tower supports.

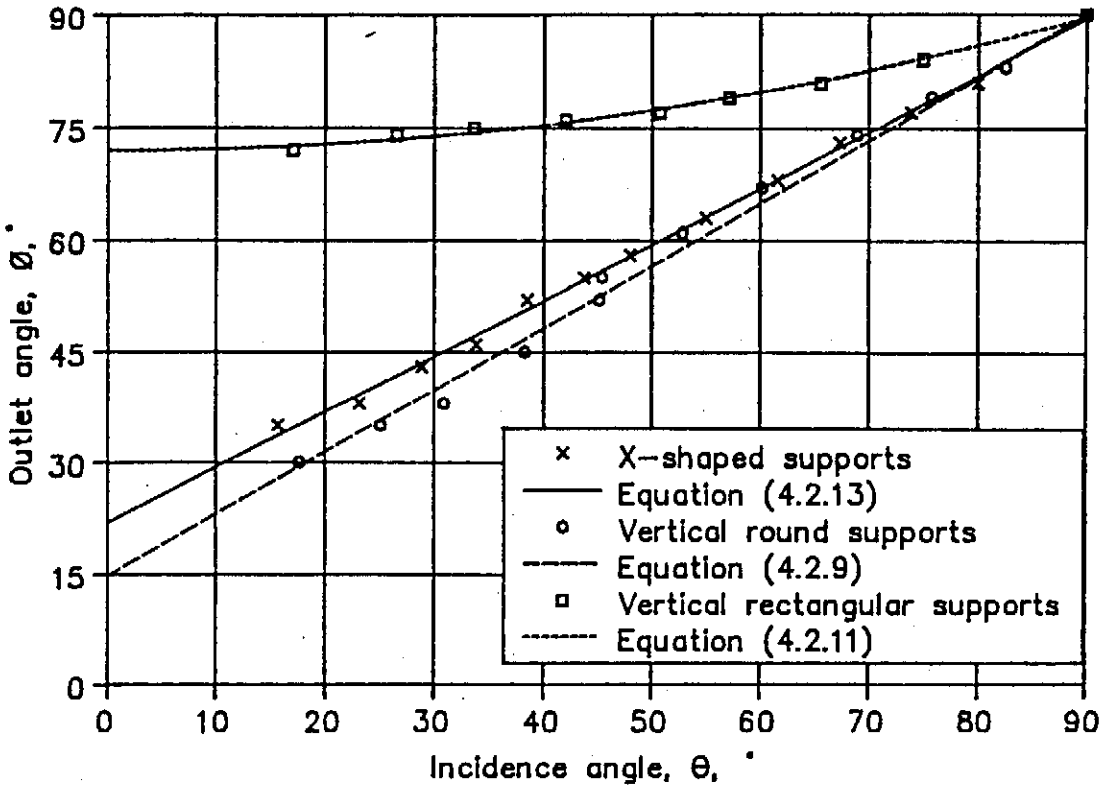

Figure 4.2.9: Mean outlet flow angle for different support arrangements.

4.3: Predicted heat rejection rate of tower in the absence of atmospheric disturbances.

By following an iterative procedure PHOENICS provides solutions for the internal and external aerodynamic and thermal flow field of the tower. Additional GROUND coding was added in the GROUND subroutine, see Appendix J, to calculate the amount of heat rejected by the tower and the mean air mass flow rate through the tower at the end of each iteration cycle whereupon these values were stored in the RESULT.DAT file. These results were used to determine when a stable solution was reached, i.e. when there is no change in the values of the dependant variables for each successive iteration. Convergence was normally reached after 60 iteration cycles whereupon the run was terminated after the values of the variables were stored on disk to be used as the initial conditions for the next run. To ensure convergence, under-relaxation was employed for all the variables which were solved. This was done by introducing a false time step for the velocity vectors and the temperature while a linear under-relaxation factor was applied to the pressure.

The amount of heat rejected by a three dimensional model of one of the Kendal cooling towers was determined for different initial temperature differences, $T_{wi} - T_{ai}$, with the results shown in figure 4.3.1. Compared to the results of full scale measurements made under similar conditions, also shown in the figure, the heat rejection rate of the tower as calculated by PHOENICS is found to be roughly 1.6% conservative.

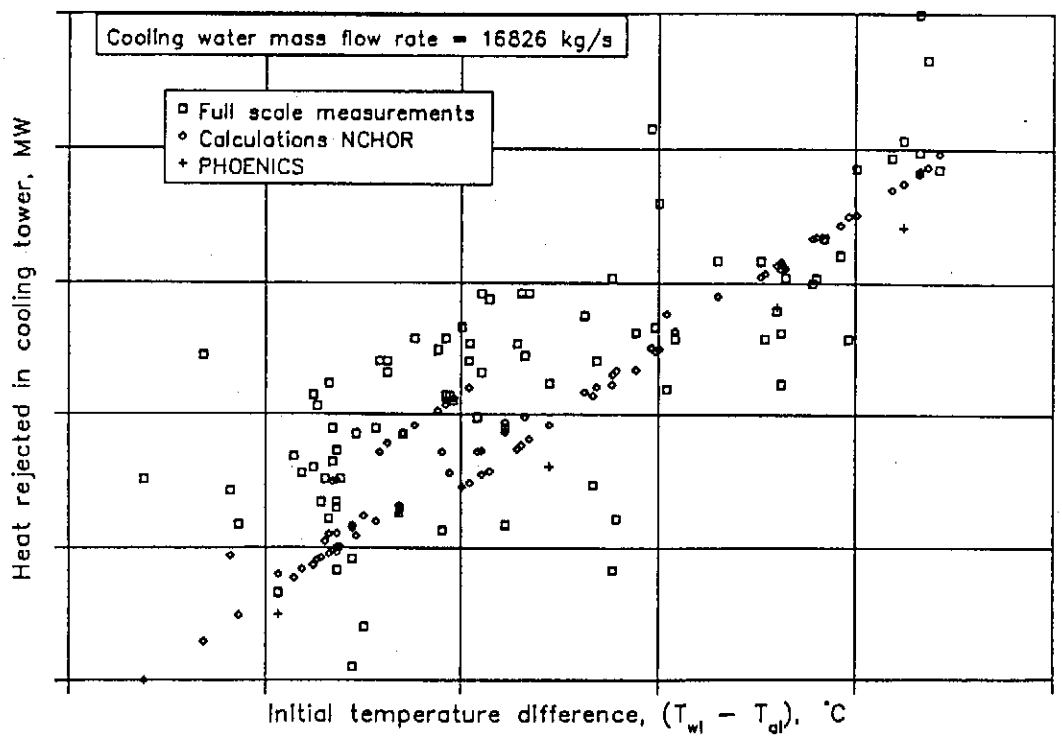

Figure 4.3.1: Heat rejected in a dry-cooling tower in windless conditions.

A vector representation of the flow field of the tower in windless conditions is shown in figure 4.3.2. An almost uniform air velocity is obtained through the heat exchangers when the pressure loss coefficient is high, as shown by Geldenhuys [86GE1].

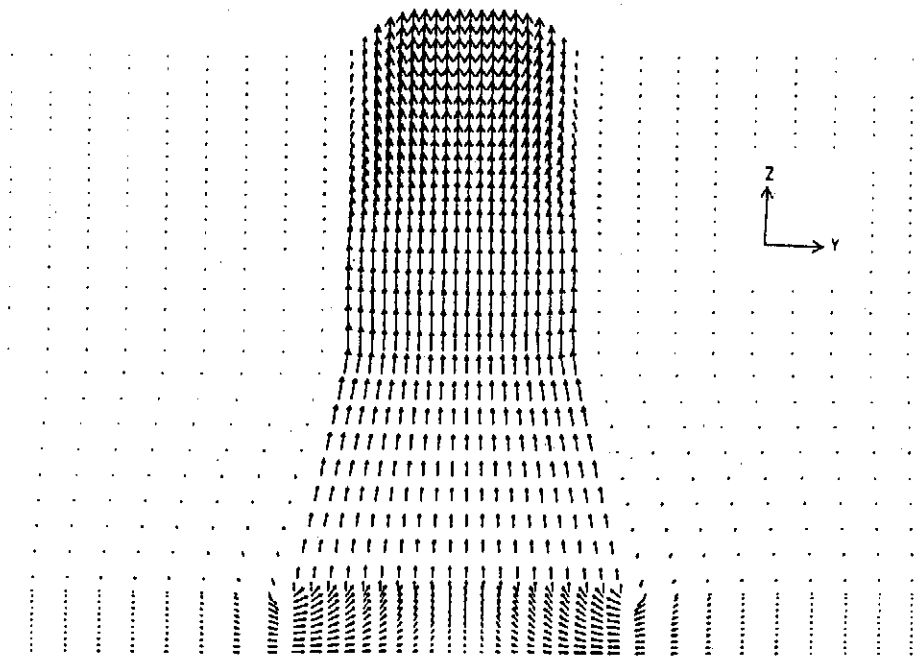

Figure 4.3.2: Vector representation of flow field.

By entering the water and air inlet temperatures as measured on the full scale tower into the program NCHOR, briefly described in section 2.5, the corresponding amount of heat rejected by the tower was calculated with the results also shown in figure 4.3.1. The heat rejection rate obtained from the computer code, not including radiation effects, proved to be 0.6% less compared to the full scale measurements.

4.4: Prediction of the wind effect on natural draft dry-cooling towers.

By varying the wind velocity specified at the inlet of the computational domain, the rise in the inlet water temperature needed to maintain the heat rejection rate of the tower was calculated for different wind speeds. The tower dimensions and characteristics of the heat exchangers used for all the calculations were similar to those employed in the cooling towers of the Kendal power station except where stated differently. Figure 4.4.1 shows the rise in the approach temperature of the tower for different support arrangements as a function of the wind velocity at the outlet height of the tower. The calculations were done for a tower with the heat exchangers arranged uniformly and horizontally, i.e. not A-frames, over the entire inlet cross-section of the tower.

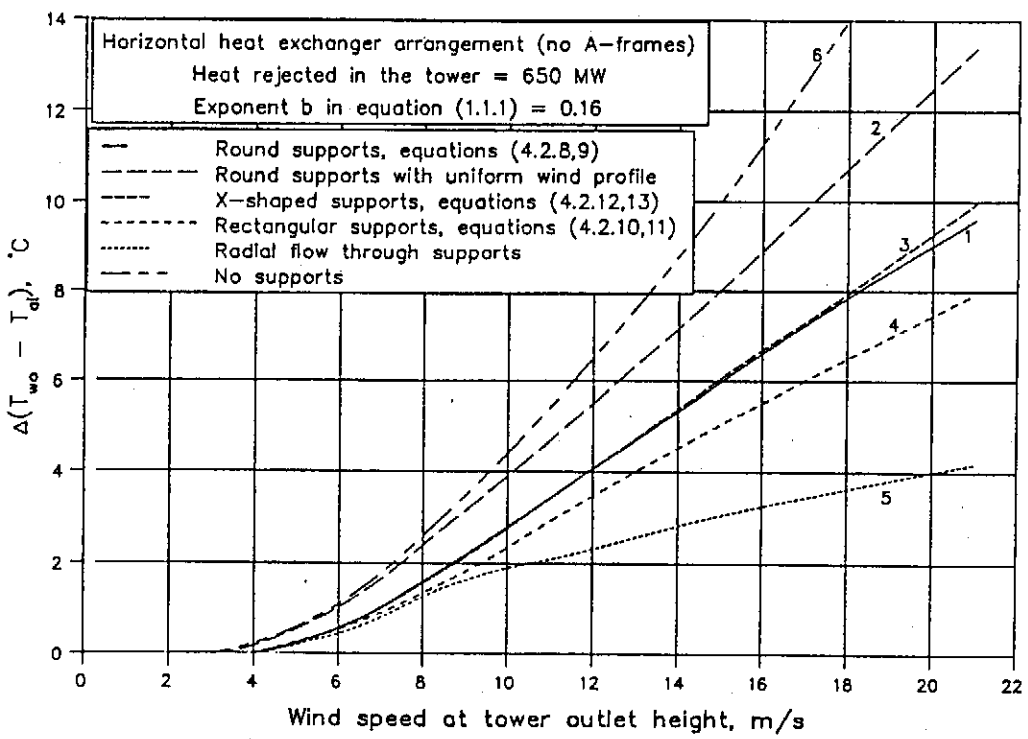

Figure 4.4.1: Wind effect on tower with different support arrangements.

For the first curve in the figure, round tower supports were considered. These supports had a similar pressure loss coefficient to those used in the model tests as discussed in Appendix D. Figure 4.4.2 shows a vector representation of the velocity field in the vertical cross-sectional plane of the tower and immediate surroundings for a wind speed of 12 m/s. The wind is entering the computational domain from the positive Y-direction while the wind profile was approximated by the power law with exponent b in equation (1.1.1) equal to 0.16.

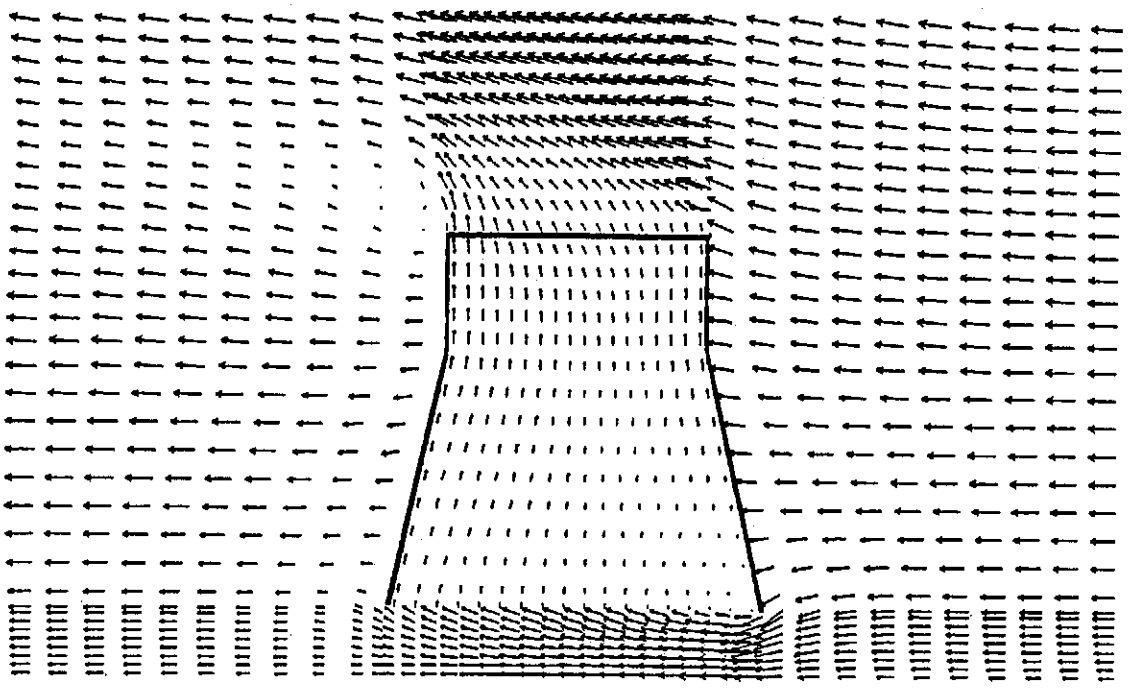

Figure 4.4.2: Flow field in and outside a cooling tower.

On the upstream side of the tower, below the heat exchangers, the incoming flow is accelerated and separates from the inlet edge of the tower. Consequently the static pressure in this region drops, see figure 4.4.3, which causes a reduction in the air flow rate through the bundles. For sufficiently high wind velocities, a recirculating flow pattern was observed with hot air flowing from inside the tower through the heat exchangers. Figure 4.4.4 shows the distorted flow pattern through the horizontal heat exchangers for three different values of the relative wind velocity. The latter is found to be in good agreement with measurements made on a model of a similar tower as shown in figure 2.3.1. The kinetic energy coefficient, α, as defined by equation (A.1.3) was calculated for the velocity distributions obtained for different support arrangements with the results shown in figure 4.4.5. The latter may be compared with similar experimental results shown in figure 2.3.2. Due to the distorted flow pattern through the heat exchangers, the air temperature distribution inside the tower becomes increasingly more non uniform as the wind speed increases. It was shown that the maximum air velocity is found on the lee side of the tower, therefore it is expected that the minimum air temperature will also be found in that position. The latter is confirmed by the temperature contours shown in figure 4.4.6. As a result of the recirculating flow pattern on the upstream side of the tower, the air below the heat exchanger in that region is heated. Furthermore the air inside the tower is not mixed because the unstable large scale vortices found in full scale towers were not represented

by the time-independent numerical simulation.

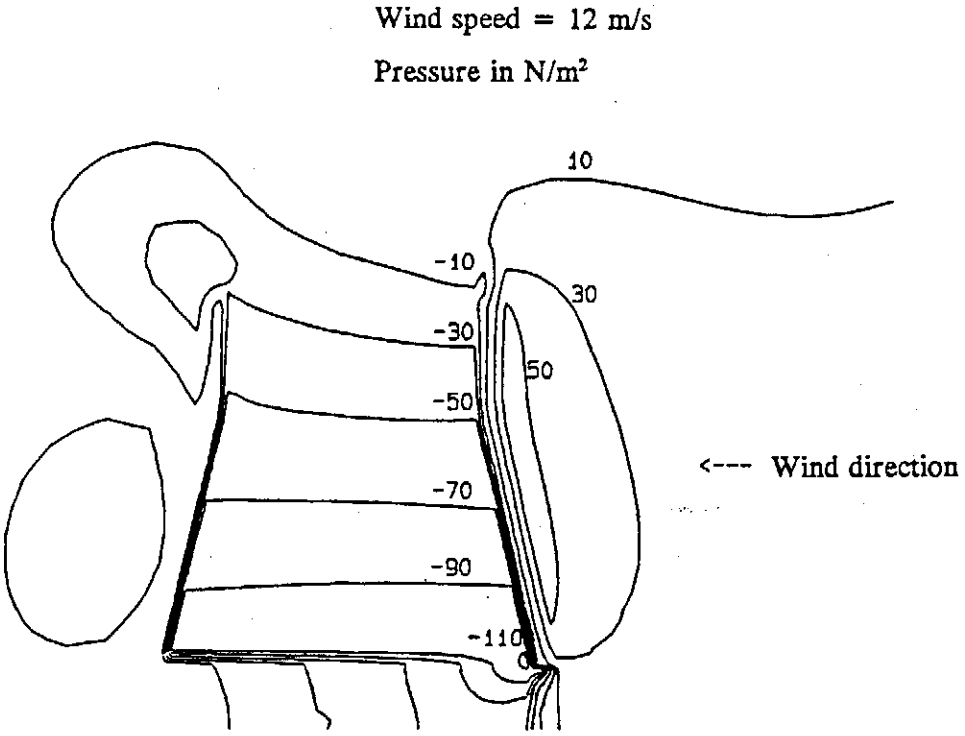

Figure 4.4.3: Relative static pressure contours for a wind speed of 12 m/s.

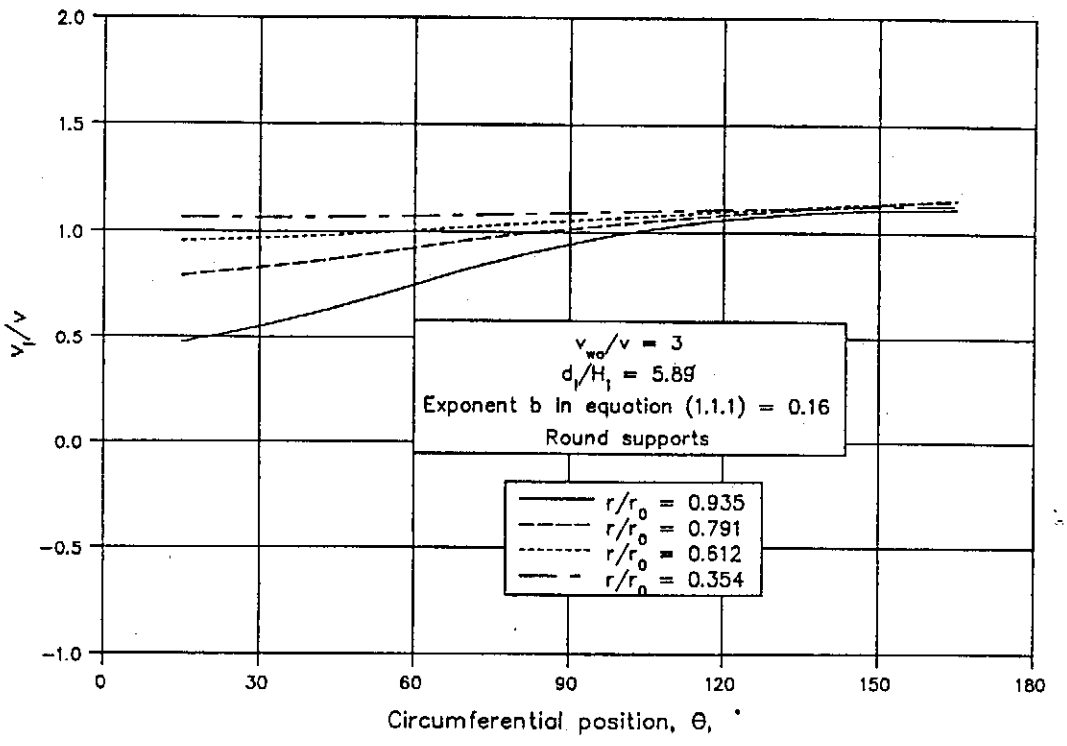

(a)

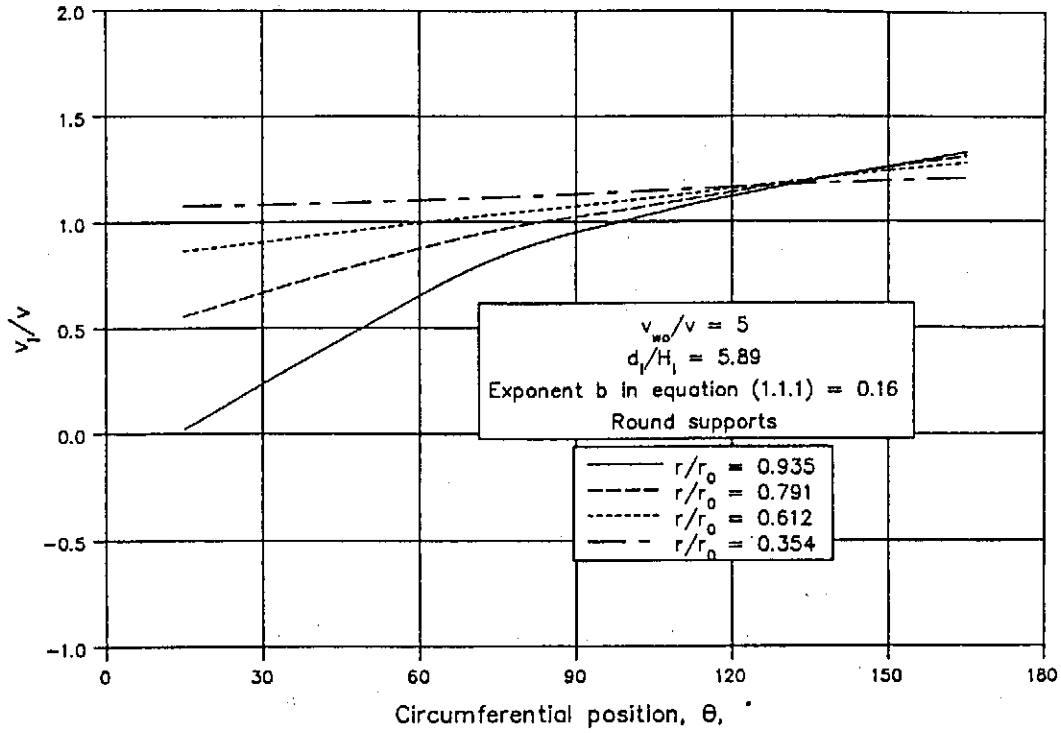

(b)

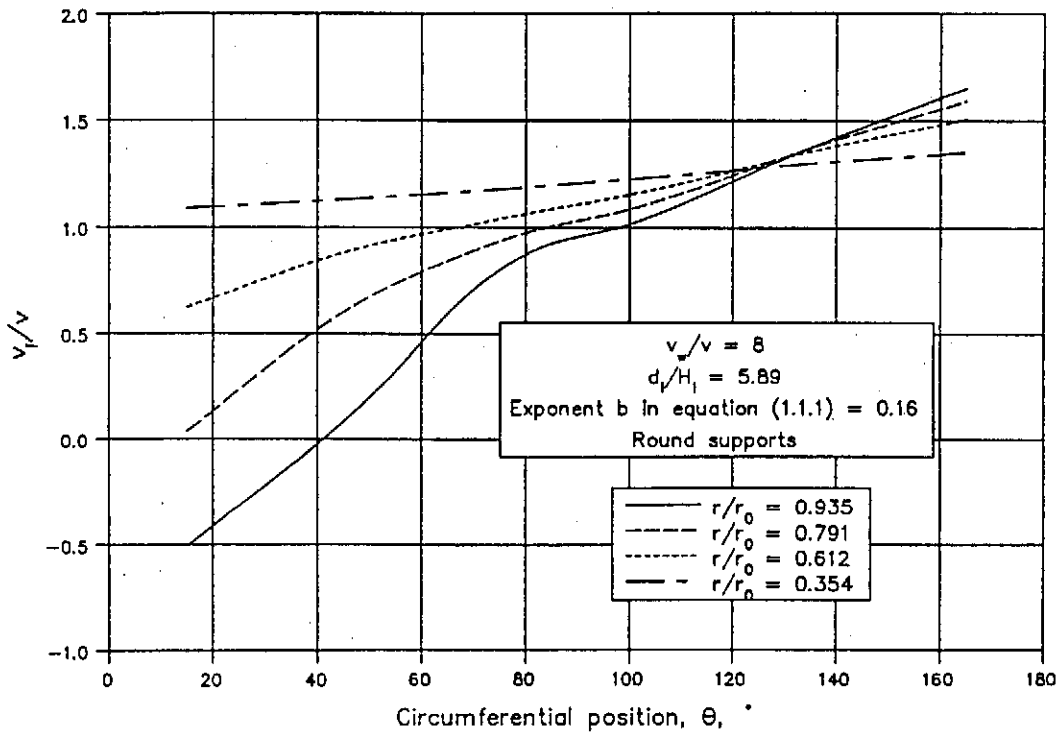

(c)

Figure 4.4.4: Velocity distribution through the horizontal heat exchangers.

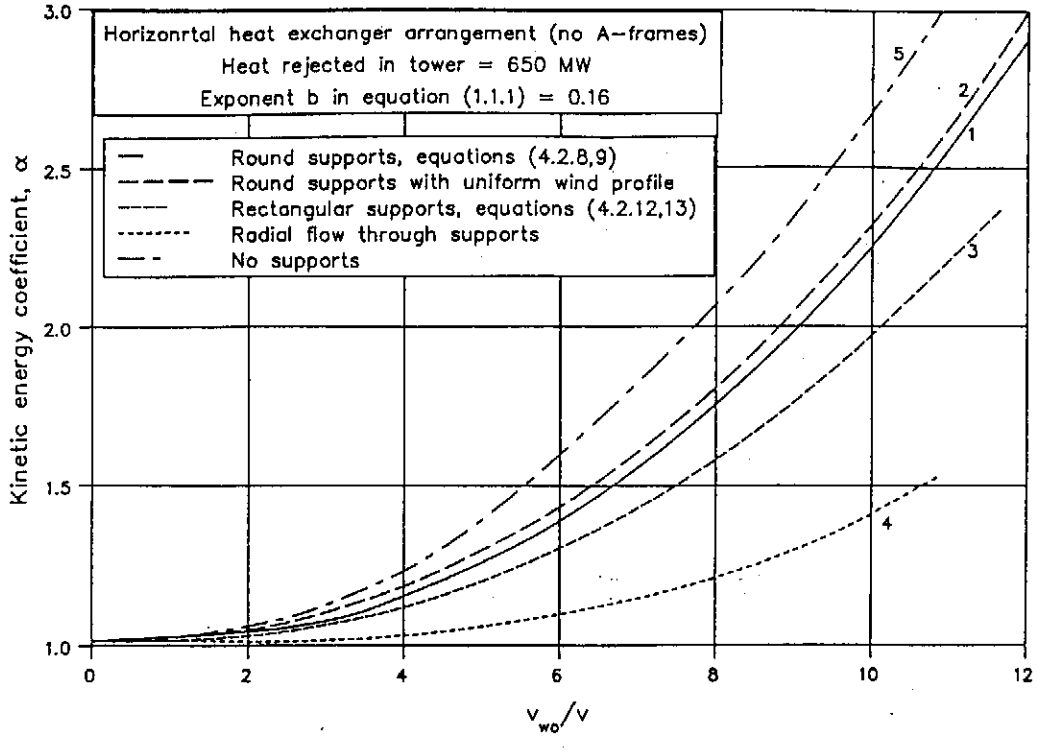

Figure 4.4.5: α for different support arrangements.

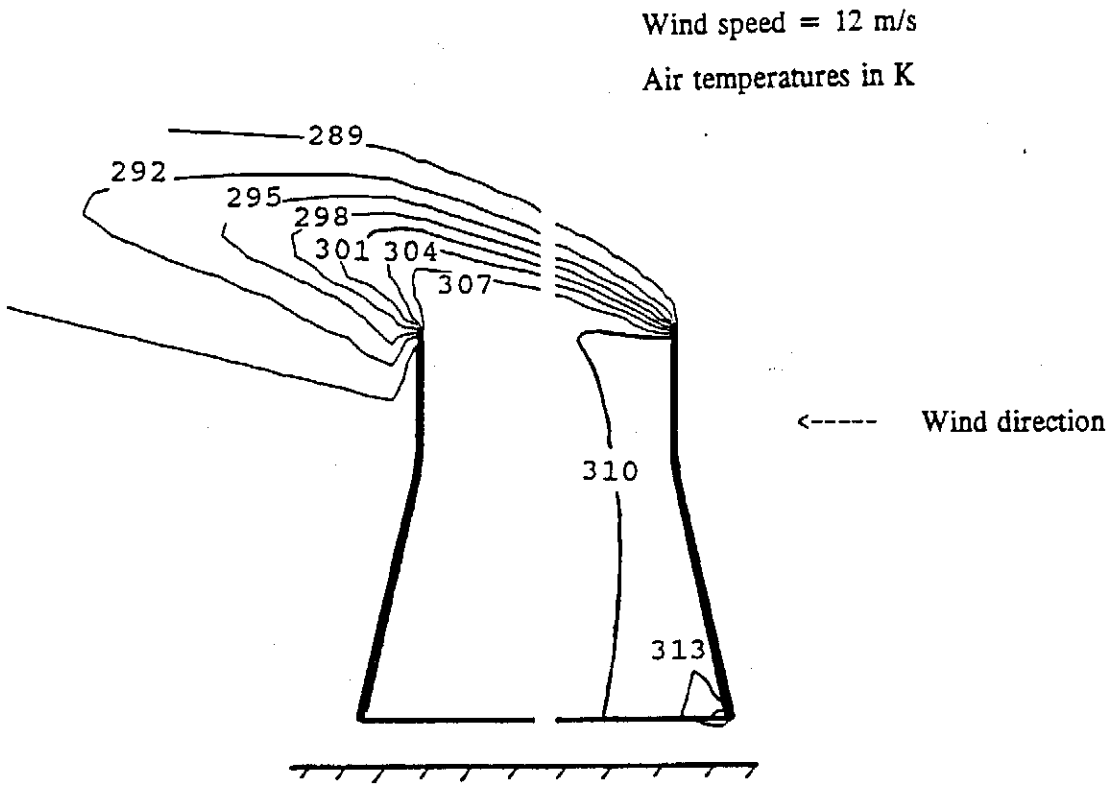

Figure 4.4.6: Temperature contours for a wind speed of 12 m/s.

In the second curve in figure 4.4.1, the calculations were repeated with a uniform wind velocity specified at the inlet of the computational domain. In comparison with the first curve, a significant reduction in the tower performance is found for high wind speeds as the wind profile becomes more uniform. The latter is mainly caused by a reduction in the static pressure below the heat exchangers due to the higher air velocity at ground level. A slight deterioration of the velocity distribution through the heat exchangers is also observed as shown by the second curve in figure 4.4.5 which is in agreement with the results shown in figure 2.3.2.

Curve three in figure 4.4.1 shows that the change in the tower performance is negligible if the round supports are replaced by X-shaped supports. The reason for the latter is found in figure 4.2.9 where it was shown that the mean outlet angle for these two support shapes is approximately the same for a given incidence angle. Also shown in figure 4.2.9 is the outlet angle for an array of rectangular supports for different incidence angles. Since a much greater deflection in the air stream is found with this arrangement, it is expected that the performance of the tower in a cross-wind will also be affected if these supports are installed in the tower inlet. This is confirmed by curve 4 in figure 4.4.1 which shows a reduction in the influence of the wind on the tower [86VA1]. The latter is partly due to the improvement in the velocity distribution through the heat exchangers as shown by curve three in figure 4.4.5.

Sabaton [82SA1] suggested that the influence of a cross-wind on the performance of a tower can be reduced by arranging a series of radial walls around the circumference of the tower. In effect, this is an array of tower supports with a very large depth to width ratio by which the entering flow is directed in a radial direction. In the numerical model the latter was simulated by allowing only the radial velocity component to pass through the cells in which the tower supports were represented. The favourable effect on the rise in the approach temperature of the tower as found by Sabaton [82SA1] is confirmed and is clearly shown by curve 5 in figure 4.4.1 with the corresponding kinetic energy coefficient shown by curve 4 in figure 4.4.5.

With no tower supports installed in the inlet of the tower, the tower performance deteriorates dramatically as shown by curve 6 in figure 4.4.1. The large difference between the different curves shown in the figure, indicate that both the pressure loss coefficient and the shape of the tower supports have a significant influence on the performance of a tower subjected to cross-winds. Radially elongated supports by which the incoming flow is directed in a radial direction proved to have the most favourable effect.

The rise in the approach temperature for the same tower may also be calculated for different wind speeds by using the computer program NCHOR as described in section 2.5. For this purpose the experimental results shown in chapter two were employed in the program to calculate the inlet and outlet pressure coefficients and the heat transfer correction factor. Figure 4.4.7 shows the results of the calculations for two different support arrangements and different forms of the approaching wind profile. These curves may be compared with the results of the numerical model, shown in figure 4.4.1, since the same tower geometry and heat exchanger characteristics were used in both cases.

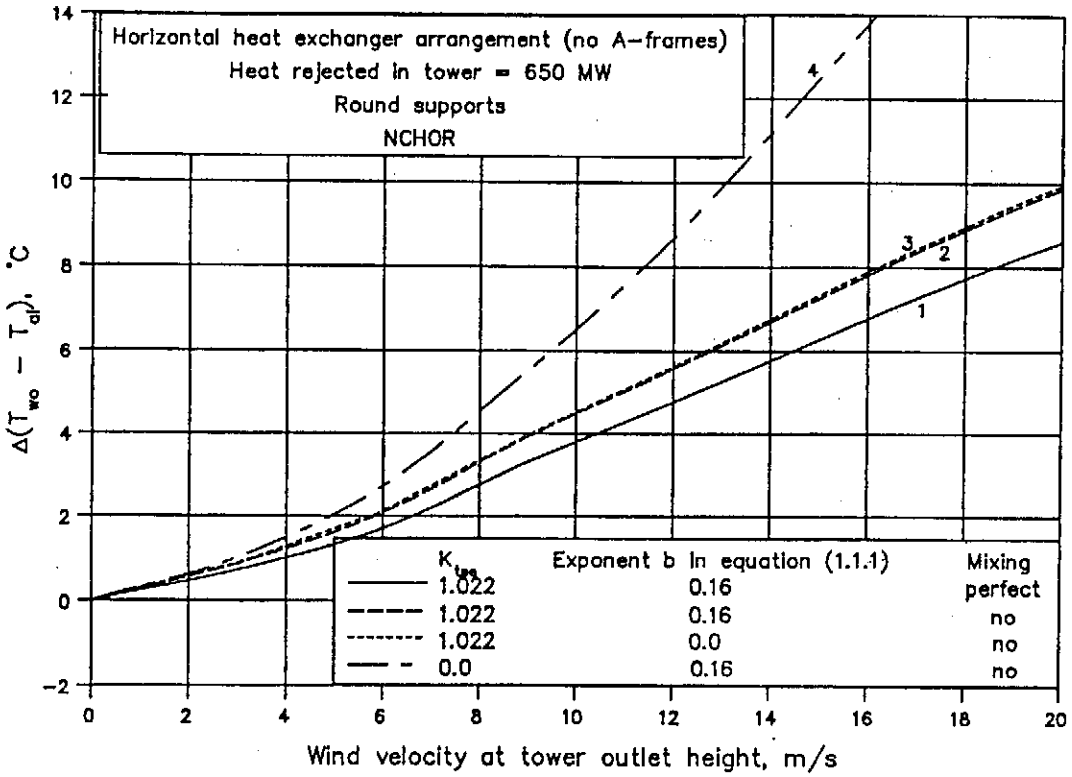

Figure 4.4.7: Prediction of the wind effect on a cooling tower based on experimental results.

For the first and second curves in figure 4.4.7 round tower supports were considered while the wind profile was described by the power law with exponent b = 0.16. Because the amount of mixing of the warm air above the heat exchanger is not known, curve 1 was calculated by assuming perfect mixing while no mixing was considered for curve 2. For high wind velocities the agreement between the numerical results and those based on the experimental data is excellent. As the wind speed decreases, the curves shown in the two figures diverge with the results according to the numerical model somewhat more optimistic. Changes in the wind profile have almost no influence on the wind effect on the tower as shown by the third curve in figure 4.4.7. Conversely a noticeable rise in the approach temperature of the tower was found with the numerical model as the wind profile becomes more uniform.

In agreement with the results shown in figure 4.4.1, curve 4 in figure 4.4.7 indicates a significant rise in the approach temperature of the tower if the tower supports are removed from the tower inlet. The latter is mainly due to the reduction in the static pressure below the heat exchangers caused by the high air velocity in this region.

Although there are a few minor differences between the results obtained with the numerical model and those based on the experimental results, as discussed in the previous paragraphs, there is in general a favourable agreement between the two sets of results.

In section 2.6 it was shown that the erection of windbreak walls below the horizontal heat exchangers may result in significant reductions in the wind effect on the tower. The effect of such a device on the performance of the tower was also investigated by means of the PHOENICS code by modelling a flow resistance below the heat exchangers with the results shown in figure 4.4.8. The windbreak walls were positioned perpendicular to the approaching wind direction, see figure 4.4.8, with a pressure loss coefficient which corresponds to the loss coefficient of K_{wall2} as shown in figure 2.6.7. The pressure loss coefficient of the wall was correlated by

$$K_{wall} = 37.298\ v^{-0.52317}$$

where v is the local approach velocity through the wall. Figure 4.4.8 shows the results of the numerical model as well as the results obtained with the program NCHOR. If the air above the heat exchangers is assumed to be perfectly mixed, excellent agreement is found between the numerical and experimental results. The favourable effect of the walls can be seen when the curves in figure 4.4.8 are compared to those shown in figure 4.4.1 which were obtained for the same cooling tower.

The change in the mean air mass flow rate through the tower is shown in figure 4.4.9 as a function of the wind velocity. As explained in section 2.6, the presence of the windbreak walls tend to increase the static pressure below the heat exchangers which will ensure a more uniform velocity distribution through the heat exchangers. In figure 4.4.10 the velocity distribution through the heat exchangers is shown for different values of the relative wind velocity which can be compared to those obtained with a model test as shown in figure 2.6.11.

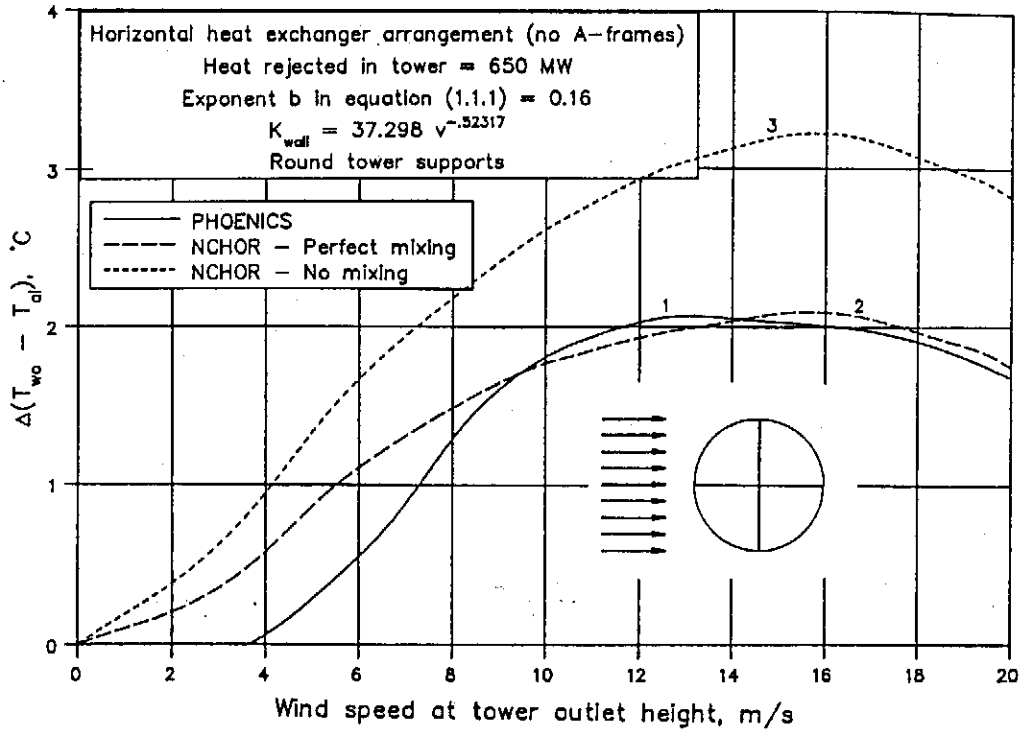

Figure 4.4.8: Wind effect on tower with windbreak walls below heat exchanger.

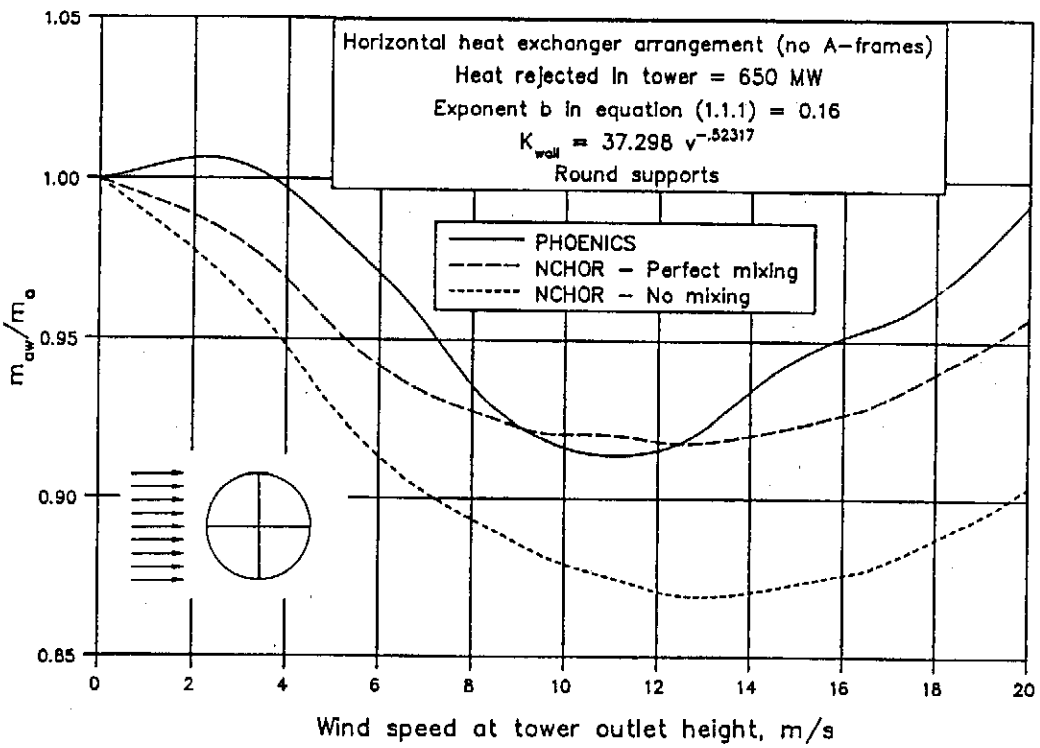

Figure 4.4.9: Effect of cross-winds on the mean air mass flow rate through tower.

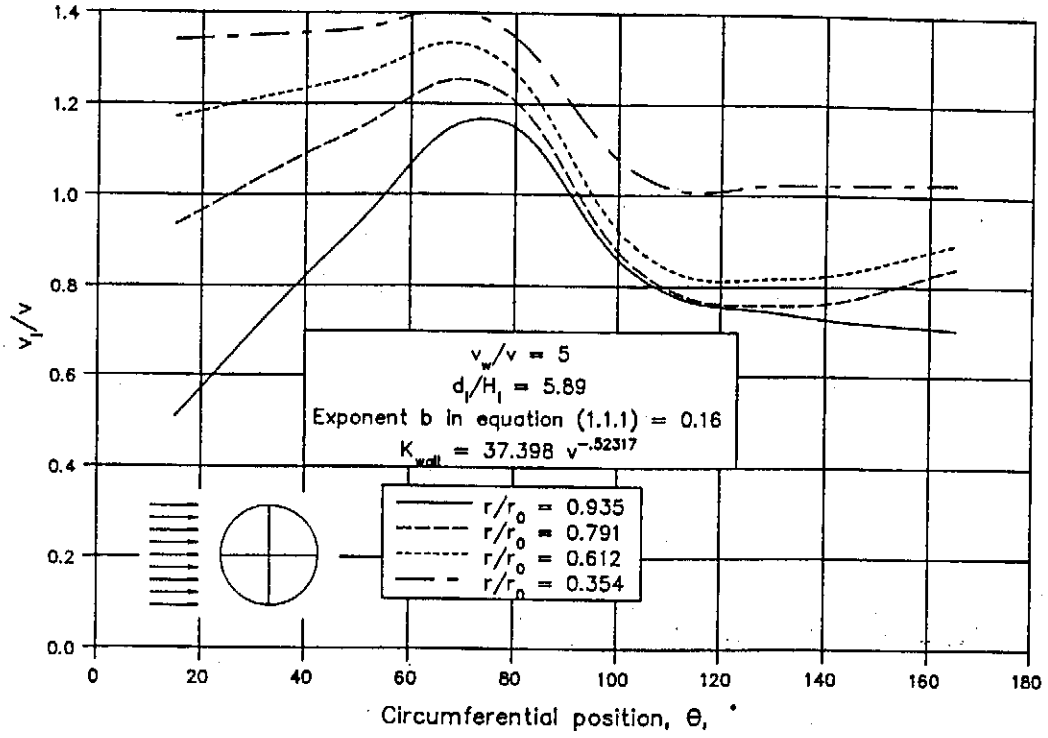

(a)

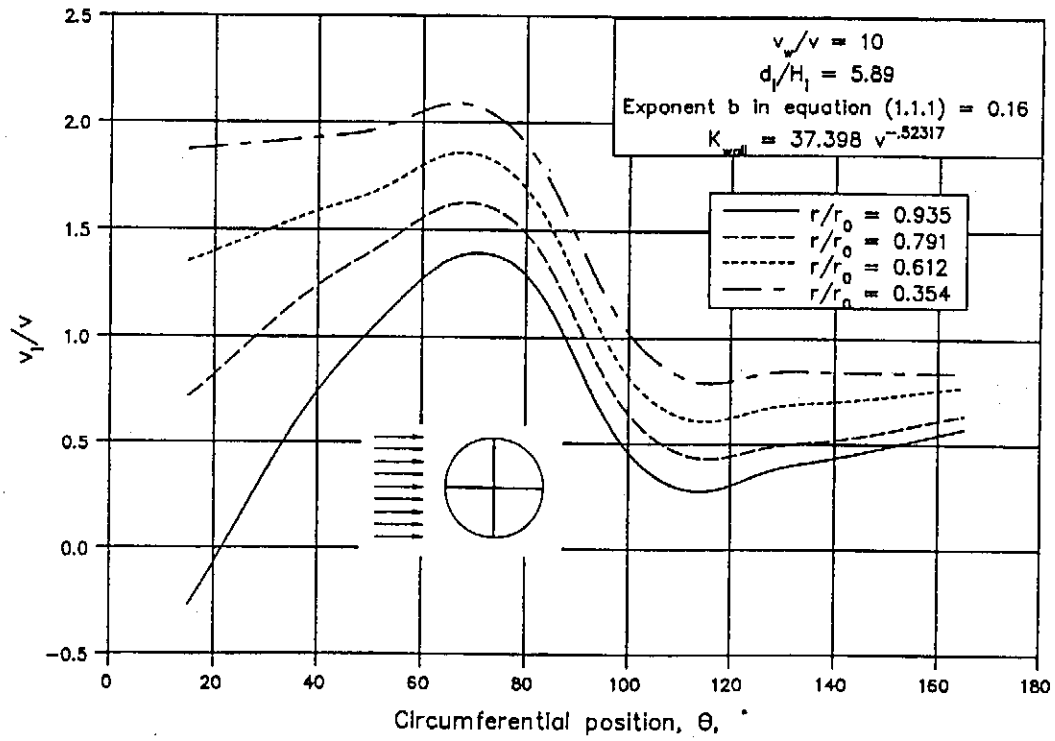

(b)

Figure 4.4.10: Velocity distribution through horizontal heat exchangers.

Both the experimental and numerical models predict an increase in the wind effect on a cooling tower for an increase in the heat rejection rate of the tower as shown in figure 4.4.11. These curves were obtained for a cooling tower with the heat exchangers arranged uniformly and horizontally (not A-frames) over the entire inlet cross-section of the tower. The latter seems to be in direct contrast with results obtained on full scale towers where the heat exchangers are arranged in the form of A-frames. In figure 3.4.5 a reduction in the wind effect on the cooling tower, with the heat exchangers arranged in a horizontal radial pattern, i.e. in the form of A-frames, was observed for an increase in the heat rejection rate of the tower. Results published by Markòczy [77MA1] indicate the same tendency for a cooling tower where the heat exchangers are arranged vertically around the circumference of the tower. Markòczy [77MA1] furthermore suggests that the latter is due to the fact that the disturbances caused by the wind is not only a function of the wind velocity, but also of the cooling air velocity through the heat exchangers. For an increase in the tower performance, the mean air velocity through the heat exchangers also increases, which will result in a reduction in the wind effect on the tower.

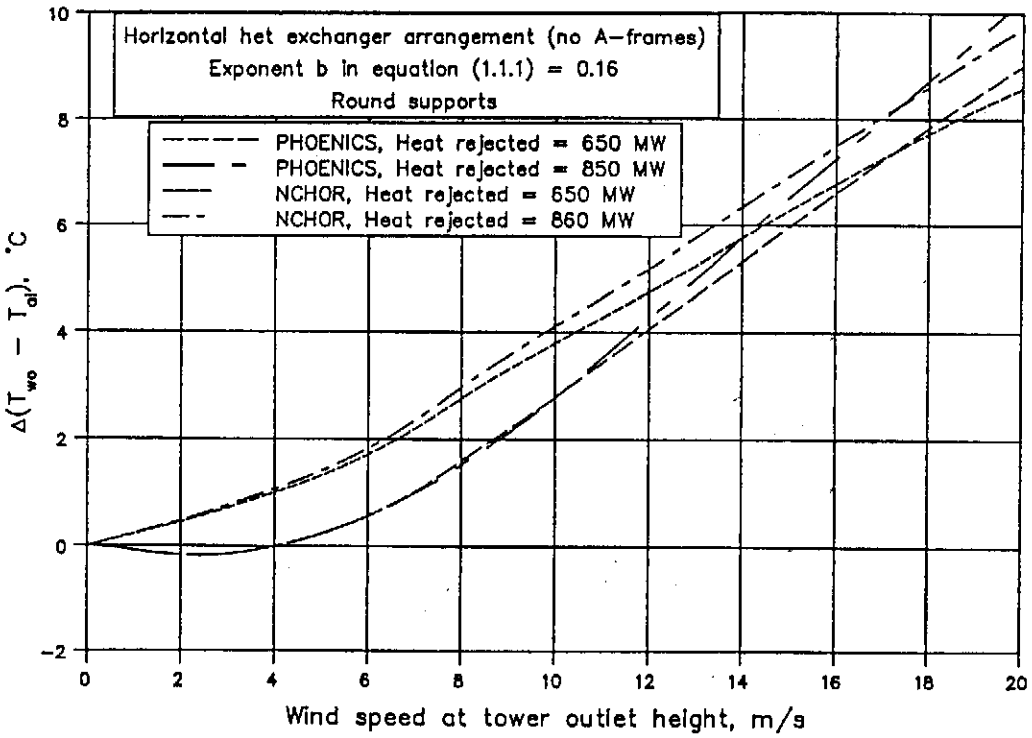

Figure 4.4.11: Wind effect on tower for different heat rejection rates.

The negative effect on the characteristics of an A-frame due to a distorted flow pattern is discussed in appendix K where it is shown that the efficiency of an A-frame becomes increasingly less as the flow incidence angle to the A-frame decreases. Upon closer investigation of the flow field below the heat exchangers, it was found that the incidence angle

to the A-frames becomes very small for large values of the relative wind velocity w_{wo}/v. Based on the results obtained from the numerical model, the flow incidence angle experienced by the A-frames was calculated for a cooling tower with the heat exchangers arranged horizontally and radially in the inlet cross-section of the tower. The results are shown in figure 4.4.12 and suggest a significant reduction in the value of the incidence angle for an increase in the velocity ratio v_{wo}/v. A reduction in the heat rejection rate of the cooling tower implies an increase in the velocity ratio with the incidence angles correspondingly less. Since the latter will in turn cause a reduction in the efficiency of the A-frames, an increase in the wind effect on the tower can be expected. This was also confirmed by further calculations (see figure 4.4.13), after the correlations for the temperature and pressure correction factor for an A-frame (figures K.5 and K.7), were employed in the PHOENICS code. In agreement with the observations made on a similar dry-cooling tower (figure 3.4.5), the wind effect on the tower becomes increasingly less for an increase in the heat rejection rate on the tower. The intersection of the curves for high wind velocities is caused by uncertainties in the correct values of the correction factors due to a lack of reliable data for small incidence angles. The present calculations are based on values obtained by extrapolating the correlations which might lead to erroneous results.

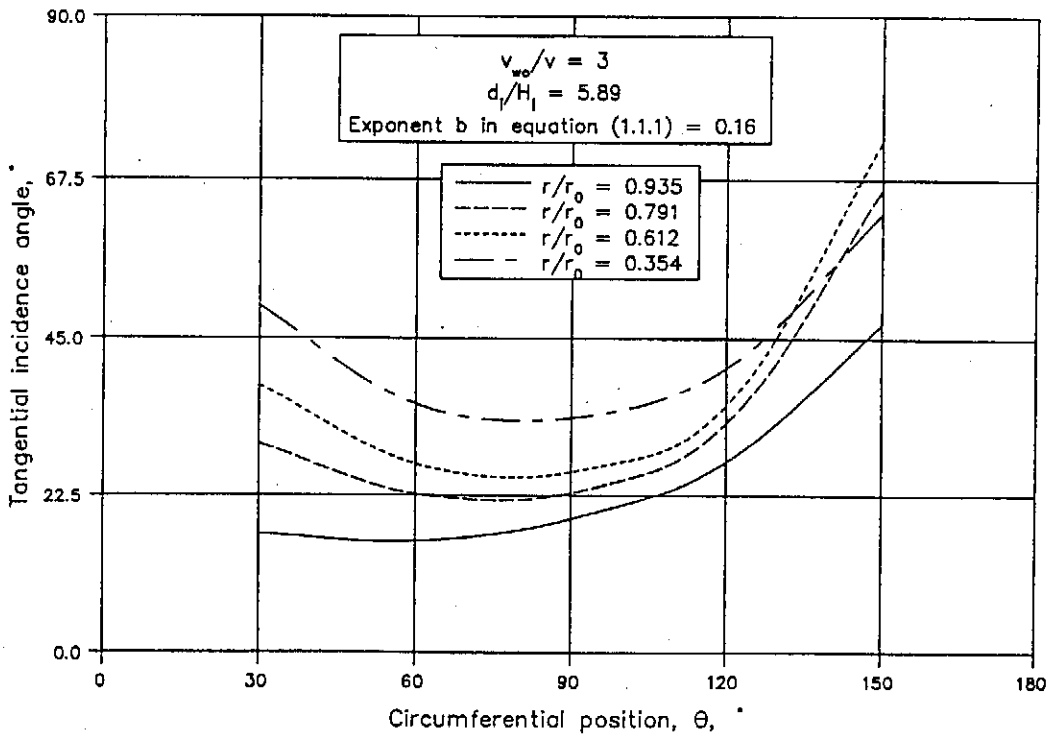

(a)

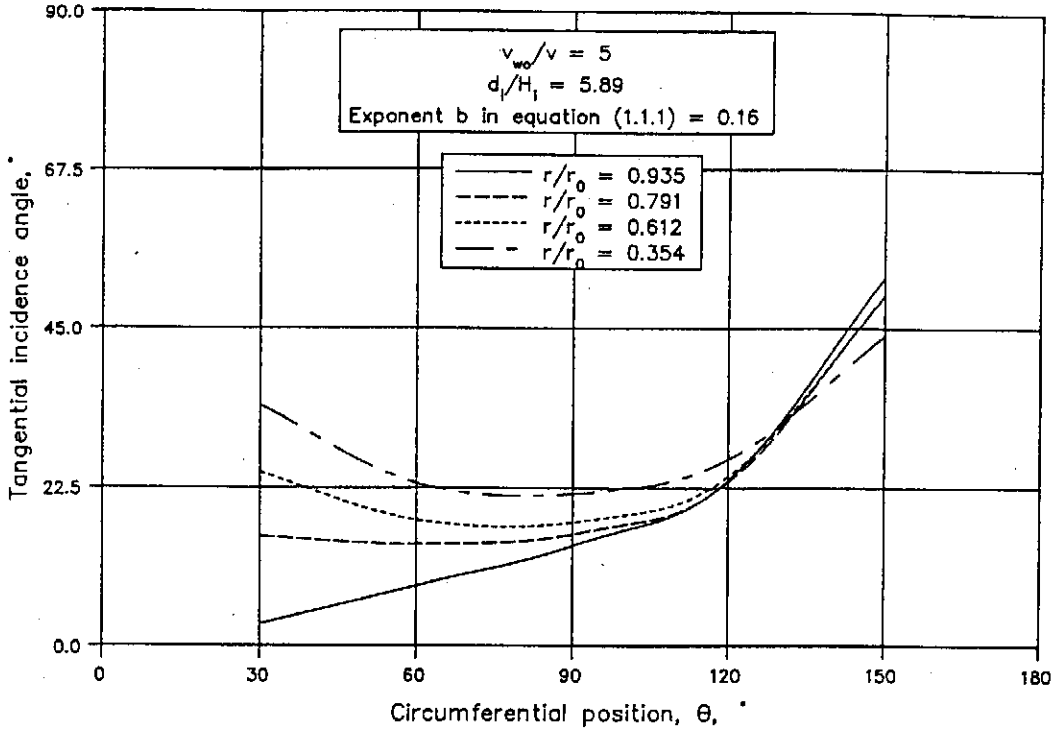

(b)

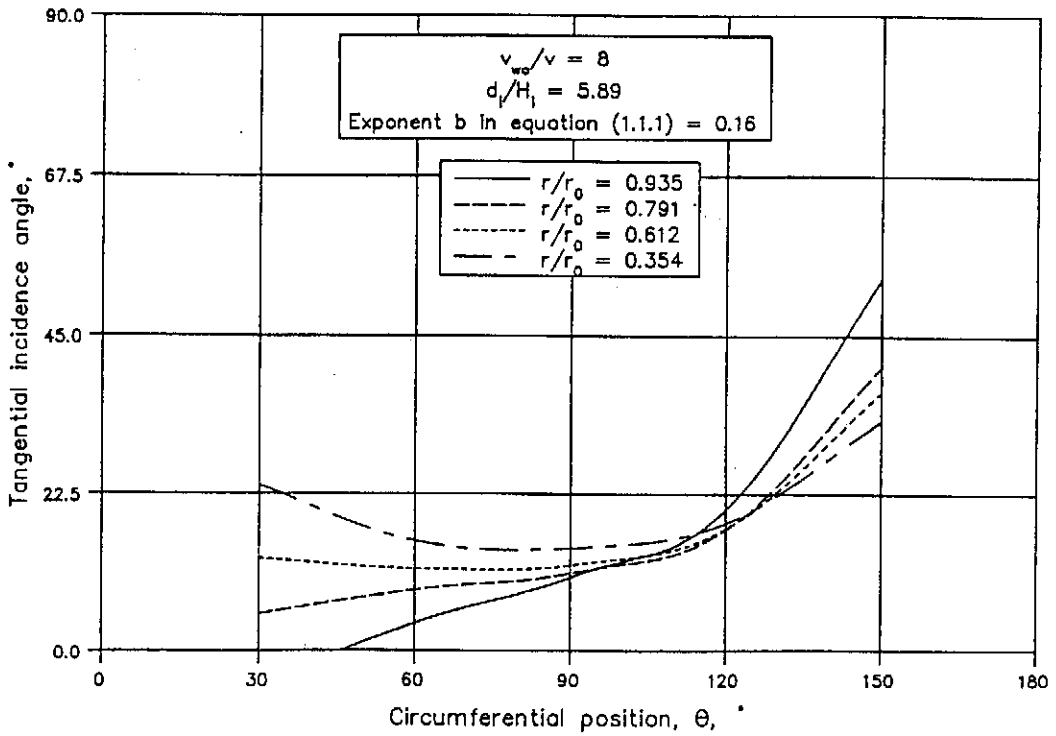

(c)

Figure 4.4.12: Tangential incidence angles to horizontal heat exchangers.

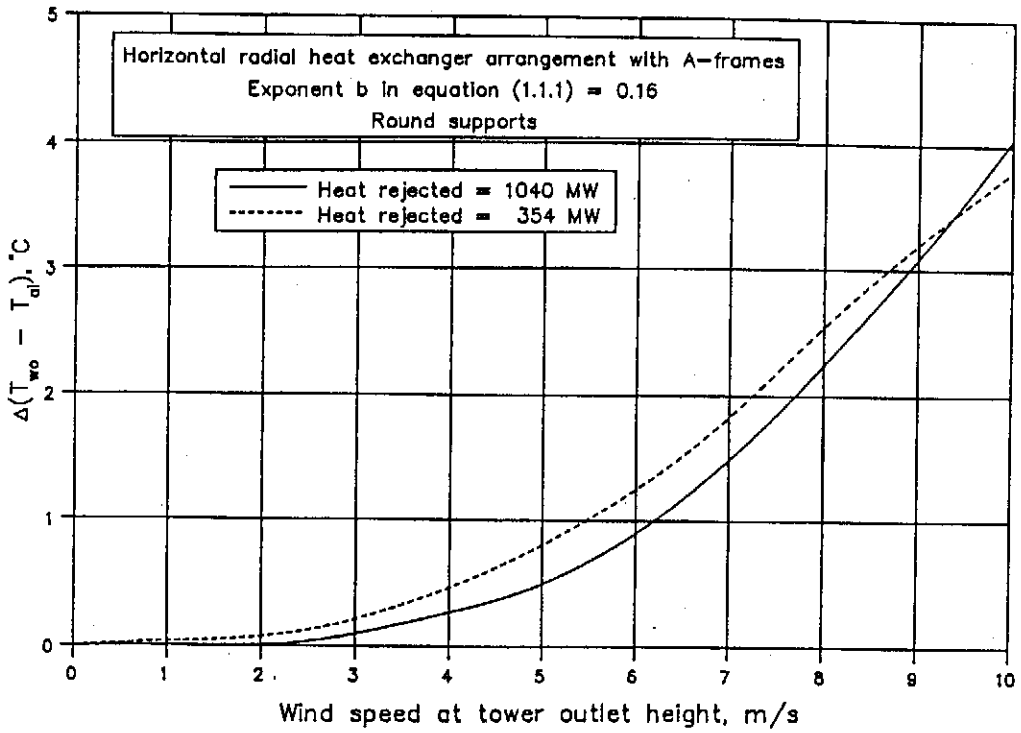

Figure 4.4.13: Wind effect on tower with the heat exchangers arranged horizontally and radially in the inlet cross-section of the tower.

The influence of the A-frames on the wind effect on the tower is shown by curves one and two in figure 4.4.14 which were calculated for the same cooling tower with the heat exchangers arranged horizontally (no A-frames) and in a horizontal radial layout respectively. Since the heat exchanger arrangement in the Kendal tower corresponds to the arrangement in the second curve, the latter may be compared to the results obtained on the full scale tower. The prediction according to the numerical model agrees favourably with the full scale measurements as shown in figures 4.4.15 and 4.4.16 for heat transfer rates of 650 MW and 860 MW respectively. It should furthermore be mentioned that the heat exchanger layout in the full scale tower is slightly conical, with a cone angle $2\theta_c \approx 173°$, which may also have an effect on the wind influence on the tower. The reduction in the mean air mass flow rate through the tower as a function of the wind velocity is shown in figure 4.4.17 which may be compared to the data as measured on the full scale tower shown in figure 3.4.8.

Generally it would appear that towers where the heat exchangers are arranged horizontally in the inlet cross-section are less affected by cross-wind than those where the heat exchangers are arranged vertically around the circumference of the tower, see figure 1.1.1. The influence of the heat exchanger arrangement on the wind effect on a dry-cooling tower was also investigated

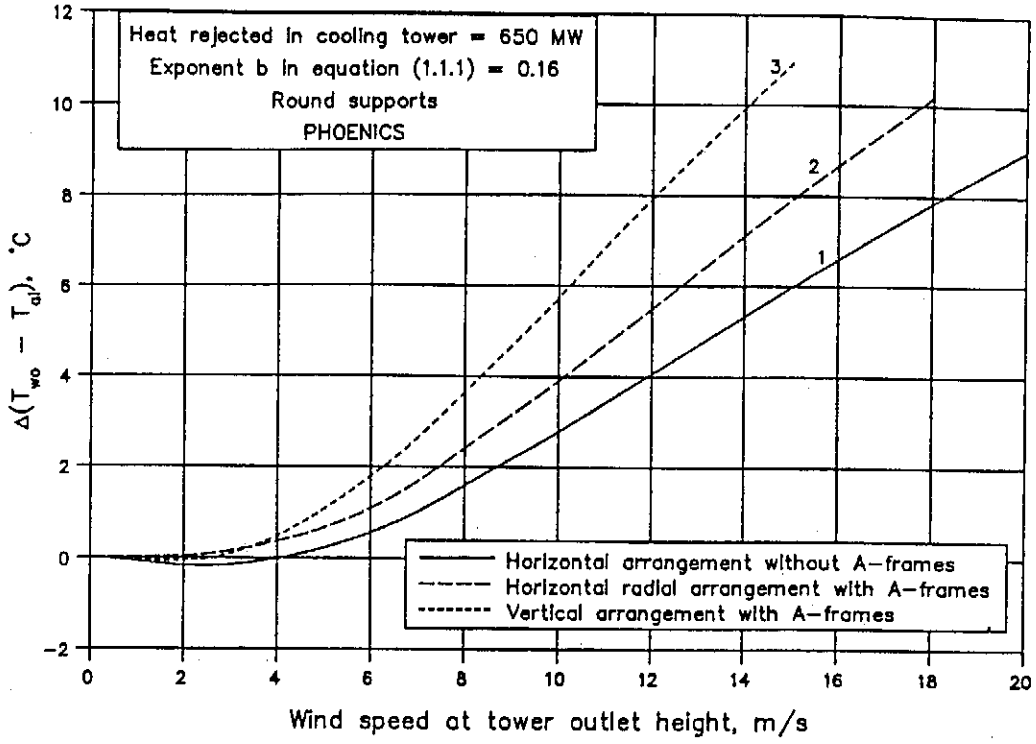

Figure 4.4.14: Wind effect on tower with different heat exchanger arrangements.

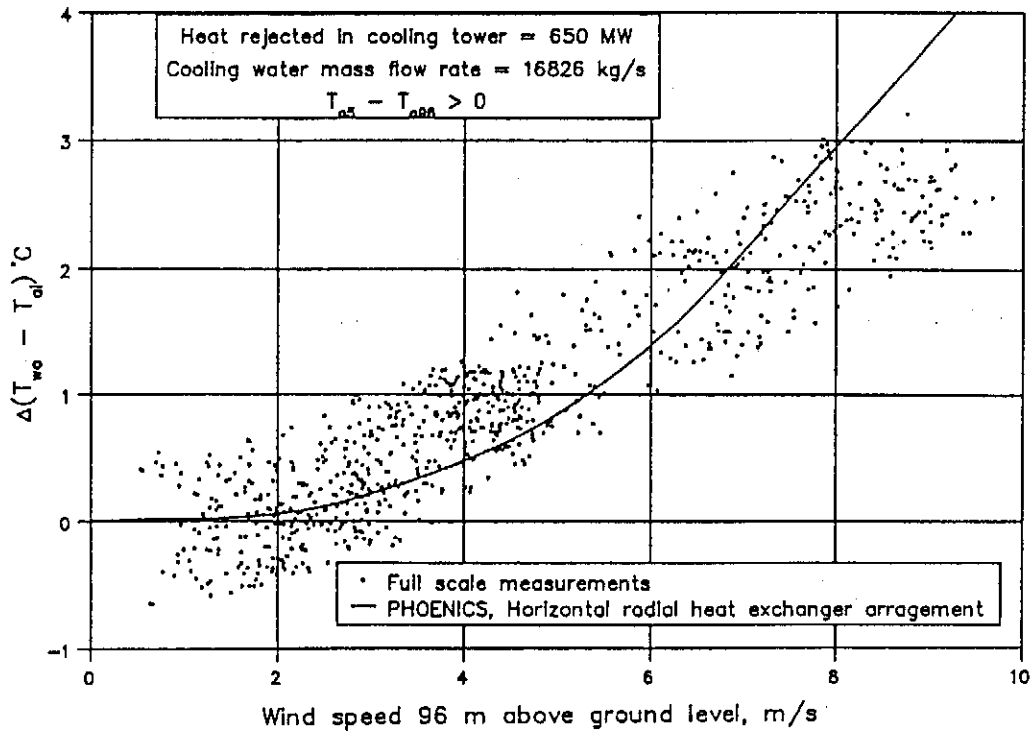

Figure 4.4.15: Wind effect on tower, Heat rejected by tower = 650 MW.

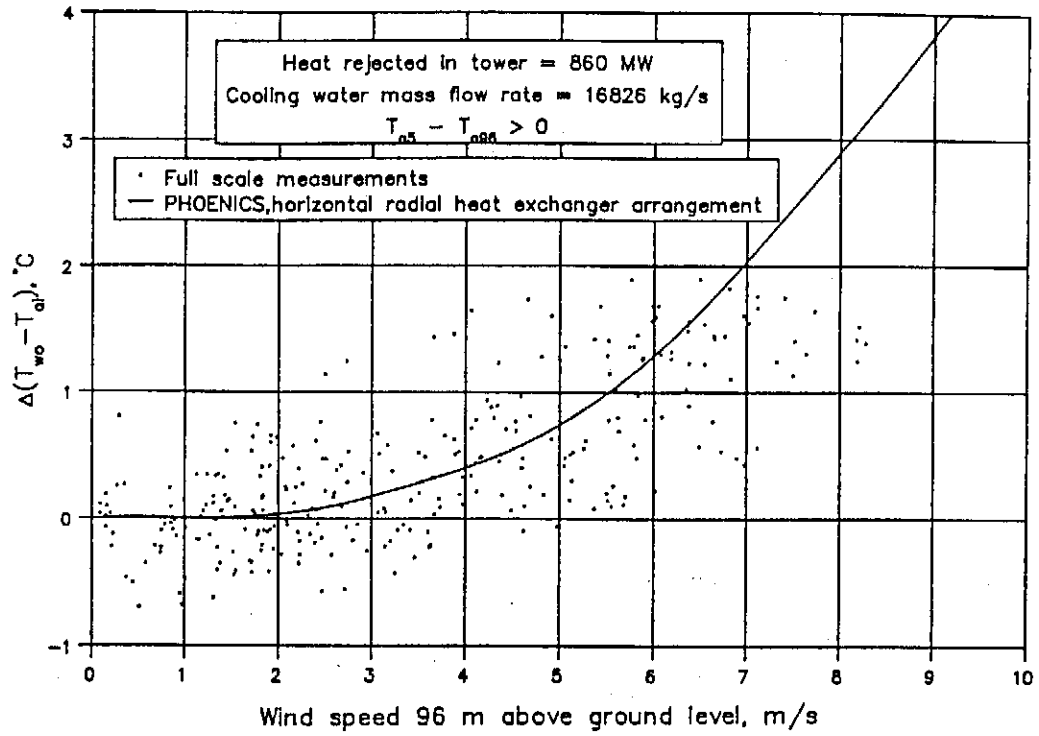

Figure 4.4.16: Wind effect on tower, Heat rejected by tower = 860 MW.

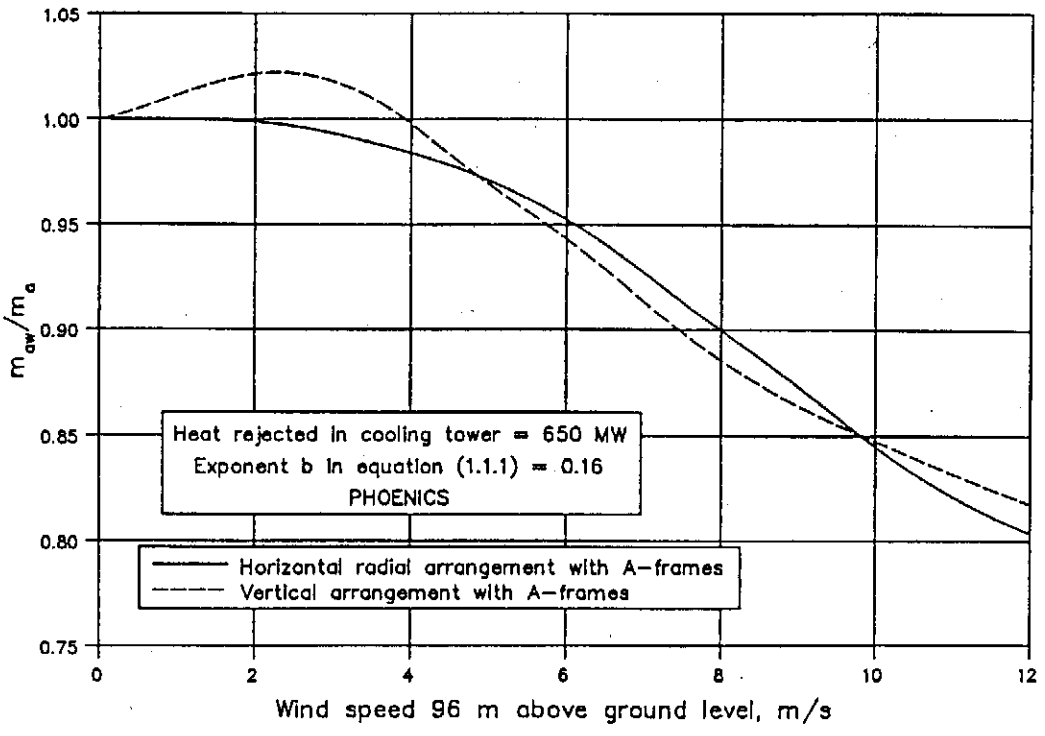

Figure 4.4.17: Reduction in the mean air mass flow rate through the tower due to the wind.

by means of the numerical model. The same tower geometry was used in the calculations but the A-frames, previously arranged horizontally and radially in the tower, were positioned vertically around the circumference of the tower directly below the inlet edge of the tower shell. Although the apex angle of the A-frames were kept at 60°, the length of the fin tubes, and therefore also the inlet height of the tower, were changed to retain the total frontal area of the heat exchangers. With a tube length of 19 m the d_i/H_i ratio of the tower was found to be 7.7 in comparison with the 5.89 of the previous model.

In the absence of atmospheric disturbances the amount of heat rejected by the tower with the vertical heat exchanger arrangement is found to be 3% more than that rejected by the same tower with a horizontal heat exchanger arrangement. However, in the presence of a cross-wind, the performance of a tower with vertically arranged heat exchangers is affected more in comparison with a tower where heat exchangers are arranged horizontally in the inlet cross-section of the tower as shown in figure 4.4.14. Since the wind effect on the mean air mass flow rate through towers with different heat exchanger arrangement is approximately the same (figure 4.4.17), the poor performance of the vertically arranged exchangers is mainly due to the severely distorted air flow distribution as shown in figure 4.4.18. The latter is caused by the variation in the static pressure around a cylinder during a cross-flow [80LE1, 85VO1]. The incidence angle to the A-frames in the vertical arrangement is shown in figure 4.4.19 and compares very well with experimental measurements made by Völler [85VO1].

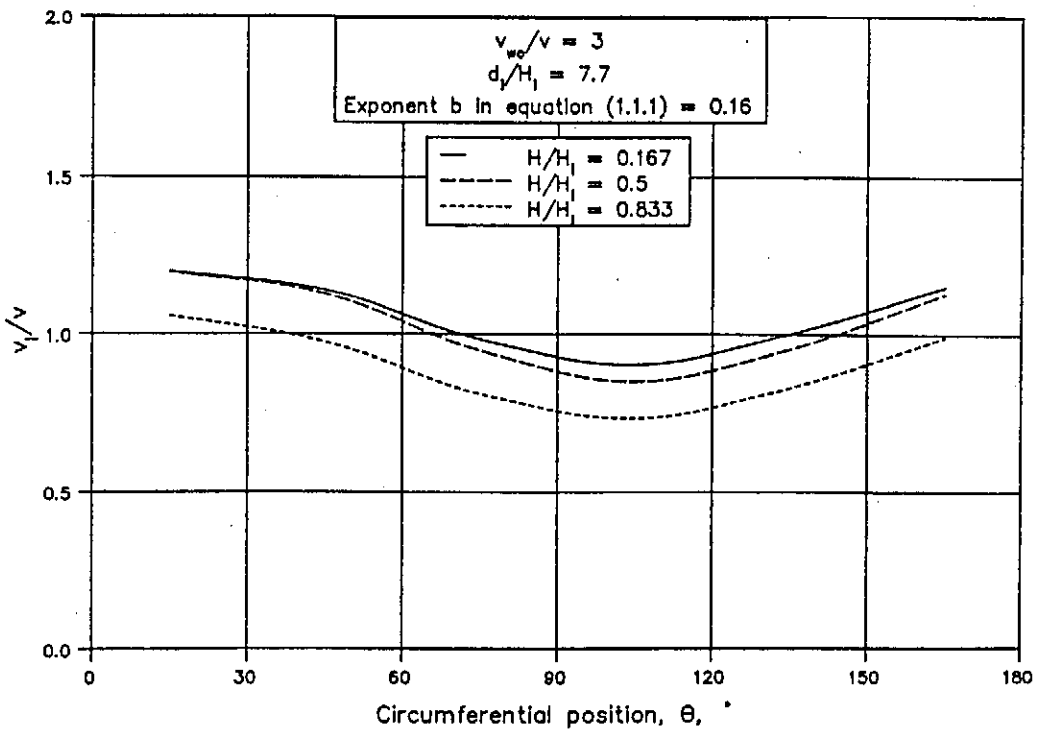

(a)

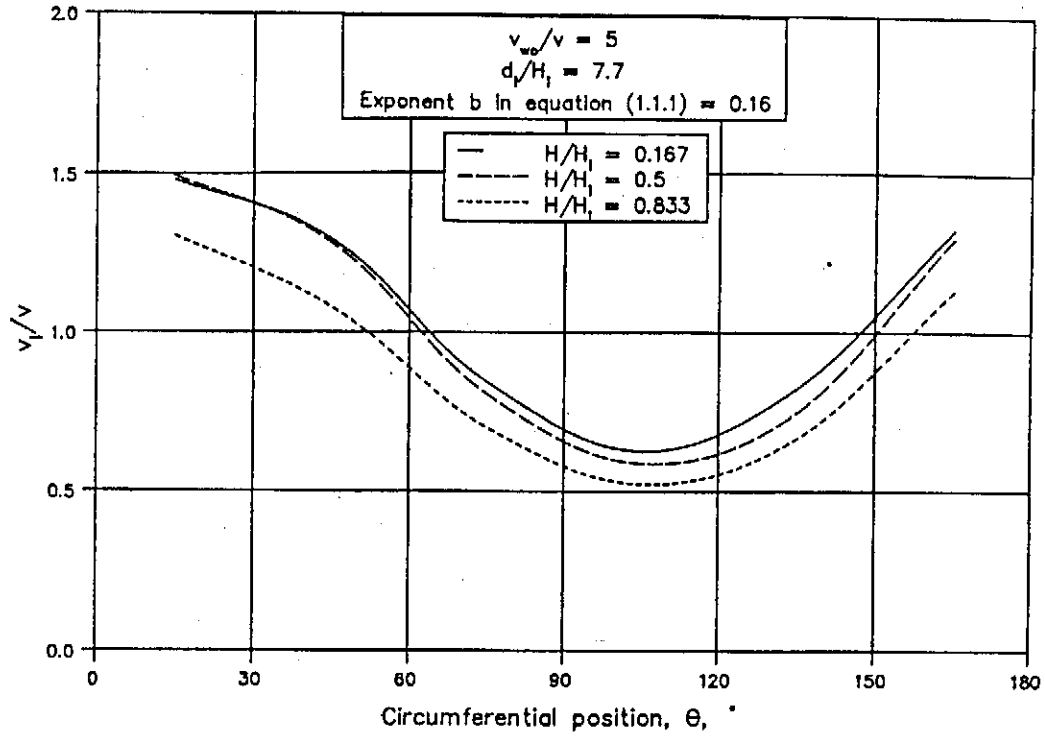

(b)

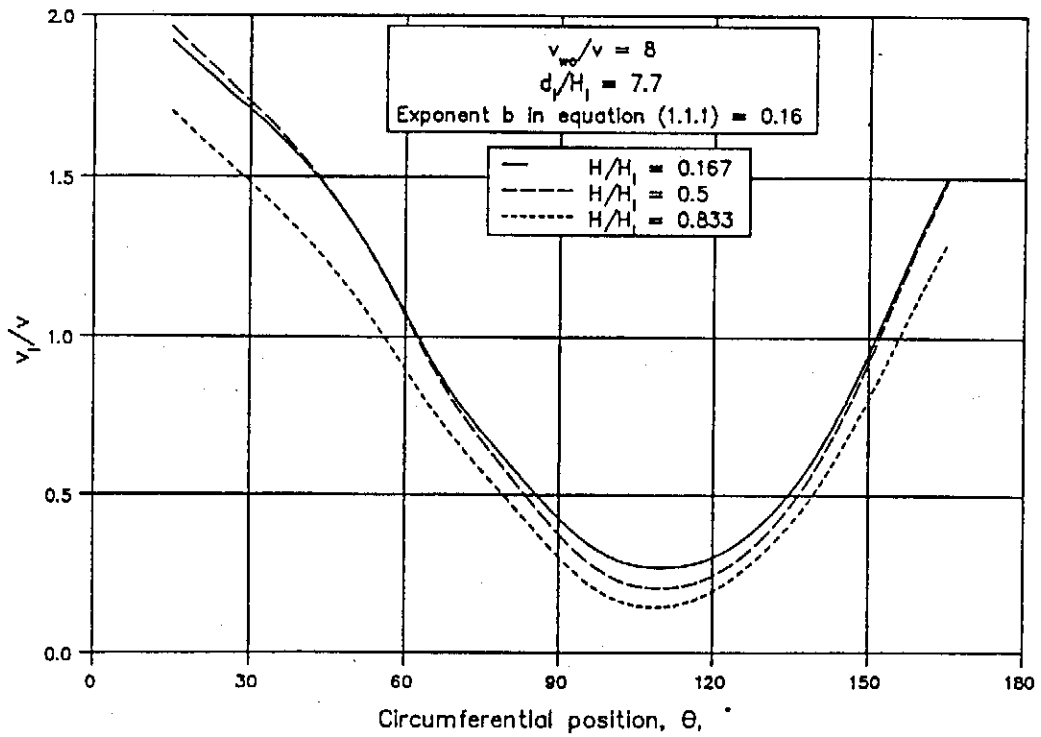

(c)

Figure 4.4.18: Velocity distribution through vertical arrangement.

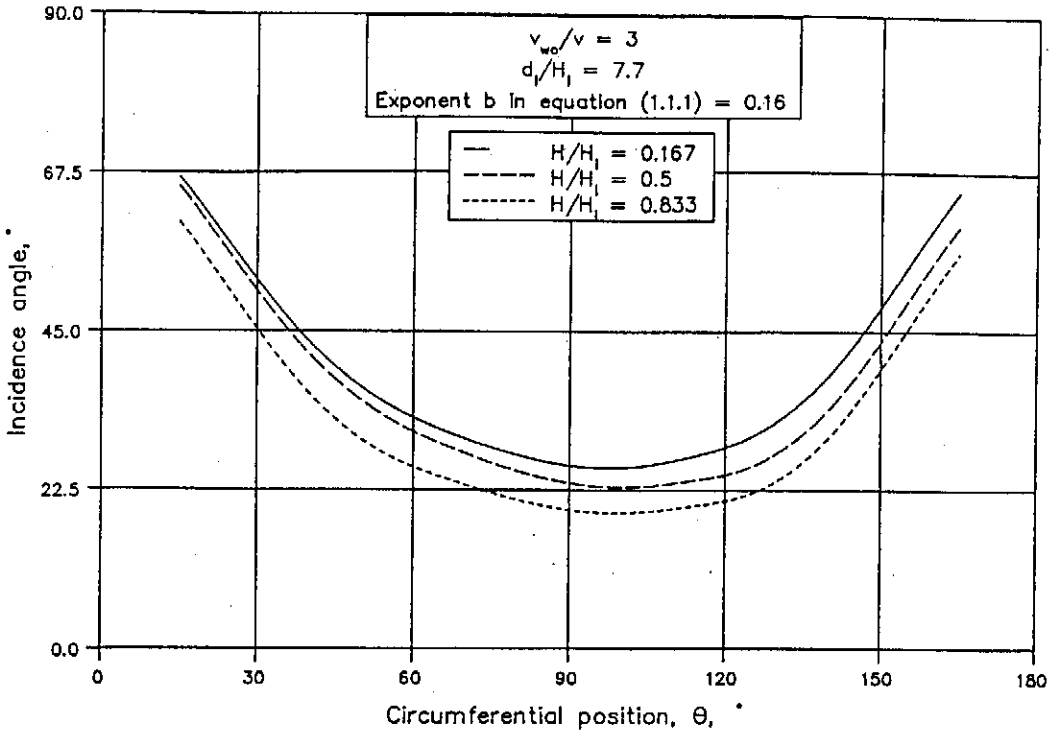
v_{wo}/v = 3
d_1/H_1 = 7.7
Exponent b in equation (1.1.1) = 0.16
H/H_1 = 0.167
H/H_1 = 0.5
H/H_1 = 0.833
90.0
67.5
45.0
22.5
0.0
Incidence angle, °
0
30
60
90
120
150
180
Circumferential position, θ, °

(a)

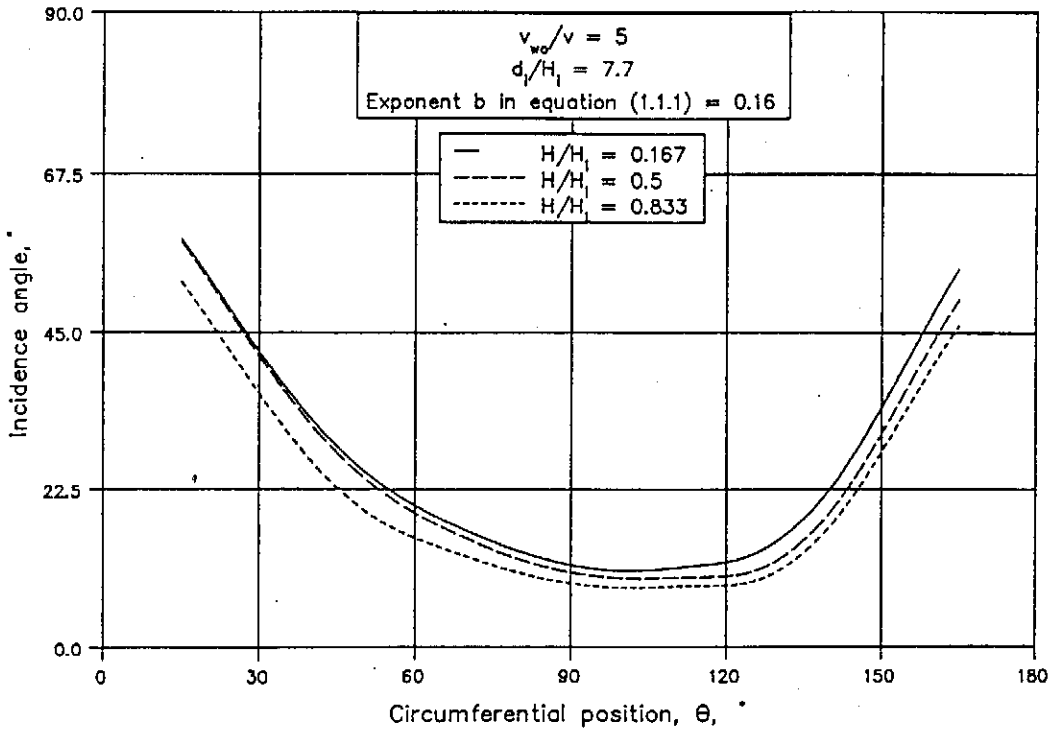
v_{wo}/v = 5
d_1/H_1 = 7.7
Exponent b in equation (1.1.1) = 0.16
H/H_1 = 0.167
H/H_1 = 0.5
H/H_1 = 0.833
90.0
67.5
45.0
22.5
0.0
Incidence angle, °
0
30
60
90
120
150
180
Circumferential position, θ, °

(b)

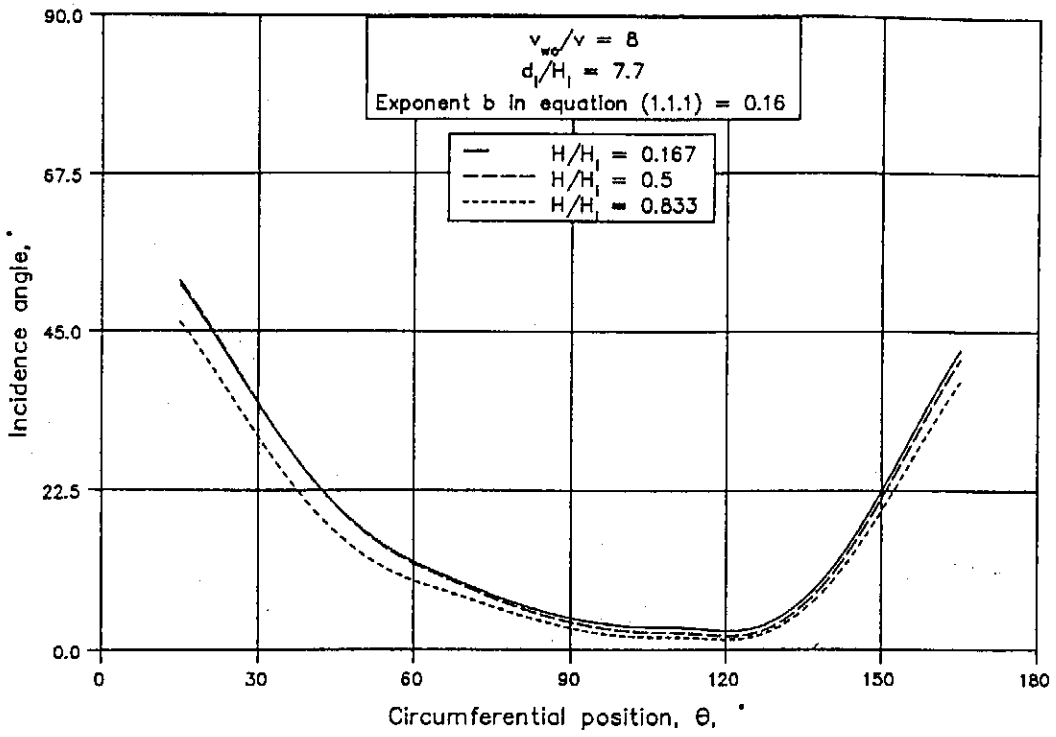

(c)

Figure 4.4.19: Incidence angle for vertical arrangement.

4.5: Conclusions

Computational fluid dynamics proved to be a helpful tool to reliably predict the wind effect on a natural draft dry-cooling tower. By incorporating the effect of different support arrangements and A-frames in the numerical model, the effect of these components on the wind influence on the tower performance was investigated. In conclusion the results of the investigation are summarized.

1. As the wind speed increases, a rise in the inlet water temperature is needed to maintain the amount of heat rejected by the tower.

2. As the wind speed increases the air mass flow rate through the tower becomes increasingly less.

3. Figure 4.4.4 shows that the local air velocity through horizontally arranged heat exchangers on the upstream side of the tower is affected the most by a cross-flow.

4. As the wind speed increases the velocity distribution through horizontally and vertically arranged heat exchangers becomes increasingly more non-uniform (see figures 4.4.4 and 4.4.18).

5. If the wind speed increases, a reduction in the flow incidence angles to the heat exchangers is found. This is found to be true for both a vertical and horizontal heat exchanger arrangement.

6. As the approaching wind profile becomes more uniform, the wind effect on the tower performance increases.

7. Both the pressure loss coefficient and the shape of the tower supports have significant influences on the wind effect of the tower. Radially elongated supports by which the incoming flow is directed in a radial direction have the most favourable effect.

8. Significant reductions in the wind effect on a dry-tower are achieved by installing porous windbreak walls in the base of the tower under the heat exchangers.

9. For a horizontal arrangement of the heat exchangers (no A-frames) an increase in the wind effect on the tower is found if the amount of heat rejected by the tower increases. Conversely a reduction in the wind influence on the tower is found if the heat rejection rate of a tower is increased when the heat exchangers are arranged in the form of A-frames.

10. The performance of a tower is adversely affected in a cross-wind if the heat exchangers are arranged in the form of A-frames.

11. Towers where the heat exchangers are arranged vertically around the circumference of the tower are more affected by a cross-wind compared to those where the heat exchangers are arranged horizontally in the inlet cross-section of the tower.

Finally the results obtained by means of the numerical procedure, as listed above, can be compared to the model and full scale observations discussed in chapters 2 and 3 respectively.

Scale model vs. Numerical simulation (no A-frames).

1. Both methods indicate an increase in the wind effect on the tower with increasing wind speeds as shown in figures 4.4.1 and 4.4.7. For high wind velocities the agreement between the numerical results and those based on the experimental data is excellent. As the wind speed decreases the prediction according to the numerical model is optimistic.

2. Results obtained on the scale model suggest that changes in the wind profile have almost no effect on the wind influence on the tower. Conversely a noticeable rise in the approach temperature of the tower was found with the numerical model as the wind profile became more uniform as shown in figure 4.4.1.

3. The numerical model shows that the presence of tower supports causes an improvement in the velocity distribution through the horizontally arranged tower supports. The latter is contradictive to results obtained on the experimental model.

4. Both methods indicate a significant reduction in the tower performance if the tower supports are removed from the tower inlet.

5. The velocity distribution through the horizontally arranged heat exchangers as predicted by the numerical model (see figure 4.4.4) is in good agreement with the distribution measured on the experimental model as shown in figure 2.3.1.

6. The effect of a porous windbreak wall, installed below the heat exchangers, on the performance and air mass flow rate through the tower is shown in figures 4.4.8 and 4.4.9 respectively. The results predicted by the numerical and experimental methods are found to be in excellent agreement.

7. For a horizontal arrangement of the heat exchangers both the numerical and experimental models indicate an increase in the wind effect on the tower for an increase in the amount of heat rejected by the tower.

8. The incidence angles to vertically arranged heat exchangers compare well with experimental results published by Völler [85VO1].

Full scale measurements vs. numerical simulation (with A-frames).

1. The predicted wind effect on a tower with a radial A-frame arrangement agrees favourably with measurements made on a full scale tower with a similar heat exchanger arrangement.

2. Once the effect of the A-frames is incorporated in the numerical model, a reduction in the wind effect on the tower is found for an increase in the amount of heat rejected by the tower. The latter is in agreement with full scale observations.

3. The predicted reduction in the air mass flow rate through the tower shown in figure 4.4.17 can be compared to the measured results as shown in figure 3.4.8.

4. Finally it is shown that dry-cooling towers with vertically arranged heat exchangers are more sensitive to cross-winds than those where the heat exchangers are arranged vertically in the inlet cross-section of the tower [76MO1].

CHAPTER 5

Conclusions and recommendations.

The reduction in the performance of natural draft dry-cooling towers subjected to cross-winds was studied by means of isothermal model tests, a numerical simulation and full scale measurements. Since each of these techniques offers its own advantages, but also limitations, a combination of these methods was used to study different aspects of the problem.

Due to economical reasons most investigators preferred model tests to study the wind effect on cooling towers. By using a flexible model it is possible to perform a large number of relatively inexpensive tests to determine the influence of various parameters on the wind effect on the cooling tower. It is shown that C_{pi} is strongly dependent on the flow resistance of the tower supports, the pressure loss coefficient of the heat exchangers and the inlet diameter to inlet height ratio of the tower. Generally it would appear that a tower becomes less sensitive to the wind for a reduction in the K_{he} value of the heat exchangers, for a reduction in the d_i/H_i ratio of the tower and for an increase in the pressure loss coefficient of the tower supports. Furthermore it is found that the conical shape of the tower shell and the form of the approaching wind profile have a very small effect on the value of C_{pi} provided that the pressure loss coefficient of tower supports is sufficiently large. At high wind speeds the tower draft is enhanced due to increased suction at the outlet of the tower.

Further reductions in the performance of the tower are caused by the distorted flow pattern through the heat exchangers. This is due to the reduction in the effectiveness of the heat exchanger and the non-uniform air temperature distribution in the tower. The velocity distribution through the heat exchangers becomes increasingly more non-uniform as the d_i/H_i ratio of the tower increases and also for a reduction in the pressure loss coefficient of the heat exchangers. By erecting windbreak walls below the heat exchangers, for a horizontal arrangement of the latter, significant reductions in the wind effect of the tower can be achieved.

By using the results obtained by the model tests, the rise in the approach temperature of the cooling tower can be calculated for different wind speeds. Since the model tests were performed on a model of a tower where the heat exchangers are arranged uniformly and horizontally over the entire inlet cross-section of the tower (no A-frames), the results are only applicable for similar towers. Further calculations revealed that the wind effect on such towers

increases for an increase in the heat rejection rate of the tower. A reduction in the wind effect on the tower is also observed as the height of the tower increases.

The size of cooling tower models is usually limited by the size of available wind tunnels. The Reynolds numbers obtained with a small scale model are much smaller compared to those found in full scale towers. Furthermore is it almost impossible to model certain tower details such as the shape of the tower supports and the A-frame arrangement of the heat exchangers correctly.

The PHOENICS computer code proves to be a useful tool for determining the flow patterns about a natural draft dry-cooling tower. Although the flow instabilities are not represented in the present numerical model, the results obtained with the calculations compare favourably with those measured in a similar full scale tower. By using the computer code, the influence of different support arrangements on the wind effect of the tower was investigated numerically. Since tower supports tend to reduce the wind speed below the heat exchangers the static pressure in that region is correspondingly higher. The latter will cause an increase in the mean air mass flow rate and therefore an enhancement in the performance of the tower. If the shape of the tower supports is such that the incoming flow is directed in a radial direction, significant reductions in the wind effect on the tower can be achieved under certain conditions. With a numerical model the incidence angle to the heat exchangers is easily determined, thereby making it possible to incorporate the effect of A-frames on the tower performance. It is found that the heat rejection rate of a tower in the presence of a cross-wind is adversely affected if the heat exchangers are arranged in the form of A-frames. If the A-frames are represented in the numerical model, a reduction in the wind effect on the cooling tower is found for an increase in the heat rejection rate which corresponds to full scale observations. It is furthermore found that towers where the heat exchangers are arranged horizontally in the inlet cross-section of the tower are less affected by the wind than those where the heat exchangers are arranged vertically around the circumference of the tower. The latter is mainly due to the severely distorted air flow distribution through the vertically arranged heat exchangers.

Full scale measurements are expensive and much time is usually needed for adequate preparations and the installation of the instruments. Since none of the independent variables can be controlled by the investigator, the measurements can easily be misinterpreted and such tests should be thoroughly documented. These measurements are however of great value when evaluating results of model tests or numerical calculations. It was shown in chapter 4 that if

the characteristics of all tower components are known and interpreted correctly, measurements obtained on full scale towers can be successfully reproduced.

The factors affecting the performance of natural draft dry-cooling towers may therefore be summarized as follows:

1. Wind speed
2. Velocity distribution of approaching wind profile.
3. Heat rejected by cooling tower.
4. Mean air velocity through heat exchangers.
5. Degree of mixing of air after heat exchangers.
6. Transfer characteristics of heat exchangers.
7. Pressure loss coefficient of heat exchangers.
8. Location and arrangement of heat exchangers.
9. Height of cooling tower.
10. Ratio of inlet diameter to tower height, d_i/H_i.
11. Inlet taper and shape of shell.
12. Loss coefficient of tower supports.
13. Shape of tower supports.
14. Any structures or obstacles in tower base below the heat exchangers.

Recommendations.

Although many of the uncertainties concerning the problem addressed in this dissertation have been solved, much more remains to be done to clarify certain aspects of the problem:

1. In the present investigation specific reference was made to dry-cooling towers with a horizontal arrangement of the heat exchangers. Although the wind effect on a tower with a vertical heat exchanger was determined by means of a numerical procedure, very little useful information was obtained for heat exchanger arrangements other than the horizontal layout. The influence of the different tower components on the wind effect on a tower with a vertical arrangement remains to be determined. Furthermore, the effect of a conical heat exchanger arrangement on the wind influence on the tower is

still unknown.

2. The available information concerning the effect of oblique inlet conditions on the performance of heat exchangers arranged in an A-frame is insufficient. Future investigations should be extended to include effects such as variations in the pressure loss coefficients of the heat exchangers, the apex angle of the A-frames and transfer characteristics of the heat exchangers.

3. At present the wind effect on a tower with the heat exchangers arranged horizontally in the form of A-frames can only be predicted by means of numerical methods. Since almost no information, for example the incidence angles, of the flow field below the heat exchangers is available, the effect of the A-frames cannot be incorporated in the experimental model.

4. The influence of the tower supports on the velocity distribution through the heat exchangers and the effect of variations in the form of the wind profile in the tower performance are still uncertain. Results obtained with the model tests and numerical simulation concerning these two areas were in disagreement and more work should be done to clarify the problem.

5. The degree of mixing of the air after the heat exchangers and the corresponding effect on the heat transfer rate of the tower is still unknown to a great extent.

6. The current numerical model can be extended to include flow instabilities in and outside the tower.

REFERENCES

29FA1 Fage, A. and Warsap, J.H., The Effects of Turbulence and Surface Roughness on the Drag of a Circular Cylinder, Rept. Mem. 1283, Brit. Aeronaut. Res. Comm., October, 1929.

29LO1 Lock, C.N.H., The Interference of a Wind Tunnel on a Symmetrical Body, ARC R.&M. 1275, 1929.

52PA1 Pankhurst, R.C. and Holder, D.W., Wind-Tunnel Technique, Sir Isaac Pitman & Sons, LTD, London, 1952.

65HO1 Hoerner, S.F., The Fluid Dynamics of Drag, Hoerner, 2nd ed. Midland Park, New Jersey, 1965.

66PO1 Pope, A. and Harper, J.J., Low-Speed Wind Tunnel Testing, John Wiley & Sons, Inc., New York, 1966.

67PR1 Preussag, A.G., Steinkohlenbergwerke Ibbenbüren, Kraftwerke Ibbenbüren - 150 MW Block. Bericht über die am 22 und 23.8.1967 durchgeführten Messungen am Kühlturm der luftgekühlten Kondensationsanlage, 6 Nov, 1967.

69CH1 Christopher, P.J. and Forster, V.T., Rugeley Dry Cooling Tower System, Proc. Instn. Mech. Engrs. (London), Vol. 184, Pt. 1, No. 11, pp. 197-211, 1969-1970.

72EC1 Eck, B., Ventilatoren, Entwurf und Betrieb der Radial-, Axial- und Querstromventilatoren, Springer-Verlag, Berlin, 1972.

73FO1 Fox, R.W. and McDonald, A.T., Introduction to Fluid Mechanics, John Wiley & Sons, Inc., New York, 1973.

75GN1 Gnielinski, V., Forsch. Ing. Wesen, Vol. 41, No. 1, 1975.

76MO1 Moore, F.K., Dry Cooling Towers, Advances in Heat Transfer, Vol. 12, 1976

76VA1 Van der Walt, N.T., West, L.A., Sheer T.J. and Kuball, D., The Design and Operation of a Dry Cooling System for a 200 MW Turbo-generator at Grootvlei Power Station, South Africa, The South African Mechanical Engineer, Vol. 26, No. 12, pp. 498-511, 1976.

77MA1 Markòczy G. and Stämpfli, E., Experimentelle Untersuchung des Einflusses Atmosphärischer Umgebungsbedingungen auf das Betriebsverhalten von Naturzug - Trockenkühltürmen, EIR-Bericht, No. 324, Würenlingen, Switzerland, 1977.

77VA1 Van Rooyen, R.S., Warmte-oordrag van Laminêre Olievloei in Gladde en Intern Gevinde Pype met Wentellint-insetsels, M.Ing. Tesis, Universiteit van Stellenbosch, bl.142, 1977.

78BO1 Bouton, F., Design Studies for Natural Draught Dry Towers, SHF Conference, Paris, 1978.

78MO1 Moore, F.K., Effects of Aerodynamic Losses on the Performance of Large Dry Cooling Towers, ASME Paper 78-WA/HT-18, WAM, 1978.

78RU1 Russell, C.M.B., McChesney, H.R., Holder, D.W., Jones, T.V. and Verlinden, M., Cross Wind and Internal Flow Characteristics of Dry Cooling Towers, Combustion, May, 1978.

78VD1 Thermal Acceptance and Performance Tests on Dry Cooling Towers, VDI-Guide Lines, VDI 2049, 1978.

79DI1 Dibelius, G. and Ederhof, A., Der Windeinfluss auf den Volumenstrom von Naturzugkühltürmen, BWK, Vol. 31 NO. 8, pp. 319-326, August 1979.

80BO1 Bourillot, C., Grange, J.L. and Lecoeuvre, J.M., Effect of Wind on the Performance of a Natural Wet Cooling Tower, Proc. 2nd IAHR Cooling Tower Workshop, San Francisco, 1980.

80LE1 Leene, J.A., Draught Reduction of Hyperbolic Natural-Draught Cooling Towers as a Result of Wind, Proc. of the 4th Colloq. on Industrial Aerodynamics, Part 2, Fachhochschule Aachen, pp. 71-82, 1980.

81HO1 Holman, J.P., Heat Transfer, McGraw-Hill International Book Company, 1981.

82BU1 Buchlin, J.M. and Olivari, D., Experimental Investigation of Flow in Natural Draft Cooling Towers by use of Heated Models, Proc. 3rd IAHR Cooling Tower Workshop, Budapest, 1982.

82CH1 Chaboseau, J., Calculation of the Characteristics of an Air Cooling Tower Exposed to Wind, Proc. 3rd IAHR Cooling Tower Workshop, Budapest, 1982.

82GR1 Grange, J.L. and Simon, J.Y., Behaviour of Crossflow and Natural Draft Cooling Towers in the Presence of Wind, Proc. 3rd IAHR Cooling Tower Workshop, Budapest, 1982.

82RU1 Ruscheweyh, H., Modelluntersuchung zum Einfluss der Kühlturmkronenform auf das Zugverhalten grosser Naturzugkühltürme unter Querwindeinfluss, Brennst-Wärme-Kraft, Vol. 34, No. 7, pp. 361-369, 1982.

82SA1 Sabaton, M., Caytan, Y. and Goussebaile, J., Numerical and Experimental Studies for the Cooling Tower Optimization, Proc. 3rd IAHR Cooling Tower Workshop, Budapest, 1982.

83BU1 Buxmann, J., Strömungsverteilung und Wärmeübertragung bei unterschiedlichen Elementanordnugen im Trockenkühlturm, Sonderforschungsbereich 61, Teilproject E10, Bericht Nr. 54, Universität Hannover, 1983.

83HA1 Haaland, S.E., Simple and Explicit Formulas for the Friction Factor in Turbulent Pipe Flow, Trans. ASME J. Fluids Engineering, Vol. 105, No. 3, pp.89-90, Mach 1983.

83PA1 Panofsky, H.A. and Dutton, J.A., Atmospheric Turbulence, John Wiley & Sons, New York, 1983.

83RU1 Ruscheweyh, H., Full-scale Measurements on a Large Natural Draught Cooling Tower, Proc. 6th. International Conference on Wind Engineering, Australia, 1983.

83WI1 Witte, R., Das Betriebsverhalten atmosphärisch beeinflusster Trockenkühltürme, Fortschr.-Ber VDI-Z, Reihe 6, No. 132, VDI-Verlag, Düsseldorf, 1983.

84RO1 Roetzel, W., Berechnung von Wärmeübertragen, VDI- Wärmeatlas, pp. Ca1 - Ca31, VDI-Verlag GmbH, Düsseldorf, 1984.

85VO1 Völler, G., Untersuchungen zum Windeinfluss auf die Strömung im Naturzug-Trockenkühlturm, Dr. Ing.- thesis, Universität Hannover, 1985.

86BL1 Blanquet, J.C., Goldwirt, F. and Manas, B., Wind Effects on the Aerodynamic Optimization of a Natural Draft Cooling Tower, Proc. 5th IAHR Cooling Tower Workshop, Monterey, 1986.

86BU1 Buxmann, J., Dry Cooling Tower Characteristics Effected by Cooling Circuit and the Top Shape of the Tower, Proc. 5th IAHR Cooling Tower Workshop, Monterey, 1986.

86GE1 Geldenhuys, J.D. and Kröger, D.G., Aerodynamic Inlet Losses in Natural Draft Cooling Towers, Proc. 5th IAHR Cooling Tower Workshop, Monterey, 1986.

86KO1 Kotzè, J.C.B., Bellstedt, M.O. and Kröger, D.G., Pressure Drop and Heat Transfer Characteristics of Inclined Finned Tube Heat Exchanger Bundles, Proc. 8th Int. Heat Transfer Conf., San Francisco, 1986.

86KR1 Kröger, D.G., Performance Characteristics of Industrial Finned Tubes Presented in Dimensional Form, Int. J. Heat Mass Transfer, Vol. 29, No. 8, 1986.

86VA1 Vauzanges, M. and Ribier, G., Variation of the Head Losses in the Air Inlets of Natural Draft Cooling Towers with the Shape of the Lintel and Shell Supports, Proc. 5th IAHR Cooling Tower Workshop, Monterey, 1986.

87TR1 Trage, B. and Hintzen, F.J., Design and Construction of Indirect Dry Cooling Units, Proc. VGB Conference, South Africa, Vol. 1, pp. 70-79, Johannesburg, November 1987.

88CA1 Caytan, Y. and Fabre, L., Wind Effects on the Performance of Natural Draft Wet Cooling Towers Comparison of Constructors Proposals and Realisation of Performance Control Tests, Proc. 6th IAHR Cooling Tower Workshop, Pisa, Italy, 1988.

88DU1 Du Preez, A.F. and Kröger, D.G., Experimental Evaluation of Aerodynamic Inlet Losses in Natural Draft Dry Cooling Towers, Proc. 6th IAHR Cooling Tower Workshop, Pisa, Italy, 1988.

88RA1 Radosavljevic, D. and Spalding, D.B., Simultaneous Prediction of Internal and External Aerodynamic and Thermal Flow Fields of a Natural-Draft Cooling Tower in a Cross-Wind, Proc. 6th IAHR Cooling Tower Workshop, Pisa, 1988.

APPENDIX A

Inlet-and-outlet pressure loss coefficients in a natural draft dry-cooling tower.

A.1 Inlet loss coefficient.

At the inlet of an empty cooling tower, the same flow distortions are found as observed in duct inlets. The flow field for an empty cooling tower is shown schematically in figure A.1.1 with the separated flow region clearly visible at the inlet.

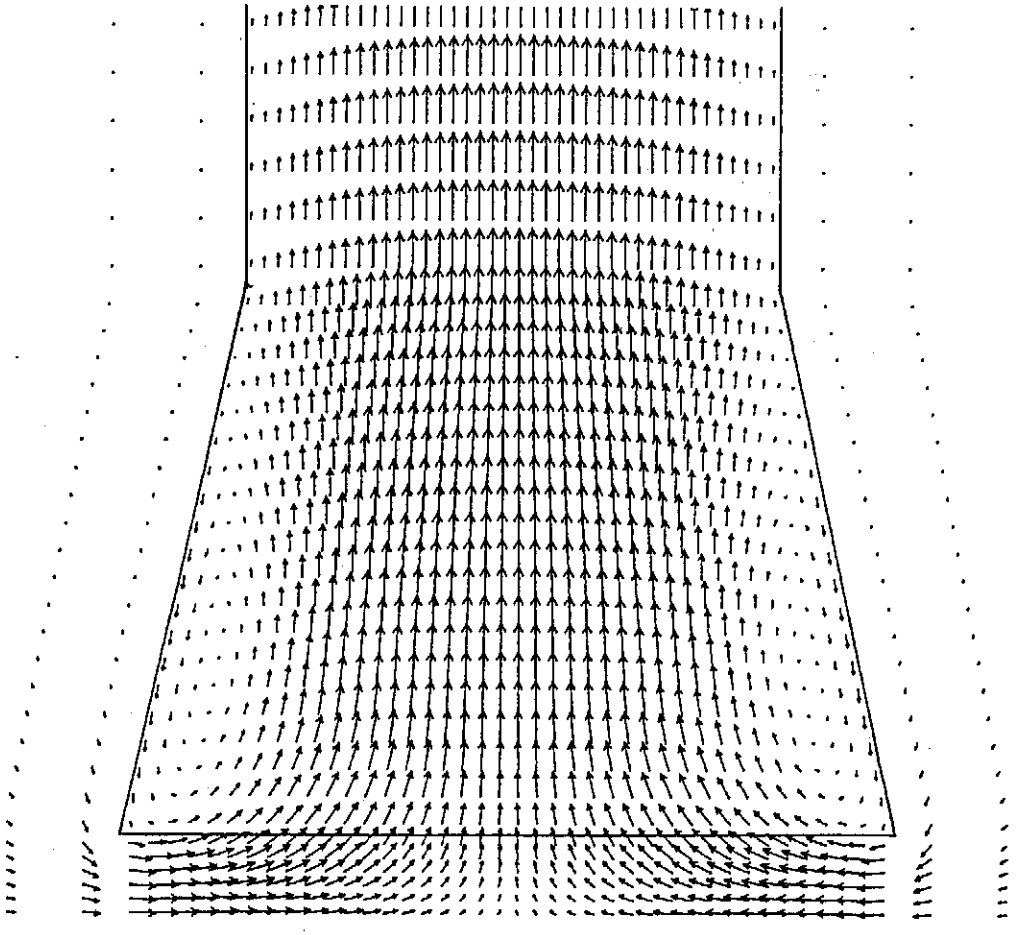

Figure A.1.1: Flow pattern in at inlet of an empty cooling tower.

A static inlet loss coefficient ,K_{cts}, may be defined as:

$$K_{cts} = \frac{(p_\infty - p_s)}{0.5\rho v^2} \qquad (A.1.1)$$

where p_∞ is the stagnant ambient pressure and p_s is the static pressure inside the tower just above the inlet edge of the shell. Furthermore v is the mean air velocity based on the inlet cross-section of the tower.

The static inlet loss coefficient, K_{cts}, was determined with the present cooling tower model and is compared in figure A.1.2 with similar results which Geldenhuys and Kröger [86GE1] obtained at a much higher Reynolds number. The results suggest that K_{cts} is independent of the Reynolds number for the range of the latter shown in the figure.

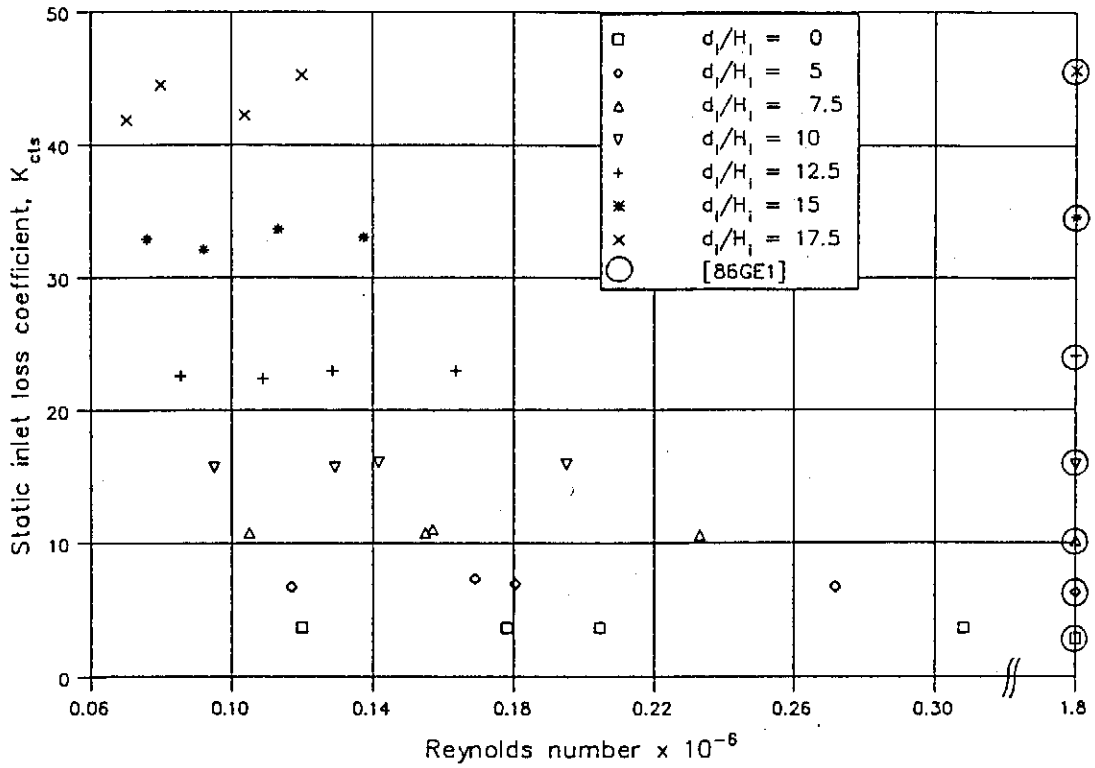

Figure A.1.2: Static inlet loss coefficient for empty cooling tower.

If the Reynolds number is further reduced to values less than 30 x 10^3, the static inlet loss coefficient becomes a function of the former as shown in figure A.1.3. It is therefore preferable that model tests should not be performed in this range of Reynolds numbers.

It was furthermore found that the inlet shape (taper) of the tower shell has no effect on the value of K_{cts}, because the flow separates from the inlet edge and a free jet is formed. This is also observed by Russell [78RU1].

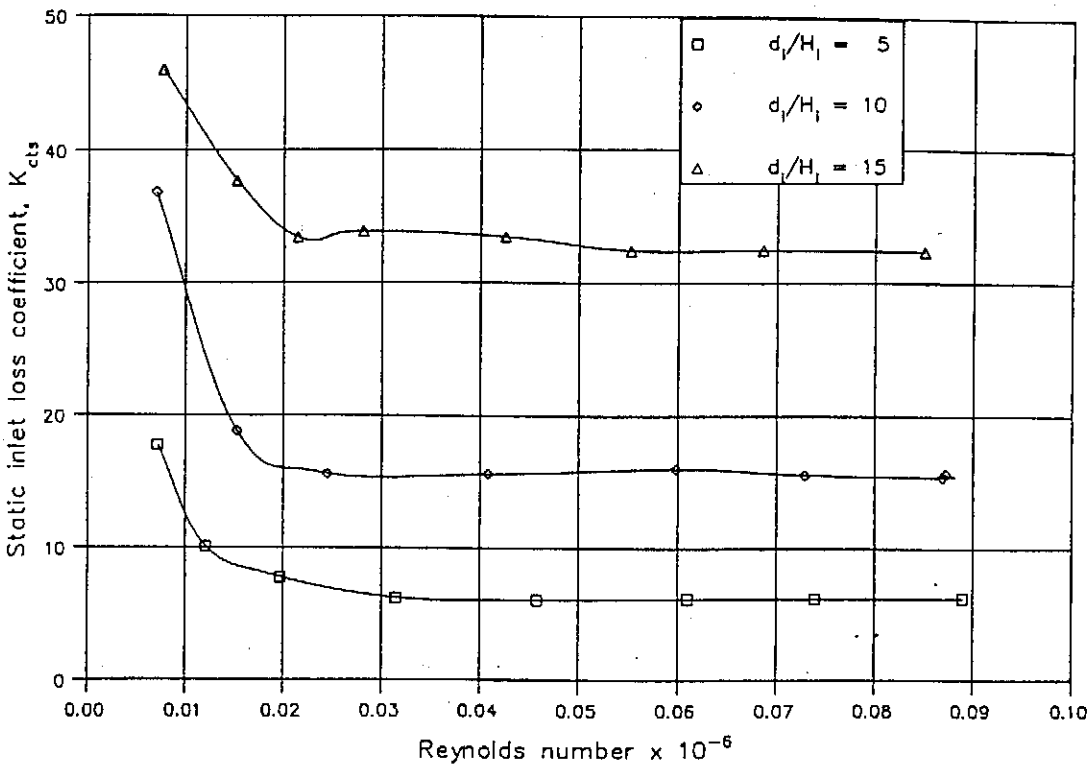

Figure A.1.3: K_{cts} at very low Reynolds numbers.

Finned tube heat exchangers as commonly found in existing dry-cooling towers are conveniently simulated in the present tests with two pieces of honeycomb in series with additional flow resistances in the form of perforated plates or screens as shown in figure A.1.4. The honeycomb is used to direct the air flow at the inlet of the model in an axial direction.

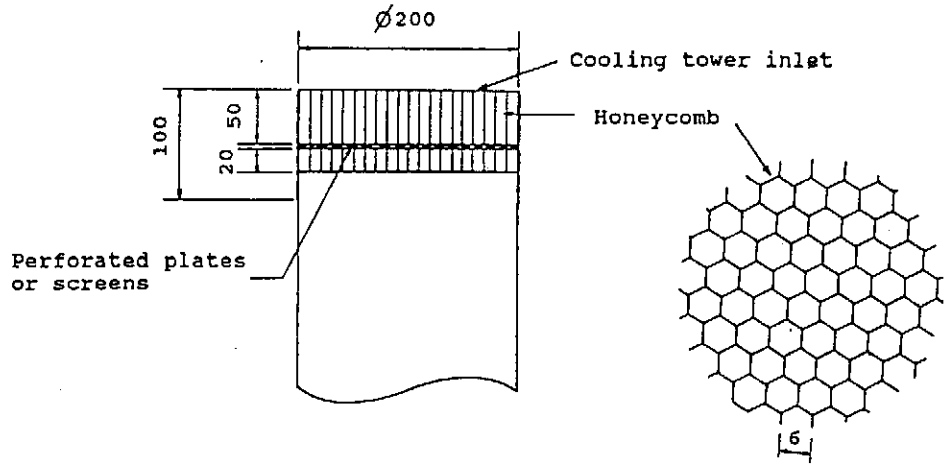

Figure A.1.4: Horizontal heat exchanger model.

The heat exchanger loss coefficient, K_{he}, as defined in equation (2.1.2), is determined under normal flow conditions by adding a rounded inlet to the model. In figure A.1.5 the heat exchanger loss coefficient is shown with five additional resistances in series with the honeycomb as a function of the characteristic flow parameter, Ry, as defined in equation (2.1.3).

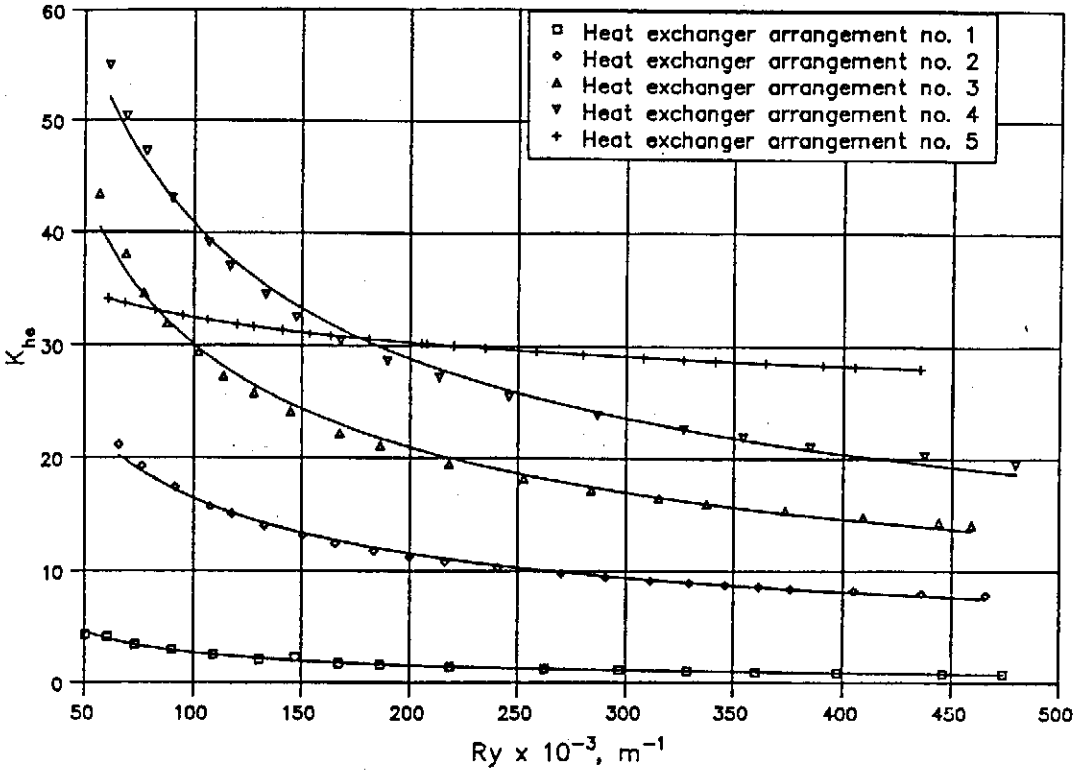

Figure A.1.5: Heat exchanger loss coefficients.

Geldenhuys and Kröger [86GE1] and Du Preez and Kröger [88DU1] performed isothermal model tests to determine the cooling tower loss coefficient as a function of the heat exchanger pressure loss coefficient. The cooling tower loss coefficient was expressed in terms of the total pressure above the horizontal heat exchangers.

$$K_{ct}=\frac{p_\infty-\left(p_s+\alpha 0.5\rho v_{he}^2\right)}{0.5\rho v^2}-K_{he}\left(\frac{v_{he}}{v}\right)^2 \qquad (A.1.2)$$

where p_s is the static pressure after the horizontal heat exchanger and v_{he} is the air velocity based on the frontal area of the heat exchangers. If the heat exchangers are arranged in the form of A-frames or V-bundles, v_{he} is based on their projected frontal area. In an empty cooling tower or a tower with a low K_{he} value, the axial velocity distribution in the inlet cross-section is non-uniform and therefore a kinetic energy coefficient is defined as

$$\alpha = \int_A v_l^3 \, dA / (A \, v^3) \qquad (A.1.3)$$

where v_l is the local air velocity. For practical dry-cooling towers with a horizontal heat exchanger arrangement, the air velocity distribution after the heat exchangers tends to be more uniform and α is correspondingly less. Data presented by Geldenhuys and Kröger suggests that for $K_{he} = 11$, $\alpha = 1.044$ and for $K_{he} = 30$ $\alpha = 1.020$ for a d_i/H_i ratio of 7.5. The loss due to flow distortions therefore becomes very small and α can be taken equal to unity. In the present model the heat exchangers fill the entire inlet cross-section of the tower, therefore equation (A.1.2) can be simplified

$$K_{ct} = \frac{p_\infty - p_s}{0.5\rho v^2} - 1 - K_{he} \qquad (A.1.4)$$

In figure A.1.6 the inlet loss coefficient is shown as a function of the Reynolds number for different d_i/H_i values. Similar results published by Du Preez and Kröger [88DU1] for much higher Reynolds numbers are also shown.

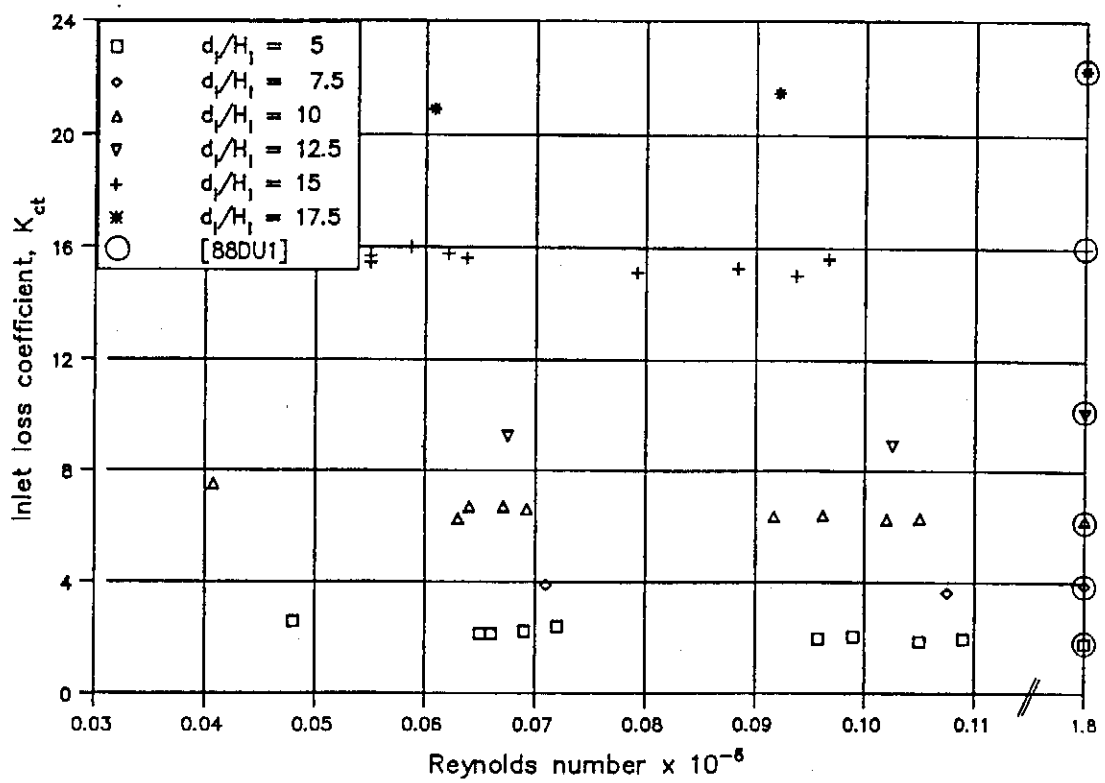

Figure A.1.6: Inlet loss coefficient for a cooling tower with a horizontal heat exchanger arrangement.

When the tower model is positioned in a cross-flow, the flow pattern in the inlet of the tower will be disturbed with corresponding changes in the value of the inlet loss coefficient. Model tests were performed to investigate the influence of a cross-flow on the dynamic inlet losses of a natural draft cooling tower. For a uniform cross-flow the total pressure far away from the tower model is constant and is given by:

$$p_\infty + 0.5\rho v_w^2 \tag{A.1.5}$$

where v_w is the air velocity of the cross-flow. In the atmosphere it is found that the wind velocity is a function of the height above ground level, and for engineering purposes the velocity profile is commonly described by a power law as defined in equation (1.1.1). Because both the barometric pressure and the wind velocity vary for different elevations, the total pressure will also not be constant. To obtain kinematic similarity a similar wind velocity profile has to be used with the model tests. The velocity profile given by equation (1.1.1) can be modelled by arranging dowels upstream of the tower as described in chapter 2 with the model height being used as the reference height. In terms of the difference in total pressure, the inlet loss coefficient in the presence of a cross-wind for the current heat exchanger arrangement is defined as:

$$K_{ctw} = \frac{\left(p_\infty + 0.5\rho v_{wref}^2\right) - \left(p_s + \alpha 0.5\rho v^2\right)}{0.5\rho v^2} - K_{he} \tag{A.1.6}$$

$$= \frac{(p_\infty - p_s)_w}{0.5\rho v^2} + \left[\frac{v_{wref}}{v}\right]^2 - (K_{he} + \alpha) \tag{A.1.7}$$

where v_{wref} is the wind velocity at any reference height. As shown in Appendix B, the reference height can be chosen at any convenient elevation, provided that the draft equation of the cooling tower is defined accordingly. For consistency however, the reference height is chosen at 10 m above ground level as suggested by VDI 2049 [78VD1].

In chapter 2 it was shown that one of the effects of a cross-wind in a natural draft cooling tower is a distorted velocity profile through the heat exchangers. Depending on the value of the relative wind velocity and cooling tower characteristics, the value of α can be as high as 2.7,

see figure 2.3.2, and can therefore not be neglected. By substituting equation (A.1.4) and (A.1.7) into equation (2.1.1), K_{ctw} can be expressed in terms of the inlet pressure coefficient i.e.

$$K_{ctw}=\left(-C_{piref}+1\right)\left[\frac{v_{wref}}{v}\right]^2 + K_{ct} + (1-\alpha) \qquad (A.1.8)$$

where K_{ct} is the tower inlet loss coefficient for the same tower in windless conditions as defined by equation (A.1.4) and C_{piref} is the inlet pressure coefficient based on the wind velocity on the reference elevation.

A.2 Outlet pressure coefficient.

The wind effect on the outlet of a cooling tower can also be defined as an outlet loss coefficient, similar to the coefficient defined at the inlet. The loss coefficient at the outlet is expressed in terms of the difference in total pressure just after the heat exchangers and the total pressure external to the tower at the tower outlet height.

$$K_{ctow} = \frac{(p_s+\alpha 0.5\rho v^2)-(p_\infty+0.5\rho v_{wo}^2)}{0.5\rho v_o^2} \qquad (A.2.1)$$

The variables in the first term are the same as those used in equation (A.1.6) while v_o is the mean air velocity at the outlet of the tower while v_{wo} is the wind velocity at the tower outlet height. If it is assumed that the air flow through the tower is isentropic in windless conditions, equation (2.1.1) can be rewritten as follows:

$$C_{po} = \frac{(p_s-p_\infty)_w-(0.5\rho v_o^2-0.5\rho v^2)}{0.5\rho v_{wo}^2} \qquad (A.2.2)$$

By substituting equation (A.2.2) in (A.2.1), K_{ctow} is expressed in terms of the outlet pressure coefficient

$$K_{ctow} = (C_{po}-1)\left[\frac{v_{wo}}{v_o}\right]^2+(\alpha-1)\left[\frac{v}{v_o}\right]^2+1 \qquad (A.2.3)$$

APPENDIX B

B.1 Draft equation for a dry-cooling tower in a cross-wind.

Consider the hyperbolic cooling tower shown in figure B.1.1. The heat exchanger bundles are arranged uniformly and horizontally (not A-frames) over the entire inlet cross section of the tower. The density of the heated air inside the tower is less than that of the cold atmosphere outside the tower, with the result that the pressure inside the tower is less than the external pressure at the same elevation. This pressure difference causes the air to flow through the tower at a rate which is dependent on the various flow resistances, the cooling tower dimensions and the heat exchanger characteristics.

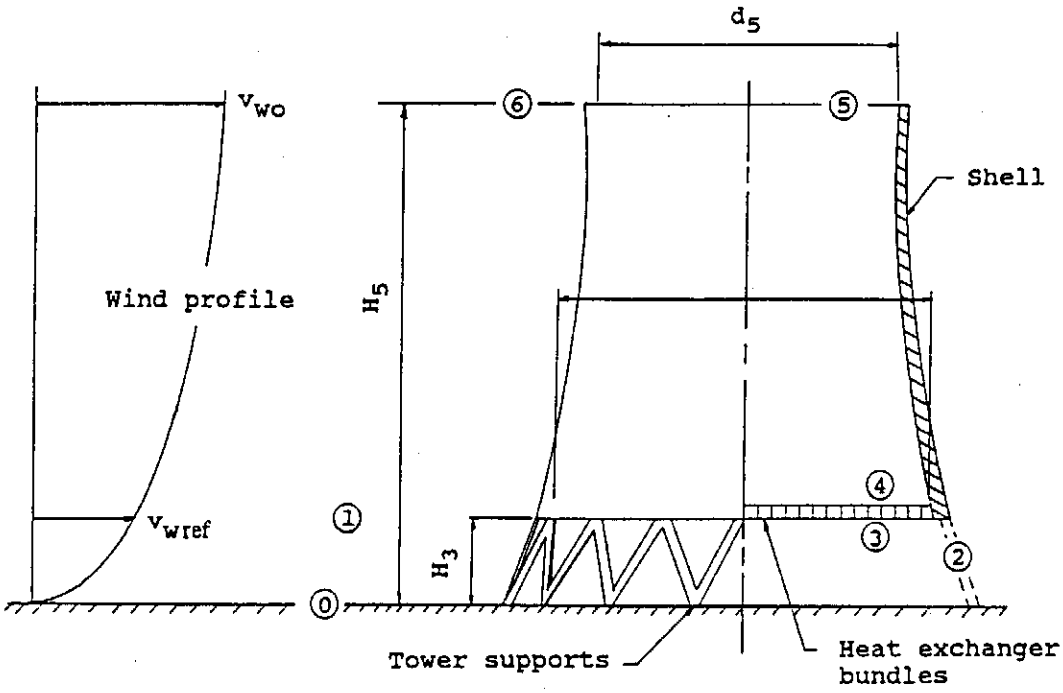

Figure B.1.1: Natural draft dry-cooling tower.

In this analysis it is assumed that the variation of the dry-bulb air temperature in the surface boundary layer is given by the dry adiabatic lapse rate (DALR). The ambient air temperature at any elevation outside the tower will then be given by

$$T_a = T_{ao} - 0.00975\ z \qquad (B.1.1)$$

where T_{ao} is the air temperature at the ground level. In the atmosphere external to the tower, the variation in pressure with elevation in a gravity field is given by

$$dp_a = - \rho_a \, g \, dz \tag{B.1.2}$$

For dry air the air density, ρ_a, is calculated with the perfect gas law, i.e.

$$\rho_a = p_a / R \, T_a \tag{B.1.3}$$

Substitute equations (B.1.1) and (B.1.3) in (B.1.2) and integrate between 0 and 6.

$$p_{a0} - p_{a6} = p_{a0} \left[1 - (1\text{-}0.00975 \, H_5/T_{a0})^{102.564g/R}\right] \tag{B.1.4}$$

where $H_5 = H_6$ is the tower height, $g = 9.8$ m/s^2 and $R = 287.08$ J/kgK. Similarly is it found that

$$p_{a0} - p_{a4} \approx p_{a0} \left[1 - (1\text{-}0.00975 \, (H_3 + H_4)/2T_{a0})^{102.564g/R}\right] \tag{B.1.5}$$

Choose point 1 at any convenient reference position upstream of the tower, say 10 m above ground level with the wind velocity and air density at that position given by v_{wref} and ρ_{wref} respectively. The air at reference point 1 flows through the supports at 2 before flowing through the heat exchanger bundles from 3 to 4. A total pressure balance between 1 and 4 yields

$$(p_{a1} + 0.5\rho_{wref} v_{wref}^2) - \left[p_{a4} + \frac{\alpha}{2\rho_{a4}} \left(\frac{m_a}{A_4}\right)^2\right]$$

$$= (K_{ts} + K_{ctw} + K_{he})_{he} \left[\frac{1}{2\rho_{a34}}\right] \left[\frac{m_a}{A_{fr}}\right]^2 + (p_{a1} - p_{a4}) \tag{B.1.6a}$$

where m_a is the air mass flow rate through the tower. All loss coefficients are based on the frontal area of the heat exchangers, i.e. the inlet cross-section of the cooling tower for the heat exchanger arrangement under consideration, and the mean density through it. If the static pressure p_{a1} on the left and right hand sides in equation (B.1.6a) is replaced by p_{a0} and equation (B.1.5) is substituted into equation (B.1.6a), the following is found

$$(p_{a0}+0.5\rho_{wref}v_{wref}^2)-\left[p_{a4}+\frac{\alpha}{2\rho_{a4}}\left(\frac{m_a}{A_4}\right)^2\right] = (K_{ts}+K_{ctw}+K_{he})_{he}\left(\frac{1}{2\rho_{a34}}\right)\left(\frac{m_a}{A_{fr}}\right)^2$$

$$+ p_{a0}\left[1 - (1-0.00975\ (H_3+H_4)/2T_{a0})^{102.564g/R}\right] \qquad \text{(B.1.6b)}$$

The air temperature at position 4 will not be uniform due to the non-uniform velocity distribution through the heat exchangers. Because the draft of a natural draft tower is primarily a function of the temperature difference between the in and outside of the tower, a distortion of the temperature profile inside the tower will also affect the available tower draft. In a full scale cooling tower warm air inside the tower is mixed due to large scale vortices. The effectiveness of the mixing process, however is not known and therefore an assumption has to be made. One extreme would be to assume that the air is perfectly mixed directly above the heat exchangers and the draft equation will be based on the mass mean air temperature, T_{a4}, given by

$$T_{a4} = \frac{Q}{m_a\ c_{pa34}} + T_{a3} \qquad \text{(B.1.7)}$$

This will result in a somewhat optimistic solution.

The other extreme would be to assume that there is absolutely no mixing in the air stream above the heat exchangers. In this case, as shown in appendix F, the warmer air is accelerated while the less buoyant cold air is decelerated. The static pressure gradient above the heat exchangers was also found to be almost the same as the hydrostatic pressure gradient of the coldest air leaving the heat exchangers. Therefore the air temperature of the coldest air has to be used to calculate the tower draft and a pessimistic result will be obtained. Because the coldest air outlet temperature is usually associated with the highest air velocity through the heat exchangers, equation (2.3.4) can be employed to calculate the maximum air velocity for a known air mass flow rate through the tower. In Appendix G the above-mentioned proposals to calculate the air temperature above the heat exchangers is illustrated by means of a numerical example.

The correct solution of the problem is expected to be found somewhere between the two extremes mentioned above, depending on the effectiveness of the mixing process. By using one

of the two options given above, a value of the mean air temperature after the heat exchangers, T_{a4}, is found and is used to calculate the tower draft.

A total pressure balance between 4 and 6 in figure B.1.1 yields

$$\left[p_{a4}+\frac{\alpha}{2\rho_{a4}}\left(\frac{m_a}{A_4}\right)^2\right]-(p_{a6}+0.5\rho_{wo}v_{wo}^2)$$

$$= K_{ctow}\left(\frac{1}{2\rho_{a5}}\right)\left(\frac{m_a}{A_5}\right)^2$$

$$+ p_{a4}\left[1-\{1-0.00975(H_5-H_3/2-H_4/2)/T_{a4}\}^{102.564g/R}\right] \qquad (B.1.8)$$

The change in total pressure through the cooling tower is obtained by adding equations (B.1.6b) and (B.1.8)

$$(p_{a0}+0.5\rho_{wref}v_{wref}^2)-(p_{a6}+0.5\rho_{wo}v_{wo}^2)$$

$$= (K_{ts}+K_{ctw}+K_{he})_{he}\left(\frac{1}{2\rho_{a34}}\right)\left(\frac{m_a}{A_{fr}}\right)^2 + K_{ctow}\left(\frac{1}{2\rho_{a5}}\right)\left(\frac{m_a}{A_5}\right)^2$$

$$+ p_{a4}\left[1-\{1-0.00975(H_5-H_3/2-H_4/2)/T_{a4}\}^{102.564g/R}\right]$$

$$+ p_{a0}\left[1-\{1-0.00975(H_3+H_4)/2T_{a0}\}^{102.564g/R}\right] \qquad (B.1.9)$$

By substituting equations (A.1.8) and (A.2.3) into equation (B.1.9), the static pressure difference through the tower is given in terms of the inlet- and outlet pressure coefficients.

$$(p_{a0}-p_{a6}) = (K_{ts}+K_{ct}+K_{he})_{he}\left(\frac{1}{2\rho_{a34}}\right)\left(\frac{m_a}{A_{fr}}\right)^2$$

$$- C_{piref}0.5\rho_{wref}v_{wref}^2 + C_{po}0.5\rho_{wo}v_{wo}^2 + \frac{1}{2\rho_{a5}}\left(\frac{m_a}{A_5}\right)^2$$

$$+ p_{a4}\left[1-\{1-0.00975(H_5-H_3/2-H_4/2)T_{a4}\}^{102.564g/R}\right]$$

$$+ p_{a0}\left[1-\{1-0.00975(H_3+H_4)/2T_{a0}\}^{102.564g/R}\right] \qquad \text{(B.1.10)}$$

where C_{piref} is the inlet pressure coefficient based on the wind velocity at the reference height.

If dynamic effects are neglected, an approximate expression for p_{a4} may be obtained.

$$p_{a4} = p_{a0}\{1-0.00975(H_3+H_4)/2T_{a0}\}^{102.564g/R}$$

$$- (K_{ts}+K_{ct}+K_{he})_{he}\left[\frac{1}{2\rho_{a34}}\right]\left[\frac{m_a}{A_{fr}}\right]^2 + C_{piref}0.5\rho_{wref}v_{wref}^2 \qquad \text{(B.1.11)}$$

By substituting equations (B.1.4) and (B.1.11) into equation (B.1.10), the draft equation of a cooling tower with a horizontal heat exchanger arrangement in a cross-wind is found

$$p_{a0}\left[\{1-0.00975(H_3+H_4)/2T_{a0}\}^{102.564g/R}\right.$$

$$x\ \{1-0.00975(H_5-H_3/2-H_4/2)/T_{a4}\}^{102.564g/R}$$

$$\left.-\left(1-0.00975H_5/T_{a0}\right)^{102.564g/R}\right]-C_{po}0.5\rho_{wo}v_{wo}^2$$

$$+ C_{piref}0.5\rho_{wref}v_{wref}^2 x\{1-0.00975(H_5-H_3/2-H_4/2)/T_{a4}\}^{102.564g/R}$$

$$= (K_{ts}+K_{ct}+K_{he})_{he}\left[\frac{1}{2\rho_{a34}}\right]\left[\frac{m_a}{A_{fr}}\right]^2$$

$$x\ \{1-0.00975(H_5-H_3/2-H_4/2)/T_{a4}\}^{102.564g/R} + \frac{1}{2\rho_{a5}}\left[\frac{m_a}{A_5}\right]^2 \qquad \text{(B.1.12)}$$

The pressure loss coefficients used in equation (B.1.12) are all determined in windless conditions. Any changes in the value of the latter because of the wind is included in the value of C_{piref}. It is also clear that the draft equation is independent of the reference position 1. For the sake of simplicity, however, the velocity v_{wref} is defined as the wind velocity 10 m above ground level and therefore C_{piref} has to be based on the same velocity. Since (C_{piref} 0.5

$\rho_{wref}\, v_{wref}) = (C_{pi}\, 0.5\, \rho_{wo}\, v_{wo})$, the latter can also be substituted into equation (B.1.12)

Equation (B.1.3) is used to determine the various air densities at different positions of the tower. At position 3 under the heat exchangers, the air density is approximately given by

$$\rho_{a3} \approx p_{a0}/R\, T_{a3} \tag{B.1.13}$$

Similarly ρ_{a4} is for all practical purposes

$$\rho_{a4} \approx p_{a0}/R\, T_{a4} \tag{B.1.14}$$

The harmonic mean density of the air through the heat exchanger is:

$$1/\rho_{a34} = 0.5(1/\rho_{a3} + 1/\rho_{a4}) \tag{B.1.15}$$

If all the dynamic effects are neglected, equation (B.1.1) can be used to calculate T_{a5} if T_{a4} is known.

$$T_{a5} \approx T_{a4} - 0.00975\, (H_5 - H_4) \tag{B.1.16}$$

If it is assumed that $p_{a5} = p_{a6}$ at the outlet of the tower, the outlet air density is calculated with

$$\rho_{a5} \approx p_{a6}/R\, T_{a5} = p_{a6}/R\, (T_{a4} - 0.00975\, (H_5 - H_4)) \tag{B.1.17}$$

where p_{a6} is given by equation (B.1.4). Similarly

$$\rho_{a6} \approx p_{a6}/R\, T_{a6} = p_{a6}/R\, (T_{a0} - 0.00975\, H_5) \tag{B.1.18}$$

If the loss coefficient of the tower supports, given by equation (D.2), is based on the conditions at the heat exchanger, the following is found:

$$K_{ts} = 2\Delta p_{ats}\rho_{a34}\left[\frac{A_{fr}}{m_a}\right]^2 = \frac{C_{Dts}\, L_{ts}\, d_{ts}\, n_{ts}\, A_{fr}^2}{(\pi d_3 H_3)^3}\left[\frac{\rho_{a34}}{\rho_{a0}}\right] \tag{B.1.19}$$

The inlet coefficient for a cooling tower without wind was determined by Geldenhuys and

Kröger [86GE1] and Du Preez and Kröger [88DU1]. The inlet loss coefficient was found to be a function of the d_i/H_i ratio of the tower and in the case of large d_i/H_i values a gradual reduction in the inlet pressure coefficient was observed for an increase in the exchanger resistance. Du Preez and Kröger [88DU1] correlated their results with the following equation:

$$K_{ct} = \left[- 18.7 + 8.095 \left(\frac{d_i}{H_i}\right) - 1.084 \left(\frac{d_i}{H_i}\right)^2 + 0.0575 \left(\frac{d_i}{H_i}\right)^3 \right] \times K_{he}^{(0.165 - 0.035(d_i/H_i))} \qquad \text{(B.1.20)}$$

for $19 < K_{he} < 50$ and $5 < d_i/H_i < 15$

For dry-cooling towers where $K_{he} \geq 30$ and $5 \leq d_i/H_i \leq 10$ the following simplified expression is recommended [86GE1]

$$K_{ct} = 0.072 \left(\frac{d_i}{H_i}\right)^2 - 0.34 \left(\frac{d_i}{H_i}\right) + 1.7 \qquad \text{(B.1.21)}$$

Based on the conditions at the heat exchanger, the inlet loss coefficient is :

$$\left(K_{ct}\right)_{he} = K_{ct} \frac{\rho_{a34}}{\rho_{a3}} \left(\frac{A_{fr}}{A_3}\right)^2 \qquad \text{(B.1.22)}$$

APPENDIX C

Apparatus

C.1 Model of the dry-cooling tower.

In the present investigation, the effect of winds on the performance of dry-cooling towers is studied by using isothermal models, similar to those used by Völler [85VO1]. Two different models were used to simulate the shell of a dry-cooling tower. Each of these models had a sharp edged inlet of 200 mm. For the first model, a cylindrical cooling tower was simulated by using a PVC pipe with an outside diameter of 200 mm and a wall thickness of 4 mm. For the second model, a 160 mm diameter pipe was used with the inlet shape of the tower simulated by a conical section attached to the one end of the pipe. The latter had a cone apex angle, $2\theta_c$, of 24° as shown in figure 2.2.13(a). All tests were done with the axis of the cylindrical model in a horizontal position, and therefore the ground level was simulated by a vertical surface. By adjusting the distance between the ground level and the inlet edge of the model, the inlet pressure coefficient can be determined for different values of the diameter to inlet height ratio, d_i/H_i, of the tower. The experimental layout is shown in figure C.1.1.

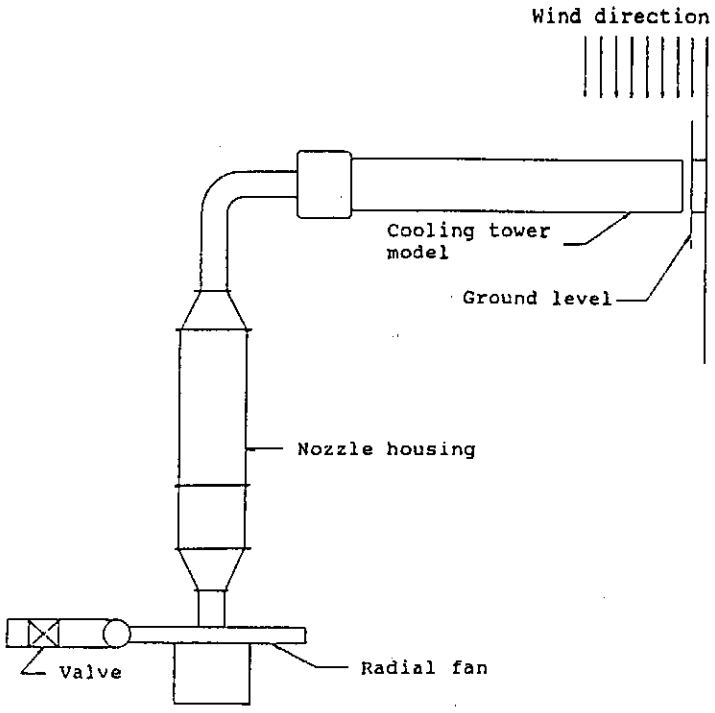

Figure C.1.1: Experimental layout.

An elliptic nozzle, placed in a wooden housing, shown in figure C.1.2, was connected to the other end of the model. Air enters the housing at 1 and moves through two air mixers at 2. By measuring the static pressure drop across the nozzle, located between perforated plates 3, the air flow is determined. The nozzle with the housing was calibrated as a unit by coupling it to a test wind tunnel. This was done by measuring the static pressure difference across the nozzle with a for air flow rate through it, with the results of the calibration shown in figure C.1.3. The data is correlated by the following equation, also shown in the figure in its range of applicability.

$$m_a = - 0.0033503 + 0.0061966 \left(\Delta p_n \rho_u\right)^{0.5} \qquad (C.1.1)$$

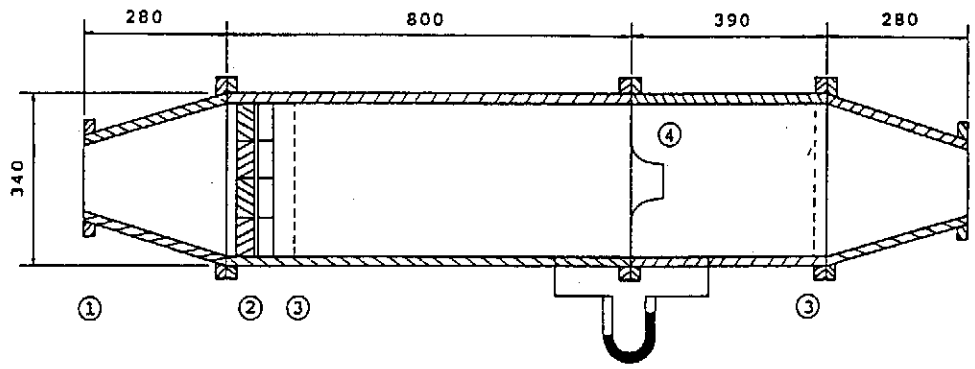

Figure C.1.2: Layout of nozzle housing.

where ρ_u is the air density upstream of the nozzle and Δp_n is the pressure drop across it. To confirm the above mentioned procedure, the mass flow rate through the nozzle was also determined theoretically by using the following equation

$$m_a = C_n \phi_g Y \alpha A_n \left(2 \rho_n \Delta p_n\right)^{0.5} \qquad (C.1.2)$$

where A_n is the throat area of the nozzle with a diameter of 75 mm. The results obtained with equation (C.1.2) are compared to the experimental results in figure C.1.3. According to Van Rooyen [77VA1] the nozzle coefficient of discharge C_n, is a function of the nozzle Reynolds number.

For $30000 < Re_n < 100\,000$,

$$C_n = 0.954803 + 6.37817\text{x}10^{-7}\ Re_n - 4.65394\text{x}10^{-12}\ Re_n^2 + 1.33514\text{x}10^{-17}\ Re_n^3 \quad \text{(C.1.3)}$$

For $100\,000 < Re_n < 350\,000$

$$C_n = 0.9758 + 1.08\text{x}10^{-7}\ Re_n - 1.6\text{x}10^{-13}\ Re_n^2 \quad \text{(C.1.4)}$$

and for $Re_n > 350\,000$, $C_n = 0.994$ (C.1.5)

The gas expansion factor ϕ_g may be approximated by the following relation.

$$\phi_g = 1 - \frac{3\ \Delta p_n}{4\ p_u\ c_p/c_v} \quad \text{(C.1.6)}$$

where $c_p/c_v = 1.4$ for air and p_u is the static pressure upstream of the nozzle. For compressible fluid, it can be shown that the approach velocity factor is approximately

$$Y = 1 + 0.5\left[\frac{A_n}{A_{ts}}\right]^2 + 2\left[\frac{A_n}{A_{ts}}\right]^2 \frac{\Delta p_n}{p_n\ c_p/c_v} \quad \text{(C.1.7)}$$

where A_{ts} is the housing cross-section. The thermal expansion coefficient α, was neglected because all the tests were performed at room temperature.

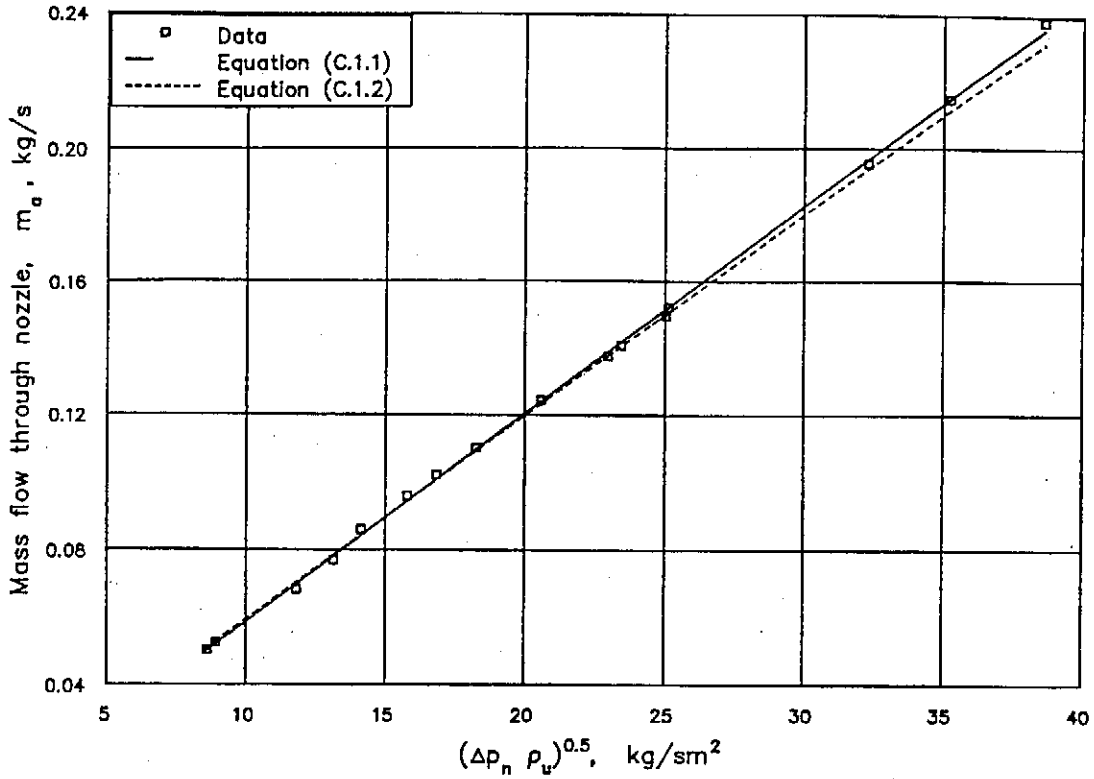

Figure C.1.3: Air mass flow rate through nozzle.

C.2 Wind tunnels used to simulate cross-wind.

Two different wind tunnels were used to simulate the cross-winds. The one tunnel which was used has a much smaller outlet section than the other one, but because of the availability of this tunnel, shown in figure C.2.1, it was used for most of the tests.

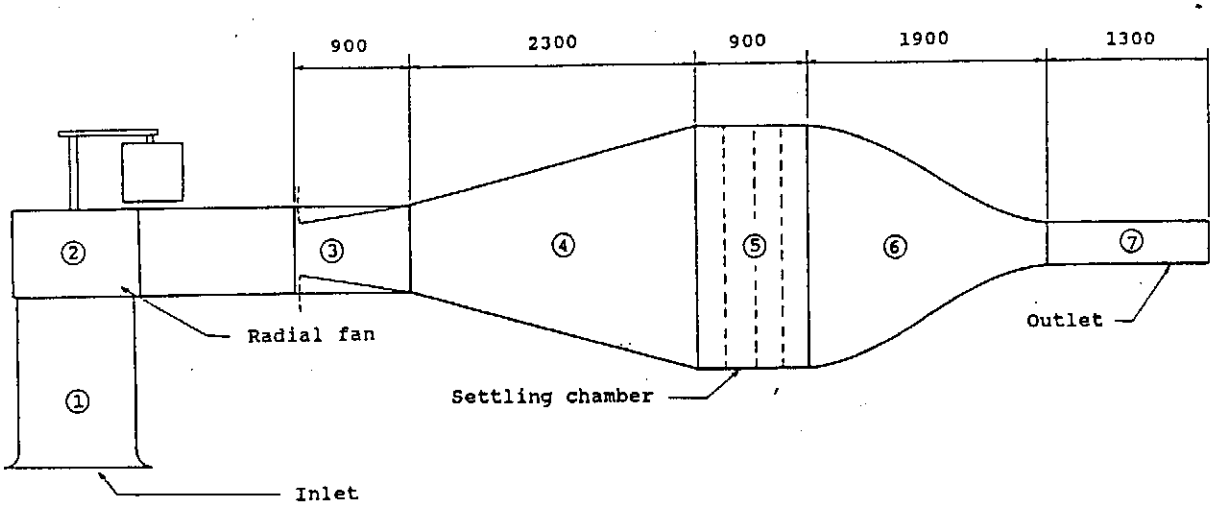

Figure C.2.1: Layout of the smaller wind tunnel.

A constant velocity radial fan 2 draws air from the surroundings and blows it through the divergent section 4 to a settling chamber which contains a number of screens 5. From there the flow is accelerated by the contraction 6 and leaves the tunnel through the test section 7. By adjusting the flaps at 3, the air velocity in the test section can be varied continuously from zero to a maximum of 38 m/s. The dimensions of the rectangular outlet section of the tunnel are 660 x 330 mm.

The velocity profile at the outlet of the wind tunnel was determined, by measuring the dynamic pressure at various positions in the jet. For the maximum wind speed the variation in velocity was less than 0.1% of the mean air speed. According to Pope [66PO1] this variation should be less than 0.25%. It was also found that the outlet velocity tends to vary slightly with time. The difference between the maximum and minimum value was found to be less than 0.35% of the mean velocity for the duration of the test. During the tests, the wind velocity was measured continuously, therefore this variation should not cause any serious inaccuracies. The outlet velocity was determined by measuring the static pressure drop across the contraction. A pitot-static tube was used to calibrate the contraction, and the following relation is found.

$$0.5\rho v_o^2 = 1.006844\ \Delta p_{con} + 0.00008\ \Delta p_{con}^2 \qquad \text{(C.2.1)}$$

where v_o is the mean outlet velocity and Δp_{con} is the static pressure drop across the contraction.

The cooling tower model was placed 450 mm from the outlet edge of the tunnel. The one side of the outlet section, that simulates the ground level, was extended with a wooden board. To cut the boundary layer on the ground surface, a disc was fastened to the board with a false cylinder placed between the disc and the board to prevent any distortion in the velocity profile.

With the model in position the velocity profile at the outlet becomes non-uniform. With a pitot-static traverse the velocity profile was measured and by integrating the profile, the mean velocity was calculated. The pressure drop across the contraction was measured simultaneously and the mean dynamic head was calculated by applying equation (C.2.1). The mean velocities obtained with the two methods differ with less than 0.1%, suggesting that velocity profile at the outlet of the test section has no influence on the pressure drop across the contraction and equation (C.2.1) is still applicable.

According to Pankhurst [52PA1] the blockage effect in an open jet will cause the effective velocity across the model to be less than that of the free stream velocity. Lock [29LO1] determined a solid-blockage factor that can be expressed in the form:

$$\frac{v_e}{v_\infty} = 1 + \tau \lambda \left[\frac{A_{model}}{A_{jet}} \right]^{1.5} \qquad \text{(C.2.2)}$$

where λ is a factor depending on the shape of the model and τ depends on the shape of the cross-section of the wind tunnel. For a cylinder $\lambda = 1$ and $\tau \approx -0.23$ for the present outlet section. The effective wind velocity across the tower model is therefore:

$$\frac{v_e}{v_\infty} = 1 - 0.23 \left[\frac{0.2 \times 0.33}{0.66 \times 0.33} \right]^{1.5} = 0.962 \qquad \text{(C.2.3)}$$

This correction is used with equation (C.2.1) to obtain the effective wind velocity across the model.

Due to uncertainties which were caused by the solid blockage effect, some of the tests were repeated in another wind tunnel with a round outlet cross-section with a diameter of 1.71 m. The layout of the wind tunnel is shown in figure C.2.2.

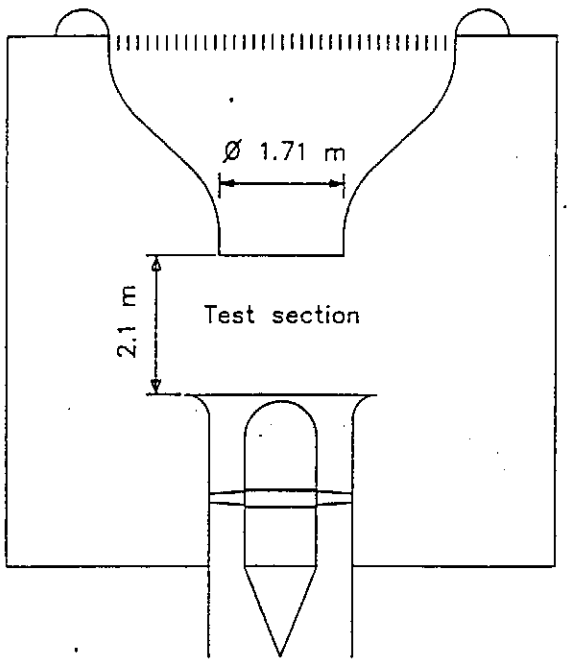

Figure C.2.2: layout of wind tunnel.

The air velocity in the test section can be varied from zero to approximately 29 m/s by adjusting the speed of the fan. A metal sheet, placed vertically in the centre of the test section, simulated the ground surface. The same cooling tower model described in the previous section was positioned on the one side of the sheet, 450 mm from the inlet of the test section. For symmetrical reasons a false cylinder was placed on the opposite side of the sheet.

With the model in position, the velocity profile at the inlet of the test section was distorted as shown in figure C.2.3. By integrating the profile, the mean velocity was calculated and the position on the curve which corresponds to the mean velocity was determined. By placing a pitot-static tube on this position, the mean velocity in the test section was measured directly.

By applying equation (C.2.2), the effective velocity across the model was calculated. For a round outlet section τ = -0.206

$$\frac{v_e}{v_\infty} = 1 - 0.206\left[\frac{0.2 \times 1.71 \times 4}{\pi \times 1.71^2}\right]^{1.5} \qquad (C.2.4)$$

$$= 0.988$$

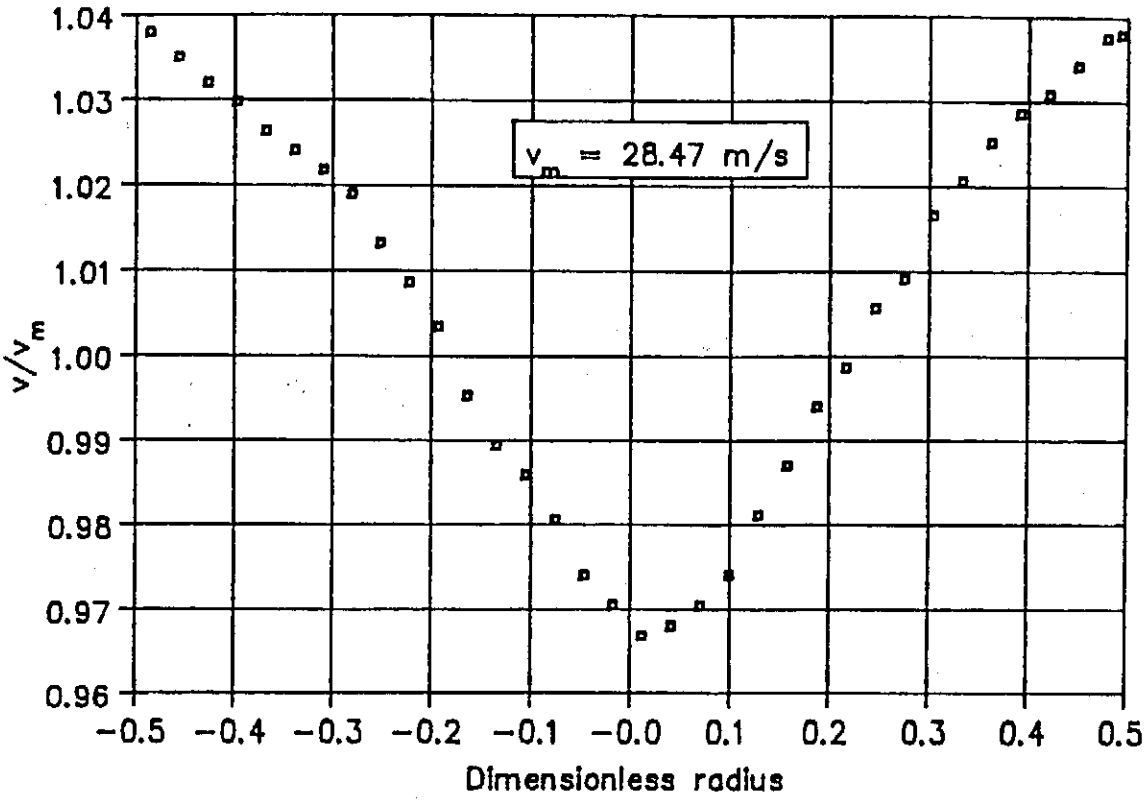

Figure C.2.3: Velocity profile 450 mm upstream of the model.

APPENDIX D

Modelling of the tower supports for a cooling tower with a horizontal heat exchanger arrangement.

Data presented by Vauzanges [86VA1] suggests that the tower supports have a noticeable effect on the inlet pressure coefficient of the tower in the presence of a cross-wind. For a vertical arrangement of the heat exchanger bundles, supports are needed only around the circumference of the tower on which the shell rests, while more supports are needed for a horizontal arrangement to support the bundles.

The tower supports should be modelled in such a way that the pressure loss coefficients of the latter is similar for the model and the full scale tower. A model of the tower support arrangement in the dry-cooling towers of the Kendal power station, presently under construction in South Africa, was used in the tests. In figure D.1 the arrangement of the supports of these towers are shown with further details given in table D.1.

Table D.1: Detail of tower supports.

Support no.	No. of supports	Cross-section area, m^2
a	112	0.75 x 1.4
b	29	0.7 x 0.7
c	29	0.7 x 0.7
d	16	0.75 x 0.75
e	19	0.7 x 0.7

The mean pressure loss coefficient of the supports can approximately be calculated by using their drag coefficient. Normally the drag coefficient of bodies in a free stream is a function of the Reynolds number across the body, but for objects with sharp corners, the drag coefficient is essentially independent of Reynolds number because separation points are fixed by the geometry of the object [73FO1]. Hoerner [65HO1] listed the drag coefficients of various two

dimensional bodies, and for a square the latter is given as 2.05 in the range $10^4 < Re < 10^6$. For the X-shaped tower supports with a rectangular cross-section, the drag coefficient is slightly less. The depth to width ratio of these supports is 1.87 and for the latter the drag coefficient is roughly 1.9 [65HO1].

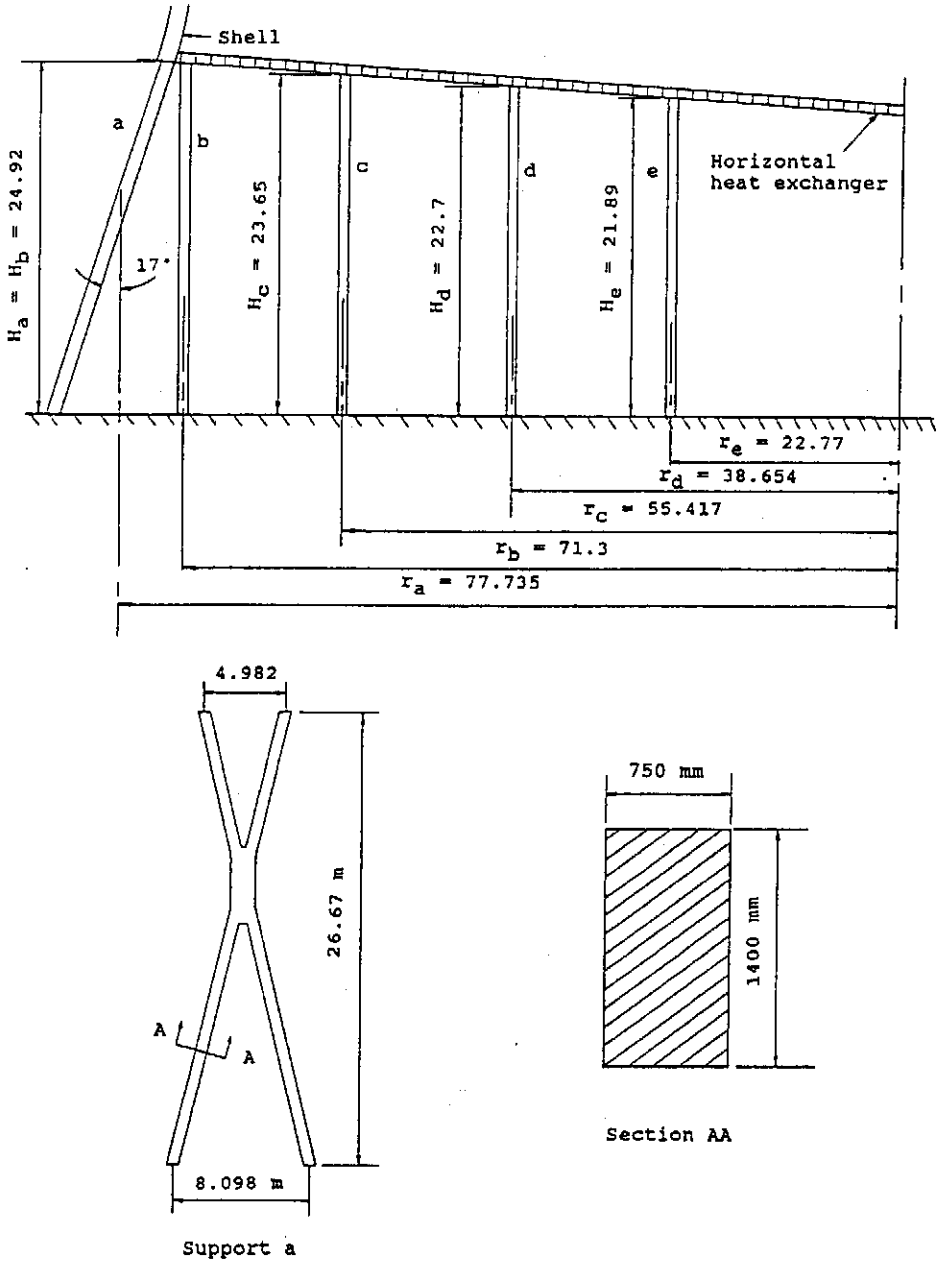

Figure D.1: Tower supports.

In the model the tower supports were simulated with round metal rods with diameters of 3 and 1.5 mm respectively. The drag coefficient for a cylinder is a function of the Reynolds number and therefore the approximate air velocity across the supports has to be known to obtain the

corresponding drag coefficient.

Approximate values for the minimum and maximum values of the local Reynolds numbers through the tower supports can be obtained by using results of measurements performed by Völler [85VO1]. He measured the velocity distribution through the tower supports for different values of the relative wind velocity, v_w/v_2, where v_2 is the mean air velocity at the tower supports as shown in figure B.1.1. The results of these tests are shown graphically with the velocity ratio $v_{2\theta}/v_2$ plotted as a function of the circumferential position, θ [85VO1]. $v_{2\theta}$ is the radial velocity component at the circumferential position θ in the vertical inlet cross-section.

Most of the tests in the present investigation were performed at the maximum wind velocity, namely 38 m/s, therefore this value was also used to calculate the number of tower supports needed in the model. The maximum air velocity through the tower supports is expected to be found for the largest values of the relative wind velocity. For the latter the mean air velocity inside the tower is small and therefore most of the air which flows through the supports at the upstream side of the tower, will flow out from underneath the tower through the supports at the lee side. If it is furthermore assumed that the velocity distribution through the supports is uniform, the maximum Reynolds number is

$$Re_{tsmax} = \rho\, v_{tsmax}\, d_{max} / \mu = 1.2 \times 38 \times 0.003 / 1.83 \times 10^{-5} = 7516$$

At this Reynolds number the drag coefficient for a cylinder is 1.05.

The minimum local support Reynolds number is found at the supports at the lee side of the tower for the smallest values of the relative wind velocity, v_w/v_2. In the present tests, the minimum v_w/v_2 value obtained for a wind velocity of 38 m/s and a d_i/H_i value of 5 equals 4.5. According to the results presented by Völler [85VO1], it is found that for a relative wind velocity of 4.5, the velocity ratio $v_{2\theta}/v_2$ at the lee side of the tower is -1.17. The negative sign indicates that the air at this position is flowing in the wind direction.

The mean air velocity in the vertical cross-section of the tower is

$$v_2 = v_w/(v_w/v_2) = 38 / 4.5 = 8.44$$

The local air velocity through the supports at the lee side of the tower is therefore

$v_{tsmin} = 1.17 \times 8.44 = 9.88$ m/s

and the corresponding minimum Reynolds number is:

$Re_{tsmin} = \rho\, v_{tsmin}\, d_{min} / \mu = 1.2 \times 9.88 \times 0.0015 / 1.82 \times 10^{-5} = 977$

At this Reynolds number the drag coefficient has a value of 1. In the range $977 < Re < 7516$, the average value of the drag coefficient, C_D, for a cylinder is therefore 0.975 which will be used to calculate the loss coefficient for the supports in the model.

If the air velocity through the tower supports , $v_{ats,}$ is assumed to be uniform, the pressure drop across the supports is given by

$$\Delta p_{ats} = \frac{0.5\, \rho\, v_{ats}^2\, C_{Dts}\, L_{ts}\, d_{ts}\, n_{ts}}{\pi\, d_i\, H_i} \qquad (D.1)$$

where L_{ts} is the support length, d_{ts} is the effective diameter and n_{ts} is the number of supports. The loss coefficient across the supports is therefore given by

$$K_{ts} = \frac{2\Delta p_{ats}}{\rho v_{ats}^2} = \frac{C_{Dts}\, L_{ts}\, d_{ts}\, n_{ts}}{\pi\, d_i\, H_i} \qquad (D.2)$$

The pressure loss coefficient for the X-shaped tower supports for the Kendal Power station is found from equation (D.2)

$K_{ts} = 1.9 \times 27.61 \times 0.75 \times 112 / (\pi\ 155.47 \times 24.92) = 0.362$

Experimental tests indicated that for a small lateral displacement between the tower supports, the actual value of K_{ts} tends to be larger due to the interaction between the supports. Although the value of 0.362 as calculated above may be to small, the same, but opposite, mistake will be made when the number of tower supports in the model is calculated in D.3. With a d_i/H_i ratio of 5 the inlet height of the model and therefore also the length of the supports is equal to 38.4 mm. The number of supports with a 3 mm diameter needed in the model to obtain the same loss coefficient, is found by rearranging equation (D.2).

$$n_{tsmodel} = K_{ts}\ \pi\ d_i\ H_i\ /\ C_{Dts}\ L_{ts}\ d_{ts}$$
$$= 0.362\ \pi\ 0.196\ x\ 0.0384\ /\ 0.975\ x\ 0.0384\ x\ 0.003 \qquad (D.3)$$
$$= 76$$

Equation (D.2) was obtained by assuming that the velocity distribution through the tower supports is uniform, which is not true with a cross-wind. If, however, the non-uniform velocity distribution through the supports and the model is the same, the error made in equation (D.2) is corrected in equation (D.3).

The rest of the supports in the model were simulated with rods with a diameter of 1.5 mm. The number of the rods needed to obtain the required loss coefficients for the different rings of tower supports, is also calculated as shown above, with the results shown in table D.2. The tower supports in the model were arranged uniformly in 5 concentric circles, similar to that in the full scale tower. The ratio of the diameter of the different rings of tower supports to the inlet diameter of the tower is given in the fifth column of the table.

Table D.2: Tower supports in model.

Support no.	d_{ts} [mm]	K_{ts} based on C_{Dts}	Number of supports	d/d_i
a	3	0.362	76	1.000
b	1.5	0.0929	36	0.918
c	1.5	0.1195	36	0.714
d	1.5	0.1029	22	0.497
e	1.5	0.1906	22	0.293

For substitution in equation (2.2.1), the effective pressure loss coefficient, K_{tse}, of the tower supports has to be calculated. The latter is defined as the sum of the loss coefficients of the different rings of tower supports based on the circumferential inlet area of the cooling tower. Based on experimental tests (see section 4.2), $K_{tse} = 1.02$ for the support arrangement under consideration.

APPENDIX E

Pressure distribution around the outside of a cylinder in a cross-flow.

One of the dimensionless quantities, listed in table 1.2.1, which should be kept constant for the model and full scale tower, is the wind Reynolds number based on the diameter of the tower. For a cooling tower with a diameter of 100 m and a uniform wind velocity of 10 m/s, the wind Reynolds number equals 6.7×10^7. If a model with a diameter of say 200 mm is employed, an air speed of 5000 m/s is needed to obtain the same Reynolds number.

It is well known that a sudden drop in the drag coefficient of a smooth cylinder occurs near Re $= 5 \times 10^5$. This phenomenon is related to changes in the flow in the boundary layer and in particular to the transition from laminar to turbulent flow. The transition causes the point of separation to move, from a point just upstream of the equator for laminar flow, over to a considerable distance in the downstream direction.

Fage [29FA1] performed experimental tests to determine the effect of free stream turbulence and surface roughness on the drag coefficient of a circular cylinder. By applying different grades of sandpaper to the surface of the cylinder, Fage found that the Reynolds number for which the drag coefficient shows a sudden drop, known as the critical Reynolds number, decreases with increasing relative roughness. The relative roughness, k/d, is defined as the ratio of the mean height of the roughness elements, k, to the diameter of the cylinder. The boundary layer appears to be disturbed by the roughness to such a degree that transition occurs at considerable lower Reynolds numbers than with smooth cylinders.

With the present model tests, the outer surface of the cooling tower model was roughened with sandpaper to increase the effective wind Reynolds number. The height of the roughness elements of the sandpaper were 0.35 mm which for a 200 mm diameter model, corresponds to a relative roughness of 0.00175. According to Fage [29FA1] the critical Reynolds number for a cylinder with a relative roughness of 0.00175 is 1.6×10^5.

In figure E.1 the pressure distribution round the roughened cooling tower model is shown for different Reynolds numbers. A static pressure coefficient is defined as:

$$C_p = \frac{p_\theta - p_\infty}{0.5\rho_\infty v_\infty^2} \qquad \text{(E.1)}$$

where p_θ is the local static pressure while the other variables refer to the free stream. The results can be compared to the distribution which Ruscheweyh [83RU1] measured around a full scale tower.

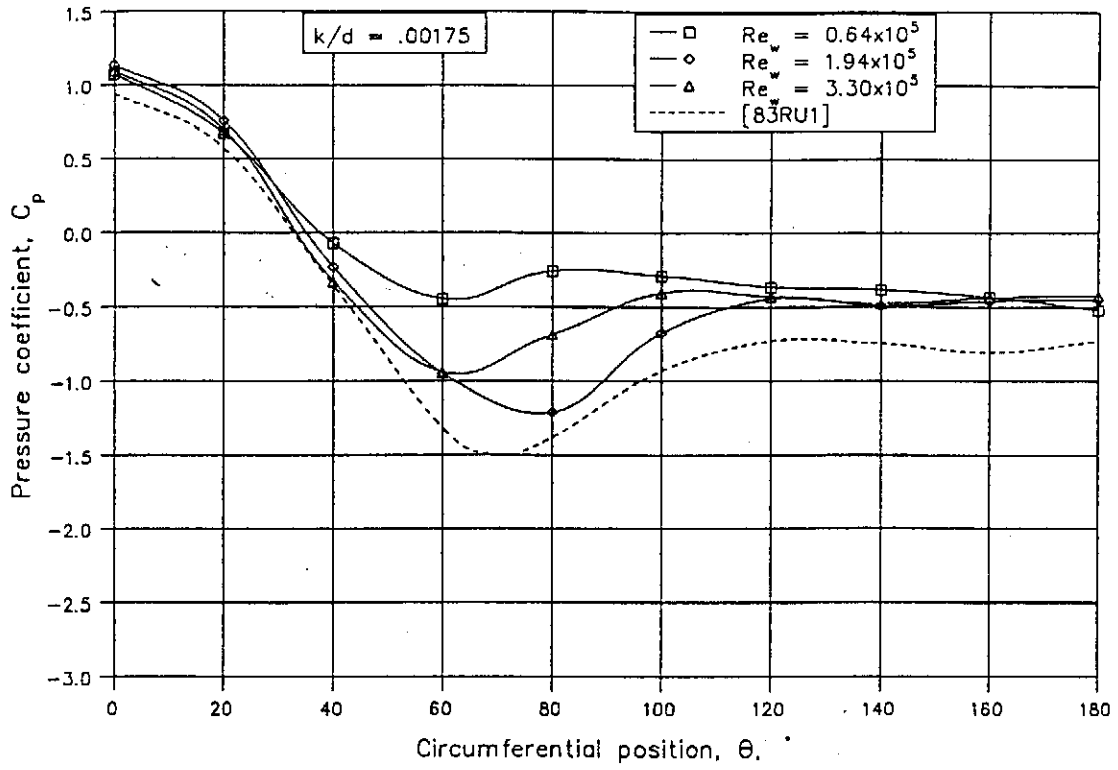

Figure E.1: Pressure distribution around a cylinder.

In figure E.2, the minimum pressure coefficient, C_{pmin}, is shown as a function of the Reynolds number for both the roughened and smooth cylinders. Good agreement in the trend of the data is found for both cylinders with similar data published by Fage [29FA1].

Tests were also performed to determine whether the inlet pressure coefficient of the tower in the presence of wind is affected by the pressure distribution on the outside of the shell. The static pressure after the heat exchangers was measured for different wind velocities with no flow in the model. The pressure difference between the surroundings and the inside of the model is therefore only caused by the cross-wind. The results of the tests are shown in figure E.3 as a function of the wind Reynolds number.

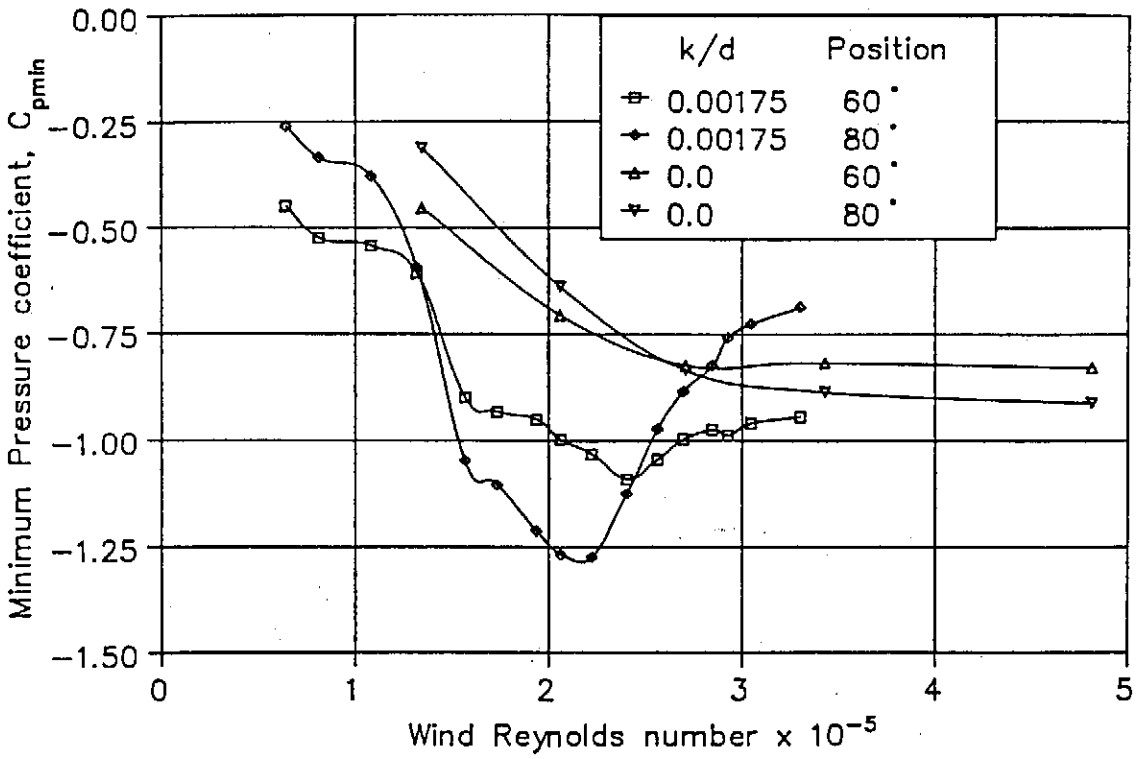

Figure E.2: C_{pmin} for flow across a cylinder.

The similarity in the trends of the curves shown in figure E.2 and E.3 suggest that the value of C_{pi} is affected by the pressure distribution around the outside of the tower. C_{pi} would therefore also be a function of the wind Reynolds number. To eliminate this, most of the tests in the present investigation were performed at the maximum Reynolds number of 4.8×10^5, except where stated differently. As mentioned before, the critical Reynolds number for the cooling tower model is 1.6×10^5, therefore the present tests were performed in the supercritical range of Reynolds numbers. This however is still at least two orders of magnitude less than the Reynolds numbers commonly found in full scale towers.

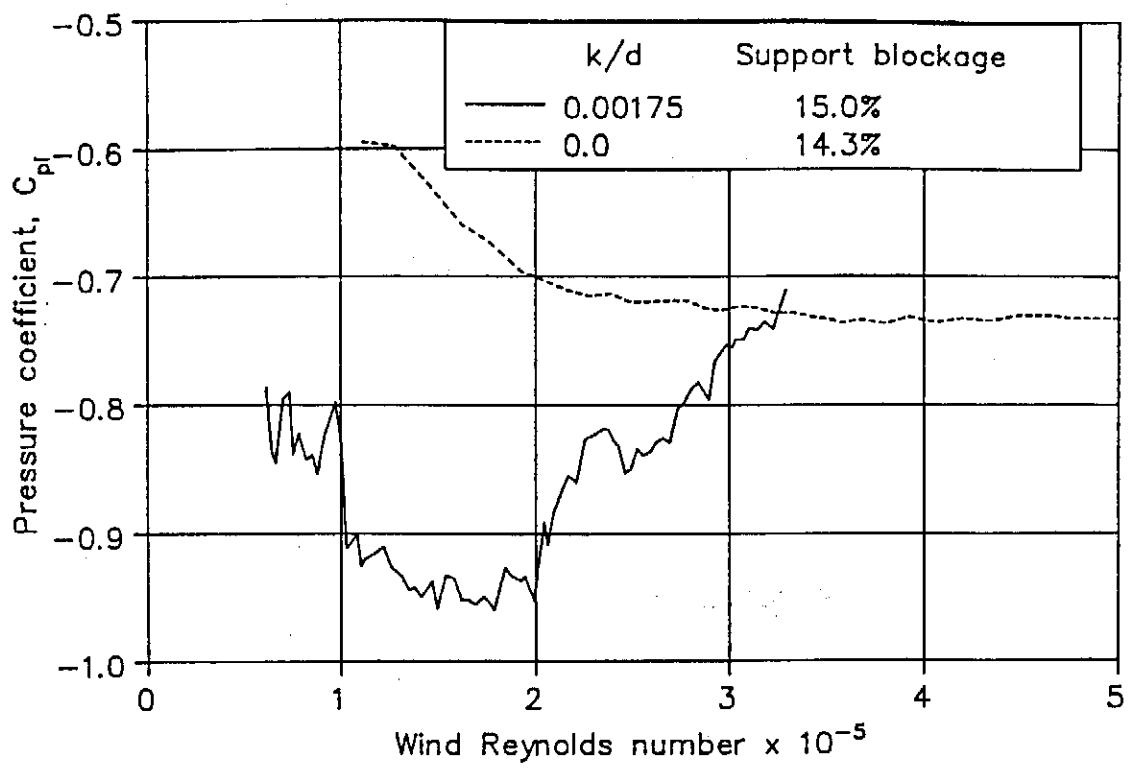

Figure E.3: C_{pi} with no flow in tower.

APPENDIX F

Potential flow analysis of the flow pattern in cooling tower.

Since the heat transfer phenomenon is not represented during isothermal tests, effects which exist in full scale towers like the buoyancy are not simulated. As shown in figure 2.3.1, the velocity distribution through the heat exchangers is distorted in the presence of a cross-wind, which on its turn will cause a non-uniform temperature distribution in the tower. Due to buoyancy effects, the warmer air in the tower will be accelerated, while the less buoyant colder air will be decelerated. By using potential flow theory, the influence of these dynamic effects on the tower draft is investigated.

Consider a round conical cooling tower with the horizontal heat exchanger at an elevation H_i above the ground level. Assume a two dimensional velocity distribution through the heat exchangers as shown in figure F.1 with the colder air stream entering the cooling tower in a vertical direction with a relative high velocity, v_{c0}, and the hot stream with a low velocity, v_{h0}. The discontinuity in the velocity profile is assumed to be in the centre of the tower inlet.

Further assumptions which are made is that there is no mixing between the two air streams and that the temperature and density for each stream is constant and uniform for all values of z. Viscous effects and heat transfer between the two streams are also neglected. The static pressure is also considered to be constant at any elevation over the entire cross-section of the tower.

By applying Bernoulli's equations for the cold stream between the inlet, $z = 0$, and any elevation z, the following is found:

$$p_0 + 0.5\ \rho_c\ v_{c0}^2 = p_z + g\ \rho_c\ z + 0.5\ \rho_c\ v_{cz}^2 \qquad \text{(F.1)}$$

and similar for the hot stream

$$p_0 + 0.5\ \rho_h\ v_{h0}^2 = p_z + g\ \rho_h\ z + 0.5\ \rho_h\ v_{hz}^2 \qquad \text{(F.2)}$$

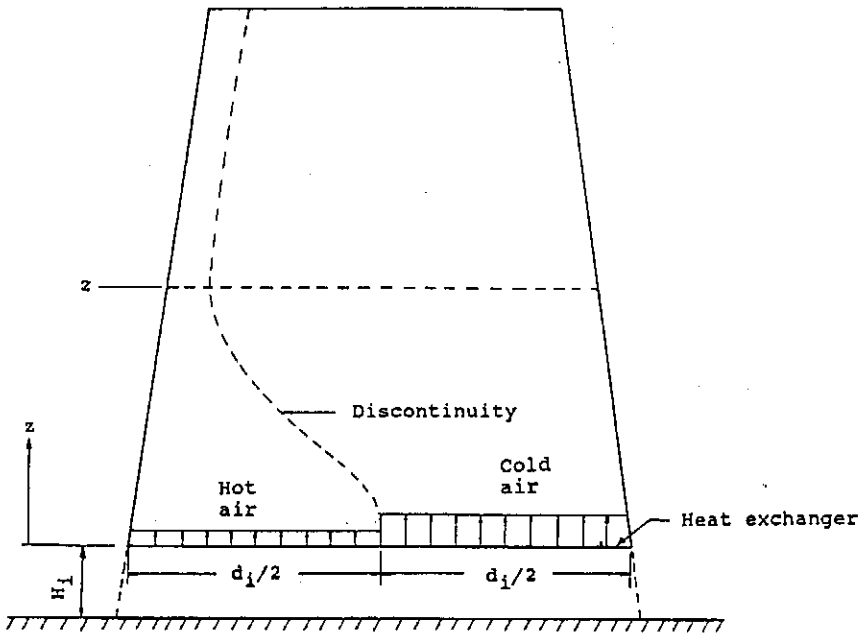

Figure F.1: Flow pattern in cooling tower.

Subtract equation (F.2) from (F.1) and find:

$$0.5\ (\rho_h\ v_{h0}^2 - \rho_c\ v_{c0}^2) = g\ z\ (\rho_h - \rho_c) + 0.5\ (\rho_h\ v_{hz}^2 - \rho_c\ v_{cz}^2) \qquad \text{(F.3)}$$

By rearranging the previous equation, it can be written in the following dimensionless form:

$$\frac{g\ z\ (\rho_h - \rho_c)}{\rho_h\ v_{h0}^2 - \rho_c\ v_{c0}^2} = 0.5\left[1 - \frac{(\rho_h\ v_{hz}^2 - \rho_c\ v_{cz}^2)}{(\rho_h\ v_{h0}^2 - \rho_c\ v_{c0}^2)}\right] \qquad \text{(F.4)}$$

The air velocity for each stream is given by

$$v_z = \frac{m_a}{\rho\ A_z} \qquad \text{(F.5)}$$

where A_z is the flow area for the hot or cold stream at a specific elevation and m_a is the corresponding mass flow rate. The air mass flow rate for each stream is constant for all values of z. At any elevation, the sum of the hot and cold flow areas should be equal to the cross-sectional flow area of the tower at that elevation.

$$A_{hz} + A_{cz} = A_z \tag{F.6}$$

By using equations (F.4), (F.5) and (F.6), the velocity of the hot and the cold stream can be calculated at any elevation for the cooling tower.

The above-mentioned equations have been solved numerically for the cooling tower shown in figure F.1 with inlet and outlet diameter of 100 m and 70 m respectively while the tower height equals 120 m. Calculations have been done for different values of the initial hot air velocity, v_{h0}, while the initial velocity of the cold air stream, v_{c0}, is kept constant at 2.5 m/s. For each chosen value of the inlet velocities, the corresponding air temperatures have to be calculated. The heat exchanger characteristics used in this example are such that the outlet air temperature and the uniform outlet air velocity is correlated by the following equation

$$T_{a0} = 53.1 - 6.6\, v_{a0} + 0.48\, v_{a0}^2 + 0.0023\, v_{a0}^3 \tag{F.7}$$

for $0.0 < v_{a0} < 2.7$

The corresponding air density for each stream is obtained by using the perfect gas relation, i.e.

$$\rho_a = p_a / R\,(T_{a0} + 273.15) \tag{F.8}$$

where p_a is the atmospheric pressure which is kept at a constant value of 84600 N/m^2 for the calculations.

The results of the analysis are shown in figure F.2 with the velocity ratio v_h/v_c plotted as a function of the dimensionless tower height. As the value of v_{h0}/v_{c0} increases, the density difference decreases and therefore the velocity distribution in the tower tends to become uniform as v_{h0}/v_{c0} moves towards 1. By substituting the velocities obtained by the previous calculation back in equations (F.1) or (F.2), the static pressure at any elevation in the tower can be

calculated. If dynamic effects are neglected, the hydrostatic pressure at an elevation for the hot and cold air column is given by

$$p_z = p_0 - \rho\, g\, z \tag{F.9}$$

where ρ is the density of the hot or cold air. In figure F.3 the difference in static pressure according to Bernoulli at a specific elevation and the hydrostatic pressure for the hot and cold air column at the same elevation is shown. The results suggest that the pressure difference between the in and outlet of the cooling tower is for all practical purposes given by the hydrostatic pressure difference of the colder air stream.

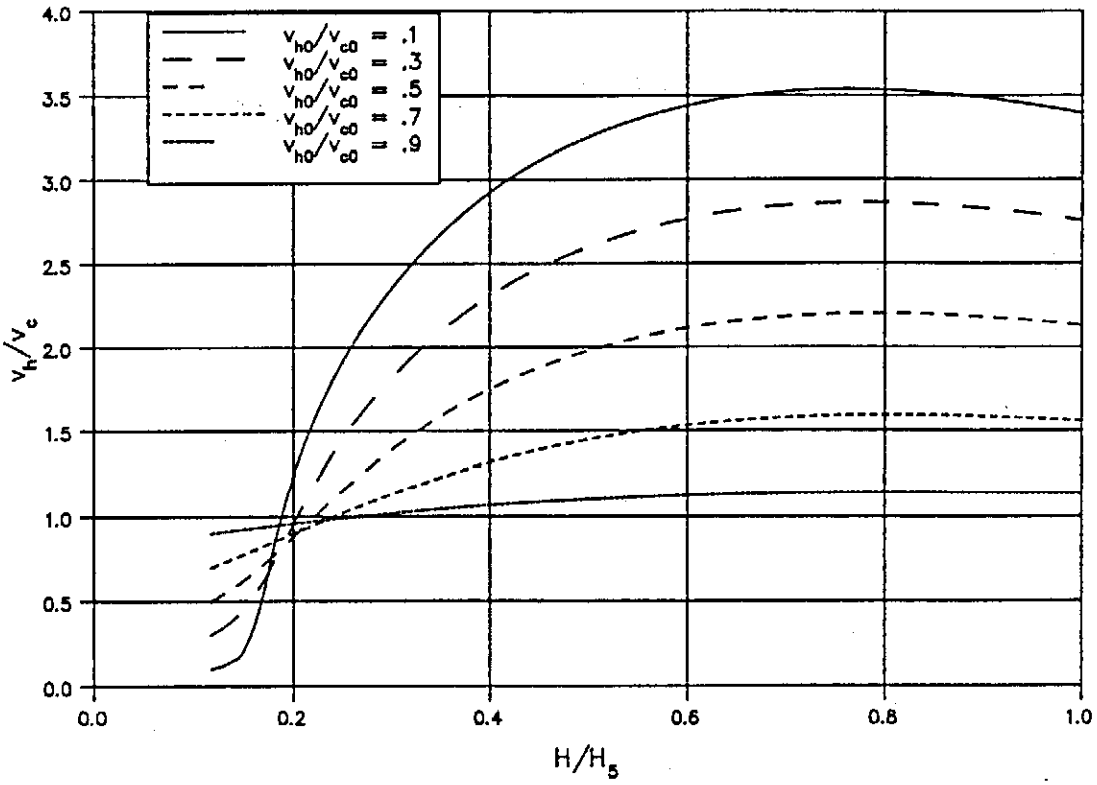

Figure F.2: Velocity ratio of the two streams in the cooling tower.

The kinetic energy coefficient, as defined by equation (A.1.3), can be calculated at the inlet and outlet of the tower if the density difference between the two streams is neglected. For the tower geometry and heat exchanger characteristics used in this analysis, the outlet kinetic coefficient has a maximum value of 1.85 for a initial velocity ratio of 0.2. This can be explained by the fact that α at the outlet have to be equal to 1 for both $v_{h0}/v_{c0} = 0$ and $v_{h0}/v_{c0} = 1$. If the initial velocity ratio is zero, if follows that v_{h0} is zero and therefore the entire cooling tower will be filled with cold air. For the case where the initial velocity distribution is 1, there is no temperature difference between the two streams and therefore the outlet velocity distribution will

be uniform.

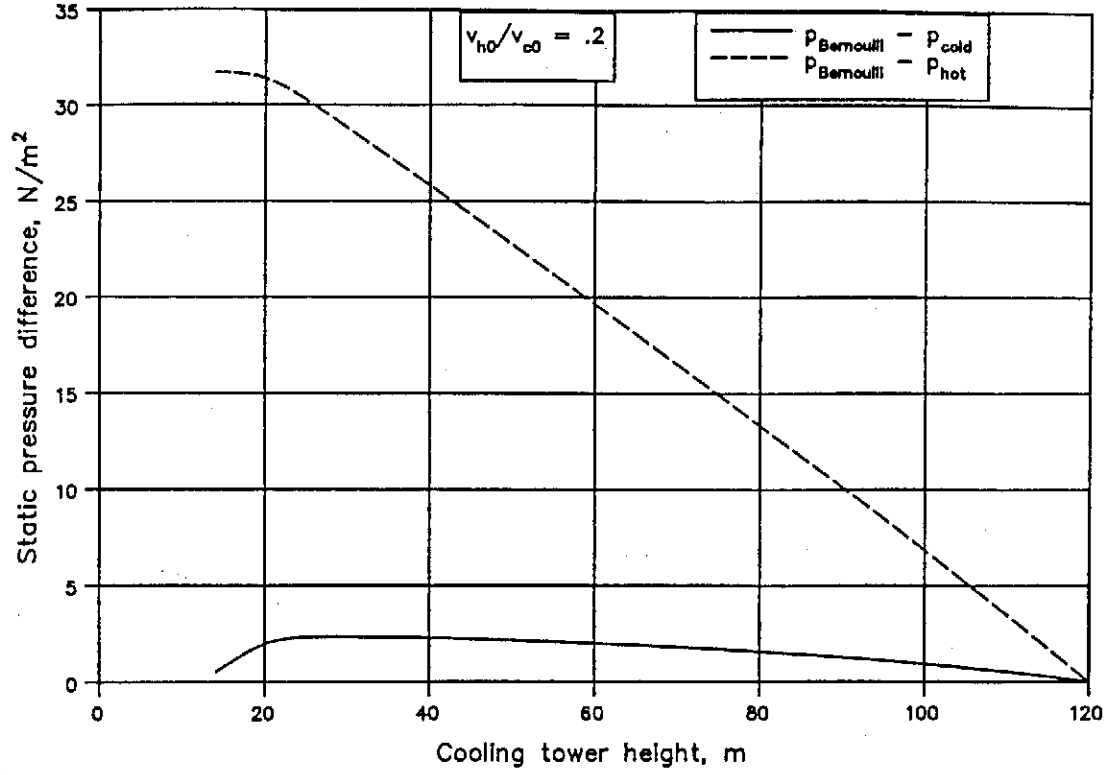

Figure F.3: Pressure distribution in tower.

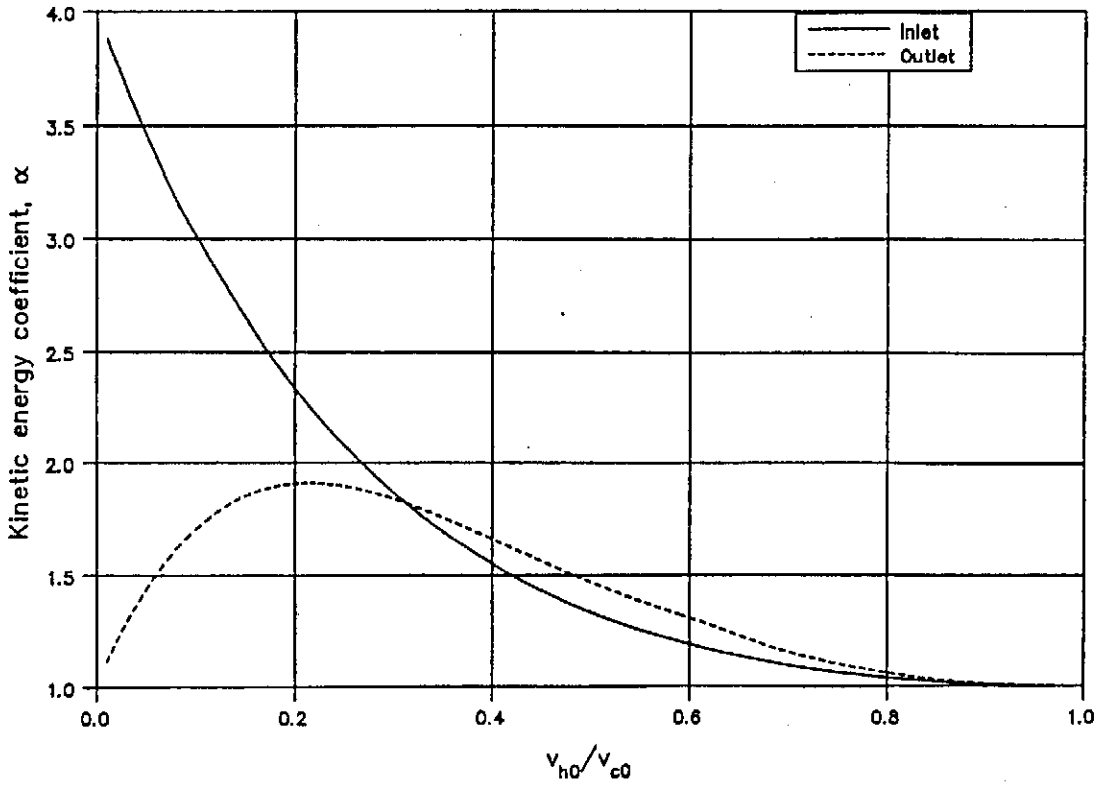

Figure F.4: Kinetic energy coefficients at inlet and the outlet of the tower.

APPENDIX G

Sample calculation for the prediction of the wind influence on a natural draft dry-cooling tower with a horizontal heat exchanger arrangement.

G.1: Perfect mixing of the air in the tower.

In section 2.5 the results of the model tests were used to predict the effect of a cross-wind on a specific dry-cooling tower. The heat rejected by the tower, of which all the available data is given in the same section, with no atmospheric disturbances is found to be 354.39×10^6 W for a water inlet temperature of T_{wi} = 61.45 °C and a corresponding water outlet temperature T_{wo} = 42.136 °C.

If a cross-wind of 6 m/s, as measured on the reference height 10 m AGL, acts on the tower while the heat rejection rate of the tower is kept at a constant value, the following values of the independent variables are found to satisfy the energy and draft equations:

Water inlet temperature	T_{wi}	= 66.82794 °C
Water outlet temperature	T_{wo}	= 47.52647 °C
Air mass flow rate	m_a	= 10171.213 kg/s
Air outlet temperature to satisfy the energy equation	T_{a4}	= 51.5887 °C
Air outlet temperature to satisfy the draft equation	T_{a4}	= 50.059 °C

The air temperature before the heat exchangers is according to equation (B.1.1):

$$T_{a3} = 15.6 - 0.00975 \times 13.67 = 15.4667 \text{ °C}$$

with the corresponding air density according to equation (B.1.3) equal to ρ_{a3} = 1.021048 kg/m^3 $\approx \rho_{ref}$. The mean air temperature through the heat exchanger is therefore

$$T_{a34} = 0.5\ (15.4667 + 51.5887) = 33.5277 \text{ °C}$$

The air properties of dry air, as given in Appendix H, at this temperature is:

Density	ρ_{a34}	= 0.960916 kg/m^3
Specific heat	c_{pa34}	= 1007.213 J/kgK
Dynamic viscosity	μ_{a34}	= 1.8774805x10^{-5} kg/sm
Thermal conductivity	k_{a34}	= 0.02673676 W/mK
Prandtl number	Pr_{a34}	= 0.707274

If the air above the heat exchangers is perfectly mixed the mass mean air temperature above the heat exchangers is given by equation (B.1.7)

$$T_{a4} = 354.39x10^6/(10171.213 \times 1007.213) + 15.4667 = 50.059\ ^\circ C$$

The air density after the heat exchangers as based on the mass mean air temperature is calculated from equation (B.1.14)

$$\rho_{a4} = 84600 / (287.08 \times (273.15 + 50.059) = 0.911766\ kg/m^3$$

The harmonic mean air density through the heat exchanger is according to equation (B.1.15):

$$\rho_{a34} = 2/(1/1.021048 + 1/0.911766) = 0.963318\ kg/m^3$$

The wind velocity at the outlet height of the tower is calculated from equation (1.1.1)

$$v_{wo} = v_{wref}\ (z / z_{ref})^{0.2} = 6.0\ (120 / 10)^{0.2} = 9.86251\ m/s$$

The mean air inlet velocity based on the inlet cross-sectional area of the tower and the mean air density through the heat exchanger is

$$v = 4\ m_a / \rho_{a34}\ \pi\ d_3^2 = 4 \times 10171.213 / 0.963318\ \pi\ 78.3233^2 = 2.19145\ m/s$$

The relative wind velocity, defined as the wind velocity at the outlet height of the tower divided by the mean air velocity through the heat exchangers is found to be

$$v_{wo}/v = 9.86251 / 2.19145 = 4.50045$$

The heat transfer correction factor is obtained from equation (2.3.3). The value of the heat

exchanger pressure loss coefficient used in the equation is evaluated for an arbitrary Ry value of 200×10^3. Substitute the latter into equation (2.5.2) and find

$$K_{he} = 1383.94795 \times 200\,000^{-0.332458} = 23.91938$$

Substitute the latter into equation (2.3.3) and find

$$\alpha_Q = \left\{1 - \frac{(4.50045)^{3.6}\exp\left[-\frac{4.50045}{3.75}\right]\ 2.19145^{0.576}}{3561}\right\}$$

$$\times \left[0.98 + 0.02\left\{\exp\left[5.2 - \frac{78.3233}{13.67}\right] + \exp(-4.50045)\right\}\right]$$

$$-(1.5 - 0.05 \times 23.91938) \times \left[\left\{0.013 - 0.0048\left[\frac{78.3233}{13.67}\right] + 0.000302\left[\frac{78.3233}{13.67}\right]^2\right\}\right.$$

$$+ \left\{0.0134 - 0.00129\left[\frac{78.3233}{13.67}\right] + 0.000038\left[\frac{78.3233}{13.67}\right]^2\right\} \times (4.50045)$$

$$\left. + \left\{0.0035 + 0.00206\left[\frac{78.3233}{13.67}\right] - 0.000085\left[\frac{78.3233}{13.67}\right]^2\right\}\sin\left[\frac{4.50045}{1.9}\right]\right]$$

$$- \left[0.0053 - \frac{23.91938}{9182}\right](11.26 - 25.64 \times 0.46) \times 4.50045$$

$$= 0.957662$$

The heat transfer rate to the air stream is therefore according to equation (2.5.1) equal to:

$$Q = 10171.213 \times 1007.213 \times (51.5887 - 15.4667) \times 0.957662 = 354.39 \times 10^6 \text{ W}$$

The air side characteristic flow parameter is defined by equation (2.1.3) and is found to be

$$Ry = 10171.213 / 1.8774805 \times 10^{-5} \times 4818.06 = 112441.11 \text{ m}^{-1}$$

The corresponding heat transfer parameter according to equation (2.5.4) is

$Ny = 383.61731 \times 112441.11^{0.523761} = 169580.452\ m^{-1}$

The heat transfer parameter is based on the maximum number of tubes that can be installed in a bundle. Because it is impractical to install half-tubes in the bundles employed in the tower, a correction has to be made when calculating the effective heat transfer coefficient as defined by Kröger [86KR1]

$$h_{ae}A_a = k_{a34}\, Pr_{a34}^{0.333}\, A_{fr}\, Ny\, (n_{tb\ actual} / n_{tb\ maximum})$$
$$= 0.02673676 \times 0.707274^{0.333} \times 4818.06 \times 169580.452 \times 154 / 156$$
$$= 19216115.3\ W/K$$

The mean water temperature is

$$T_w = 0.5\,(T_{wi} + T_{wo}) = 0.5(66.82794 + 47.52647) = 57.1772\ °C$$

At this temperature the water properties are according to appendix H:

Specific heat	c_{pw}	$= 4182.36$ J/kgK
Dynamic viscosity	μ_w	$= 4.8384425 \times 10^{-4}$ kg/sm
Thermal conductivity	k_w	$= 0.6504133$ W/mK
Prandtl number	Pr_w	$= 3.111269$

The heat transferred from the water stream is calculated similar as that for the air stream

$$Q = 4390 \times 4182.36 \times (66.82794 - 47.52647) = 355.48 \times 10^6\ W$$

The Reynolds number for the water flow inside the pipes is:

$$Re_w = \frac{m_w\, n_{wp}\, d_e}{A_{ts}\, n_{tb}\, n_b\, \mu_w}$$

$$= \frac{4390 \times 2 \times 0.0216}{3.664 \times 10^{-4} \times 154 \times 142 \times 4.8384425 \times 10^{-4}} = 48919.07$$

The friction factor inside the tubes can be calculated from an equation as recommended by Haaland [83HA1]

$$f_D = 0.3086/\left[\log_{10}\left\{\frac{6.9}{Re_w}+\left(\frac{\epsilon/d}{3.7}\right)^{1.11}\right\}\right]^2$$

$$= 0.3086/\left[\log_{10}\left\{\frac{6.9}{48919.07}+\left(\frac{5.24\text{x}10^{-4}}{3.7}\right)^{1.11}\right\}\right]^2$$

$$= 0.02240693$$

According to Gnielinski [75GN1] the heat transfer coefficient inside the tubes is given by:

$$h_w = \frac{k_w \left(\frac{f_D}{8}\right)\left(Re_w-1000\right) Pr_w \left[1+\left(\frac{d_e}{L_t}\right)^{0.67}\right]}{d_e\left[1+12.7\left(\frac{f_D}{8}\right)^{0.5}\left(Pr_w^{0.67}-1\right)\right]}$$

$$= \frac{0.6504133 \text{ x } 0.02240693 \text{ x } 47919.07 \text{ x } 3.111269 \text{ x } \left[1+\left(\frac{0.0216}{15}\right)^{0.67}\right]}{8 \text{ x } 0.0216\left[1 + 12.7\left(\frac{0.02240693}{8}\right)^{0.5}\left(3.111269^{0.67} - 1\right)\right]}$$

$$= 7209.95 \text{ W/m}^2$$

The total surface area on the water side is

$$A_w = A_{ti}\, L_t\, n_{tb}\, n_b = 0.0679 \text{ x } 15 \text{ x } 154 \text{ x } 142 = 22272.558 \text{ m}^2$$

The overall heat transfer coefficient is therefore

$$UA = \left[\frac{1}{h_{ae}\, A_a} + \frac{1}{h_w\, A_w}\right]^{-1}$$

$$= \left[\frac{1}{19216115.3} + \frac{1}{7209.95 \text{ x } 22272.558}\right]^{-1}$$

$$= 17162395.7 \text{ W/°C}$$

The logarithmic mean temperature difference is:

$$\Delta T_{lm} = \frac{(T_{wi} - T_{ao}) - (T_{wo} - T_{a3})}{\ln[(T_{wi} - T_{ao}) / (T_{wo} - T_{a3})]}$$

$$= \frac{(66.82794 - 51.5889) - (47.52647 - 15.4667)}{\ln[(66.82794 - 51.5889) / (47.52649 - 15.4667)]}$$

$$= 22.6165 \text{ °C}$$

The cross-flow correction factor according to Roetzel [84RO1] is found to be

$$F_T = 0.953369$$

The heat transfer rate from the air to the water stream is therefore:

$$Q = UA\, F_T\, \Delta T_{lm}\, \alpha_Q$$
$$= 17162395.7 \times 0.953369 \times 22.6165 \times 0.957662 = 354.39 \times 10^6 \text{ W}$$

This is in agreement with the heat transfer rate to and from the air and water stream respectively.

To calculate the draft equation (B.1.12) the various loss coefficients have to be determined. For non-isothermal normal flow situations, the pressure loss coefficient is given by Kröger [86KR1] as

$$K_{he} = 1383.94795\, Ry^{-0.332458} + \frac{2}{\sigma^2}\left[\frac{\rho_{a3} - \rho_{a4}}{\rho_{a3} + \rho_{a4}}\right]$$

$$= 1383.94795 \times 112441.11^{-0.332458} + \frac{2}{0.433^2}\left[\frac{1.021048 - 0.911766}{1.021048 + 0.911766}\right]$$

$$= 29.56985$$

The tower inlet loss coefficient can be found by substituting equation (B.1.21) into equation (B.1.22)

$$K_{ct} = \left[0.072\left[\frac{78.3233}{13.67}\right]^2 - 0.34\left[\frac{78.3233}{13.67}\right] + 1.7\right]\left[\frac{0.963318}{1.021048}\right]\left[\frac{4818.06 \times 4}{\pi \times 78.3233^2}\right]^2$$

$$= 1.99595$$

The loss coefficient of the tower supports is obtained from equation (B.1.19)

$$K_{ts} = \frac{2 \times 15.79 \times 0.5 \times 60 \times 4818.06^2}{(\pi\ 78.3233 \times 13.67)^3}\left[\frac{0.963318}{1.021048}\right]$$

$$= 0.45522$$

The atmospheric pressure at the top of the tower is calculated from equation (B.1.4)

$$p_{a6} = 84600\ (1 - 0.00975 \times 120 / 288.75)^{102.564 \times 9.8 / 287.08}$$

$$= 83405.873\ N/m^2$$

For an horizontal bundle arrangement is

$$H_4 \approx H_3 = 13.67\ m$$

The air density at the tower outlet can therefore be obtained from equation (B.1.17)

$$\rho_{a5} = 83405.873 / \{287.08\ [\ 323.209 - 0.00975\ (120 - 13.67)]\} = 0.90179\ kg/m^3$$

Likewise the ambient air density on the tower outlet height given by equation (B.1.18) is

$$\rho_{a6} = 83405.873 / 287.08\ [\ 288.75 - 0.00975 \times 120] = 1.010264\ kg/m^3$$

The relative wind speed at the tower outlet height is therefore

$$v_{wo}/v_o = 9.86251 \times 0.90179\ \pi \times 58^2 / 4 \times 10171.213 = 2.31028$$

The outlet pressure coefficient for a cylindrical tower outlet is given by equation (2.4.1)

$$C_{po} = -0.405 + \frac{1.07}{2.31028} + 1.8 \log_{10}\left[\frac{2.31028}{2.7}\right] \frac{1}{2.31028^2}$$

$$= 0.035316$$

The inlet pressure coefficient is obtained from equation (2.2.1).

$$C_{pi} = \left[- 0.57 + 0.0503 \times 4.50045^{0.8} \times \left[\frac{78.3233}{13.67}\right]^{-0.64} \right.$$

$$\left. -1.2/\exp\left\{2.4 \times 4.50045 \times \left[\frac{78.3233}{13.67}\right]^{-0.8}\right\}\right]$$

$$\times \left[1 - \left\{\frac{0.0067}{\exp(0.2 \times 23.91938)}\right\}\left\{40 - 6 \times 4.50045\left[\frac{78.3233}{13.67}\right]^{-0.8}\right\}\right]$$

$$+ \left[\left[-0.6+0.01x\left[\frac{78.3233}{13.67}\right]+\left\{-0.65+0.06\left[\frac{78.3233}{13.67}\right]+0.1x23.91938\right.\right.\right.$$

$$\left.\left.\left. \times \left[0.23-0.039\left[\frac{78.3233}{13.67}\right]+0.001\left[\frac{78.3233}{13.67}\right]^2\right]\right\} x0.054(24-4.50045)\right]\right.$$

$$\left. + \frac{\sin\{4.50045/(1+0.17x4.50045)\}}{\exp\left[\frac{4.50045}{7}+0.2\left[15-\frac{78.3233}{13.67}\right]+\frac{23.91938}{20}\right]}\right]$$

$$\times (1 - 0.978 \times 1.0) \times [1-(0.003 \times 20 + 2 \times 0.2$$

$$+ 0.027 \times 20 \times 0.2)] = -0.60406$$

To be substituted into equation (B.1.12), C_{pi} has to be based on the reference wind velocity as measured 10 m above ground level, therefore

$$C_{piref} = -0.60406 \frac{\rho_{a6}\, v_{wo}^2}{\rho_{wref}\, v_{wref}^2} = -0.60406 \times \frac{1.010264 \times 9.86251^2}{1.021048 \times 6^2} = -1.61492$$

Evaluate the left hand side of the draft equation, (B.1.12)

$$84600\ [\{1 - 0.00975(13.67 + 13.67)/2 \times 288.75\}^{3.50121}$$
$$\times \{1 - 0.00975(120 - 13.67/2 - 13.67/2)/323.209\}^{3.50121}$$
$$- (1 - 0.00975 \times 120 / 288.75)^{3.50121}]$$
$$- 0.035316 \times 0.5 \times 1.010264 \times 9.86251^2$$
$$- 1.61492 \times 0.5 \times 1.021048 \times 6^2$$
$$\times [1 - 0.00975(120 - 13.67/2 - 13.67/2)/323.209]^{3.50121}$$
$$= 81.64\ N/m^2$$

and for the right hand side

$$[0.54522 + 1.99595 + 29.56985\ ] \times \left[\frac{1}{2 \times 0.963318}\right]\left[\frac{10171.213}{4818.06}\right]^2$$
$$\times [1 - 0.00975(120 - 13.67/2 - 13.67/2)/323.209]^{3.50121}$$
$$+ \frac{1}{2 \times 0.90179}\left[\frac{10171.213 \times 4}{\pi\ 58^2}\right]^2 = 81.66\ N/m^2$$

Because the values obtained for the left and right hand side of the draft equation are practically the same, the draft equation is satisfied. Thus, if it is assumed that the air is perfectly mixed, the increase in the approach temperature of this particular tower for a wind speed of 6 m/s at 10 m AGL is found to be 47.52647 - 42.136 = 5.39047 °C while the heat rejected by the tower is kept constant at 354.39×10^6 W. This data point shown amongst others in figure 2.5.1 with the increase of the approach temperature shown as a function of the wind speed.

G.2: No mixing of the warm air in the tower.

In the present section the numerical example in the previous section is repeated, but it is assumed that there is absolutely no mixing in the air stream above the heat exchangers. As discussed in Appendix B, the static pressure gradient above the heat exchangers in this case is almost the same as the hydrostatic pressure gradient of the coldest air stream leaving the bundles. The variables found to satisfy the energy and draft equations if the tower draft is based on the coldest air temperature above the heat exchangers are:

Water inlet temperature	T_{wi}	= 68.2888 °C
Water outlet temperature	T_{wo}	= 48.9912 °C
Air mass flow rate	m_a	= 9756.793 kg/s
Air outlet temperature to satisfy the energy equation	T_{a4}	= 53.21745 °C
Air outlet temperature to satisfy the draft equation	T_{a4}	= 47.58163 °C

By repeating the calculations shown in section G.1, the mean air inlet velocity, v, is found to be 2.093648 m/s while the relative wind velocity v_{wo}/v = 4.710681. By applying equation (2.3.4), the ratio of the maximum air velocity to the mean velocity through the heat exchanger is found.

$$\frac{v_{max}}{v} = 1.014-0.0095\left[\frac{78.3233}{13.67}\right]+0.0014\left[\frac{78.3233}{13.67}\right]^2$$

$$+\left\{-0.1265+0.0509\left[\frac{78.3233}{13.67}\right]-0.00245\left[\frac{78.3233}{13.67}\right]^2\right\} \times 4.710681(1-0.26 \times 0.2)$$

$$+\left[-.362+.0865\left[\frac{78.3233}{13.67}\right]-0.00321\left[\frac{78.3233}{13.67}\right]^2\right.$$

$$\left.+\left\{0.288-.0572\left[\frac{78.3233}{13.67}\right]+0.00242\left[\frac{78.3233}{13.67}\right]^2\right\} \times 4.710681\right](1.5-0.05 \times 23.91938)$$

$$=1.44926$$

The maximum air velocity through the heat exchanger is therefore = 1.44926 x 2.093648 = 3.03424 m/s which is to be used to calculate the minimum air temperature above the heat exchangers. The characteristics of the heat exchangers used in the calculation are such that the air minimum outlet temperature is found to be 47.58163 °C with a water inlet temperature of 68.2888 °C. For the rest of the calculations, exactly the same procedure as that in section G.1 is followed. The rise in the outlet water temperature for a wind speed of 6 m/s, 10 m AGL, is therefore found to be 48.9912 - 42.136 = 6.8552 °C as also shown in figure 2.5.1.

APPENDIX H

Properties of fluids

H.1: The thermophysical properties of dry air from 220 K to 380 K.

Density:

$\rho_a = p_a/RT$, kg/m^3 (H.1.1)

with R = 287.08 J/kgK

Specific heat:

$c_{pa} = a + bT + cT^2 + dT^3$, J/kgK (H.1.2)

a = 1.045356×10^{3}

b = -3.161783×10^{-1}

c = 7.083814×10^{-4}

d = -2.705209×10^{-7}

Dynamic viscosity

$\mu_a = a + bT + cT^2 + dT^3$, kg/sm (H.1.3)

a = 2.287973×10^{-6}

b = 6.259793×10^{-8}

c = $-3.131956 \times 10^{-11}$

d = 8.150380×10^{-15}

Thermal conductivity:

$k_a = a + bT + cT^2 + dT^3$, W/mK (H.1.4)

a = -4.937787×10^{-4}

b = 1.018087×10^{-4}

c = -4.627937×10^{-8}

d = 1.250603×10^{-11}

H.2: The thermophysical properties of saturated water liquid from 273.15K to 380K.

Density

$$\rho_w = (a + bT + cT^2 + dT^6)^{-1}, \text{ kg/m}^3 \quad \text{(H.2.1)}$$

$a = 1.49343 \times 10^{-3}$

$b = -3.7164 \times 10^{-6}$

$c = 7.09782 \times 10^{-9}$

$d = -1.90321 \times 10^{-20}$

Specific heat

$$c_{pw} = a + bT + cT^2 + dT^6, \text{ J/kgK} \quad \text{(H.2.2)}$$

$a = 8.15599 \times 10^{3}$

$b = -2.80627 \times 10$

$c = 5.11283 \times 10^{-2}$

$d = -2.17582 \times 10^{-13}$

Dynamic viscosity

$$\mu_w = a10^{b/(T-c)}, \text{ kg/ms} \quad \text{(H.2.3)}$$

$a = 2.414 \times 10^{-5}$

$b = 247.8$

$c = 140$

Thermal conductivity

$$k_w = a + bT + cT^2 + dT^4, \text{ W/mK} \quad \text{(H.2.4)}$$

$a = -6.14255 \times 10^{-1}$

$b = 6.9962 \times 10^{-3}$

$c = -1.01075 \times 10^{-5}$

$d = 4.74737 \times 10^{-12}$

APPENDIX I

Q1 instruction file.

```
TALK=F;RUN( 1, 1);VDU=T4107
   GROUP 1. Run title and other preliminaries
TEXT(Wind effect on Kendal tower
   Declare variables
   CON      1 - Inlet diameter / Outlet diameter
   CPAIR    Specific heat                                   J/kgK
   HEATCO   Coefficient in K_he correlation
   HEATEX   Exponent in K_he correlation
   RAIR     Universal gas constant                          J/kgK
   RAMB     Density of ambient air                          kg/m^3
   TAMB     Temperature of ambient air                      K
   TOWH     Effective height of tower shell                 m
   TSWI     Water inlet temperature                         K
   VISCO    Kinematic viscosity of air                      m^2/s
   WIND     Wind velocity                                   m/s
   WPRO     Exponent b in equation (1.1.1)
   YAMB     Radial distance from tower inlet to outer
            limit of computational domain                   m
   YTOW     Inlet radius of tower                           m
   ZAMB     Distance from tower outlet edge to upper
            limit of computational domain                   m
   ZHEAT    Height of heatexchanger cell                    m
   ZTOI     Inlet height of tower                           m
   ZTOOC    Height of conocal part of tower shell           m
   ZTOWC    Height of cylindrical part of tower shell       m
   ISWEP    Number of sweeps
   NXTOW    Number of cells in X-direction
   NYAMB    Number of cells in Y-direction to the
            outer limit of computational domain
   NYTOW    Number of cells in Y-direction up to tower shell
   NZAMB    Number of cells in Z-direction
            to the outer limit of computational domain
   NZHEAT   Number of cells in Z-direction from the ground
            level to heat exchanger outlet
   NZTOI    Number of cells in Z-direction from ground level to
            tower inlet
   NZTOO    Number of cells in Z-direction from the
            ground level tower inlet the tower outlet
REAL(CON,CPAIR,HEATCO,HEATEX,PI,RAIR,RAMB,TAMB,TOWH,TSAO1)
REAL(TSAO2,TSAO3,TSAO4,TSWI,VISCO,WIND,WPRO,YAMB,YTOW,ZAMB)
REAL(ZHEAT,ZTOI,ZTOOC,ZTOWC)
INTEGER(ISWEP,NXTOW,NYAMB,NYTOW,NZAMB,NZHEAT,NZTOI,NZTOO)
ISWEP=70
TSWI=273.155+39.2
   Calculate the air outlet temperature from equation (4.2.6)
TSAO1= a + b *TSWI
TSAO2= c + d *TSWI + e *TSWI**2.0
TSAO3= f + g *TSWI + h *TSWI**2.0
```

```
TSAO4= i + j *TSWI + k *TSWI**2.0
VISCO=1.0E-3
CPAIR=2.0*1007.0
PRESS0=83330.0
TAMB=287.15
RAIR=287.08
RAMB=PRESS0/(TAMB*RAIR)
WIND=-3.
WPRO=0.16
NXTOW=6
NYTOW=10
NYAMB=10+NYTOW
NZTOI=10
NZHEAT=NZTOI+1
NZTOO=15+NZHEAT
NZAMB=15+NZTOO
PI=3.14159
YTOW=73.6
YAMB=144.0
ZTOI=24.5
ZHEAT=1.0
TOWH=139.5
CON=0.31
ZTOOC=TOWH*0.65
ZTOWC=TOWH-ZTOOC
ZAMB=75.0
  Calculate the pressure loss coefficient of the heat exchanger
  according to equation (4.2.5)
HEATCO= a
HEATEX= 1.+b
   GROUP 2. Transience; time-step specification
   GROUP 3. X-direction grid specification
NX=NXTOW
   GROUP 4. Y-direction grid specification
NY=NYAMB
   GROUP 5. Z-direction grid specification
NZ=NZAMB
   GROUP 6. Body-fitted coordinates or grid distortion
BFC=T;NONORT=T
    Tower inlet
DOMAIN(1,NXTOW+1,1,NYTOW+1,1,NZTOI+1)
SETLIN(XC,YTOW*LNJ*SIN(PI*LNI))
SETLIN(YC,YTOW*LNJ*COS(PI*LNI))
SETLIN(ZC,ZTOI*LNK)
DOMAIN(1,NXTOW+1,NYTOW+1,NYAMB+1,1,NZTOI+1)
SETLIN(XC,YTOW*SIN(PI*LNI)+YAMB*LNJ*SIN(PI*LNI))
SETLIN(YC,YTOW*COS(PI*LNI)+YAMB*LNJ*COS(PI*LNI))
SETLIN(ZC,ZTOI*LNK)
     Heat exchanger
DOMAIN(1,NXTOW+1,1,NYTOW+1,NZTOI+1,NZHEAT+1)
SETLIN(XC,YTOW*LNJ*SIN(PI*LNI))
SETLIN(YC,YTOW*LNJ*COS(PI*LNI))
SETLIN(ZC,ZTOI+ZHEAT*LNK)
```

```
DOMAIN(1,NXTOW+1,NYTOW+1,NYAMB+1,NZTOI+1,NZHEAT+1)
SETLIN(XC,(YTOW+YAMB*LNJ)*SIN(PI*LNI))
SETLIN(YC,(YTOW+YAMB*LNJ)*COS(PI*LNI))
SETLIN(ZC,ZTOI+ZHEAT*LNK)
     Conical inlet of tower
DOMAIN(1,NXTOW+1,1,NYTOW+1,NZHEAT+1,NZTOO-5)
SETLIN(XC,YTOW*(1-CON*LNK)*LNJ*SIN(PI*LNI))
SETLIN(YC,YTOW*(1-CON*LNK)*LNJ*COS(PI*LNI))
SETLIN(ZC,ZTOI+ZHEAT+ZTOOC*LNK)
DOMAIN(1,NXTOW+1,NYTOW+1,NYAMB+1,NZHEAT+1,NZTOO-5)
SETLIN(XC,(YTOW*(1-CON*LNK)+(YAMB+CON*YTOW*LNK)*LNJ)*SIN(PI*LNI))
SETLIN(YC,(YTOW*(1-CON*LNK)+(YAMB+CON*YTOW*LNK)*LNJ)*COS(PI*LNI))
SETLIN(ZC,ZTOI+ZHEAT+ZTOOC*LNK)
    Cylindrical outlet of tower
DOMAIN(1,NXTOW+1,1,NYTOW+1,NZTOO-5,NZTOO+1)
SETLIN(XC,YTOW*(1-CON)*LNJ*SIN(PI*LNI))
SETLIN(YC,YTOW*(1-CON)*LNJ*COS(PI*LNI))
SETLIN(ZC,ZTOI+ZHEAT+ZTOOC+ZTOWC*LNK)
DOMAIN(1,NXTOW+1,NYTOW+1,NYAMB+1,NZTOO-5,NZTOO+1)
SETLIN(XC,(YTOW*(1-CON)+(YAMB+CON*YTOW)*LNJ)*SIN(PI*LNI))
SETLIN(YC,(YTOW*(1-CON)+(YAMB+CON*YTOW)*LNJ)*COS(PI*LNI))
SETLIN(ZC,ZTOI+ZHEAT+ZTOOC+ZTOWC*LNK)
     Ambient above the tower
DOMAIN(1,NXTOW+1,1,NYTOW+1,NZTOO+1,NZAMB+1)
SETLIN(XC,YTOW*(1-CON)*LNJ*SIN(PI*LNI))
SETLIN(YC,YTOW*(1-CON)*LNJ*COS(PI*LNI))
SETLIN(ZC,ZTOI+ZHEAT+TOWH+ZAMB*LNK)
DOMAIN(1,NXTOW+1,NYTOW+1,NYAMB+1,NZTOO+1,NZAMB+1)
SETLIN(XC,(YTOW*(1-CON)+YAMB*(1+SS)*LNJ)*SIN(PI*LNI))
SETLIN(YC,(YTOW*(1-CON)+YAMB*(1+SS)*LNJ)*COS(PI*LNI))
SETLIN(ZC,ZTOI+ZHEAT+TOWH+ZAMB*LNK)
   GROUP 7. Variables stored, solved & named
SOLVE(P1,H1,V1,W1,U1)
SOLUTN(P1,Y,Y,Y,N,N,N)
STORE(DEN1,ENUL,TEMP1)
   GROUP 8. Terms (in differential equations) & devices
TERMS(H1,N,Y,Y,Y,Y,Y)
   GROUP 9. Properties of the medium (or media)
ENUL=VISCO
PRNDTL(H1)=0.71
RHO1=GRND5
RHO1B=1.0/RAIR
RHO1A=1.0;RHO1C=1.0/1.4
DRH1DP=GRND5
TMP1=GRND2
TMP1A=0;TMP1B=1.0
   GROUP 10. Inter-phase-transfer processes and properties
   GROUP 11. Initialization of variable or porosity fields
RESTRT(ALL)
CONPOR(0.0,NORTH,1,NX,NYTOW,NYTOW,NZHEAT,NZTOO)
   GROUP 12. Convection and diffusion adjustments
   GROUP 13. Boundary conditions and special sources
PATCH(BUOY,PHASEM,1,NX,1,NY,1,NZ,1,1)
```

```
COVAL(BUOY,U1,FIXFLU,GRND2)
COVAL(BUOY,V1,FIXFLU,GRND2)
COVAL(BUOY,W1,FIXFLU,GRND2)
PATCH(BFCIN,NORTH,1,NX/2,NY,NY,1,NZ,1,1)
COVAL(BFCIN,P1,FIXFLU,GRND1)
COVAL(BFCIN,U1,ONLYMS,GRND1)
COVAL(BFCIN,H1,ONLYMS,TAMB)
COVAL(BFCIN,V1,ONLYMS,GRND1)
COVAL(BFCIN,W1,ONLYMS,GRND1)
COVAL(BFCIN,UCRT,0.0,0.0)
COVAL(BFCIN,VCRT,0.0,WIND)
COVAL(BFCIN,WCRT,0.0,0.0)
  Boundary conditions for non-uniform wind profile
  PATCH(ININ1,NORTH,1,1,NY,NY,1,NZ,1,1)
  COVAL(ININ1,P1,FIXFLU,GRND2)
  COVAL(ININ1,U1,ONLYMS,GRND2)
  COVAL(ININ1,V1,ONLYMS,GRND2)
  COVAL(ININ1,W1,ONLYMS,0.0)
  COVAL(ININ1,H1,ONLYMS,TAMB)
  PATCH(ININ2,NORTH,2,2,NY,NY,1,NZ,1,1)
  COVAL(ININ2,P1,FIXFLU,GRND3)
  COVAL(ININ2,U1,ONLYMS,GRND3)
  COVAL(ININ2,V1,ONLYMS,GRND3)
  COVAL(ININ2,W1,ONLYMS,0.0)
  COVAL(ININ2,H1,ONLYMS,TAMB)
  PATCH(ININ3,NORTH,3,3,NY,NY,1,NZ,1,1)
  COVAL(ININ3,P1,FIXFLU,GRND4)
  COVAL(ININ3,U1,ONLYMS,GRND4)
  COVAL(ININ3,V1,ONLYMS,GRND4)
  COVAL(ININ3,W1,ONLYMS,0.0)
  COVAL(ININ3,H1,ONLYMS,TAMB)
  Boundary conditions for uniform wind profile
PATCH(NORBOU,NORTH,NX/2+1,NX,NY,NY,1,NZ,1,1)
COVAL(NORBOU,P1,8.0,0.0)
COVAL(NORBOU,U1,ONLYMS,SAME)
COVAL(NORBOU,V1,ONLYMS,SAME)
COVAL(NORBOU,W1,ONLYMS,SAME)
COVAL(NORBOU,H1,ONLYMS,SAME)
PATCH(UITLAT,HIGH,1,NX,1,NY,NZ,NZ,1,1)
COVAL(UITLAT,P1,8.0,0.0)
COVAL(UITLAT,H1,ONLYMS,SAME)
COVAL(UITLAT,V1,ONLYMS,SAME)
COVAL(UITLAT,W1,ONLYMS,SAME)
COVAL(UITLAT,U1,ONLYMS,SAME)
PATCH(HEAT,LOW,1,NX,1,NYTOW,NZHEAT,NZHEAT,1,1)
COVAL(HEAT,V1,FIXVAL,0.0)
COVAL(HEAT,U1,FIXVAL,0.0)
COVAL(HEAT,W1,GRND3,0.0)
COVAL(HEAT,H1,FIXVAL,GRND1)
PATCH(SUPPORT,NORTH,1,NX,NYTOW,NYTOW,1,NZTOI,1,1)
COVAL(SUPPORT,U1,GRND1,0.0)
COVAL(SUPPORT,V1,GRND1,0.0)
PATCH(GROUND,LWALL,1,NX,1,NY,1,1,1,1)
```

```
COVAL(GROUND,V1,1.,0.0)
COVAL(GROUND,U1,1.,0.0)
PATCH(SHELL,NWALL,1,NX,NYTOW,NYTOW,NZHEAT,NZTOO,1,1)
COVAL(SHELL,W1,1.0,0.0)
COVAL(SHELL,U1,1.0,0.0)
PATCH(SSHELL,SWALL,1,NX,NYTOW+1,NYTOW+1,NZHEAT,NZTOO,1,1)
COVAL(SSHELL,W1,1.0,0.0)
COVAL(SSHELL,U1,1.0,0.0)
   GROUP 14. Downstream pressure for PARAB=.TRUE.
   GROUP 15. Termination of sweeps
LSWEEP=ISWEP
   GROUP 16. Termination of iterations
   GROUP 17. Under-relaxation devices
RELAX(V1,FALSDT,100.)
RELAX(U1,FALSDT,100.)
RELAX(W1,FALSDT,100.)
RELAX(H1,FALSDT,100.)
RELAX(P1,LINRLX,0.5)
   GROUP 18. Limits on variables or increments to them
   GROUP 19. Data communicated by satellite to GROUND
RSG1=RAMB;RSG10=-9.8
RG(1)=TSWI
RG(4)=HEATCO
RG(5)=HEATEX
RG(6)=TAMB
RG(7)=CPAIR
RG(8)=TSAO1
RG(9)=TSAO2
RG(10)=TSAO3
RG(11)=TSAO4
RG(12)=ZTOI+ZHEAT+TOWH
RG(13)=WPRO
RG(14)=WIND
IG(1)=1
IG(2)=NX
IG(3)=1
IG(4)=NYTOW
IG(5)=NZHEAT
IG(6)=ISWEP-1
   GROUP 20. Preliminary print-out
   GROUP 21. Print-out of variables
OUTPUT(P1,Y,N,N,Y,N,N)
OUTPUT(H1,Y,N,N,Y,N,N)
OUTPUT(DEN1,Y,N,N,Y,N,N)
OUTPUT(V1,Y,N,N,Y,N,N)
OUTPUT(W1,Y,N,N,Y,N,N)
OUTPUT(TEMP1,N,N,N,N,N,N)
   GROUP 22. Spot-value print-out
TSTSWP=1
ISWPRF=LSWEEP
ISWPRL=LSWEEP
IYPRF=1;IYPRL=NYTOW
IZPRF=1;IZPRL=NZTOO
```

IXPRF=1;IXPRL=NX
NYPRIN=1;ITABL=0
NZPRIN=1
NXPRIN=1
GROUP 23: Field print-out and plot control
STOP

APPENDIX J

GROUND Subroutine

```
C FILE NAME GROUND.FTN----------22 April 87
C THIS IS THE MAIN PROGRAM OF EARTH
C
C   (C) COPYRIGHT 1984, LAST REVISION 1987.
C   CONCENTRATION HEAT AND MOMENTUM LTD. ALL RIGHTS RESERVED.
C   This subroutine and the remainder of the PHOENICS code are
C   proprietary software owned by Concentration Heat and Momentum
C   Limited, 40 High Street, Wimbledon, London SW19 5AU, England.
```

Material omitted

```
C 5  The numbers in the next two statements (which must be ident-
C     ical) indicate how much computer memory is to be set aside
C     for storing the main and auxiliary variables. The user may
C     alter them if he wishes, to accord with the number of
C     grid nodes and dependent variables he is concerned with.
      COMMON F(3200000)
      NFDIM=   3200000
```

Material omitted

```
C*****************************************************************
C$DIR**GROUND
      SUBROUTINE GROUND
      INCLUDE 'PUBLIC_DIR:SATEAR'
      INCLUDE 'PUBLIC_DIR:GRDLOC'
      INCLUDE 'PUBLIC_DIR:GRDEAR'
      EQUIVALENCE (IZ,IZSTEP)
CXXXXXXXXXXXXXXXXXXXXXXXXXXXXXXXXXXXXXXXXX   USER   SECTION
STARTS:
C
C 1  Set dimensions of data-for-GROUND arrays here. WARNING: the
C     corresponding arrays in the MAIN program of the satellite
C     and EARTH must have the same dimensions.
      COMMON/LGRND/LG(20)/IGRND/IG(20)/RGRND/RG(100)/CGRND/CG(10)
      LOGICAL LG
      CHARACTER*4 CG
C
C 2  User dimensions own arrays here, for example:
C     DIMENSION UUH(10,10),UUC(10,10),UUX(10,10),UUZ(10)
      DIMENSION UUAREA(50,50),UUZ(10)
C
C 3  User places his data statements here, for example:
```

```
C     DATA NXDIM,NYDIM/10,10/
      DATA ISWEP/0/
C
C
C 4   Insert own coding below as desired, guided by GREX examples.
C     Note that the satellite-to-GREX special data in the labelled
C     COMMONs /RSG/, /ISG/, /LSG/ and /CSG/ can be included and
C     used below but the user must check GREX for any conflicting
C     uses. The same comment applies to the EARTH-spare working
C     arrays EASP1, EASP2,....EASP10. If the call to GREX has been
C     deactivated then they can all be used without reservation.
C
      IXL=IABS(IXL)
        IF(IGR.EQ.13) GO TO 13
        IF(IGR.EQ.19) GO TO 19
      GO TO (1,2,3,4,5,6,24,8,9,10,11,12,13,14,24,24,24,24,19,20,24,
     124,23,24),IGR
```

Material omitted

```
C*********************************************************************
C
C*********************************************************************
C
C--- GROUP 13. Boundary conditions and special sources
C
   13 CONTINUE
      GO TO (130,131,132,133,134,135,136,137,138,139,1310,
     11311,1312,1313,1314,1315,1316,1317,1318,1319,1320,1321),ISC
  130 CONTINUE
C------------------ SECTION  1 ------------ coefficient = GRND
      RETURN
  131 CONTINUE
C------------------ SECTION  2 ------------ coefficient = GRND1
C  Pressure loss coefficients for U1 and V1 across tower supports
        CALL ONLYIF(U1,V1,'SUPPORT')
      L0U1=L0F(U1)
      L0V1=L0F(V1)
      L0CO=L0F(CO)
      L0UN=L0F(NORTH(U1))
      L0VN=L0F(NORTH(V1))
      L0US=L0F(SOUTH(U1))
      L0VS=L0F(SOUTH(V1))
      DO 1231 IX=IXF,IXL
        DO 1232 IY=IYF,IYL
        ICELL=IY+NY*(IX-1)
        UUV=(F(L0V1+ICELL))
        UUU=(F(L0U1+ICELL))
          IF(UUV.LT.0.0)THEN
            UIV=ABS(F(L0VN+ICELL))
            UIU=ABS(F(L0UN+ICELL))
```

```
        ELSE
          UIV=ABS(F(L0VS+ICELL))
          UIU=ABS(F(L0US+ICELL))
        ENDIF
      UUV=ABS(UUV)
      UUU=ABS(UUU)
        IF(UUU.GT.0.01) THEN
          UTR=ATAN(UIV/UIU)
          UTG=UTR*180./3.141592
C
C                   Calculate outlet flow angle for vertical
C                   round supports, equation (4.2.9)
C
          UPG=14.78+0.8358*UTG
          UPR=UPG*3.141592/180.
C
C                   Calculate K_ts for vertical round supports,
C                   equation (4.2.8)
C
          UTS=(-0.09584+0.025532*UTG-0.0001682*UTG**2.
     *     +11.59337/exp(UTG/10))
C
C                   Calculate K_tsu, equation (4.2.16)
C
          UUKU=TAN(UTR)*(2.-2.*TAN(UTR)/TAN(UPR)+UTS*
     *     (SIN(UTR))**2.)
          IF(UUKU.LT.0.0)UUKU=0.0
C
C                   Calculate K_tsv, equation (4.2.17)
C
          UUKV=UTS*(SIN(UTR))**2.
C
C                   Add effective pressure loss coefficient
C                   of inner rings rings of supports
C
          UUKV=UUKV+.181
        ELSE
C
C                   Calculate K_tsu and K_tsv for normal flow through supports
C
          UUKU=0.0
          UUKV=0.84105+.181
        ENDIF

        IF(INDVAR.EQ.U1)THEN
          F(L0CO+ICELL)=RSG1*UUU*0.5*UUKU
        ELSE IF(INDVAR.EQ.V1)THEN
          F(L0CO+ICELL)=RSG1*UUV*UUKV*0.5
        ENDIF
1232   CONTINUE
1231  CONTINUE
      RETURN
 132 CONTINUE
```

```
C------------------ SECTION  3 ------------ coefficient = GRND2
C
      RETURN
  133 CONTINUE
C------------------ SECTION  4 ------------ coefficient = GRND3
C  Pressure loss coefficient through heat exchanger
      CALL ONLYIF(W1,W1,'HEAT')
      L0W1=L0F(W1)
      L0DEN=L0F(AUX(DEN1))
      L0CO=L0F(CO)
      DO 1331 IX=IXF,IXL
        DO 1332 IY=IYF,IYL
        ICELL=IY+NY*(IX-1)
        UUV=ABS(F(L0W1+ICELL))*(F(L0DEN+ICELL)/RSG1)
        F(L0CO+ICELL)=RSG1*UUV**RG(5)*RG(4)*0.5
     *  *(F(L0DEN+ICELL)/RSG1
 1332   CONTINUE
 1331  CONTINUE
      RETURN
  134 CONTINUE
C------------------ SECTION  5 ------------ coefficient = GRND4
C
      RETURN
  135 CONTINUE
```

Material omitted

```
C------------------ SECTION 13 -------------------- value = GRND1
C  Temperature of air immediately after the heat exchanger.
      CALL ONLYIF(H1,H1,'HEAT')
      L0DEN=L0F(AUX(DEN1))
      L0W1=L0F(W1)
      L0VAL=L0F(VAL)
      L0LOW=L0F(LOW(H1))
      DO 1333 IX=IXF,IXL
        DO 1334 IY=IYF,IYL
        ICELL=IY+NY*(IX-1)
        UUV=(F(L0W1+ICELL))*F(L0DEN+ICELL)/RSG1
          IF (UUV.GT.0.0)THEN
            F(L0VAL+ICELL)=273.15+(RG(8)+RG(9)*
     *       UUV+RG(10)*UUV**2+RG(11)*UUV**3)+
     *       (F(L0LOW+ICELL)-RG(6))*UUV*0.127348
          ELSE
            F(L0VAL+ICELL)=RG(1)
          ENDIF
          IF(F(L0VAL+ICELL).GT.RG(1))THEN
            F(L0VAL+ICELL)=RG(1)
          ENDIF
 1334     CONTINUE
 1333   CONTINUE
      RETURN
```

```
 1313 CONTINUE
C------------------ SECTION 14 ---------------------- value = GRND2
C Wind velocity components at inlet of computational domain
C for IX=1
      CALL ONLYIF(P1,V1,'ININ1')
      CALL GETPT(1,1,IZ,UUZ(1),UUZ(2),UUZ(3))
      CALL GETPT(1,1,IZ+1,UUZ(4),UUZ(5),UUZ(6))
      UUZ(7)=(UUZ(3)+UUZ(6))/2.0
      L0VAL=L0F(VAL)
        DO 1337 IX=IXF,IXL
          DO 1338 IY=IYF,IYL
          ICELL=IY+NY*(IX-1)
            IF(INDVAR.EQ.P1)THEN
              F(L0VAL+ICELL)=-1.*RG(14)*RSG1*0.965926*
     *         (UUZ(7)/RG(12))**RG(13)
            ELSE IF(INDVAR.EQ.V1)THEN
              F(L0VAL+ICELL)=RG(14)*0.965925*(UUZ(7)/RG(12))**RG(13)
            ELSE IF(INDVAR.EQ.U1)THEN
              F(L0VAL+ICELL)=-1.*RG(14)*0.258819*
     *         (UUZ(7)/RG(12))**RG(13)
            ENDIF
1338        CONTINUE
1337      CONTINUE
      RETURN
 1314 CONTINUE
C------------------ SECTION 15 ---------------------- value = GRND3
C Wind velocity components at inlet of computational domain
C for IX=2
      CALL ONLYIF(P1,V1,'ININ2')
      CALL GETPT(1,1,IZ,UUZ(1),UUZ(2),UUZ(3))
      CALL GETPT(1,1,IZ+1,UUZ(4),UUZ(5),UUZ(6))
      UUZ(7)=(UUZ(3)+UUZ(6))/2.0
      L0VAL=L0F(VAL)
        DO 1339 IX=IXF,IXL
          DO 1340 IY=IYF,IYL
          ICELL=IY+NY*(IX-1)
            IF(INDVAR.EQ.P1)THEN
              F(L0VAL+ICELL)=-1.*RG(14)*RSG1*0.7071067*
     *         (UUZ(7)/RG(12))**RG(13)
            ELSE IF(INDVAR.EQ.V1)THEN
              F(L0VAL+ICELL)=RG(14)*0.7071067*(UUZ(7)/RG(12))**RG(13)
            ELSE IF(INDVAR.EQ.U1)THEN
              F(L0VAL+ICELL)=-1.*RG(14)*0.7071067*
     *         (UUZ(7)/RG(12))**RG(13)
            ENDIF
1340        CONTINUE
1339      CONTINUE
      RETURN
 1315 CONTINUE
C------------------ SECTION 16 ---------------------- value = GRND4
C Wind velocity components at inlet of computational domain
C for IX=3
      CALL ONLYIF(P1,V1,'ININ3')
```

```
      CALL GETPT(1,1,IZ,UUZ(1),UUZ(2),UUZ(3))
      CALL GETPT(1,1,IZ+1,UUZ(4),UUZ(5),UUZ(6))
      UUZ(7)=(UUZ(3)+UUZ(6))/2.0
      L0VAL=L0F(VAL)
        DO 1342 IX=IXF,IXL
          DO 1343 IY=IYF,IYL
          ICELL=IY+NY*(IX-1)
            IF(INDVAR.EQ.P1)THEN
              F(L0VAL+ICELL)=-1.*RG(14)*RSG1*0.258819*
     *         (UUZ(7)/RG(12))**RG(13)
            ELSE IF(INDVAR.EQ.V1)THEN
              F(L0VAL+ICELL)=RG(14)*0.258819*(UUZ(7)/RG(12))**RG(13)
            ELSE IF(INDVAR.EQ.U1)THEN
              F(L0VAL+ICELL)=-1.*RG(14)*0.965926*
     *         (UUZ(7)/RG(12))**RG(13)
            ENDIF
1343        CONTINUE
1342      CONTINUE
      RETURN
 1316 CONTINUE
C------------------ SECTION 17 ------------------- value = GRND5
      RETURN
 1317 CONTINUE
```

Material omitted

```
C   * ------------------ SECTION 6 ---- FINISH OF IZ SLAB.
C   Calculate heat transfer rate in the cooling tower.
      IF(IZ.EQ.IG(5))THEN
      L0DEN=L0F(AUX(DEN1))
      L0W1=L0F(W1)
      L0H1=L0F(H1)
      L0LOW=L0F(LOW(H1))
      L0HIGH=L0F(HIGH(H1))
      CALL GTIZYX(10,IG(5),UUAREA,50,50)
      UUQ=0.0
      UUWW=0
      UUOP=0
      UUMASS=0
      DO 1335 IX=IG(1),IG(2)
        DO 1336 IY=IG(3),IG(4)
        ICELL=IY+NY*(IX-1)
        UUV=F(L0W1+ICELL)
        UUTL=F(L0LOW+ICELL)
        UUTH=F(L0HIGH+ICELL)
        UUMASS=UUMASS+UUV*UUAREA(IY,IX)*F(L0DEN+ICELL)*2.
        UUOP=UUOP+UUAREA(IY,IX)
         IF (UUV.GT.0.0)THEN
           UUQ=UUQ+F(L0DEN+ICELL)*UUAREA(IY,IX)
     *      *UUV*RG(7)*ABS(F(L0H1+ICELL)-UUTL)
        ELSE
```

```
          UUQ=UUQ+F(L0DEN+ICELL)*UUAREA(IY,IX)
     *       *(ABS(UUV))*RG(7)*ABS(F(L0H1+ICELL)-UUTH)
         ENDIF
1336     CONTINUE
1335  CONTINUE
      UUWW=UUMASS/UUOP/RSG1/2.
      ENDIF
      RETURN
  197 CONTINUE
C     * ------------------ SECTION 7 ---- FINISH OF SWEEP.
      ISWEP=ISWEP+1
      CALL WRIT3R('Heat T  ',UUQ,'VELOCITY',UUWW,'MASS    ',UUMASS)
      RETURN
  198 CONTINUE
C     * ------------------ SECTION 8 ---- FINISH OF TIME STEP.
      CALL WRIT3R('Heat T  ',UUQ,'VELOCITY',UUWW,'MASS    ',UUMASS)
      RETURN
C*****************************************************************
```

Material omitted

APPENDIX K

A two-dimensional investigation of the maldistribution through an A-frame due to a cross-flow.

Markòczy [77MA1] suggests that a part of the negative action of a cross-wind on a the performance of a natural draft dry-cooling tower is due to the maldistribution of the air flow through the heat exchangers. For a tower with the heat exchangers arranged vertically around the circumference of the tower, the performance of the A-frames on the flanks of the tower are the most affected by this flow distortion due to oblique inlet flow [69CH1]. If the horizontal radial layout is chosen for a particular tower, the A-frames arranged perpendicularly to the wind direction will experience similar distorted inflow conditions. By using the PHOENICS computer code the effect of oblique inlet conditions on the heat transfer rate and pressure drop across a two-dimensional A-frame was investigated.

The grid distribution used to solve the flow field through an array of A-frames is shown in figure K.1. To indicate the position of the A-frames the cells in which they are represented are shaded. The A-frames modelled in the analysis each have an apex angle of 60°, while the pressure loss coefficient for normal flow through the individual heat exchanger bundles is given by

$$K_{he} = 10206\, Ry^{-0.5207} \qquad (K.1)$$

The pressure drop through the heat exchanger is assumed to be such that the air flow will pass through it in a direction essentially normal to the face of the heat exchanger. By specifying a low pressure above the A-frames at the exit of the computational domain, air is sucked through the heat exchangers with the resulted flow field shown in figure K.2. In the analysis only the flow distribution through the A-frame located in the middle of the array was considered, while the flows through the other A-frames were used to simulate the effective boundary conditions.

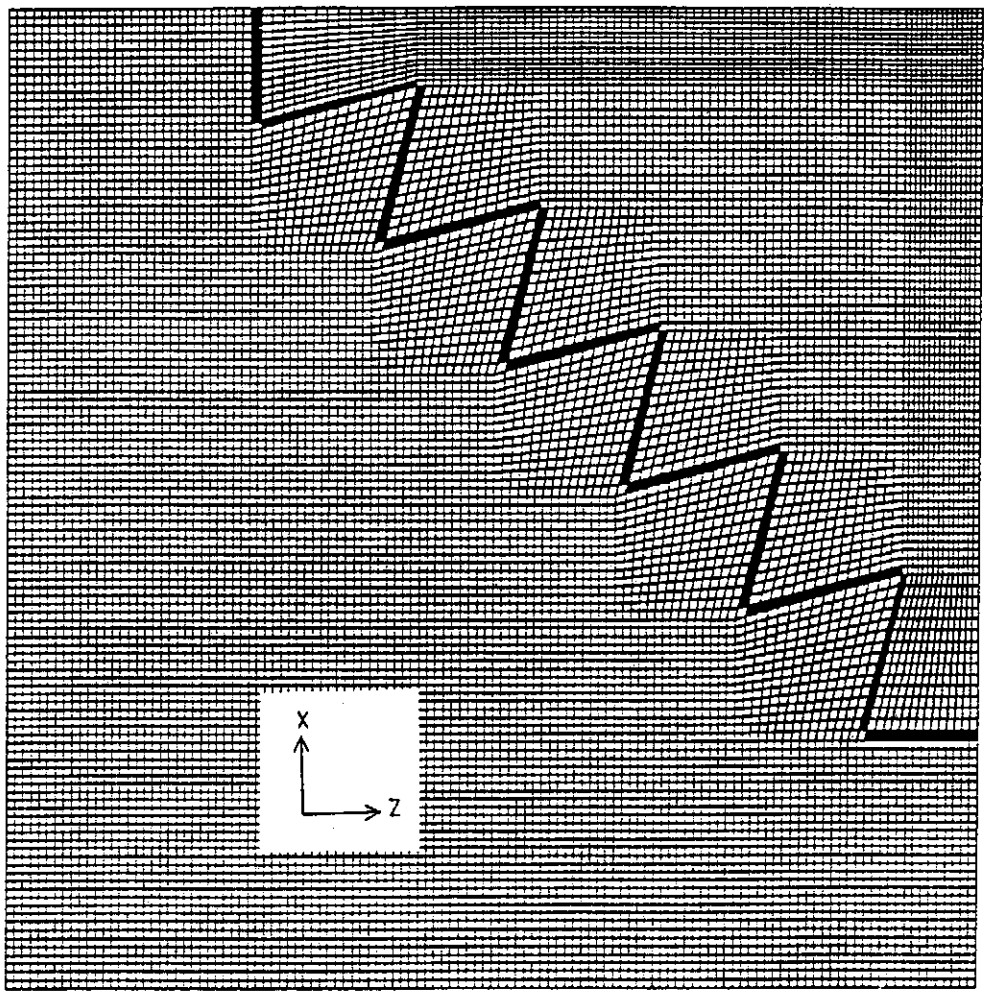

Figure K.1: Grid distribution.

To solve the flow field through the A-frame in a cross-flow, the following boundary conditions were specified on the inlet of the computational domain. On the lower x-plane an uniform inlet velocity was specified in a direction parallel to the A-frames while the lower z-plane was left "open". The low pressure specified above the heat exchangers caused the air in the main stream to be deflected and flow through the heat exchangers at a rate which is dependent on the pressure difference and the flow resistances. By varying the air inlet velocity at the inlet of the domain with a constant pressure difference across the heat exchangers, the mean incidence angle of the flow to the A-frame under consideration was changed. A vector diagram of the flow field through the array of A-frames for a given air inlet velocity is given in figure K.3.

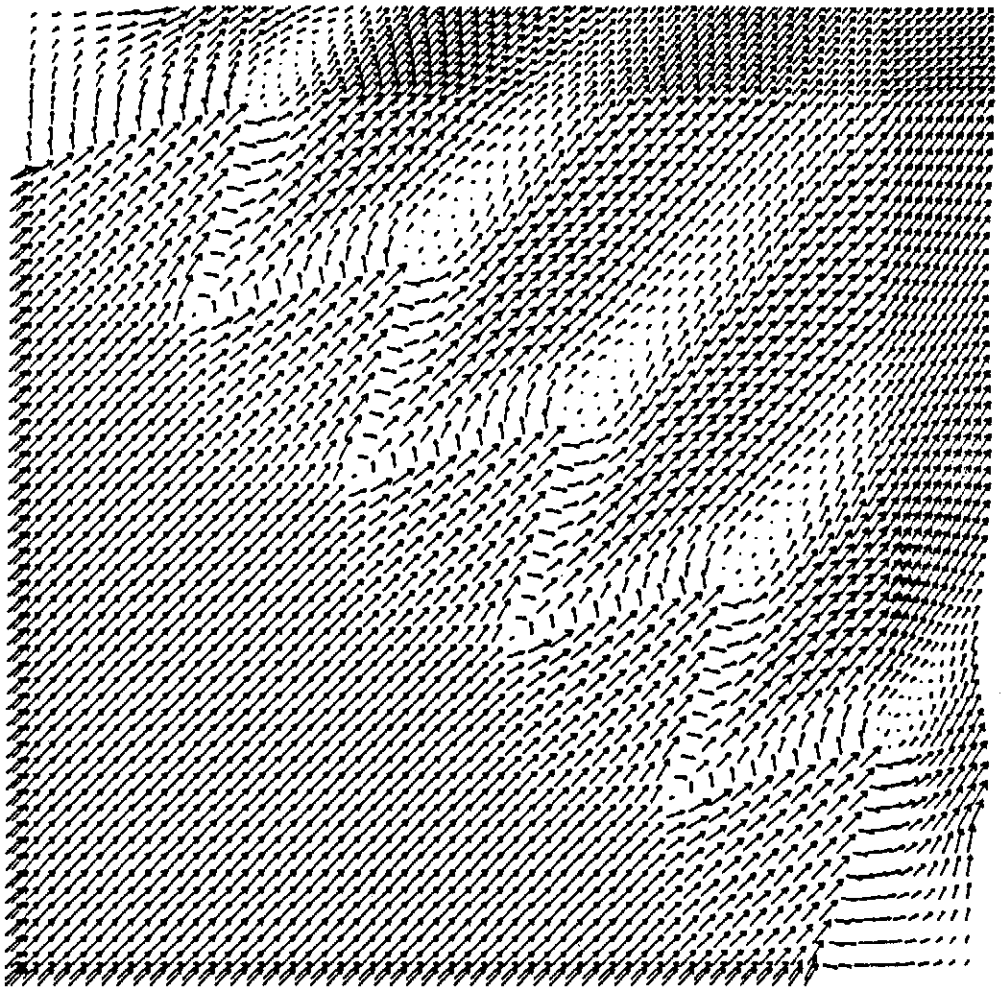

Figure K.2: Flow field through an array of A-frames in windless conditions.

As the incidence angle decreases from 90°, i.e. normal flow, the flow distribution through the A-frame becomes increasingly more non-uniform. Figure K.4 shows the air velocity distribution through the up and downstream heat exchangers for a mean incidence angle of 41.6°. As indicated in the figure, the flow through the heat exchanger on the upstream side of the A-frame decreases as a result of the inclined flow. Similar flow patterns were observed by Markòczy [77MA1] through the A-frames of a full scale tower and are compared to the numerical results in figure K.4.

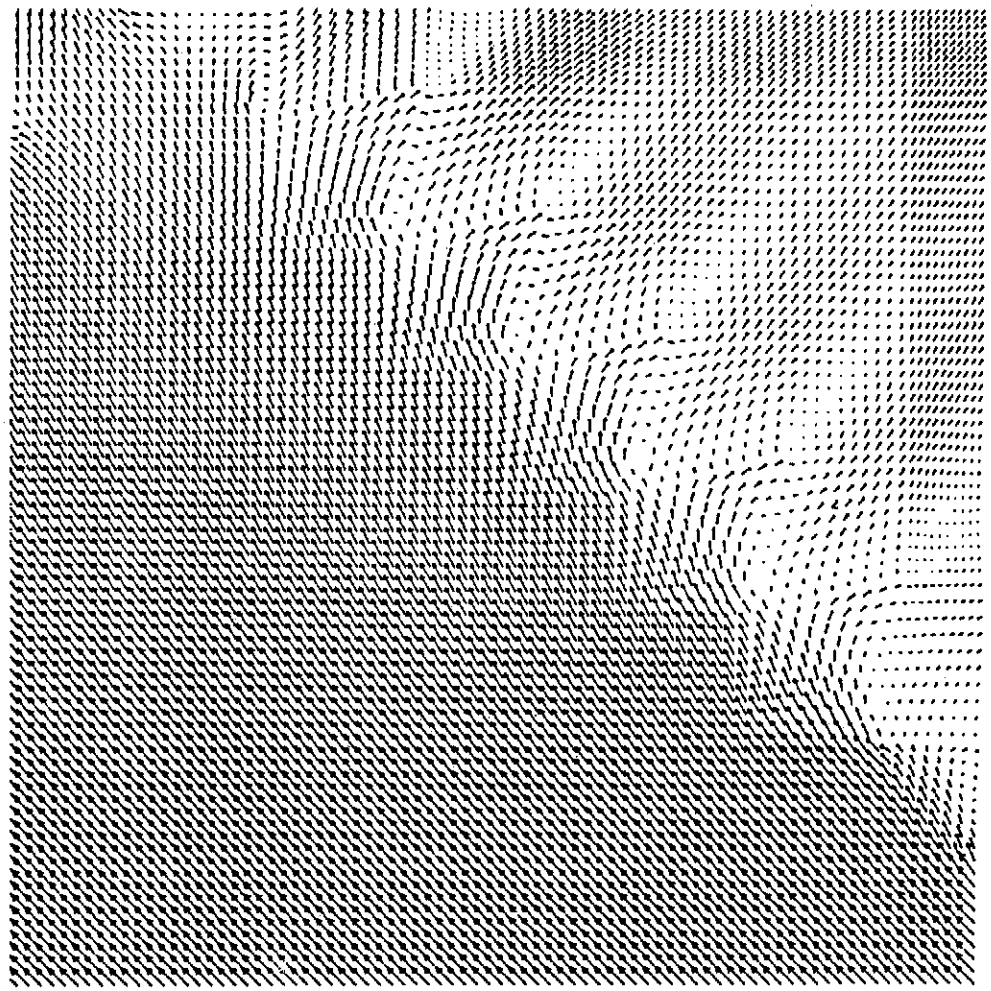

Figure K.3: Flow field through A-frames in a cross-flow.

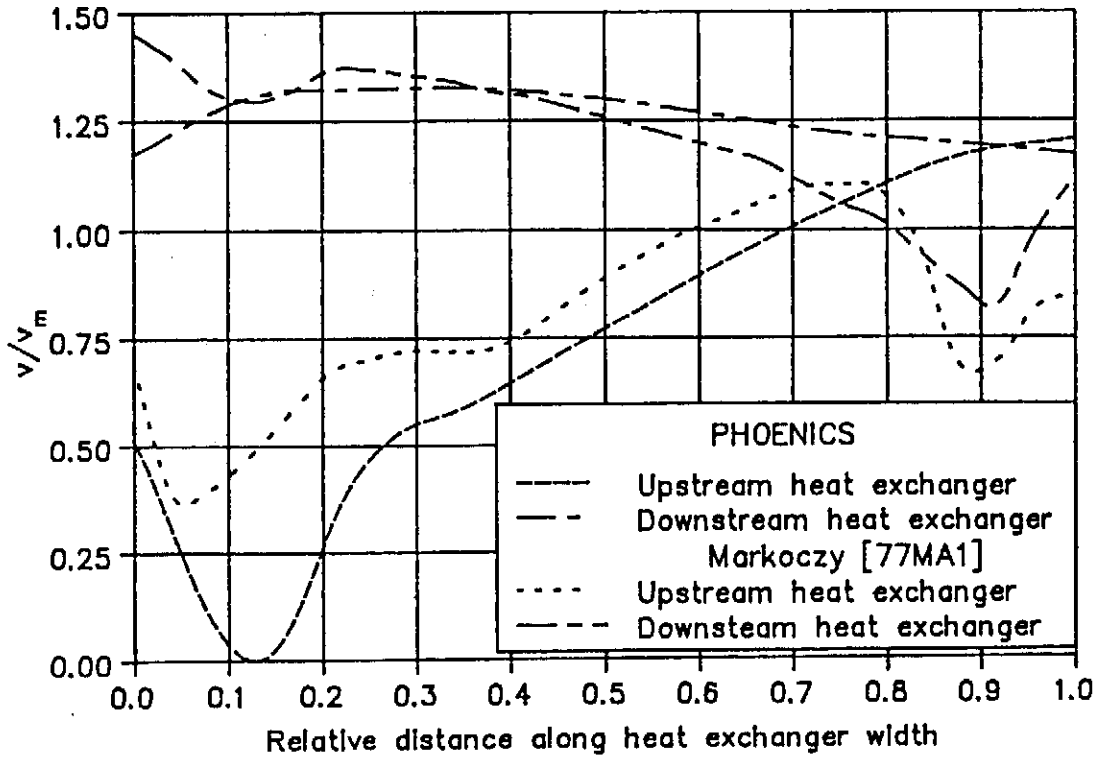

Figure K.4: Velocity distribution through an A-frame, Apex angle = 60°.

Due to the distorted flow pattern, the mass mean temperature of the air leaving the heat exchangers is less than that which will be found for a uniform velocity distribution. Based on the results obtained with the numerical model, an air temperature correction factor was calculated and is shown in figure K.5 as a function of the incidence angle to the A-frames. By applying this factor, the effect of the maldistribution through the A-frame on the mean air outlet temperature can be calculated for a known incidence angle and a given mean air mass flow rate through it.

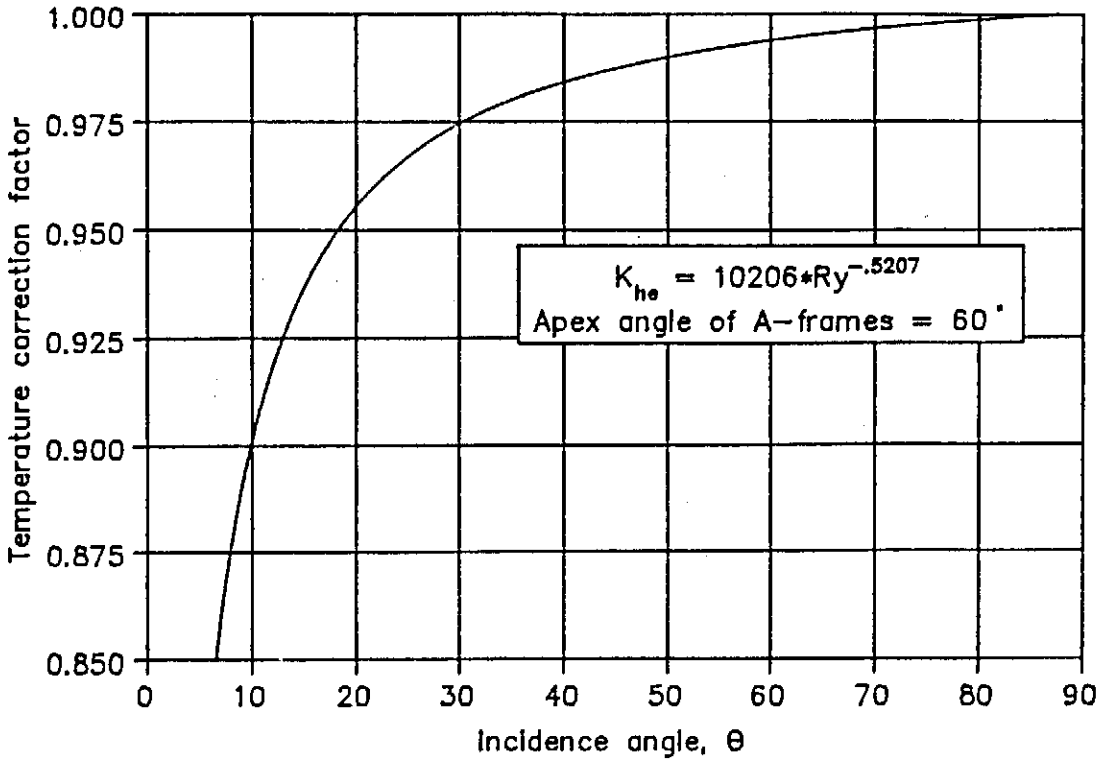

Figure K.5: Temperature correction factor.

As a result of the lower air outlet temperature, the effectiveness of the A-frame also decreases as shown in figure K.6. The effectiveness of the A-frame is defined as the ratio of the actual heat transfer rate to the heat transfer rate obtained for a uniform air distribution. Furthermore, if the A-frame is employed in a natural draft dry-cooling tower operating in a cross-wind, the lower air outlet temperature will cause a reduction in the available tower draft. As a result less air will be sucked through the tower which will cause a further reduction in the amount of heat dissipated by the tower.

As the incidence angle to the A-frame decreases, a reduction in the mean air mass flow rate through the A-frame is found due to an increase in the effective pressure loss coefficient through the heat exchangers. Based on the mean air mass flow rate through the A-frame, a pressure

loss coefficient correction factor was calculated and is shown in figure K.7.

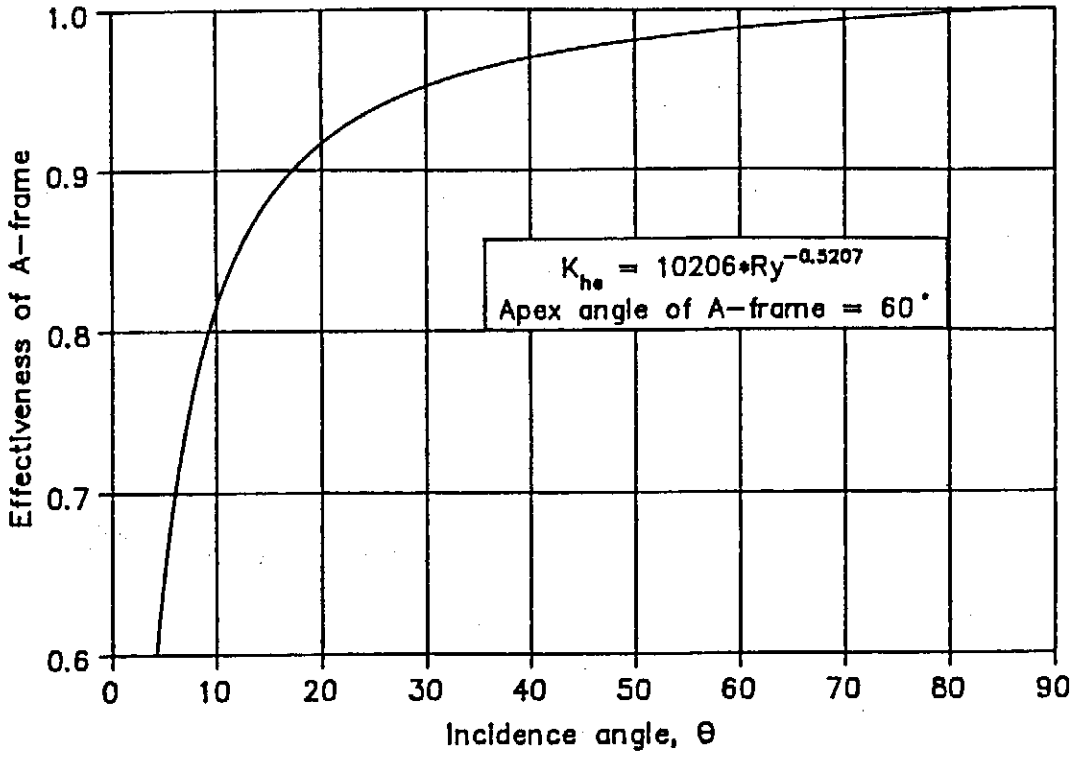

Figure K.6: Effectiveness of an A-frame in a cross-flow.

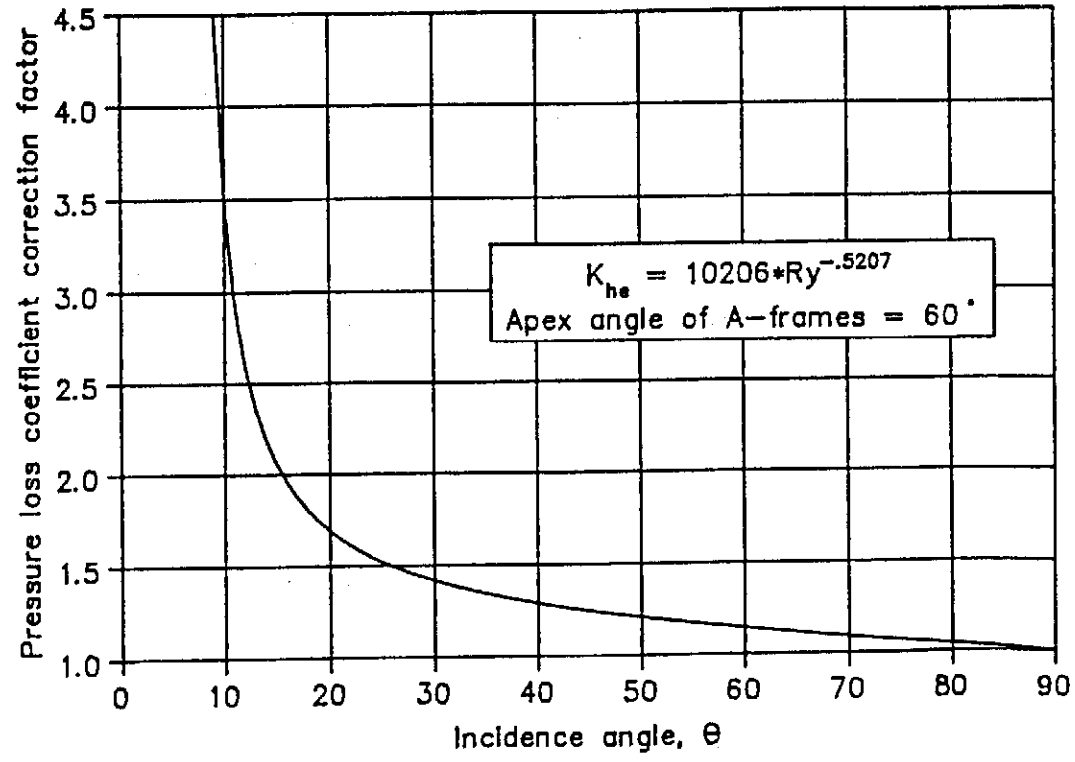

Figure K.7: Pressure loss coefficient correction factor.